Structures and symmetry-breaking in the fluctuations of nonequilibrium systems

TESIS DOCTORAL

Programa de Doctorado en Física y Matemáticas (FisyMat)

Nicolás Tizón Escamilla

Directores

Pedro Luis Garrido Galera
Pablo Ignacio Hurtado Fernández

UNIVERSIDAD
DE GRANADA

Grupo de Física Estadística y Sistemas Complejos
Departamento de Electromagnetismo y Física de la Materia
Universidad de Granada
2018

El doctorando / *The doctoral candidate* NICOLÁS TIZÓN ESCAMILLA, y los directores de la tesis / *and the thesis supervisors* PEDRO LUIS GARRIDO GALERA y PABLO IGNACIO HURTADO FERNÁNDEZ,

Garantizamos, al firmar esta tesis doctoral, que el trabajo ha sido realizado por el doctorando bajo la dirección de los directores de la tesis y hasta donde nuestro conocimiento alcanza, en la realización del trabajo, se han respetado los derechos de otros autores a ser citados, cuando se han utilizado sus resultados o publicaciones.

Guarantee, by signing this doctoral thesis, that the work has been done by the doctoral candidate under the direction of the thesis supervisors and, as far as our knowledge reaches, in the performance of the work, the rights of other authors to be cited (when their results or publications have been used) have been respected.

Granada, a 13 de Noviembre de 2018,

Directores de la Tesis / *Thesis supervisors*:

Dr. Pedro Luis Garrido Galera	Dr. Pablo Ignacio Hurtado Fernández
Catedrático de Universidad	Prof. Titular de Universidad
Grupo de Física Estadística y Sistemas Complejos	Grupo de Física Estadística y Sistemas Complejos
Departamento de Electromagnetismo y Física de la Materia	Departamento de Electromagnetismo y Física de la Materia
Universidad de Granada	Universidad de Granada

Doctorando / *Doctoral candidate*:

Nicolás Tizón Escamilla

Financiación

Contents

List of publications

The contents and results of this thesis are included in the following set of publications.

Paper I **Structure of the optimal path to a fluctuation.**
N. Tizón-Escamilla, P.I. Hurtado, and P.L. Garrido.
Physical Review E , *95* , 032119 (2017).

Paper II **Order and symmetry-breaking in the fluctuations of driven systems.**
N. Tizón-Escamilla, C. Pérez-Espigares, P.L. Garrido, and P.I. Hurtado.
Physical Review Letters , *119*, 090602 (2017).

Paper III **Effective driven dynamics for one-dimensional conditioned Langevin processes in the weak-noise limit.**
N. Tizón-Escamilla, V. Lecomte, and E. Bertin.
arXiv:1807.06438 ,
Accepted in Journal of Statistical Mechanics: Theory and Experiments.

Paper IV **Infinite family of universal profiles for heat current statistics in Fourier's law.**
P.L. Garrido, P.I. Hurtado, and N. Tizón-Escamilla.
arXiv:1810.10778 ,
Under revision in Physical Review E.

Chapter 1

Introduction

1.1 Background

Unraveling the mysteries of Nature has always been one of the main challenges of humanity. During centuries, questions such as *what is the different substances made of?*, *why does it rain?* or *why does the Sun rise and set every day?* were tried to be solved. Finding answers to these fundamental questions opens the door to a new interesting dilemma: would it be possible to anticipate what is going to happen under the light of this new information? Or in other words, are we able to detect general patterns from these answers and use them to predict future behaviour? These elements constitute the foundations in which physics relies on. Loosely speaking, physics aims to understand natural phenomena by characterizing their causes and deduce basic principles and theories which allow to make quantitative predictions about future observations[1]. In this sense, physics occupies a special place among the different fields comprehending modern Natural Science. In words of Richard P. Feynman: "Physics is the most fundamental and all-inclusive of the sciences [...]. Students of many fields find themselves studying physics because of the basic role it plays in all phenomena" [1]. Indeed, physics, as a science which tries to obtain general laws governing Nature , has a wide range of applicability in Chemistry, Biology, Geology or even social sciences.

The spectrum of phenomena described by physics wide from the very tiny (e.g. particles that constitute matter and radiation) to the extremely large (e.g. galaxies,

---

[1]We do not aim to establish here a formal definition of what physics is, just to point out, from the point of view of the author, some of the most important goals of this science.

clusters of galaxies, superclusters,...). When dealing with the ambitious task of understanding the universe, one realizes that Nature presents a hierarchical structure. Reality is divided into different *levels of description*, each of them defined by their typical *length and time scales*. For instance, let us imagine a litre of water inside an isolated Dewar flask. The length and time scales that we can measure with the naked eye in a laboratory define the *macroscopic level*. However, it is well-known that the litre of water is composed by a number of H_2O molecules of the order of Avogadro's number, N_A. These much smaller length and time scales define a new level of description called *microscopic level*[2]. Studying the properties of each level separately, one discovers that they are characterized by their own observables which satisfies certain relations. These *laws* govern the behaviour of each hierarchical structure. In our water example, the macroscopic level is completely characterized by quantities such as temperature, volume, pressure, etc. Furthermore, there exists a macroscopic theory establishing relations among these observables: Thermodynamics. Nevertheless, when we think about molecules composing water, their behaviour is described by their position, velocity, energy, etc., and laws that govern their evolution are defined by Classical or Quantum Mechanics. Some examples of this hierarchical division are shown in Fig.1.

The clear separation between different scales lead to a fundamental question: if both level of descriptions are parts of the same reality, which is the connection between microscopic and macroscopic levels? The field trying to find a solution of this dilemma is *Statistical Mechanics*, whose main goal is to describe the macroscopic properties of a system from laws governing the microscopic world. We think again in the example of water in a Dewar flask. For simplicity, let us assume that laws which describe the behaviour of water molecules are given by Classical Mechanics. Therefore, equations defining the dynamics of each particle are deterministic, i.e. their evolution is fully determined once initial conditions of each molecule are fixed. Nevertheless, although this situation is formally solvable, finding the solution of N_A coupled differential equations is, in general, impracticable. Furthermore, it is also impossible to experimentally fix and determine N_A initial conditions. Consequently, the existence of such large number of particles leads to a statistical treatment of this problem. Statistical Mechanics deal with the many microscopic degrees of freedom in order to obtain statistical laws which will allow us to understand the complex macroscopic behaviour. Under this scheme, one can determine the *mean* or *average* value of a macroscopic observable, which corre-

---

[2]This division is not unique and represent a simplified version of the whole reality. Certainly, H_2O molecules are composed by a number of sub-atomic particles such as electrons, quarks, etc., with their own scales. Furthermore, the litre of water could be just a little fraction of the Atlantic Ocean, which again presents its typical length and time scales.
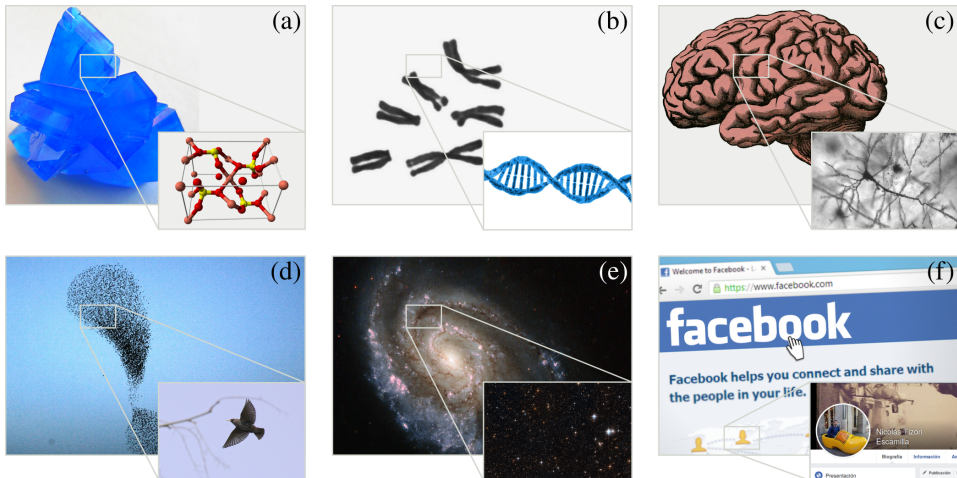
Figure 1.1: Several examples of system seen at different scales. (a) Copper(II) sulfate is a crystal of triclinic structure formed by atoms of Cu, S and O. (b) Each human cell has 46 chromosomes of size of order $10^{-4} - 10^{-6}$ m inside the nucleus. In the chromosomes the DNA exists in a wrapped structure, but if stretched out in one cell, DNA would form very thin thread, of about 3 m long [2]. (c) The human brain has a volume of the order of 10^3 m^3 and it is composed by around 10^{10} neurons, which length varies from $10^{-6} - 10^{-4}$ m. [3]. (d) A flock of birds and a single starling. (e) The spiral galaxy NGC 6984 is one of the 10^{11} galaxies in the observable universe, and in each galaxy there is an estimated amount of 10^{11} stars [4]. (f) The number of active users of the largest social network is of the order of 10^{10}. Image sources: Wikimedia Commons, the free media repository (a, d, e), ESA/Hubble (b), Facebook (c), Graphodatsky et al., Molecular Cytogenetics 2011, 4-22 (d), Pixabay (d, f), COBBS (Sapienza University, Rome) (f).

sponds to the typical value that we will observe during a measure in the laboratory[3]. However, one can find *deviations* from the mean value of such a quantity as a consequence of its statistical nature. In this case, it said that the value of the observable *fluctuates* [7–9]. Hence, fluctuations are understood to be a microscopic reminiscence at the macroscopic world. The study of fluctuations is a fundamental object in modern physics, and it will the central topic of this Thesis.

In 1905, Albert Einstein introduced a formalism to describe the Brownian motion, i.e. the random motion of a particle suspended in a fluid, based on a statistical description of the phenomena [10–13]. This work is broadly considered one of the first evidences of the strong influence of fluctuations. The randomness of the parti-

---

[3]This will be not always the case. A system satisfying this condition is call *ergodic system*. Proving that a system is ergodic is far from being a easy task, only solved in a few particular cases (see for instance, Sinai's billiards system [5, 6]). In most cases, this property is assumed to be satisfied, what it is known as *Ergodic Hypothesis*.

cle's movement emerge from its collisions with the molecules composing the fluid. In this way, Einstein was able to determine Avogadro's number and, consequently, the size of fluid molecules by analysing the statistic of fluctuations of the particle displacement. Many other examples highlighting the importance of fluctuations can be found, for instance, in critical phenomena, hydrodynamics or even cosmology, where the study of fluctuations of the cosmic background radiation has provided crucial information to understand the origin of our universe.

1.2   Why do we study macroscopic fluctuations?

The probability of observing a given fluctuation usually decays with the number of particles of the system. Consequently, measuring a deviation from the mean value of a macroscopic quantity in a laboratory is, in general, unlikely. The situation is even more dramatic if we are interested in large deviations. To illustrate this fact, let us imagine that we are in an isolated room and, suddenly, the air of the place condenses in the upper corner of the room. This event is a paradigmatic example of what we understand by a large fluctuation. Even though this rare event is not physically forbidden, the probability of taking place is so small that, in practice, it will luckily never occur. In Nature, there exists several phenomena which are known to be an outgrowth of such a behaviour, usually with dramatic consequences (see Fig. 2). Thus, the question that naturally arises is: why are we interested in studying phenomena which rarely happen? Or reformulating it, why the characterization of arbitrarily large fluctuations result of special relevance in physics? In the following lines we will provide three powerful arguments to support the importance of analysing the statistic of arbitrarily large fluctuations.

   Nonequilibrium dilemma. Describing macroscopic behaviour in terms of the microscopic dynamics is an arduous task which remains challenging in most cases. Let us imagine an isolated system presenting no hysteresis. Under these conditions, after a transient time it will settle into a state in which its macroscopic variables do not change with time, known as *thermodynamical equilibrium state*. Dealing with systems in equilibrium, Statistical Mechanics has achieved a great success, providing a general theory capable of connecting both levels of description: the *Ensemble Theory*. Under this framework, one can construct and relate the different (macroscopic) thermodynamic quantities (e.g. entropy, free energy, temperature, pressure,...) from the knowledge of the laws of Classical (or Quantum) Mechanics controlling the evolution of the microscopic components. In this way, by postulating that each microscopic state which realizes a given equilibrium macroscopic state has *a priori* the same probability of occurring (i.e. *equal a priori*

Figure 1.2: Rogue wave in Avila Bay (California). A paradigmatic example of large fluctuations taking place in Nature. These waves could reach 30 metres high. Their rarity and unpredictability make them an extremely dangerous phenomena.

probability postulate), Statistical Mechanics establishes that entropy (macroscopic observable) could be related to the number of microstates $\Omega(U, \Delta U; V, N)$ compatible with macrostates of energy $E \in [U, U + \Delta U]$ (with $\Delta U << U$), volume V and number of particles N, as:

$$S(U, V, N) = k_{\mathrm{B}} \ln \Omega(U, \Delta U; V, N) \,, \tag{1.1}$$

where k_{B} is the Boltzmann constant. The relation between this two quantities was first established by Ludwig Boltzmann in 1875 [14], and later formulated as (20) by Max Planck in early 1900's [8]. The number of microstates Ω is the main element of the *microcanonical ensemble*, which describes a system characterized by $E \in [U, U + \Delta U]$, V and N. However, it is difficult to fix experimentally the system energy. Using a heat bath, we can control its temperature, leting the energy fluctuates. Hence, one can define the *canonical* ensemble describing a system characterized by T, V and N. The probability density function of observing a

microscopic state α is now given by Gibbs distribution:

$$\rho(\alpha) = \frac{1}{Z(T,V,N)} e^{-\beta E(\alpha)} , \qquad (1.2)$$

where $\beta = (k_{\mathrm{B}}T)^{-1}$, $E(\alpha)$ is the energy associated to microstate α and $Z(T,V,N)$ is the *partition function*, central object of the canonical ensemble. Canonical ensemble provides a definition of the *free energy* or *Helmhotz potential*,$F(T,V,N)$, in terms of the partition function, namely:

$$F(T,V,N) = -\beta^{-1} \ln Z(T,V,N) , \qquad (1.3)$$

Furthermore, one could write Ω in terms of Z via a sort of Laplace transform, while the entropy and free energy can also be related, as it was predicted by Thermodynamics, via the Legendre transform:

$$F = U - TS . \qquad (1.4)$$

In the context of equilibrium Statistical Mechanics, fluctuations play a prominent role since by characterizing their statistics one can compute relevant thermodynamic potentials. One particularly interesting relation is given by Einstein formula [7, 8, 15] which allow us to write the fluctuations of the system energy E in terms of a measurable macroscopic quantity, the heat capacity at constant volume $C_V = \left(\frac{\partial U}{\partial T}\right)_{V,N}$:

$$\langle \Delta E \rangle \equiv \langle E^2 \rangle - \langle E \rangle^2 = k_{\mathrm{B}} T^2 C_V , \qquad (1.5)$$

where $U = \langle E \rangle$ and $\langle \cdot \rangle$ indicates an average over the canonical (Gibbs) distribution.

Considering a real system to be in thermodynamic equilibrium has become an exceptional approximation in many situations, where Statistical Mechanics has lead to outstanding predictions. Nevertheless, there exists no real equilibrium systems in Nature (they will require, for instance, perfect insulating materials). Even more, most of the phenomena we found in Nature are *out of equilibrium*. Let us think about ourselves. Our brain is composed by billions of neurons which are in continuous activity, sending and receiving electrical signals, leading to a highly complex structure working far from equilibrium. In our heart, a blood flow enters and is pumped to the whole body through a purely nonequilibrium process, in which the different parts contract and expand in a non-trivial way. Breathing, cell division or DNA replication are a few more examples of nonequilibrium processes occurring in our body. Far away living organisms, nonequilibrium systems abound in Nature at all scales. For instance, liquid crystals under the action of

external electric or magnetic fields found in cell membranes or LCD screens; seas and oceans where complex and turbulent flows are paradigms of their behaviour; or stars which present temperature and pressure gradients, convection phenomena, etc. In general, they are open or hysteric systems, often under the action of external forces or noise sources, subject to mass or energy fluxes. One interesting situation arise when the system evolves to a state in which their macroscopic varibles remain constant in time. We say that they settle into a nonequilibrium *steady state*. They are the most similar situations to equilibrium states, becoming the main object of study in most works characterizing out of equilibrium phenomena.

Despite their ubiquity, there no exists a general theory which predicts macroscopic behaviour in terms of the microscopic laws in nonequilibrium systems. The crucial role played by the microscopic dynamics out of equilibrium hinders the development of a scheme connecting both levels of description. As a direct consequence, the system's *trajectories* or *histories*, i.e. sequences of states, followed by the system during its evolution, emerge as the central elements to characterize nonequilibrium features. In general, such trajectories are described by phenomenological equations obtained using *ad hoc* approximations valid for a particular system (or class of systems), as for instance Langevin, Fokker-Planck or Navier-Stokes equations. Furthermore, in a similar way to what happens in equilibrium, one can find phenomena related to the breaking of a symmetry, self-organization, phase coexistence, etc., far from equilibrium in the space of trajectories. The instabilities behind these processes are known as *dynamical phase transitions* (DPTs) which separates regions where histories characterizing the evolution of the system present different properties and structures.

Inspired by Einstein formula and the capital relevance of fluctuations in equilibrium, it is nowadays expected that a deeper understanding of nonequilibrium macroscopic fluctuations could fill in part this lack of a general theory linking both level of descriptions [16–19]. To support this idea, we briefly describe in the following lines the main features of the *Large Deviation Theory* (LDT), the mathematical framework characterizing large fluctuations [19–26], and its connection to equilibrium Statistical Mechanics. The LDT relies on a fundamental statistical principle, cornerstone of the study of rare events. Let A_n be a random variable depending on the parameter n, and let $p(A_n = a)$ the probability of having a given value $A_n = a$. We say that $p(A_n = a)$ satisfies a *large deviation principle* if the limit:

$$G(a) = \lim_{n \to \infty} \left\{ -\frac{1}{n} \ln p(A_n = a) \right\} \qquad (1.6)$$

exists [19]. The function $G(a)$ is called *Large Deviation Function* (LDF) or *rate*

function, the central element of LDT characterizing the statistic of fluctuations. From Eq. (25), one can write:

$$p(A_n = a) \asymp e^{-nG(a)} \,, \tag{1.7}$$

where "$\asymp$" stands for "asymptotic logarithmic equivalence". The LDF is a positive function $G(a) \geq 0 \;\forall a$. Assuming that $G(a)$ has an unique global zero value and minimum [4], it can be proved that it is located at $a^* = \lim_{n\to\infty}\langle A_n\rangle_{\text{noise}}$, called *typical* or *expected* value. Remarkably, $p(A_n = a^*)$ does not decay exponentially, and thus the LDF indicates how the probability $p(A_n = a)$ peaks around a^* when $n \to \infty$, which is nothing more that an expression of the Law of Large Numbers. Finally, in this scheme one can study fluctuations around the typical value a^* by expanding the LDF:

$$G(a) \approx \frac{1}{2}G''(a^*)(a - a^*)^2 + \mathcal{O}((a - a^*)^3) \,, \tag{1.8}$$

which at first order different from zero leads, as it was expected, to Gaussian fluctuations:

$$p(A_n = a) \asymp e^{-n\frac{1}{2}G''(a^*)(a-a^*)^2} \,. \tag{1.9}$$

Therefore, Large Deviation Theory can be considered as a generalization of the Central Limit Theorem (CLT), since it provides information about what happens both near the expected value (where LDT and CLT agree) and for large deviations from a^*, where the Gaussian approximation is no more valid. We encourage the reader to see the review by Touchette [19], where the features of Large Deviation Theory are studied in depth.

Ensemble Theory, nucleus of equilibrium Statistical Mechanics, can be now understood in terms of Large Deviation Theory [19,24,25,27–36]. Let us show in brief this correspondence. Indeed, if the random variable whose fluctuations are going to be studied is the energy of the system E_N, following (25) one can define[5]:

$$G(e) = \lim_{N\to\infty} \left\{ -\frac{1}{N} \ln P(e_N \in [e, e + de]) \right\} \,, \tag{1.10}$$

where N is again the number of particles, $e_N = E_N/N$ is the energy per particle (or molar energy) and $P(e_N \in [e, e + de])$ is the probability of observing an energy $e_N \in [e, e + de]$. Such a probability is proportional to the number of

---

[4]In general, this will be the case along this Thesis.
[5]This can be trivially proved (see [19]) by using $P(E_N \in [E, E + dE]) = p(E_N = E)dE$

microstates $\Omega(e, de; v)$ compatible with $e_N \in [e, e + de]$ (with v=V/N), so it can proved that [19]:

$$G(e) = \lim_{N \to \infty} \left\{ -\frac{1}{N} \ln \Omega(e, de; v) \right\} . \qquad (1.11)$$

Writing $G(e) = -s(e)/k_{\mathrm{B}}$ and according to previously mentioned LDF properties, we realize that such expression corresponds to (20) with $s = S/N$ the *entropy per particle*. Hence, the energy LDF indeed corresponds to the entropy in equilibrium systems. One can know define the *scaled Cumulant Generating Function* (sCGF) of the distribution $P(e_N \in [e, e + de])$ as:

$$\mu(T) = \lim_{N \to \infty} \left\{ -\frac{1}{N} \ln Z_N(T) \right\} , \qquad (1.12)$$

with T the temperature and $Z_N(T) = \langle e^{-n\beta e_N} \rangle$ the partition function (note that $\langle \cdot \rangle$ stands for the average over $P(e_N \in [e, e + de])$). Defining $\mu(T) = \beta f(T)$, we again realize that the previous equation corresponds to (22) with $f = F/N$ the *free energy per particle*. Thus, in equilibrium, the sCGF corresponds to the free energy. Furthermore, according to Gärtner-Ellis Theorem [19, 24, 37], both G and μ are related via a Legendre-Fenchel transform, leading to:

$$s(e) = \inf_{T} \left\{ \frac{e - f(T)}{T} \right\} , \qquad (1.13)$$

in complete analogy with (23). Finally, we focus on fluctuations around the mean value $u = \langle e_N \rangle$, which according to (28), lead to:

$$\langle e_N^2 \rangle - \langle e_N \rangle^2 = -k_{\mathrm{B}} s''(u) . \qquad (1.14)$$

Noticing that $C_V = -N \frac{1}{T^2} \left(\frac{\partial^2 s(u,v)}{\partial u^2} \right)_v$, this equation is nothing more that Einstein formula (24).

The connection between equilibrium ensemble theory and Large Deviation Theory breaks new ground for facing nonequilibrium situations. The LDT methodology provides a robust scheme from which general far from equilibrium predictions could be derived. In the core of this framework, the large deviations functions, in a natural extension, could be considered as nonequilibrium analogs to thermodynamic potentials, bridging the gap between the microscopic and macroscopic levels of descriptions. Furthermore, it is expected that LDF exhibit a far more complex structure out of equilibrium, encoding key information on nonequilibrium properties[6]. However, these ideas are not deprived of problems. One of

---

[6]For instance, the LDF will be, in general, non-local which reflects the existence of long-range correlations standards of nonequilibrium situations

the main difficulties is the identification of the relevant macroscopic observables. The lacking of such a theory as Thermodynamics out of equilibrium leads to a gap in the proper definition (if any) of the quantities fully characterizing the behaviour of a macroscopic system (an essential element in the development of equilibrium ensemble theory). For systems which could be described by the evolution of some conserved quantities (e.g. temperature, energy, density of particles,...), it is broadly accepted that essential nonequilibrium observables are the associated currents or fluxes emerging in response of the external forces or gradients driven the system out of equilibrium. Indeed, understanding current fluctuations is nowadays considered as one of the main goals in nonequilibrium physics, becoming a source of number of very general results, as for instance [16–18, 38–52]. In other situations, space- and time-integrated observables could be good candidates, but in general, they will strongly depend on each system features.

In spite of being able to identify the relevant observables characterizing nonequilibrium behaviour, obtaining the large deviation function is still highly complex task since, in general, we do not know the structure of the probability distribution of microscopic dynamical states, or even if such a distribution indeed exits. The computation of the LDF from the microscopic dynamics have only succeeded in a few oversimplified stochastic lattice gases [16, 17]. Nevertheless, in the last decades, Bertini, De Sole, Gabrielli, Jona-Lasinio and Landim has formulated a theory to study dynamic fluctuations in driven diffusive systems far from equilibrium: the *Macroscopic Fluctuation Theory* (MFT) [16, 38, 53–55]. Starting from a mesoscopic description of the system in terms of fluctuating hydrodynamics (fully characterized by only a few transport coefficients which can be easily determined in experiments or simulations), the MFT offers detailed predictions for the large deviation functions of interest in the large time and size[7] limits. Note that time and size will play the role of the large-n parameter in LDT. As an interesting by-product, MFT also determines the *most probable trajectory* that the system follows to sustain a given fluctuation. Understanding the properties and spatio-temporal structure of these optimal histories is of paramount importance, as they contain information on possible dynamic phase transitions appearing at the fluctuating level [18, 41, 52, 56–63], while their symmetry properties lead to new fluctuation theorems [44, 46, 48–50, 64–71]. The application of such scheme has been proved to provide deep and very general results helping us to improve our understanding on nonequilibrium behaviour.

Effective dynamics. The second reason to justify the importance of studying rare events is related to the determination of what it is called *effective driven dy-*

---

[7]In this situation, large size means large scale of separation between level of descriptions.

namics. As it was previously mentioned, it is in general nearly impracticable to measure a rare fluctuation in an experiment. However, recent breakthroughs have shown that fluctuations admit a control-theory (or active) interpretation [72–77]. In this way, by using a generalised version of Doob's h-transform [78, 79], one can construct an effective dynamics whose typical trajectories corresponds to the rare events of the original dynamics. In addition, this mechanism provides the external effective force which should be apply to our original system to make rare events become typical. Many advances and explicit examples on the determination of such effective dynamics have been done in the last years [72, 73, 80–88]. In the light of such mechanisms, the determination of rare events probability distribution, as well as characterization of interesting phenomena such as DPTs, symmetry-breaking, ordered structures, etc., are now more accessible both in simulations and experiments.Certainly, this methodology opens the door to a whole new world of possible applications of the large number of results and techniques developed in large fluctuations studies.

Small systems. Finally, the last argument supporting the interest in large fluctuations is based on the main role they played when dealing with small systems. We have shown that the probability of observing a deviation from the mean value decays exponentially with the number of particles of the system, which is the main reason why rare events rarely occurs in experiments. Nevertheless, if the system is small the difference between the scales of microscopic and macroscopic description notably reduces, as well as its number of particles. Consequently, large fluctuations become far more probable rising as essential elements to understand the system behaviour. This fact will be of crucial relevance in, for instance, nano-electronic devices, where fluctuations severely condition properties and features of such systems and their effects must be taken into account [89–92].

1.3 Outline of the Thesis

On the basis of the foregoing, it seems clear that the study of fluctuations is an essential object in modern physics. The aim of this Thesis will be to delve into the role of fluctuations arbitrarily far from equilibrium under the frameworks of Macroscopic Fluctuation Theory and Large Deviation Theory. In the following pages we will explore the two firsts arguments exposed above and their deep implications, developing a number a tools, techniques and results for a wide spectrum of situations ranging from general driven diffusive systems to systems composed by a single particle under the action of an external force both in and out of equilibrium. In this way, Chapters 2, 3, 4, 5, 6 will be devoted to the study and characterization

of MFT and its consequences, showing general results in the structure of the trajectories sustaining a given fluctuation, LDFs and dynamic phase transitions. On the other hand, Chapter 7 will focus on the construction of the effective dynamics associated to fluctuations of very general observables for a stochastic particle in a ring subjected to an external drift. We show then the outline of this Thesis.

In **Chapter 2** we present an introduction to Macroscopic Fluctuation Theory. Focusing on systems with one conserved quantity, we will describe their evolution at a mesoscopic level, which will serve as a starting point to develop the different aspects characterizing MFT. In particular, we will show how the study of probability distributions of relevant observables fluctuations converts into a variational problem whose solutions are the optimal trajectories sustaining a given fluctuation, leading to the determination of the corresponding LDF. Furthermore, we will present some essential and very general results on fluctuations and we will translate to the language of large deviations and MFT. Finally, we will briefly describe the mesoscopic evolution of other classes of systems, such as systems with no conserved quantities, to which the different techniques of MFT could be generalized.

As we have seen, trajectories leading to a given fluctuation encode key information on their statistical properties. This makes the understanding of optimal histories features a central issue. In **Chapter 3** we will derive a fundamental relation which strongly constraints the architecture of these optimal paths for general d-dimensional nonequilibrium diffusive systems, which implies a non-trivial structure for the dominant current vector fields. This general relation makes manifest the spatio-temporal non-locality of the current statistics and the associated optimal trajectories. In addition, we will also show how this outcome encompasses and explains many previous results obtained in the large deviation field.

Chapter 4 is devoted to the study of fluctuations of the heat current in a model of d-dimensional incompressible fluid driven out of equilibrium by a temperature gradient. Macroscopically, this system is govern by Fourier's law of heat conduction and its behaviour is fully described by the temperature field along the system. We will find that the most probable temperature fields sustaining atypical values of the global current can be naturally classified in an infinite set of curves, allowing us to exhaustively analyze their topological properties and to define universal profiles onto which all optimal fields collapse. We will also compute the statistics of empirical heat current, where we find remarkable logarithmic tails for large current fluctuations orthogonal to the thermal gradient. Finally, we will determine explicitly a number of cumulants of the current distribution, finding remarkable relations between them.

In **Chapter 5** we focus on the study of dynamic phase transitions at a fluctu-

ating level in the spaces of trajectories, one of the most intriguing phenomena of nonequilibrium physics. Here we will discover a DPT in the current vector statistics of an archetypal two-dimensional ($2d$) driven diffusive system, and characterize its properties using MFT. Interestingly, this is the first work which analyses DPTs of a d'-dimensional observable in d'-dimensional systems with $d' > 1$, a situation which until now had remained puzzling. The complex interplay among the external field, system anisotropy and vector currents in $2d$ leads to a rich phase diagram, with different symmetry-broken fluctuation phases separated by lines of 1st- and 2nd-order DPTs. Remarkably, different types of $1d$ order in the form of jammed density waves emerge to hinder transport for low-current fluctuations, revealing a connection between rare events and self-organized structures which enhance their probability.

Originally, MFT was developed to study large fluctuations of driven diffusive systems. However, these techniques could be extended to other situations characterized by mesoscopic evolution equations. In this way, in **Chapter 6**, we will characterize fluctuations in Ginzburg-Landau models at equilibrium. These systems are described by a scalar field which evolves following a locally non-conserved dynamics whose mesoscopic equations are given by Hohenberg-Halpering model A [93]. Interestingly, these systems present two different beheviour regimes characterized by a single or double equilibrium states. We will focus on fluctuations of the magnetization, i.e. the space- and time-integrated scalar field, revealing the existence of a DPT when asking for the probability of having small values of such observable in the "double-well" regime. Furthermore, we will show an exotic homogeneous but time-periodic trajectory which could appear below the transition point.

In **Chapter 7** we determine explicitly the effective probability-conserving dynamics in the case of fluctuations of general space- and time-integrated observables for a particle diffusing in a one-dimensional periodic potential in the weak-noise and large time asymptotes (which will play now the role of large-n in LDT). For 'current-type' additive observables, we find criteria for the emergence of a propagative trajectory for large enough deviations, revealing the existence of a dynamical phase transition at a fluctuating level, whose singular behaviour is between first and second order. In addition, we will provide a new method to determine the sCGF of the observable without having to solve the variational problem derived from MFT. It will allow us to show that the weak-noise and the large-time limits commute in this problem. Lastly, we will show how the original dynamics can be mapped in practice to an explicit effective driven dynamics, which takes the form of a driven Langevin dynamics in an effective potential. The non-trivial shape of

this effective potential is key to understand the link between the dynamical phase transition in the large deviations of current and the standard depinning transition of a particle in a tilted potential.

Finally, in **Chapter 8** we will summarize the different results exposed along this Thesis, pointing out the main implications and novelties which such contributions could involve to the field of macroscopic fluctuations and, in general, to Statistical Mechanics.

Chapter 2

An Introduction to Macroscopic Fluctuation Theory

2.1   Introduction

Fluctuations arise macroscopically as a consequence of the statistical nature of microscopic elements composing our world. Their appearance could involve severe consequences in the properties and behaviour of the system, so determining the probability distribution of fluctuations has become an interesting, although extremely hard, issue. In the context of equilibrium systems, Gibbs [94] and Einstein [15] provide, from different perspectives, a deep description of this problem. Under the light of this works, it is possible to establish a connection between the thermodynamic variables (e.g. entropy, internal energy, volume,...) and the probability of a fluctuation. To illustrate this fact, let us consider an isolated closed system composed by a small body A embedded in a (large) reservoir B. We suppose that both systems are macroscopic and they are in thermal and mechanical equilibrium. The reservoir is considered to be much larger than A, so its temperature T, pressure p and chemical potential μ remain fixed. While the total internal energy, U, volume, V and number of particles, N remains constant, there exists a mutual exchange of these quantities between both subsystems, opening the door to the emergence of fluctuations. The equilibrium entropy of the whole system, denoted by S_0, takes the maximum accessible value. When a fluctuation takes place, the value of total entropy changes to S, in such a way that $\Delta S = S - S_0 < 0$. Under these conditions, it can be proved [7–9] that the probability of such fluctuation

obeys Boltzmann-Einstein formula:

$$P \asymp \exp\left(-\frac{W_{\min} - \mu\Delta N_A}{k_B T}\right), \tag{2.1}$$

where subindex A indicates that variations of the observables between the fluctuation and equilibrium state are considered for subsystem A, k_B is the Boltzmann constant, and:

$$W_{\min} = \Delta U_A - T\Delta S_A + p\Delta V_A \tag{2.2}$$

is the minimum reversible work necessary to carry out such a fluctuation, i.e. to produce the given change of the observable's values, in the body A in a reversible way, for a fixed number of particles [95, 96]. For instance, if the volume remains constant during the process, this work corresponds to the variation of the free energy from one state to the other, $W_{\min} = (\Delta F)_{T,V}$ (in other words, the exponent in (2.1) is the variation of the grand potential). Interestingly $-W_{\min}$ is the maximum "useful" work which could be extracted from the system when it is forced to sustain the given fluctuation, i.e. to achieve a new equilibrium state whose variables correspond to the fluctuation state.

Out of equilibrium, the situation becomes harder. Indeed, there is no general theory describing the probability distribution of a fluctuation. During decades, a number of works tried to shed light on this problem, developing fundamental results which are considered as the basis of the way in which nonequilibrium fluctuations are understood nowadays [44, 48–50, 97–101]. A special remark should be made for Onsager [102, 103] and Onsager and Machlup [104] works, which characterized fluctuations near equilibrium and provided a mathematical approach to describe the statistics of a full trajectory. However, it was in the 2000's when the study of far from equilibrium fluctuations undergoes a true revolution. Bertini, De Sole, Gabrielli, Jona-Lasinio and Landim [16, 38, 53–55] settled the basis of general theoretical scheme which describes fluctuations of driven diffusive systems out of equilibrium: the *Macroscopic Fluctuation Theory* (MFT). Under this framework, the problem of characterizing the probability distribution of fluctuations turns into a variational problem on the most probable paths the system follows to sustain such a given fluctuation. The mathematical techniques underlying MFT relies on the well-known *large deviation theory*, developed by Cramér [105], Donsker and Varadhan [21, 106–108], and Freidlin and Wentzell [26], which, as it was shown in the Introduction, has been proved to provide an efficient framework to formulate problems of statistical mechanics [19, 24, 25, 28–30, 35].

The aim of this chapter is to establish the foundations for characterizing the statistics of macroscopic fluctuations in a broad variety of general systems, under the MFT (and large deviations) formalism. In this direction, we will describe

the different features constituting MFT, as well as the mechanisms and techniques widely employed to study large fluctuations in systems both in and out of equilibrium. The structure of the chaper is the following: in Section 2.2 we will describe the general class of system we are going to deal with, d-dimensional systems with conserved dynamics, providing a mesoscopic description of its evolution by means of Langevin equation. We will also present a particular kind of systems, included in the general case, with special relevance in physics: the driven diffusive systems. In Section 2.3, we will show other possible formulations describing the evolution at the mesoscopic level, i.e. the Fokker-Planck equation and Path Integral representation, and their equivalences. In Section 2.4, we will describe the procedure to study macroscopic fluctuations under the MFT framework, paying special attention to fluctuations of the final structure of conserved field characterizing the behaviour of the system and of relevant space- and time-integrated observables. In Section 2.5, we will present some remarkable results in the realms of fluctuations which have been obtained in the last decades. Finally, in Section 2.6, we will characterize the evolution at a mesoscopic level of two other systems which will be also studied along this Thesis: systems with non-conserved dynamics and a particle under the action of a force and a thermal noise.

2.2 A mesoscopic description of d-dimensional driven systems with locally conserved dynamics

The broad class of systems we are interested in are the d-dimensional driven systems characterized by one conservation law. These systems are completely described by a locally-conserved scalar field $\phi(\mathbf{r}, t)$ (e.g. particle density, temperature, charge,...), where $\mathbf{r} \in \Lambda \equiv [0, 1]^d$ is the (macroscopic) spatial dimension and $t \in [t_0, t_f]$ is the (macroscopic) time, which evolves according to the hydrodynamic (or macroscopic) equation [109, 110]:

$$\partial_t \phi(\mathbf{r}, t) + \boldsymbol{\nabla} \cdot \mathbf{j_D}(\mathbf{r}, t) = 0 \,. \tag{2.3}$$

The field $\mathbf{j_D}(\mathbf{r}, t)$ is the local current associated to $\phi(\mathbf{r}, t)$. This evolution equation is known as *continuity equation*. In order to close Eq. (2.3), one can express the local current as a function of $\phi(\mathbf{r}, t)$:

$$\mathbf{j_D}(\mathbf{r}, t) = \mathbf{J_E}[\phi(\mathbf{r}, t)] \,, \tag{2.4}$$

with $\mathbf{J_E}[\phi(\mathbf{r}, t)]$ depending on the external drift $\mathbf{E}(\mathbf{r}, t)$, the scalar field $\phi(\mathbf{r}, t)$ and its derivatives. The relation (2.4) is called *constitutive equation* and its structure is determined by the physical properties of the problem. Interestingly, these

equations are also known in literature as *phenomenological* relations since, in their origin, they were introduced *ad hoc* under the light of experimental results. Nowadays, while some of them have still a phenomenological basis, most constitutive equations can be deduced theoretically from first principles. Some examples of constitutive equations are Fick's law of diffusion, Fourier's law of thermal conduction or Ohm's law of electric conduction.

The current field (2.4) represent a dissipative flux related to the necessary work made by the thermodynamic forces acting on the system in a relaxation or excursion between two states (both in or out of equilibrium) or to the dissipation needed to sustain a nonequilibrium state [16, 110, 111]. Furthermore, it vanished when the system is in thermodynamic equilibrium[1]. As a consequence, the current plays a foundamental role in describing and characterizing nonequilibrium behaviour.

Finally, to fully define the problem, one must supplement equations (2.3)-(2.4) with the appropriate boundary and initial conditions, namely:

$$\phi(\mathbf{r}, t) = \bar{\phi}(\mathbf{r}, t), \ \mathbf{r} \in \partial \Lambda \quad , \quad \phi(\mathbf{r}, 0) = \phi_0(\mathbf{r}), \tag{2.5}$$

where $\partial \Lambda$ denotes system boundary. Some examples of boundary conditions could be periodic ones, if Λ is the d-dimensional torus $\mathbb{T}^d$, or non-homogeneous and time-independent conditions inducing an external boundary-drift (e.g. a one dimensional bar in contact with two thermostat at different temperatures). Remarkably, the structure of boundary conditions are crucial to define whether the system described by (2.3)-(2.4) reach an equilibrium state after an appropriated transient. A detailed example of this fact will be exposed in Section 2.2.1 when dealing with driven diffusive systems.

The set of equations (2.3)-(2.4), together with boundary conditions (2.5), defines the *deterministic* (or *classical*) evolution of a d-dimensional driven system with locally conserved dynamics at a macroscopic level of description. Thus, we will obtain the same system evolution once the initial conditions are fixed. Nevertheless, as we have seen, the values of physical observables fluctuate in real systems as a result of molecular-scale random behaviour. This fact could be taken into account by describing the system at an intermediate scale between the microscopic and the macroscopic ones: the *mesoscopic* level.

The new variables characterizing mesoscopic scale are integrated out in a "coarse-graining" procedure from the microscopic to the macroscopic by an appropriate rescaling of the spatial coordinates $\mathbf{r} = L^{-1}\mathbf{r}'$ and time $t = L^{-2}t'$, where

---

[1]In general, nonequilibrium systems are characterized by a non-vanishing current. However, it is important to remark that there exists out of equilibrium systems with zero net current. For an interesting discussion about which conditions should be satisfied by systems with one or no conserved quantities to be at equilibrium we refer to [112]

$\mathbf{r}'$ and t' are the microscopic spatial dimension and time, respectively. The L factor could be interpreted as a parameter proportional to the inverse of the size of a microscopic region which is averaged to obtain the local field mesoscopic value. This coarse-grained fields become random variables with the noise preserving information about the many fast microscopic degrees of freedom at the mesoscopic level. Deriving a continuum mesoscopic equation from the laws governing the microscopic dynamics is really hard task, which has been rigorously done for a few systems, such as stochastic lattice gas models (we refer the reader to [113–115] for a detailed description). In general, the construction of such equations is done by introducing *ad hoc* arguments based on intuitive heuristic reasonings. We are going to assume in our case that random microscopic motions leave a fingerprint in the form of small perturbation of the current field, in such a way that the average value will correspond to the one predicted by macroscopic equations (2.3)-(2.4). Furthermore, the amplitude of the noise will be, in general, nontrivial, depending on the the field ϕ. Hence, we can write the new "mesoscopic" current field as:

$$\mathbf{j}(\mathbf{r}, t) = \mathbf{j_D}(\mathbf{r}, t) + \boldsymbol{\xi}(\mathbf{r}, t), \tag{2.6}$$

where $\mathbf{j_D}(\mathbf{r}, t)$ is the deterministic current defined in (2.4) and $\boldsymbol{\xi}(\mathbf{r}, t)$ is a Gaussian white noise with:

$$\langle \boldsymbol{\xi}(\mathbf{r}, t) \rangle = 0 \tag{2.7}$$

$$\langle \xi_\alpha(\mathbf{r}, t) \xi_\beta(\mathbf{r}', t') \rangle = \frac{1}{\Omega} \sigma_{\alpha\beta}[\phi(\mathbf{r}, t)] \delta(t - t') \delta(\mathbf{r} - \mathbf{r}'), \quad \alpha, \beta \in [1, d]. \tag{2.8}$$

The variance $\hat{\sigma}[\phi(\mathbf{r}, t)]$ is the *mobility* matrix and it is coupled to the deterministic part of the current (2.6) via a fluctuation-dissipation theorem [100] which guarantees the correct equilibrium state in the absence of driving [109, 110]. This structure of this noise term defines the evolution of the system as a Markov process. Moreover, $\Omega \equiv L^{-d}$ is a (large) parameter controlling the strength of the noise that arise because of the law of large numbers when rescaling space and time keeping x^2/t fixed in the coarse-graining procedure [113]. In the limit $\Omega \to \infty$ the amplitude of the noise vanish, which corresponds to the macroscopic hydrodynamic description of the system (2.3)-(2.4). Interestingly, it is possible to see the effect of strong intrinsic fluctuations by tuning this parameter, which can be useful when studying nanosize systems with an unclear scale separation between microscopic and macroscopic descriptions. In our case, we are interested in large but finite values of Ω (i.e. *weak noise description*).

Therefore, the field ϕ now obeys a stochastic differential equation of the form:

$$\partial_t \phi(\mathbf{r}, t) + \boldsymbol{\nabla} \cdot (\mathbf{j_D}(\mathbf{r}, t) + \boldsymbol{\xi}(\mathbf{r}, t)) = 0, \tag{2.9}$$

which, together with constitutive equation (2.4) and boundary conditions (2.5), describes the evolution of the system at a mesoscopic level.

Equation (2.9) is a non-linear *Langevin equation*, i.e. a stochastic differential equation describing the evolution of the stochastic field ϕ. In general, the main interest of this equation is not to compute the evolution of the fluctuating field for one realization of the noise, but to obtain the probability distribution at all times characterizing the stochastic process ϕ [116]. However, this problem remains challenging in most cases. One way to proceed now, commonly used in fluctuating hydrodynamics, consist in linearizing the Langevin equation (2.9) around the steady macroscopic fields and solving the resulting linear deterministic equation to obtain the form of the fluctuations [110, 117]. This procedure allows to compute the lower-order correlators of the mesoscopic fields, information about large fluctuations and higher-order correlators is lost as a consequences of the linearization. Taking into account non-linear corrections (within the framework of non-linear fluctuating hydrodynamics) can help in understanding the long-time tail behavior of lowest-order correlation functions (the reader could find interesting examples in [118–123]). Nevertheless, it has been long recognized that in order to explore arbitrary fluctuations an alternative scheme is needed, one based on the computation of the full stationary probability distribution for the observable of interest. This can be achieved using Macroscopic Fluctuation Theory (MFT) [16], which offers a variational formula for this probability distribution. From a mathematical point of view, the starting point for building the MFT is the path integral representation of the system at hand. Hence, we firstly present in Section 2.3 two formalism which describes the evolution of the system at a mesoscopic level: the Fokker-Planck equation and the path integral representation.

2.2.1 An interesting example: driven diffusive systems.

Before proceeding with the alternative mesoscopic formulations, with the aim of illustrating the previous scheme, we show here a paradigmatic example of driven systems with one conserved field which will be used along this Thesis: the driven diffusive systems [124, 125]. This broad class of systems describes a wide range of physical situations as, for instance, population dynamics, molecular diffusion, semiconductor dopping processes or thermal conduction. Furthermore, from the perspective of fluctuations, driven diffusive systems result of special relevance as they are the objects of study used by Bertini et al. [16] to develop the Macroscopic Fluctuation Theory. Although this theory has been recently generalized to others classes of system (see [112]), they are still the central elements of numerous and interesting works in the world of large deviations [16–18, 38, 40, 41, 52–56, 63, 114,

126, 127].

Mathematically, driven diffusive systems are described (at the mesoscopic level) by the set of equations (2.4)-(2.9), where the local current $\mathbf{J_E}[\phi]$ is split into two terms: one diffusive term given by Fick's (or equivalently Fourier's) law and a second term governed by the external drift $\mathbf{E}$ (Ohm's law-like term). Therefore,

$$\mathbf{J_E}[\phi] = \hat{D}[\phi]\boldsymbol{\nabla}\phi(\mathbf{r},t) + \hat{\sigma}[\phi]\mathbf{E}(\mathbf{r},t)\,, \qquad (2.10)$$

where $\hat{D}[\phi]$ is the *diffusivity* matrix and $\hat{\sigma}[\phi]$ is the mobility matrix appearing in (2.8). Both $\hat{D}$ and $\hat{\sigma}$ are known as *transport coefficients* and, as we previously mentioned, they are not independent: in order to reproduce equilibrium states in absence of any drift, both are coupled via the local Einstein relation:

$$f_0''[\phi]\hat{D}[\phi] = \hat{\sigma}[\phi]\,, \qquad (2.11)$$

with $f_0[\phi]$ the equilibrium free energy density (i.e. equilibrium free energy per unit of volume) and $''$ denoting second derivative with respect to its argument. Therefore, the evolution of the system is fully characterized by these two transport coefficients, which can be measured in experiments or simulations.

Finally, to complete the description of the system at hand one needs to specify the form of boundary conditions (2.5). Interestingly, boundary structure will be an essential element to determine whether our system is in or out of equilibrium. Indeed, we can establish that our system will reach an equilibrium state (after a transient govern by (2.4)-(2.9)) if one of the following statements is satisfied:

1. The Λ-space is the torus and there is no external field $\mathbf{E}(\mathbf{r},t) = 0$.

2. The chemical potential of the boundaries is time-independent and homogeneous and there is no external field $\mathbf{E}(\mathbf{r},t) = 0$. In terms of the field ϕ, these boundary conditions read $\bar{\phi}(\mathbf{r},t) = \bar{\phi}_{bc}$, $\forall \mathbf{r} \in \partial\Lambda$, with $\bar{\phi}_{bc}$ a given constant.

3. Boundary conditions are non-homogeneous and time-independent in such a way that the induced boundary-gradient counteracts the external drift $\mathbf{E}(\mathbf{r})$.

In any other case, the system will be out of equilibrium.

2.3 Fokker-Planck equation and path integral representation associated to a Langevin equation

As we explained in the previous section, the Langevin equation (2.9) describes the evolution of the stochastic field $\phi(\mathbf{r},t)$. Notwithstanding, there exist other

two formulations characterizing how the system evolves in time at a mesoscopic level of description, namely the Fokker-Planck equation and the path integral representation. It is important to note that the three formulations are mathematically equivalent, containing the same "physical information" when describing the system behaviour.

In order to deduce both alternative formulations, one needs to obtain a discrete version of the Langevin equation. This automatically leads to the well-known "Itô-Stratonovich" dilemma [128]. Let us divide the time-domain in N intervals of duration $\Delta t = \varepsilon$, in such a way that $t_i = t_0 + i\varepsilon$, with $t_N = t_f$. Loosely speaking, the origin of a such a problematic resides in the following question: which value $\tilde{\phi}$ of the field ϕ should one choose to evaluate $\mathbf{J_E}[\phi]$ and $\hat{\sigma}[\phi]$ in a time-interval $[t_i, t_{i+1}]$? The answer to this question reveals that there exists an infinity family of possible discretization corresponding to the same original continuum Langevin equation in the limit $\varepsilon \to 0$. Parameterizing this family by $\eta \in [0, 1]$, we can write the time-discrete version of the Langevin equation as[2]:

$$\frac{1}{\varepsilon}(\phi(\mathbf{r}, t_{i+1}) - \phi(\mathbf{r}, t_i)) + \boldsymbol{\nabla} \cdot \left(\mathbf{J_E}[\tilde{\phi}(\mathbf{r}, t_i)] + \boldsymbol{\zeta}(\mathbf{r}, t_i) \right) = 0 \,, \qquad (2.12)$$

with $\tilde{\phi}(\mathbf{r}, t_i) = \eta\phi(\mathbf{r}, t_i) + (1 - \eta)\phi(\mathbf{r}, t_{i+1})$ and:

$$\boldsymbol{\zeta}(\mathbf{r}, t_i) = \int_{t_i}^{t_{i+1}} \boldsymbol{\xi}(\mathbf{r}, t) \, dt \,. \qquad (2.13)$$

The election of the η-value fix the discretization scheme: $\eta = 1$ corresponds to Itô-discretization [129], while $\eta = 1/2$ corresponds to Stratonovich-discretization [130]. Remarkably, techniques used to compute integrals or derivative in ordinary calculus could change depending on the discretization we use. For instance, while the usual chain rule of calculus holds when using Stratonovich-discretization, it is not valid for Itô-discretization, where one needs to define new transformation laws (Itô's Lemma) [128]. Finally, while different discretization leads to different Fokker-Planck equations and path integral measures (a fact of crucial relevance when describing the evolution of a microscopic system in the mesoscopic limit [128]), it is important to note that the averaged values of physical observables are the same whichever the discretization scheme we have chosen to solve the problem.

In the following lines we will present both Fokker-Planck and path integral representations associated to Langevin equation (2.9). We refer the reader to [112, 128, 131] for a formal derivation of such formulations.

---

[2]From now on, we are going to consider the external field to be time-independent, that is $\mathbf{E}(\mathbf{r}, t) = \mathbf{E}(\mathbf{r})$.

2.3.1 The Fokker-Planck equation

Since the field $\phi(\mathbf{r}, t)$ characterizing system behaviour is a stochastic variable, one could describe its evolution by determining the probability of observing a given configuration ϕ at a fixed time t, $P[\phi; t]$. As it was previously mentioned, finding this probability directly from the Langevin equation, far away from being trivial, is an arduous task which requires to solve the stochastic equation. However, there is another way to proceed: we can write a partial differential equation describing the evolution in time of the probability $P[\phi; t]$. This partial differential equation is called *Fokker-Planck equation*.

The probability $P[\phi; t]$ can be written as:

$$P[\phi; t] = \left\langle \prod_{\mathbf{r} \in \Lambda} \delta \left[\phi(\mathbf{r}, t) - \tilde{\phi}(\mathbf{r}, t) \right] \right\rangle_{\boldsymbol{\xi}}, \tag{2.14}$$

where $\tilde{\phi}(\mathbf{r}, t)$ is the solution of the Langevin equation for a given realization of the noise, and $\langle \cdot \rangle_{\boldsymbol{\xi}}$ represents the average over the noise. The main idea behind the derivation of Fokker-Planck equation is to expressed the probability $P[\phi; t_{i+1}]$ in terms of $P[\phi; t_i]$ by using a discrete version of the Langevin equation. This fact leads to an unavoidable previously announced conclusion: the structure of the Fokker-Plank equation will depend on the chosen discretization scheme. In this way, the Fokker-Planck equation associated to the Langevin equation (2.9) is[3]:

$$
\begin{aligned}
\partial_t P[\phi; t] \quad = \quad & \int_\Lambda d\mathbf{r} \sum_{\alpha=1}^{d} \left(\partial_\alpha \frac{\delta}{\delta\phi(\mathbf{r}, t)} \right) \left[- j_{D,\alpha} P[\phi; t] \right. \\
+ \quad & \frac{1}{2\Omega} \sum_{\beta=1}^{d} \left(\partial_\beta \frac{\delta}{\delta\phi(\mathbf{r}, t)} \right) (\sigma_{\alpha\beta}[\phi] P[\phi; t]) \\
- \quad & \frac{(1-\eta)}{2\Omega} \sum_{\beta=1}^{d} \left(\left(\partial_\beta \frac{\delta}{\delta\phi(\mathbf{r}, t)} \right) \sigma_{\alpha\beta}[\phi] \right) P[\phi; t] \right], \tag{2.15}
\end{aligned}
$$

where ∂_α accounts for derivatives with respect to x_α, $\mathbf{j}_D = (j_{D,1}, ..., j_{D,d})$ and:

$$\left(\partial_\beta \frac{\delta}{\delta\phi(\mathbf{r}, t)} \right) A[\phi] = \partial_\alpha \left(\frac{\delta}{\delta\phi(\mathbf{r}, t)} A[\phi] \right) - \frac{\delta}{\delta\phi(\mathbf{r}, t)} (\partial_\alpha A[\phi]). \tag{2.16}$$

---

[3]We encourage the reader to take a look at the new work of Garrido [112] for a detailed description of this derivation.

2.3.2 Path integral representation

Works by Wiener and Feynman [132–134] showed that any stochastic process can be described in terms of path integrals. Roughly speaking, the probability of having a given configuration $\phi(\mathbf{r}, t^*) = \phi^*(\mathbf{r})$ at a time t^* can be written as an infinite sum of all possible trajectories (i.e. sequence of configurations) compatible with the system constraints, correspondingly weighted, which, starting from an initial configuration, lead to the final one $\phi^*(\mathbf{r})$. The weight of each path, i.e. the probability of occurring a given trajectory starting from an initial state to a final configuration at time t, will be the basic and fundamental object in our description. This formulation has turned out to be a crucial framework not only in statistical physics but also in quantum physics, constituting the basis of Quantum Field Theory. Path integral representation indeed provides an unified mathematical scheme for both Quantum and Statistical Field Theory.

At this point, one should note an essential fact: the knowledge of a trajectory $\phi(\mathbf{r}, t)$, with $t \in [t_0, t_f]$ corresponding to a particular noise realization does not define univocally the trajectory of the local current $\mathbf{j}(\mathbf{r}, t)$ for dimension $d > 1$. Indeed, both fields are related via continuity equation (2.9), and any current field of the form $\mathbf{j}'(\mathbf{r}, t) = \mathbf{j}(\mathbf{r}, t) + \mathbf{u}(\mathbf{r}, t)$ with $\mathbf{u}(\mathbf{r}, t)$ a divergence-free vector ($\boldsymbol{\nabla} \cdot \mathbf{u}(\mathbf{r}, t) = 0$) will satisfy the same equation. This is a direct consequence of the lost of information taking place when going from the microscopic to the mesoscopic description through the coarse-grained procedure. The strong implications of this result will be illustrated along this Thesis (see, for instance, Chapter 5). Thus, when studying systems characterized by a locally conserved dynamics, it seems more interesting to ask for the probability of observing a given trajectory $\{\phi(\mathbf{r}, t), \mathbf{j}(\mathbf{r}, t)\}$, which takes the form[4]:

$$\mathbb{P}_\Omega(\{\phi, \mathbf{j}\}_{t_0}^{t_f}) \propto \exp\left[-\Omega \mathcal{S}_{[t_0, t_f]}[\phi, \mathbf{j}] + \mathcal{O}(\Omega^0)\right] \prod_{t \in [t_0, t_1]} \prod_{\mathbf{r} \in \lambda} \delta\left(\partial_t \phi + \boldsymbol{\nabla} \cdot \mathbf{j}\right),$$

(2.17)

where $\delta[\cdot]$ is the Dirac delta function accounting for constraint imposed by continuity equation (2.9) and:

$$\mathcal{S}_{[t_0, t_f]}[\phi, \mathbf{j}] = \frac{1}{2} \int_0^\tau dt \int_\Lambda d\mathbf{r}(\mathbf{j} - \mathbf{J_E}[\phi]) \cdot \hat{\sigma}^{-1}[\phi](\mathbf{j} - \mathbf{J_E}[\phi]), \qquad (2.18)$$

is the *action* of the system. It is important to note that by P we represent the probability of a given configuration, whereas $\mathbb{P}$ accounts for the probability of a

---

[4]For the sake of simplicity, we omit to write explicitly the spatial and time dependence of $\phi(\mathbf{r}, t)$ and $\mathbf{j}(\mathbf{r}, t)$

whole trajectory. Trivially, any trajectory $\{\phi, \mathbf{j}\}$ whose fields are not coupled via continuity equation contributes with zero probability. To obtain such an expression for $\mathbb{P}(\{\phi, \mathbf{j}\}_{t_0}^{t_f})$, we have to integrate over all possible realizations of the noise, taking into account that it is coupled to fields ϕ and $\mathbf{j}$ via Eq. (2.9). We refer the reader to [112, 128, 131, 135–137] for a complete derivation.

2.4 Macroscopic Fluctuation Theory

Once the different formulations to describe the evolution of a system at a mesoscopic level are defined, we are now in position to study macroscopic fluctuations. Our starting point will be the path integral representation given by (2.17)-(2.18). As we are interested in the large, but finite, Ω limit we can write[5]:

$$\mathbb{P}(\{\phi, \mathbf{j}\}_{t_0}^{t_f}) \asymp \exp\left[-\Omega \mathcal{S}_{[t_0, t_f]}[\phi, \mathbf{j}] \right], \qquad (2.19)$$

where $\asymp$ stands for "asymptotic logarithmic equivalence" in the sense:

$$\mathcal{S}_{[t_0, t_f]}[\phi, \mathbf{j}] = \lim_{L \to 0} L^d \ln \mathbb{P}(\{\phi, \mathbf{j}\}_0^\tau), \qquad (2.20)$$

and where ϕ and $\mathbf{j}$ are coupled via continuity equation:

$$\partial_t \phi + \boldsymbol{\nabla} \cdot \mathbf{j} = 0. \qquad (2.21)$$

Interestingly, since $\hat{\sigma}$ is a positive defined matrix, the action $\mathcal{S} \geq 0$, where the equality corresponds to the classical trajectory solution of the macroscopic equation (2.3). Eqs. (2.18)-(2.19) and the associated definitions constitute the fundamental formula of Macroscopic Fluctuation Theory [16], from which many important and general results can be derived, valid arbitrarily far from equilibrium.

With this ideas in mind, we proceed with the study of fluctuations of relevant macroscopic quantities. In particular, we will focus on large deviations of the conserved field ϕ and time-integrated additive observables.

2.4.1 Fluctuations of the conserved field $\phi(\mathbf{r}, t)$

As we have seen, the field ϕ characterize the properties of the system at hand, so studying fluctuations of ϕ will provide relevant information about its behaviour. In particular, we will be interested in analysing fluctuations of the conserved field

---

[5]As we have seen in Introduction, this is a manifestation of the large deviation principle. We will delve into the features and consequences of Large Deviation Theory in Section 2.4.2

ϕ at the final time of its evolution t_f, i.e. $\phi_f(\mathbf{r}) = \phi(\mathbf{r}, t_f)$. In other words, we will study large deviations of the final configuration $\phi_f(\mathbf{r})$. As we will see in the following lines, this study is of capital relevance, leading to the construction of the *quasi-potential*.

The probability of observing a final configuration $\phi_f(\mathbf{r})$ can be written as the sum over all possible trajectories $\{\phi(\mathbf{r}, t), \mathbf{j}(\mathbf{r}, t)\}_{t_0}^{t_f}$, correspondingly weighted with (2.19), compatible with $\phi(\mathbf{r}, t_f) = \phi_f(\mathbf{r})$ and continuity equation (2.21), that is:

$$P_{[t_0, t_f]}\left(\phi(\mathbf{r}, t_f) = \phi_f(\mathbf{r})\right) = \int \mathcal{D}\phi \int \mathcal{D}\mathbf{j}\, \mathbb{P}(\{\phi, \mathbf{j}\}_{t_0}^{t_f}) \prod_{\mathbf{r} \in \Lambda} \delta\left(\phi(\mathbf{r}, t_f) = \phi_f(\mathbf{r})\right)$$
$$\prod_{t \in [t_0, t_f]} \prod_{\mathbf{r} \in \Lambda} \delta\left(\partial_t \phi + \boldsymbol{\nabla} \cdot \mathbf{j}\right), \tag{2.22}$$

where again $\delta[\cdot]$ are Dirac delta functions accounting for the different constraints. Nevertheless, since we are interested only in the final structure of the field ϕ, it would be desirable not to deal with the pair of fields $\{\phi, \mathbf{j}\}$ but focus only on the probability of observing a given path $\{\phi\}_{t_0}^{t_f}$, that is $\mathbb{P}(\{\phi\}_{t_0}^{t_f})$. In the following lines, we briefly describe two different procedures to obtain such a probability distribution. For the first one [16], one can see that:

$$\mathbb{P}(\{\phi\}_{t_0}^{t_f}) = \int \mathcal{D}\mathbf{j}\, \mathbb{P}(\{\phi, \mathbf{j}\}_{t_0}^{t_f}) \prod_{t \in [t_0, t_f]} \prod_{\mathbf{r} \in \Lambda} \delta\left(\partial_t \phi + \boldsymbol{\nabla} \cdot \mathbf{j}\right) \tag{2.23}$$

Since we are interested in the large Ω limit, we can make use of the *steepest descent* or *saddle-point method* to crack this problem. Indeed, we can write:

$$\mathbb{P}(\{\phi\}_{t_0}^{t_f}) \asymp \exp\left[-\Omega \mathfrak{S}_{[t_0, t_f]}[\phi]\right], \tag{2.24}$$

with:

$$\mathfrak{S}_{[t_0, t_f]}[\phi] = \inf_{\substack{\{\mathbf{j}\} \\ \partial_t \phi + \nabla \cdot \mathbf{j} = 0}} \mathcal{S}[\phi, \mathbf{j}]. \tag{2.25}$$

The current field $\mathbf{j}$ solution of the previous variational problem is the *optimal* or *most probable* path. In Section 2.4.2, we will study in depth the meaning and relevance of such optimal trajectories. On the other hand, the second procedure [112] consists in deriving a path integral formulation for $\mathbb{P}(\{\phi\}_{t_0}^{t_f})$ directly from the Langevin equation (2.9). In this way, we can reformulate (2.9) as:

$$\partial_t \phi(\mathbf{r}, t) + \boldsymbol{\nabla} \cdot \mathbf{J_E}[\phi(\mathbf{r}, t)] + \nu(\mathbf{r}, t) = 0, \tag{2.26}$$

where $\nu(\mathbf{r}, t) = \boldsymbol{\nabla} \cdot \boldsymbol{\xi}(\mathbf{r}, t)$ is a new gaussian white noise, obtaining by the sum of d gaussian random variables, with:

$$\langle \nu(\mathbf{r}, t) \rangle = 0 \tag{2.27}$$

$$\langle \nu(\mathbf{r}, t)\nu(\mathbf{r}', t') \rangle = \frac{1}{\Omega} \sum_{\alpha=1}^{d} \sum_{\beta=1}^{d} \partial_\alpha \partial_\beta' \left(\sigma_{\alpha\beta} \delta(\mathbf{r} - \mathbf{r}') \right) \delta(t - t'), \tag{2.28}$$

with ∂_β' denoting the derivative with respect to x_β'. Once again (see Section 2.3.2), integrating over all possible realization of the noise compatible with (2.26), we obtain that, in the large Ω limit, $\mathbb{P}(\{\phi\}_{t_0}^{t_f})$ obeys (2.24).

Whichever the mechanism we choose, one can prove that the action takes the form:

$$\mathfrak{S}_{[t_0, t_f]}[\phi] = \frac{1}{2} \int_0^\tau dt \int_\Lambda d\mathbf{r} \int_\Lambda d\mathbf{r}' \left(\partial_t \phi + \boldsymbol{\nabla} \cdot \mathbf{J_E}[\phi] \right) M^{-1} \left(\partial_t \phi + \boldsymbol{\nabla}' \cdot \mathbf{J_E}[\phi] \right), \tag{2.29}$$

where $\boldsymbol{\nabla}'$ stands for derivatives with respect to $\mathbf{r}'$ and:

$$M = \sum_{\alpha=1}^{d} \sum_{\beta=1}^{d} \partial_\alpha \partial_\beta' \left(\sigma_{\alpha\beta} \delta(\mathbf{r} - \mathbf{r}') \right). \tag{2.30}$$

Finally, the probability of observing a given configuration ϕ_f at time t_f is:

$$P_{[t_0, t_f]}(\phi(\mathbf{r}, t_f) = \phi_f(\mathbf{r})) = \int \mathcal{D}\phi \mathbb{P}(\{\phi\}_{t_0}^{t_f}) \prod_{\mathbf{r} \in \Lambda} \delta \left(\phi(\mathbf{r}, t_f) - \phi_f(\mathbf{r}) \right), \tag{2.31}$$

which in the large Ω limit, using again the steepest descent method, can be written as:

$$P_{[t_0, t_f]}(\phi(\mathbf{r}, t_f) = \phi_f(\mathbf{r})) \asymp \exp \left[\Omega \mathcal{I}_{[t_0, t_f]}[\phi_f] \right], \tag{2.32}$$

where

$$\mathcal{I}_{[t_0, t_f]}[\phi_f] = \inf_{\{\phi\}} \mathfrak{S}_{[t_0, t_f]}[\phi], \tag{2.33}$$

with the constraint $\phi(\mathbf{r}, t_f) = \phi_f(\mathbf{r})$. Therefore, the problem of studying fluctuations of the final profile ϕ_f becomes a variational problem.

Once the methodology to obtain the probability distribution of the final configuration ϕ_f has been presented, we proceed to explain why it is important to characterize such fluctuations by introducing an essential element in nonequilibrium situations. Let us assume that our system reaches, after an appropriated transient, a steady state characterized by a time-independent probability distribution

$P_{st}[\phi]$, called *stationary probability distribution*, solution of Fokker-Planck equation (2.15). For large Ω-values, this probability could be written as:

$$P_{st}[\phi] \asymp \exp\left[-\Omega V_0[\phi] + \mathcal{O}((\Omega)^0)\right], \tag{2.34}$$

where $V_0[\phi]$ is known as *quasi-potential* [26]. Remarkably, $V_0[\phi] \geq 0$ and the minimum corresponds to the stationary solution of the macroscopic equation (2.3), namely $\phi_{st}(\mathbf{r})$. Therefore:

$$V_0[\phi_{st}] = 0, \quad \left.\frac{\delta V_0[\phi]}{\delta \phi}\right|_{\phi=\phi_{st}} = 0. \tag{2.35}$$

Trivially, in the macroscopic limit $\Omega \to \infty$, the stationary probability distribution becomes a Dirac delta function of the form:

$$P_{st}[\phi] = \prod_{\mathbf{r}\in\Lambda} \delta\left(\phi(\mathbf{r}) - \phi_{st}(\mathbf{r})\right). \tag{2.36}$$

As we can see, $P_{st}[\phi]$ provides information about the probability of observing a given configuration (not a trajectory) $\phi(\mathbf{r})$. Let us a consider, for instance, a driven diffusive system at equilibrium where the particle density conserves locally (that is, the relevant field characterizing the system is the density $\rho(\mathbf{r}, t)$). The evolution of such a system is given by (2.10). It can be proved [16, 17] that the quasi-potential is of the form:

$$V_0[\phi] = \int_\Lambda d\mathbf{r}\left(f[\rho] - f[\rho_{st}] - f'[\rho_{st}](\rho - \rho_{st})\right), \tag{2.37}$$

where $f'[\rho_{st}] = \mu$ is the chemical potential. If the system at hand is homogeneous (i.e. homogeneous boundary conditions and no external drift), the stationary probability distribution is indeed given by Boltzmann-Einstein formula (2.1)-(2.2). Consequently, the quasi-potential corresponds to the minimum reversible work necessary to observe a given fluctuation ρ plus the energy contribution due to the exchange of particles with the external reservoir. From a thermodynamical point of view, the integrand in (2.37) is nothing more that the variation of the grand potential per unit of volume, characteristic function of the grand canonical ensemble. Hence, the quasi-potential could be considered as a good candidate for being the nonequilibrium extension of the available energy, representing the connection between the microscopic (probability of a fluctuations) and the macroscopic (thermodynamical quantities) levels.

Characterizing the structure of the quasi-potential out of equilibrium is usually a really hard task. Indeed, $V_0[\phi]$ will present in general a non-local behaviour reflecting the existence of long-range spatial correlations typical of nonequilibrium systems. One way to proceed is introducing the expression of the stationary probability (2.34) in the Fokker-Planck equation (2.15), obtaining a Hamilton-Jacobi equation for the quasi-potential. However, we show here another mechanism to compute $V_0[\phi]$ by studying fluctuations of the final configuration ϕ. The probability of observing a given configuration $\tilde{\phi}(\mathbf{r})$ at time $t_f = 0$ assuming that the state of the system at $t_0 = -\infty$ was the macroscopic stationary one can be written as:

$$P_{[-\infty,0]}(\phi(\mathbf{r},0) = \tilde{\phi}(\mathbf{r})|\phi(\mathbf{r},-\infty) = \phi_{\text{st}}(\mathbf{r})) = P_{\text{st}}(\phi_{\text{st}})P_{[-\infty,0]}(\phi(\mathbf{r},0) = \tilde{\phi}(\mathbf{r})),$$
(2.38)

where $P_{\text{st}}(\phi_{st})$ and $P_{[-\infty,0]}(\phi(\mathbf{r},0) = \tilde{\phi}(\mathbf{r}))$ are given by (2.34) and (2.31), respectively. Since we look for a stationary probability of a configuration, its asymptotic large Ω limit is also given by (2.34). Consequently:

$$V_0[\tilde{\phi}] = \mathcal{I}_{[-\infty,0]}[\tilde{\phi}]\,,$$
(2.39)

where the right-hand side of the equality defines a variational problem with constraint $\phi(\mathbf{r},-\infty) = \phi_{\text{st}}$ and $\phi(\mathbf{r},0) = \tilde{\phi}(\mathbf{r})$. Thus, the form of the quasi-potential is fully determined by studying fluctuations of the configuration $\tilde{\phi}$ at time $t = 0$ of a system which was, at $t = -\infty$, in the macroscopic stationary state.

To conclude with this section, we present an alternative way to reproduce Eq. (2.39). This method was developed by Bertini et al. [16] and it is based on the definition of the *dual* or *adjoint* dynamics. In 1953, Onsager and Machlup [104] proved that, in equilibrium, the path followed by the system to create a fluctuation starting from an stationary state is the time reversal of the relaxation path both along the same dynamic. However, we do not expected that both path could follow the same dynamic out of equilibrium as a consequence of dissipation. Let us define the time reversal operator θ as $\theta\phi(\mathbf{r},t) = \phi(\mathbf{r},-t)$, $\theta\mathbf{j}(\mathbf{r},t) = -\mathbf{j}(\mathbf{r},-t)$. The probability of observing a particular trajectory $\{\phi\}_{t_0}^{t_f}$ from a fixed initial state $\phi(\mathbf{r},t_0) = \phi_{t_0}(\mathbf{r})$ distributed as $P_{\text{st}}[\phi_{t_0}]$ is naturally given by:

$$\mathbb{P}(\{\phi\}_{t_0}^{t_f}|\phi(\mathbf{r},t_0) = \phi_{t_0}(\mathbf{r})) = P_s t[\phi_{t_0}]\mathbb{P}(\{\phi\}_{t_0}^{\tau})\,,$$
(2.40)

In this way, the adjoint dynamics is defined as the one to which one can associate a new trajectory weight P^* satisfying

$$P\left(\{\phi\}_{t_0}^{t_f}|\phi(\mathbf{r},t_0) = \phi_{t_0}(\mathbf{r})\right) = P^*\left(\{\theta\phi\}_{-t_f}^{-t_0}|\theta\phi(\mathbf{r},-t_f) = \phi(\mathbf{r},t_f)\right)\,.$$
(2.41)

29

This relation can be interpreted as a generalization of detailed balance condition: the probability of evolving from an initial state to another fluctuating state under the original dynamics is the same that the probability of evolving from that state to the initial one under the adjoint dynamics. Consequently, in the asymptotic large Ω limit:

$$V[\phi_{t_0}] + \mathfrak{S}_{[t_0,t_f]}[\phi] = V[\phi_{t_f}] + \mathfrak{S}^*_{[-t_f,-t_0]}[\theta\phi] \,, \qquad (2.42)$$

where $\mathfrak{S}^*$ is the action associated to the adjoint dynamic and we have written $\phi(\mathbf{r}, t_f) = \phi_{t_f}(\mathbf{r})$ for simplicity. In this way, assuming that the adjoint dynamics admits a mesoscopic description of the form (2.9), it can be proved [16, 112] that the deterministic part of Langevin equation governing the adjoint dynamic corresponds to the time reversed equations for the optimal paths evolving from ϕ_{st} to an arbitrary state $\phi(\mathbf{r})$ in the original dynamics. If we now consider again the problem of studying fluctuations of the final configuration $\tilde{\phi}$ by fixing $t_0 = -\infty$, $t_f = 0$, $\phi_{-\infty} = \phi_{\mathrm{st}}$ and $\phi_0 = \tilde{\phi}$, we can then integrated both sides of (2.41) over all possible trajectories obtaining:

$$V[\phi_{\mathrm{st}}] + \mathcal{I}_{[-\infty,0]}[\tilde{\phi}] = V[\tilde{\phi}] + \mathcal{I}^*_{[0,\infty]}[\phi_{\mathrm{st}}] \,. \qquad (2.43)$$

Following (2.35), $V[\phi_{\mathrm{st}}] = 0$. Moreover, $\mathcal{I}^*_{[0,\infty]}[\phi_{\mathrm{st}}] = 0$ since it corresponds to a relaxation in the adjoint dynamics, that is the optimal trajectory associated to I^* is the classical trajectory solving the macroscopic adjoint dynamics. Hence, we recover equation (2.39). This definition of the adjoint dynamic and later analysis lead to a nonequilibrium generalization of the Onsager-Machlup relationship: the optimal path sustaining a given fluctuation starting from the stationary state in the original dynamics is the time reversed of the relaxation path following the adjoint dynamics (see [16, 112]). Furthermore, this construction provides an useful tool to solve the difficult problem of determining the most probable trajectory to a given configuration and the quasi-potential by obtaining the adjoint dynamics and solving a relaxation process to the stationary state (see, for instance [138]).

2.4.2 Fluctuations of space- and time-integrated observables

Besides the conserved field $\phi(\mathbf{r}, t)$, there exists other observables of great relevance in describing system behaviour, e.g. work, entropy production, time-integrated total mass, activity, etc. In particular, space- and time-integrated current plays a prominent role in characterizing nonequilibrium situations [16–18, 40, 41]. Therefore, it becomes a important task to study the statistic of fluctuations of such essential quantities. Here and upon, let us consider $t_0 = 0$ and $t_f = \tau$. We define a

space- and time-integrated observable as:

$$\boldsymbol{a} \equiv \frac{1}{\tau} \int_0^\tau dt \int_\Lambda d\mathbf{r}\, \mathbf{a}[\phi, \mathbf{j}]\,, \tag{2.44}$$

where $\mathbf{a}[\phi, \mathbf{j}]$ could depend on both fields ϕ and $\mathbf{j}$. We are interested in the probability distribution for this observable, namely $P_\tau(\boldsymbol{a})$, in the large scale separation (i.e. large Ω) and τ limits. In these asymptotics, the scaling form of $P_\tau(\boldsymbol{a})$ is described within the framework of the Large Deviation Theory [139–144], which has witnessed a tremendous development in the last decades both in mathematics (within the Donsker–Varadhan approach [20–23], the Gärtner–Ellis theorem [145, 146] and the Freidlin–Wentzell framework [26]) and in statistical physics in the study of many example systems (see for instance [147–152]). Therefore, the asymptotic limit of $P_\tau(\boldsymbol{a})$ is controlled by the large deviation principle, which establishes that the probability of observing a given value $\boldsymbol{a}$ of the space- and time-integrated $\mathbf{a}[\phi, \mathbf{j}]$ scales for large Ω and τ as:

$$P_\tau(\boldsymbol{a}) \asymp \exp\left[-\tau \Omega G[\boldsymbol{a}]\right]. \tag{2.45}$$

The function $G(\boldsymbol{a}) \geq 0$ is the Large Deviation Function (LDF) controlling the statistic of fluctuations of the observable $\boldsymbol{a}_\tau$, an element of crucial relevance in MFT. Indeed, as we have shown in Introduction, the LDF is considered to be a good candidate for acting as a nonequilibrium thermodynamic potential[6]. Defining the averaged value[7] of $\boldsymbol{a}$ as:

$$\boldsymbol{a}^* = \langle \boldsymbol{a} \rangle\,, \tag{2.46}$$

one observe that:

$$G(\boldsymbol{a}^*) = 0\,, \ \ G'(\boldsymbol{a}^*) = 0\,. \tag{2.47}$$

In other words, the LDF has a global minimum in $\boldsymbol{a}^*$, so the large deviation principle shows how the probability of the observable $\boldsymbol{a}$ peaks around the averaged value $\boldsymbol{a}^*$. The LDF is, thus, a measure of the exponential rate at which the likelihood of observing a given value $\boldsymbol{a} \neq \boldsymbol{a}^*$ decays as τ and Ω increases.

Despite of being such a fundamental element, characterizing the structure of the LDF is a highly non-trivial problem. To shed light on this issue, in the following lines we will describe the study of space- and time-integrated observables

---

[6]We refer the reader to works by Ruelle, Ellis and Oono [24, 25, 27–29, 35] where the analogy between large deviation theory and equilibrium statistical mechanics is study in depth, as well as the review by Touchette [19] for a self-contained derivation of such relation and extensions to nonequilibrium situations.

[7]It is also known as stationary, typical or expected value.

fluctuations under the framework of the MFT, which will open the door to a more accessible definition of the large deviation function. In this way, we can write the probability $P_\tau(\boldsymbol{a})$ as the sum over all possible paths, correspondingly weighted, compatible with the constraint (2.44). Thus, considering an arbitrary initial state chosen from the stationary distribution (2.34), the probability density function (pdf) of the integrated observable $\boldsymbol{a}$ takes the form:

$$P_\tau(\boldsymbol{a}) = \int \mathcal{D}\phi \int \mathcal{D}\mathbf{j}\, P_{st}(\phi(\mathbf{r},0))\mathbb{P}(\{\phi,\mathbf{j}\}_0^\tau) \prod_{\mathbf{r}\in\Lambda} \prod_{t\in[0,\tau]} \delta\left(\partial_t\phi + \boldsymbol{\nabla}\cdot\mathbf{j}\right)$$

$$\cdot\ \delta\left(\boldsymbol{a} - \frac{1}{\tau}\int_0^\tau dt \int_\Lambda d\mathbf{r}\,\mathbf{a}[\phi,\mathbf{j}]\right),\qquad (2.48)$$

where the weight of each trajectory $\mathbb{P}(\{\phi,\mathbf{j}\}_0^\tau)$ is given by (2.19). Once again, the Dirac delta ensures that constraint (2.44) is satisfied. We can now just use the Fourier-Laplace representation of the δ-functionals, namely

$$\delta\left(\boldsymbol{a} - \frac{1}{\tau}\int_0^\tau dt \int_\Lambda d\mathbf{r}\,\mathbf{a}[\phi,\mathbf{j}]\right) = \int d\boldsymbol{\lambda}\, e^{-\Omega\tau\boldsymbol{\lambda}\cdot(\boldsymbol{a}-\frac{1}{\tau}\int_0^\tau dt \int_\Lambda d\mathbf{r}\,\mathbf{a}[\phi,\mathbf{j}])},\quad (2.49)$$

$$\delta\left(\partial_t\phi + \boldsymbol{\nabla}\cdot\mathbf{j}\right) = \int \mathcal{D}\psi\, e^{-\Omega\int_0^\tau dt \int_\Lambda d\mathbf{r}\,\psi(\mathbf{r},t)(\partial_t\phi+\boldsymbol{\nabla}\cdot\mathbf{j})},\quad (2.50)$$

where the function $\psi(\mathbf{r},t)$ depends on the space- and time-coordinates and its boundary conditions are defined by problem geometry. Consequently, the probability $P_\tau(\boldsymbol{a})$ reads (in the large Ω limit):

$$P_\tau(\boldsymbol{a}) = \frac{1}{\tilde{Z}}\int \mathcal{D}\phi \int \mathcal{D}\mathbf{j} \int d\boldsymbol{\lambda} \int d\psi\, P_{st}(\phi(\mathbf{r},0)) \exp\left[-\tau\Omega\, S_\tau[\phi,\mathbf{j},\boldsymbol{\lambda},\psi]\right]$$

$$(2.51)$$

with $\tilde{Z}$ a normalization constant and where the action takes the form:

$$S_\tau[\phi,\mathbf{j},\boldsymbol{\lambda},\psi] = \frac{\tau^{-1}}{2}\int_0^\tau dt \int_\Lambda d\mathbf{r}\left\{(\mathbf{j}-\mathbf{J}[\phi])\cdot\hat{\sigma}^{-1}(\mathbf{j}-\mathbf{J}[\phi]) + \psi\left(\partial_t\phi+\boldsymbol{\nabla}\cdot\mathbf{j}\right)\right\}$$

$$+\boldsymbol{\lambda}\cdot\left(\boldsymbol{a} - \frac{1}{\tau}\int_0^\tau dt \int_\Lambda d\mathbf{r}\,\mathbf{a}[\phi,\mathbf{j}]\right).\qquad (2.52)$$

Finally, in the large time limit, we can make use of the steepest descent method to obtain:

$$P(\boldsymbol{a}) \asymp \exp-\left[\tau\Omega G[\boldsymbol{a}]\right],\qquad (2.53)$$

which is nothing more that the manifestation of the large deviation principle (2.45), where the LDF is defined by:

$$G[\boldsymbol{a}] = \lim_{\tau\to\infty}\frac{1}{\tau}\left\{\min_{\{\phi,\mathbf{j},\boldsymbol{\lambda},\psi\}} S_\tau[\phi,\mathbf{j},\boldsymbol{\lambda},\psi]\right\}.\qquad (2.54)$$

Therefore, the problem of determining the LDF becomes now a variational problem in which $\boldsymbol{\lambda}$ and $\psi(\mathbf{r}, t)$ act as Lagrange multipliers guaranteeing that constraints (2.9) and (2.44) are satisfied. The set $\{\phi_{\tilde{a}}, \mathbf{j}_{\tilde{a}}, \boldsymbol{\lambda}_{\tilde{a}}, \psi_{\tilde{a}}\}$ minimizing the action are called *optimal* or *most probable paths* and they represent the trajectories followed by the system in mesoscopic phase space to sustain a given large-time fluctuation. The optimal paths are one of the most interesting results derived from MFT: we can obtain not only the probability of observing a fluctuation, but also the sequence of configurations that the system exhibits during its evolution to such an event. Finally, it is important to stress that the concept of optimal path is linked to the low-noise and large time limit: indeed, for instance, if the noise of the system is large enough and we study short time trajectories, there can exist many different and equally likely paths sustaining the same event, and thus, establishing a general theory for not only small but arbitrarily large fluctuations becomes an immeasurable problem.

Let us remark several aspects on the definition of the LDF and the associated variational problem (2.54). Firstly, when going from (2.51) to (2.53) in the large time limit via the saddle-point method, the dependence on the initial probability vanishes at leading order in τ. Indeed, since the initial state is chosen from the stationary probability distribution, the term $P_{st}(\phi_0)$ appears as subdominant orders in the scaling (2.53), providing no contribution to the computation of the LDF. Secondly, variational problem (2.54) needs to be supplemented with appropiated boundary and initial conditions. While boundary conditions are given by (2.5), the issue of initial conditions worths to be explained more in detail. As we have said, we choose the initial condition arbitrarily from the stationary distribution (2.34), which implies that one should minimize over such initial condition to obtain the proper LDF. However, as we will see along this Thesis, in many nonequilibrium situations the dependence on the initial condition will disappear for large times as a consequence of the dissipative behaviour of nonequilibrium dynamics.

The structure of the conditioned probability (2.48) remind to that of the microcanonical ensemble of equilibrium statistical physics. Inspired by that, let us introduce a "canonical version" of our problem by performing a Laplace transform of (2.48). This operation leads to the generating function:

$$\Pi_\tau(\boldsymbol{\lambda}) \equiv \langle e^{-\tau \Omega \boldsymbol{\lambda} \tilde{a}} \rangle_{\tilde{a}} = \int e^{-\tau \Omega \boldsymbol{\lambda} \boldsymbol{a}} P_\tau(\boldsymbol{a}) d\tilde{\boldsymbol{a}} \,. \qquad (2.55)$$

After some straightforward operations, it takes the form (in the large Ω limit):

$$\Pi_\tau(\boldsymbol{\lambda}) = \frac{1}{\tilde{Z}} \int \mathcal{D}\phi \int \mathcal{D}\mathbf{j} \, P_{st}(\phi(\mathbf{r}, 0)) \exp\left[-\tau \Omega \, S_\tau^{\boldsymbol{\lambda}}[\phi, \mathbf{j}, \psi]\right] \qquad (2.56)$$

with:

$$
\begin{aligned}
S_\tau^{\boldsymbol{\lambda}}[\phi, \mathbf{j}, \psi] = \quad & \frac{\tau^{-1}}{2} \int_0^\tau dt \int_\Lambda d\mathbf{r} \left\{ (\mathbf{j} - \mathbf{J}[\phi]) \cdot \hat{\sigma}^{-1} (\mathbf{j} - \mathbf{J}[\phi]) + \psi \left(\partial_t \phi + \boldsymbol{\nabla} \mathbf{j} \right) \right\} \\
& + \frac{1}{\tau} \int_0^\tau dt \int_\Lambda d\mathbf{r} \, \boldsymbol{\lambda} \cdot \mathbf{a}[\phi, \mathbf{j}] \, .
\end{aligned}
\tag{2.57}
$$

The dynamics described by the path weight $e^{-\tau L^d S_\tau^{\boldsymbol{\lambda}}}$ is known as *biased* or *tilted* dynamics. The importance of this biased description lies in the fact that, after reweighting the trajectories, rare events in the original dynamics becomes typical in the tilted one. This property is the basis of many techniques to measure the statistic of fluctuations in simulations, e.g. the cloning algorithm [153–155] or transition path samplings [156–158]. Nevertheless, the tilted dynamics described above does not preserve probability, an undesirable property in order to describe a physical systems. Recent works have shown that it is possible to define a new probability-conserved *effective* dynamics asymptotically equivalent to the biased one at large times whose typical events corresponds to the rare ones in the original dynamics [74–77]. These ideas will be study in depth in Chapter 7 in the case of a particle under the action of a periodic force in the weak-noise limit.

Coming back to generating function, in the large time limit, we can apply the steepest-descent method to write (2.55) as:

$$
\Pi_\tau(\boldsymbol{\lambda}) \asymp \exp\left[-\tau \Omega \mu(\boldsymbol{\lambda}) \right],
\tag{2.58}
$$

where:

$$
\mu(\boldsymbol{\lambda}) = \lim_{\tau \to \infty} \left\{ \frac{1}{\tau} \min_{\{\phi, \mathbf{j}, \psi\}} S_\tau^{\boldsymbol{\lambda}}[\phi, \mathbf{j}, \psi] \right\}
\tag{2.59}
$$

is the scaled Cumulant Generating Function (sCGF). This function can be seen as the conjugate "potential" to $G[\boldsymbol{a}]$, a similar relation to the free energy being the Legendre transform of the entropy in equilibrium thermodynamics. Indeed, the Gärtner-Ellis theorem [19, 24, 37] establishes that LDF and sCGF are related via the Legendre-Fenchel transform:

$$
\mu(\boldsymbol{\lambda}) = \sup_{\boldsymbol{a}} \left\{ G(\boldsymbol{a}) - \tau \Omega \boldsymbol{\lambda} \cdot \boldsymbol{a} \right\} .
\tag{2.60}
$$

Consequently, the sCGF works as a *dynamical free energy* (dFE) fully characterizing the probability distribution of $\boldsymbol{a}$. Furthermore, the vector $\boldsymbol{\lambda}$ is conjugated to integrated observable $\boldsymbol{a}$, in again a similar way to the relation between temperature and energy in equilibrium (see Eq. (29) and (31) Introduction). Under the

appropriated convexity conditions (which in our situation consist in $G(\boldsymbol{a})$ being a concave function of $\boldsymbol{a}$) we can invert (2.60) obtaining:

$$G(\boldsymbol{a}) = \inf_{\boldsymbol{\lambda}} \left\{ \mu(\boldsymbol{\lambda}) - \tau\Omega\boldsymbol{\lambda} \cdot \boldsymbol{a} \right\} . \qquad (2.61)$$

Hence, these two Legendre-Fenchel transformations describe the change of "ensemble" between microcanonical (fixed $\boldsymbol{a}$) and canonical (fixed $\boldsymbol{\lambda}$) descriptions. Furthermore, this correspondence can be extended at the level of trajectories: under the same convexity hypothesis, both trajectories conditioned to exhibit a given value $\boldsymbol{a}$ of the integrated observable and biased trajectories weighted by $e^{-\tau\Omega S_\tau^{\boldsymbol{\lambda}}}$ present an asymptotically equivalent distribution in the large time limit. A rigorous description of this equivalence and its consequences was developed by Chétrite and Touchette [74].

Finally, the cumulants of the pdf $P_\tau(\boldsymbol{a})$ can be now obtained from successive derivatives of the SCGF $\mu(\boldsymbol{\lambda})$ evaluated at $\boldsymbol{\lambda} = 0$, that is:

$$\mu_{(n_1 \ldots n_d)}^{(n)} \equiv \left[\frac{\partial^n \mu(\boldsymbol{\lambda})}{\partial \lambda_1^{n_1} \ldots \partial \lambda_d^{n_d}} \right]_{\boldsymbol{\lambda}=0} , \qquad (2.62)$$

with $\sum_{i=1}^d n_i = n$ and λ_i the i-th component of the vector $\boldsymbol{\lambda}$. Furthermore, according to the definition of sCGF, one can show for $n \leq 3$ that $\mu_{(n_1,\ldots,n_d)}^{(n)} = (\tau\Omega)^{n-1} \left\langle \Delta a_1^{n_1} \ldots \Delta a_d^{n_d} \right\rangle$, with $\Delta a_i \equiv a_i - (1 - \delta_{n,1})a_i^*$ and a_i the component of $\boldsymbol{a}$ along the i-direction. Therefore, the cummulants $\mu_{(n_1,\ldots,n_d)}^{(n)}$ are nothing but spatiotemporal integrals of n-point correlators of the observable $\mathbf{a}[\phi, \mathbf{j}]$ (see [18] for the particular case of $\mathbf{a}[\phi, \mathbf{j}] = \mathbf{j}$).

Once we have described the different tools and mechanisms characterizing MFT, we are now in position to proceed with the study of macroscopic fluctuations and rare events which will be developed in this Thesis. However, before going further, in the next section we will present some previous results obtained within the framework the Macroscopic Fluctuation Theory.

2.5 Some interesting results in fluctuations

Fluctuations have always been a target of study of Statistical Mechanics. Many very general results have been obtained to understand the nature and behaviour of fluctuations, as, for instance, the broadly known fluctuation-dissipation theorem [100], which relates the linear response of a system to an external force with the intensity of a spontaneous fluctuation of the system in equilibrium[8]. This interest

---

[8]A particular example of such theorem is the local Einstein relation (2.11)

has strongly increased in the last decades, when an enormous number of works and advances have been developed in the field of macroscopic fluctuations. In this context, the establishment of the MFT and the great progress made in simulating rare events are considered as turning points in the study of fluctuations. With the aim of putting in context and illustrating many of the concepts and outcomes which will appear in following chapters, we will now summarize some of the most relevant breakthroughs obtained in this field.

2.5.1 Gallavotti-Cohen Fluctuation Theorem

Obtaining the probability distribution of fluctuations far from equilibrium is an ambitious task hard to succeed in even in most simple cases. One of the main reasons of this adversity is the major role played by the microscopic dynamics out of equilibrium. However, some properties of such microscopic dynamics could provide clues on the behaviour of fluctuations' distribution. In particular, time-reversibility of laws governing microscopic world leads to extremely relevant results, usually valid far from equilibrium, known as *fluctuation theorems*. One of the first establishments of a fluctuation theorem was made by Evans, Cohen and Morris [50] in their study of fluctuations in shear stress of fluids in far from equilibrium steady states. Other interesting examples[9] in this sense are Bochkov and Kuzovlev relation [160, 161], Jarzynski equality[10] [163, 164], Crooks fluctuation theorem [165], Hatano-Sasa relation [166] or fluctuation theorems for quantum systems as the ones presented in works by Kurchan [167] and Esposito and Mukamel [168]. However, in this Section we will focus on the work developed by Gallavotti and Cohen [44], which formulated a fluctuation theorem for macroscopic (deterministic) nonequilibrium system in steady states. This outcome was proved to be valid also for a stochastic Langevin dynamics of a single particle (Kurchan [48]) and, later, extended to very general Markov processes (Lebowitz and Spohn [49]). In our context, considering fluctuations of the space- and time-integrated current, $\mathbf{q}$, of driven systems (let us suppose, for simplicity, that the external drift $\mathbf{E}$ is constant), the Gallavotti-Cohen (GC) fluctuation theorem (also called Gallavotti-Cohen symmetry) reads:

$$\lim_{\tau \to \infty} \frac{1}{\tau \Omega} \ln \left[\frac{P_\tau(\mathbf{q})}{P_\tau(-\mathbf{q})} \right] = 2\boldsymbol{\varepsilon} \cdot \mathbf{q}, \qquad (2.63)$$

---

[9]We refer to review by Harris and Schütz [159]

[10]Both Bochkov and Kuzovlev (1977) and Jarzynski (2007) formulated a fluctuation theorem of the work along trajectories arbitrarily far from equilibrium from an initial (equilibrium) state to a final one. Although both derivations lead to apparently different results, they turn to be mathematically equivalent. The solution of this conflict resides in the different definition of work considered in their calculations. To see a rigorous description (and resolution) of this contradiction we refer [162]

where $\varepsilon = \boldsymbol{v} + \mathbf{E}$ is the driving force, which depends on the external field and on the boundary gradient via $\boldsymbol{v}$, and it is related to the entropy production in the system. This relation establishes that the probability of observing a given value of the integrated current $\mathbf{q}$ and the one of the reverse event $-\mathbf{q}$ are related via the driving force ε. Remarkable, this highly non-trivial result is valid arbitrarily far from equilibrium. In the language of LDF, the GC symmetry takes form:

$$G(\mathbf{q}) - G(-\mathbf{q}) = 2\varepsilon \cdot \mathbf{q}, \tag{2.64}$$

which will be of special relevance, among other occasions, when one pretends to characterize the statistic of current fluctuations in the whole $\mathbf{q}$-space.

2.5.2 Additivity principle

As it was shown in the previous section, one of the main goals when studying macroscopic fluctuations consist in solving the variational problem defined by (2.54). Nevertheless, it becomes a highly complex task. Indeed, Eq. (2.54) leads to a set of coupled non-linear partial differential equations which could not be, in general, solved. Moreover, the solution of such a set of equations could not be unique, and only one of them minimizes the action. In this direction, Bodineau and Derrida [40] established an *additivity principle* (AP) for large time fluctuations of the space- and time-integrated current

$$q = \frac{1}{\tau} \int_0^\tau dt \int_0^L dx\, j(x, t), \tag{2.65}$$

in one-dimensional driven diffusive systems in contact with two boundary reservoirs $\phi(0, t) = \phi_L$ and $\phi(L, t) = \phi_R$. Trivially, assuming that macroscopic equation (2.3) associated to that systems admits a time-independent solution, i.e. the macroscopic system exhibits a stationary state, the optimal paths associated to a large-time fluctuation where the value of the integrated current q is equal to the averaged (stationary) value $\langle q \rangle$ are also time-independent. Inspired by this fact, the additivity principle hypothsize that for fluctuations near the stationary value, the optimal profiles are time-independent[11]. This conjecture have strong implications

---

[11]In the original work by Bodineau and Derrida [40], they conjectured that, if we divide the system into two subsystems, the global LDF is the result of minimizing of the sum of the LDF of each subsystem over the field ϕ at their contact surface (under an appropriate *scaling hypothesis* [40,169]). It has been proved that, for $d = 1$, this hypothesis is equivalent to consider the optimal paths to be time-independent. Nowadays, it is broadly accepted that the additivity conjecture refers to time-independence of the optimal profiles, even for different situations than the one presented Bodineau and Derrida.

in one-dimensional systems. Since ϕ and j are coupled via continuity equation (2.9), if both fields are time independent, the optimal current path is uniform with value $j(x,t) = q$. Therefore, the variational problem (2.54) eminently simplifies [17,40,62,170–172]. From a physical point of view, additivity principle establishes that the $1d$-system, after an short transient time, reaches a time-independent state with a structured field $\phi(\mathbf{r})$ and uniform current q^{12}.

In one dimension, whichever the boundary conditions are, the validity of this principle has been demonstrated in simulations for $1d$ stochastic lattice gases [18, 45, 173, 174]. However, it has been shown that this result does not hold, in general, for large current fluctuations. One example of that is the case of periodic boundary conditions which present an interesting phenomenology: while for current fluctuations near the averaged value the additivity conjecture applies, to sustain extremely rare fluctuations coherent jammed (soliton-like) structures emerge traveling around the system at a constant velocity [41, 57, 175]. This traveling waves solutions enhanced the probability of observing such rare events, breaking the additivity principle and evincing the existence of a *dynamical phase transition*.

The application of this conjecture to systems with $d > 1$ poses more problems. Indeed, considering the optimal paths to be time-independent implies, according to continuity equation, that the optimal current field is now divergence-free $\nabla \cdot \mathbf{j}_{\tilde{a}} = 0$, but not necessarily uniform. This question opens the door to two possible extensions of the additivity principle to d-dimensional systems ($d > 1$): (i) considering time-independent optimal paths and an uniform optimal current field (the straightforward one) or (ii) considering time-independent optimal paths but a non-uniform optimal current field (known as *weak* additivity principle). In a recent work, Pérez-Espigares et al. [176] have shown that, for the $2d$ Kipnis-Marchioro-Presutti (KMP) model [126] with a boundary gradient in one direction and periodic boundary conditions in the other, the solution given by imposes weak additivity principle better minimizes the action with respect to the straightforward extension of the AP. In Chapter 3, we will present an original result which provides, under very general conditions, a fundamental constraint that must be satisfied by the optimal current fields, which will clarify this dilemma.

2.5.3 Isometric Fluctuation Relation

Under the light of the straightforward extension of the additivity principle (time-independent optimal paths and uniform optimal current field) when studying fluctuations of the integrated current, Hurtado et al. [46] derived an interesting re-

---

[12]If $q = \langle q \rangle$, the field ϕ will correspond to the stationary state, ϕ_{st}. However, if $q \neq \langle q \rangle$ the system will evolve to time-independent state with $\phi \neq \phi_{\text{st}}$

lation between the probabilities of observing any pair of isometric currents, i.e. $|\mathbf{q}| = |\mathbf{q}'|$. They observed that, as a consequence of the time-reversibility of the macroscopic dynamics, the optimal field ϕ is invariant under rotations of the current $\mathbf{q}$. This result leads to what they called Isometric Fluctuation Relation (IFR), which takes the form:

$$\lim_{\tau \to \infty} \frac{1}{\tau, \Omega} \ln \frac{P_\tau(\mathbf{q})}{P_\tau(\mathbf{q}')} = \varepsilon \cdot (\mathbf{q} - \mathbf{q}'), \qquad (2.66)$$

where ε (as in GC fluctuation theorem) is a constant vector related to the rate of entropy production in the system (thermodynamic force). Interestingly, this result includes Gallavotti-Cohen symmetry in the case $\mathbf{q}' = -\mathbf{q}$. The strong consequences derived from IFR have implied relevant advances in the study and characterization of fluctuations statistics. For instance, IFR provides a hierarchies of equations for cumulants of the integrated current probability distribution and their associated response coefficients [18,46] which go beyond Onsager's reciprocity relations [102, 103] and Green-Kubo formulas [97–99]. However, it is still an open question how this relation modifies when we consider the optimal current not to be uniform, i.e. under the weak additivity principle.

2.5.4 Dynamical Phase Transitions at fluctuating level

Phase transitions are one of the most ubiquitous phenomena in Nature, representing a key element in equilibrium thermodynamics. They describe the transition between two equilibrium states, that is two states which maximize the entropy of the system or minimize the Gibbs free energy[13] whose physical properties remain constant. From a mathematical point of view, a equilibrium phase transition is characterized by a non-analiticity of the Gibbs free energy. Ehrenfest classified the different types of phase transitions into two main groups. *First-order* or *discontinuous* phase transitions are characterized by the abrupt change of some quantities revealing the presence of non-analiticities in the first derivative of the free energy. Associated to these transitions one could find phenomena such as phases coexistence or hysteresis cycles. On the other hand, *second order* or *continuous* phase transitions appears when the non-analiticity of the free energy takes place in the second derivative. In theses transitions, order emerges continuously at some critical point, as captured by an order parameter, signaling the spontaneous breaking of a symmetry. At the critical point, the system presents really interesting features such as scale-invariance or long-range correlations in its physical quantities.

---

[13]This definition can be equivalently extended to minimization of other thermodynamic potentials, e.g. Helmhotz free energy.

In recent years, these ideas have been extended to the realm of fluctuations both in equilibrium and nonequilibrium physics. We now deal with transitions not between (fixed) states but among trajectories that minimizes the action of the system: that is reason why they are known as *dynamical phase transitions* (DPTs). They describe how the trajectories that lead to an atypical value of the time-integrated observable can change from one class to another when varying the value of this observable. They have been identified in different systems, both classical [16, 17, 41, 52, 55–59, 62, 177–182] and quantum [183–185], with important examples in glass formers [61, 186–191], micromasers and superconducting transistors [192, 193], or applications such as DPT-based quantum thermal switches [194–196]. Interestingly, some dynamical phases may display emergent order and collective rearrangements in their trajectories, including symmetry-breaking phenomena [18, 41, 56, 57], while the *large deviation functions* (LDFs) [19] controlling the statistics of these fluctuations exhibit non-analyticities and Lee-Yang singularities [197–204] at the DPT reminiscent of standard critical behavior. Moreover, the emergence of coherent structures associated to rare fluctuations implies in turn that these extreme events are far more probable than previously anticipated [18, 60]. In our language, dynamical phase transitions separate regions of the fluctuating observable space (for instance, a-space) which corresponds to different solutions of the variational problem (2.54). In analogy with Ehrenfest's classification, DPTs could be of first- or second-order (depending on whether the non-analiticity appears at the first or second derivative of nonequilibrium potential), or even they can exhibit a more complex behavior. In Chapter 5 we will apply these ideas to the study of current fluctuations of a paradigmatic 2-dimensional model of driven diffusive systems, obtaining, among other results, the "dynamical" phase diagram showing the emergency of both first- and second-order dynamical phase transitions at a fluctuating level.

2.6 Mesoscopic description of other system of interest

To conclude Chapter 2, we briefly present the mesoscopic description of two models of systems which will be also object of study this Thesis. We will define their dynamics by a Langevin equation and we will show their associated Fokker-Planck and path integral formulations. Once these three descriptions are known, the study of macroscopic fluctuations will follow the same MFT techniques already described in Section 2.4.

2.6.1 Systems with a non-conserved local dynamics

These systems are described by a scalar field $\phi(\mathbf{r}, t)$, where $\mathbf{r} \in \Lambda \equiv [0, L]^d$ is the spatial coordinates and $t \in [t_0, t_f]$ the time, which evolves according to the Langevin equation:

$$\partial_t \phi(\mathbf{r}, t) = F[\phi(\mathbf{r}, t)] + \varpi(\mathbf{r}, t), \tag{2.67}$$

where $F[\phi(\mathbf{r}, t)]$ is a given function of $\phi(\mathbf{r}, t)$ and its derivatives, and $\varpi(\mathbf{r}, t)$ is a Gaussian white noise with correlations:

$$\langle \varpi(\mathbf{r}, t) \rangle = 0 \tag{2.68}$$

$$\langle \varpi(\mathbf{r}, t) \varpi(\mathbf{r}', t') \rangle = \frac{1}{\Omega} G[\phi(\mathbf{r}, t)] \delta(\mathbf{r} - \mathbf{r}') \delta(t - t'). \tag{2.69}$$

The associated Fokker-Planck equations takes the form:

$$\partial_t P[\phi; t] = \int_\Lambda d\mathbf{r} \frac{\delta}{\delta \phi(\mathbf{r})} \left[-\left(F[\phi] + \frac{(1 - \eta)}{2\Omega} \frac{\delta G[\phi]}{\delta \phi(\mathbf{r})} \right) P[\phi; t] \right.$$
$$\left. + \frac{1}{2\Omega} \frac{\delta}{\delta \phi(\mathbf{r})} \left(G[\phi] P[\phi; t] \right) \right] \tag{2.70}$$

and the weight of a given trajectory $\{\phi(\mathbf{r}, t)\}_0^\tau$ can be written as:

$$\mathbb{P}(\{\phi\}_{t_0}^{t_f}) \propto \exp\left[-\Omega \mathcal{S}_{[t_0, t_f]}^{nc}[\phi] \right], \tag{2.71}$$

with:

$$\mathcal{S}_{[t_0, t_f]}^{nc}[\phi] = \frac{1}{2} \int_{t_0}^{t_f} dt \int_\Lambda d\mathbf{r} \left[\frac{1}{G[\phi]} \left(\partial_t \phi - F[\phi] + \frac{(1 - \eta)}{\Omega} \frac{\delta G[\phi]}{\delta \phi(\mathbf{r})} \right)^2 \right.$$
$$\left. + \frac{2(1 - \eta)}{\Omega} \frac{\delta F[\phi]}{\delta \phi(\mathbf{r})} \right]. \tag{2.72}$$

2.6.2 Particle diffusing under the action of an external force

This system can be interpreted as a particular model of the previous one. Consider a particle subjected to a force $F[x(t)]$ and a thermal noise $\zeta(t)$ (for simplicity, we restrict to the one-dimensional case). At a given time $t \in [0, \tau]$, the particle is located at $x(t)$. In the overdamped limit, the evolution of its position is described by the Langevin equation

$$\dot{x}(t) = F[x(t)] + \zeta(t), \tag{2.73}$$

where $\zeta(t)$ is a Gaussian white noise with:

$$\langle \xi(t) \rangle = 0 \tag{2.74}$$

$$\langle \zeta(t)\xi(t') \rangle = \frac{1}{\Omega} G[x(t)]\delta(t - t') . \tag{2.75}$$

The dynamics of the system given by Langevin equation (2.73) is equivalently described by the Fokker-Planck equation for the evolution of the probability $P(x, t)$ of finding the particle at a position x at time t, which takes the form

$$\partial_t P(x,t) = -\partial_x \left[\left(F[x(t)] + \frac{(1-\eta)}{2\Omega} G'[x(t)] \right) P(x,t) \right] + \frac{1}{2\Omega} \partial_x^2 \left(G[x(t)]P(x,t) \right) , \tag{2.76}$$

where $'$ denotes the derivative with respect to the argument. Finally, the Onsager-Machlup weight of a trajectory $\{x(t)\}_0^\tau$ of duration τ takes the form:

$$\mathbb{P}(\{x(t)\}_0^\tau) \propto \exp\left[-\frac{\Omega}{2} \int_0^\tau dt \left\{ \frac{(\dot{x} - F + \frac{(1-\eta)}{2\Omega}G')^2}{G} + \frac{2(1-\eta)}{\Omega} F' \right\} \right] . \tag{2.77}$$

Chapter 3

Structure of the optimal paths to a fluctuation

3.1 Introduction

As we have seen, understanding the statistic of macroscopic fluctuations could pave the way to a better comprehension of nonequilibrium behaviour. However, this highly non-trivial problem remains as a major challenge of theoretical physics. Macroscopic Fluctuation Theory has shed light on this situation in the context of driven diffusive systems providing a powerful scheme to determine the large deviation function controlling the probability distribution of a fluctuation as well as the most probable paths the system follows to carry out such an event [16,38,53–55]. Among all possible observables that can be defined, the currents of locally-conserved quantities play a key role as tokens of nonequilibrium physics, so their associated LDF becomes a central object of investigation. Under MFT framework [16], the problem of characterizing the current LDF converts into a spatio-temporal variational problem for the locally-conserved fields and the associated currents (see Section 2.4.2).

The complexity of the MFT variational problem is such that most studies to date have focused on the current statistics of oversimplified one-dimensional ($1d$) transport models for which the MFT problem is somewhat simpler [40, 45, 170–174, 205, 206], specially when aided with the Additivity Principle (see Section 2.5.2). Only very recently MFT has been used to understand current fluctuations in more realistic high-dimensional ($d > 1$) systems [18, 46, 52, 176, 207–209], and these studies have unveiled a rich phenomenology which only appears for $d > 1$, including hidden symmetries leading to new fluctuation theorems [46],

a weak generalization of the Additivity Principle [176], and complex dynamic phase transitions associated to competing emergent orders and symmetry breaking phenomena [52]. Crucially, the richness found in $d > 1$ stems in all cases from the relevance of structured optimal current fields at the fluctuating level, a common trait of all these new results [52, 176, 209]. In this chapter we will show that structured optimal current fields are a *fundamental requirement* of any high-dimensional fluctuating theory, rather than a mathematical accident. In particular, a simple calculation within MFT will allow us to relate the Jacobian matrix of the reduced optimal current field (to be defined below) with the Hessian matrix of a response field which guarantees that the continuity equation expressing the local conservation law is fulfilled at all points of space and time. A natural analyticity requirement for this response field then leads to a strong condition on the reduced optimal current field: in brief, the optimal current vector field is bounded to exhibit non-trivial structure along the dominant direction in all its orthogonal components, and this structure is coupled to the optimal conserved field via the mobility transport coefficient. This coupling is explicitly non-local in space and time, a main feature of nonequilibrium physics. This result sheds new light and encompass all previous works on current fluctuations in $d > 1$, opening the door to further developments in this field.

To illustrate the meaning of the structure described above, we show in Fig. 3.1 both the optimal temperature $T(x)$ and current vector fields associated to a particular (rare) current fluctuation in a broadly studied driven diffusive system, the two-dimensional Kipnis-Marchioro-Presutti (KMP) model of heat transport [126] in contact with two boundary thermal baths located at $x = 0, 1$ and no external field [176]. In this case, the dominant direction of structure formation corresponds to that of the temperature gradient, resulting in optimal temperature fields with structure only along the x-direction (Fig. 3.1.b-c). Consequently, the optimal current vector field exhibits a non-trivial structure in its y-component along the gradient x-direction, proportional to the local temperature field squared as dictated by the KMP mobility transport coefficient, which is simply $\sigma(\phi) = \phi^2$. This structure of the current y-component, which contrasts with the constant structureless x-component (Fig. 3.1.a), is the manifestation of a general theorem for driven diffusive systems that we will prove in the following lines.

In this way, in Section 3.2 we will present the variational problem derived from MFT when studying fluctuations of the space- and time-integrated current. In Section 3.3 we will analyze the structure of Euler-Lagrange equations for such a problem, which will allow us to deduced a general theorem for the structure of the optimal current fields. Furthermore, we will study the deep consequences derived
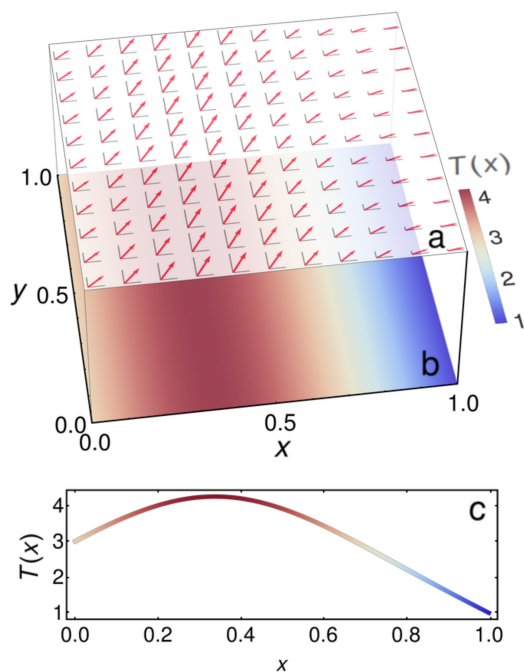
Figure 3.1: Optimal solution for the current vector field (a) and the temperature field (b and c) associated to a given current fluctuation in the $2d$ Kipnis-Marchioro-Presutti model of heat transport [126] in contact with two boundary thermal baths at temperatures $\phi(x = 0) = \phi_0 = 3$ and $\phi(x = 1) = \phi_1 = 1$ and no external field (in this model the locally-conserved field is the energy leading to the study of optimal temperature fields, as we will see in Chapter 4). Gray lines in (a) depict both local components of the optimal current vector field, while red arrows show the resultant vectors. Note the non-trivial structure of the y-component of the current field along the gradient x-direction, in stark contrast with the constant, structureless current x-component.

from this relation. In Section 3.4 we will compare this constraint on the current fields with previous results and show in which way it could contribute to future works in fluctuations of d-dimensional systems. Finally, in Section 3.5 we will summarize the main points obtained along this chapter and present an outlook of this work.

3.2 Current fluctuations in driven diffusive systems

To be more precise, we focus now on a broad class of d-dimensional anisotropic driven diffusive systems characterized by a field $\phi(\mathbf{r}, t)$, with $\mathbf{r} \in \Lambda \equiv [0, 1]^d$ and

$t \in [0, \tau]$. As we have seen in Section 2.2.1, this field evolves in time according to the following fluctuating hydrodynamics (mesoscopic) equation[1]

$$\partial_t \phi(\mathbf{r}, t) + \boldsymbol{\nabla} \cdot \left(-\hat{D}(\phi) \boldsymbol{\nabla} \phi(\mathbf{r}, t) + \hat{\sigma}(\phi) \mathbf{E} + \boldsymbol{\xi}(\mathbf{r}, t) \right) = 0 \,. \qquad (3.1)$$

The field $\mathbf{j}(\mathbf{r}, t) \equiv -\hat{D}(\phi) \boldsymbol{\nabla} \phi(\mathbf{r}, t) + \hat{\sigma}(\phi) \mathbf{E} + \boldsymbol{\xi}(\mathbf{r}, t)$ is the fluctuating current, with $\mathbf{E}$ an external driving field. The deterministic part of the current field $\mathbf{j}(\mathbf{r}, t)$ is given by Fick's law[2] under an external driving. In this way, Eq. (3.1) is nothing but the continuity equation expressing the local conservation law. We consider that diffusivity and mobility matrices can be writen as $\hat{D}(\phi) \equiv D(\phi)\hat{A}$ and $\hat{\sigma}(\phi) \equiv \sigma(\phi)\hat{A}$, respectively, with $\hat{A}$ a diagonal matrix with components $\hat{A}_{\alpha\beta} = a_\alpha \delta_{\alpha\beta}$, $\alpha, \beta \in [1, d]$, which we assume constant and independent of the local field ϕ. The matrix $\hat{A}$ encodes information about the system underlying anistropy, i.e. the possible change of microscopic jumps rates from one spatial direction to another. In other words, the system could exhibit a different diffusive behaviour in each spatial orientation. Hence, $\hat{A}$ is called *anisotropy matrix*. According to (2.7)-(2.8), the vector field $\boldsymbol{\xi}(\mathbf{r}, t)$ is a Gaussian white noise term with:

$$\langle \boldsymbol{\xi}(\mathbf{r}, t) \rangle = 0 \qquad (3.2)$$

$$\langle \xi_\alpha(\mathbf{r}, t) \xi_\beta(\mathbf{r}', t') \rangle = \frac{\sigma(\phi)}{\Omega} a_\alpha \delta_{\alpha\beta} \delta(\mathbf{r} - \mathbf{r}') \delta(t - t') \,. \qquad (3.3)$$

It is important stress again that, at this mesoscopic level of description, the diffusion and mobility matrices fully characterize the dynamic and fluctuation properties of the model at hand. In the absence of any driving mechanism, we expect the system to relax to equilirbium, implying that both transport coefficients cannot be independent. Indeed, they are coupled via a local Einstein relation $\hat{D}(\phi) = \hat{\sigma}(\phi) f_0''(\phi)$, with $f_0(\phi)$ the *equilibrium* free energy density of the system of interest and $''$ denoting second differentitation with respect to the argument (see Eq. (2.11) and below). The results we are going to derived here can be however easily generalized to more general theories violating the previous condition.

We are now in position to write the path integral representation of the given stochastic dynamics, milestone of the Macroscopic Fluctuation Theory. As it was shown in Sections 2.3.2 and 2.4, the probability of observing a particular *trajectory* $\{\phi(\mathbf{r}, t), \mathbf{j}(\mathbf{r}, t)\}_0^\tau$ of duration τ can be written, in the large Ω limit, as

$$\mathbb{P}\left(\{\phi, \mathbf{j}\}_0^\tau\right) \asymp \exp\left(-\Omega \mathcal{S}_\tau [\phi, \mathbf{j}] \right), \qquad (3.4)$$

---

[1]To facilitate reading, we include here some concepts already introduced in Chapter 2.

[2]Or, equivalently, Fourier's law.

where the action takes the form

$$\mathcal{S}_\tau\left[\phi,\mathbf{j}\right] = \int_0^\tau dt \int_\Lambda d\mathbf{r} \, \frac{1}{2\sigma(\phi)} \boldsymbol{\mathcal{J}}(\mathbf{r},t) \cdot \hat{\mathcal{A}}^{-1} \boldsymbol{\mathcal{J}}(\mathbf{r},t) \,, \tag{3.5}$$

with the definition

$$\boldsymbol{\mathcal{J}}(\mathbf{r},t) \equiv \mathbf{j} + \hat{D}(\phi)\boldsymbol{\nabla}\phi - \hat{\sigma}(\phi)\mathbf{E} \,, \tag{3.6}$$

and the additional constraint that the fields $\phi(\mathbf{r},t)$ and $\mathbf{j}(\mathbf{r},t)$ must be coupled via the continuity equation at every point of space and time (see Eq. (3.1)),

$$\partial_t\phi(\mathbf{r},t) + \boldsymbol{\nabla}\cdot\mathbf{j}(\mathbf{r},t) = 0 \,. \tag{3.7}$$

For trajectories $\{\phi,\mathbf{j}\}_0^\tau$ not obeying this continuity constraint or the appropriate boundary conditions (which depend on the particular problem at hand, see below), $\mathcal{S}_\tau\left[\phi,\mathbf{j}\right] \to \infty$. Note that the field $\boldsymbol{\mathcal{J}}(\mathbf{r},t)$ in Eq. (3.5) is nothing but the *excess current*, i.e. the departure of the current vector field $\mathbf{j}(\mathbf{r},t)$ from its constitutive form $-\hat{D}(\phi)\boldsymbol{\nabla}\phi + \hat{\sigma}(\phi)\mathbf{E}$.

Our interest is to characterize fluctuations of the space- and time-averaged empirical current $\mathbf{q}$, defined as

$$\mathbf{q} = \frac{1}{\tau}\int_0^\tau dt \int_\Lambda d\mathbf{r}\,\mathbf{j}(\mathbf{r},t) \,. \tag{3.8}$$

Therefore, the probability of observing a given value $\mathbf{q}$ of the empircal current $P_\tau(\mathbf{q})$ can be now obtained by summing up the probability of all trajectories $\{\phi,\mathbf{j}\}_0^\tau$ compatible with the constraint (3.8) and the continuity constraint (3.7). Mathematically (see Eq. (2.48)

$$P_\tau\left(\mathbf{q}\right) = \int \mathcal{D}\phi\mathcal{D}\mathbf{j}\,P_{\text{st}}(\phi(\mathbf{r},0))\mathbb{P}\left(\{\phi,\mathbf{j}\}_0^\tau\right)\prod_{\mathbf{r}\in\Lambda}\prod_{t\in[0,\tau]}\delta\left(\partial_t\phi+\boldsymbol{\nabla}\cdot\mathbf{j}\right)$$

$$\cdot\,\delta\left(\mathbf{q} - \tau^{-1}\int_0^\tau dt \int_\Lambda d\mathbf{r}\,\mathbf{j}\right)\,, \tag{3.9}$$

with the Dirac δ-functionals guaranteeing the above contraints, and where the initial condition is chosen from the stationary probability $P_{st}(\phi(\mathbf{r},0))$. As we have seen in Section 2.4.2, by introducing the corresponding Lagrange multipliers $\psi(\mathbf{r},t)$ and $\boldsymbol{\lambda}$ for constraints (3.7) and (3.8), respectively, we can write:

$$P_\tau\left(\mathbf{q}\right) \propto \int \mathcal{D}\phi\,\mathcal{D}\mathbf{j}\,\mathcal{D}\psi\,d\boldsymbol{\lambda}\,P_{st}(\phi(\mathbf{r},0))\exp\left(-\Omega\mathcal{S}_\tau\left[\phi,\mathbf{j},\psi,\boldsymbol{\lambda}\right]\right) \tag{3.10}$$

where the modified action reads

$$
\begin{aligned}
S_\tau\left[\phi, \mathbf{j}, \psi, \boldsymbol{\lambda}\right] &= \int_0^\tau dt \int_\Lambda d\mathbf{r}\left[\frac{1}{2\sigma(\phi)}\boldsymbol{\mathcal{J}}\cdot\hat{\mathcal{A}}^{-1}\boldsymbol{\mathcal{J}}+\right. \\
&+ \left. \psi(\mathbf{r}, t)\left(\partial_t\phi + \boldsymbol{\nabla}\cdot\mathbf{j}\right) + \boldsymbol{\lambda}\cdot\left[\mathbf{q} - \mathbf{j}(\mathbf{r}, t)\right]\right].
\end{aligned}
\tag{3.11}
$$

For long times (and large scale separation between levels of description, Ω), the probability of observing an empirical current $\mathbf{q}$ peaks around the average current $\langle\mathbf{q}\rangle$ as $P_\tau(\mathbf{q}) \asymp \exp[-\tau\Omega G(\mathbf{q})]$, with $G(\mathbf{q})$ the current large deviation function. According to Eq. (2.54), in the large time limit, the current LDF can be written as

$$
G(\mathbf{q}) = \lim_{\tau\to\infty}\left\{\frac{1}{\tau}\min_{\{\phi, \mathbf{j}, \psi, \boldsymbol{\lambda}\}} S_\tau\left[\phi, \mathbf{j}, \psi, \boldsymbol{\lambda}\right]\right\}.
\tag{3.12}
$$

Once the variational problem for the current LDF is defined, we can now proceed to analyze the subsequent Euler-Langrange equations.

3.3   Structure of the optimal path

The set $(\phi_\mathbf{q}, \mathbf{j}_\mathbf{q}, \psi_\mathbf{q}, \boldsymbol{\lambda}_\mathbf{q})$ of optimal fields which solve this variational problem define the most probable path leading to a current fluctuation $\mathbf{q}$. Equations for these optimal fields can be derived now by functional differentiation of the above modified action. In particular, by varying over the conserved field, $\phi(\mathbf{r}, t) \to \phi(\mathbf{r}, t) + \delta\phi(\mathbf{r}, t)$, we arrive at the following partial differential equation

$$
\partial_t\psi_\mathbf{q} = H(\phi_\mathbf{q}) - \frac{\sigma_\mathbf{q}'}{2\sigma_\mathbf{q}^2}\mathbf{j}_\mathbf{q}\cdot\hat{\mathcal{A}}^{-1}\mathbf{j}_\mathbf{q} + \frac{\sigma_\mathbf{q}'}{2}\mathbf{E}\cdot\hat{\mathcal{A}}\mathbf{E},
\tag{3.13}
$$

where we have defined

$$
H(\phi_\mathbf{q}) \equiv -\left[\boldsymbol{\nabla}\left(\frac{D_\mathbf{q}^2}{2\sigma_\mathbf{q}}\right) + \frac{D_\mathbf{q}^2}{\sigma_\mathbf{q}}\boldsymbol{\nabla}\right]\cdot\hat{\mathcal{A}}\boldsymbol{\nabla}\phi_\mathbf{q},
\tag{3.14}
$$

with $D_\mathbf{q} \equiv D(\phi_\mathbf{q})$ and $\sigma_\mathbf{q} \equiv \sigma(\phi_\mathbf{q})$. Another equation is obtained by varying over the current field, $\mathbf{j} \to \mathbf{j} + \delta\mathbf{j}$, leading to

$$
\boldsymbol{\mathcal{J}}_\mathbf{q} = \hat{\sigma}_\mathbf{q}\left(\boldsymbol{\lambda}_\mathbf{q} + \boldsymbol{\nabla}\psi_\mathbf{q}\right)
\tag{3.15}
$$

where $\boldsymbol{\mathcal{J}}_\mathbf{q} = \mathbf{j}_\mathbf{q} + \hat{D}_\mathbf{q}\boldsymbol{\nabla}\phi_\mathbf{q} - \hat{\sigma}_\mathbf{q}\mathbf{E}$ is the optimal excess current, see Eq. (3.6). Finally, variations over ψ and $\boldsymbol{\lambda}$ lead respectively to the constraints (3.7) and (3.8) for the optimal fields $\phi_\mathbf{q}(\mathbf{r}, t)$ and $\mathbf{j}_\mathbf{q}(\mathbf{r}, t)$.

Before continuing, we can now gain some insight on the physical interpretation of $\boldsymbol{\lambda}_\mathbf{q}$ and $\psi_\mathbf{q}$ by using the local Einstein formula $\hat{D}_\mathbf{q} = \hat{\sigma}_\mathbf{q} f_0''(\phi_\mathbf{q})$ to write Fick's law under external driving as $-\hat{D}_\mathbf{q} \boldsymbol{\nabla} \phi_\mathbf{q} + \hat{\sigma}_\mathbf{q} \mathbf{E} = \hat{\sigma}_\mathbf{q} [\mathbf{E} - \boldsymbol{\nabla}(\delta \mathcal{F}_0 / \delta \phi_\mathbf{q})]$, where $\mathcal{F}_0(\phi) = \int_\Lambda d\mathbf{r}\, f_0(\phi)$ is the equilibrium free energy functional of the system of interest. Using this in Eq. (3.15) we find that

$$\mathbf{j}_\mathbf{q} = \hat{\sigma}_\mathbf{q} \left[(\mathbf{E} + \boldsymbol{\lambda}_\mathbf{q}) - \boldsymbol{\nabla} \left(\frac{\delta \mathcal{F}_0}{\delta \phi_\mathbf{q}} - \psi_\mathbf{q} \right) \right] . \tag{3.16}$$

In this way, $\boldsymbol{\lambda}_\mathbf{q}$ and $\psi_\mathbf{q}(\mathbf{r}, t)$ can be interpreted respectively as the additional bulk field and boundary driving (i.e. chemical potential) necessary to obtain the current field $\mathbf{j}_\mathbf{q}(\mathbf{r}, t)$ within Fick's law under external driving. Alternatively, note also that $\psi_\mathbf{q}$ is nothing but the (optimal) Legendre multiplier associated to continuity equation, Eq. 3.7, and as such it is intimately related to the noise field. Indeed, the field ψ selects those noise realizations compatible with Fick's law and the local conservation law (this can be better seen in the Hamiltonian formulation of the problem [63, 210] where ψ plays the role of the conjugate moment to the field ϕ).

Eq. (3.15), or equivalently Eq. (3.16), sets strong conditions on the structure of the optimal current field. In particular, if we define now the reduced (optimal) excess current $\boldsymbol{\chi}_\mathbf{q}(\mathbf{r}, t) \equiv \hat{\sigma}_\mathbf{q}^{-1} \boldsymbol{\mathcal{J}}_\mathbf{q}(\mathbf{r}, t)$ and take its Jacobian matrix $\boldsymbol{\nabla} \boldsymbol{\chi}_\mathbf{q}$, with components $(\boldsymbol{\nabla} \boldsymbol{\chi}_\mathbf{q})_{\alpha\beta} = \partial_\alpha \chi_{\mathbf{q},\beta}$, we have from Eq. (3.15) that $\boldsymbol{\nabla} \boldsymbol{\chi}_\mathbf{q} = \boldsymbol{\nabla} \boldsymbol{\nabla} \psi_\mathbf{q}$, or equivalently

$$\partial_\alpha \chi_{\mathbf{q},\beta} = \partial_\alpha \partial_\beta \psi_\mathbf{q} . \tag{3.17}$$

In words, the Jacobian matrix of the reduced (optimal) excess current $\boldsymbol{\chi}_\mathbf{q}$ corresponds to the Hessian of the response field $\psi_\mathbf{q}$ associated to the continuity equation (3.7). This observation thus leads to the following strong result:

Theorem: *Let the response function $\psi_\mathbf{q} : \Lambda \times [0, \tau] \to \mathbb{R}$ be a C^2-class function of spatial coordinates, i.e. a function twice continuously differentiable in its spatial domain. Then*

$$\partial_\beta \left(\frac{j_{\alpha,\mathbf{q}}}{a_\alpha \sigma_\mathbf{q}} \right) = \partial_\alpha \left(\frac{j_{\beta,\mathbf{q}}}{a_\beta \sigma_\mathbf{q}} \right) \quad \forall\, (\mathbf{r}, t) \in \Lambda^d \times [0, \tau] . \tag{3.18}$$

Proof: Schwarz's theorem [211] states that if a function $\psi_\mathbf{q}$ has continuous second partial derivatives at any given spatial point in Λ then its Hessian matrix is symmetric at this point, $\partial_\alpha \partial_\beta \psi_\mathbf{q} = \partial_\beta \partial_\alpha \psi_\mathbf{q}$. This immediately implies, via Eq. (3.17), that the Jacobian of the reduced (optimal) excess current is itself a symmetric matrix, i.e. $\partial_\alpha \chi_{\mathbf{q},\beta} = \partial_\beta \chi_{\mathbf{q},\alpha} \; \forall \alpha, \beta \in [1, d]$. From this symmetry, and using the definitions of $\boldsymbol{\chi}_\mathbf{q}$ and $\boldsymbol{\mathcal{J}}_\mathbf{q}$ above, and the relation $\partial_\alpha (D_\mathbf{q}/\sigma_\mathbf{q}) \partial_\beta \phi_\mathbf{q} =$

$\partial_\beta(D_\mathbf{q}/\sigma_\mathbf{q})\partial_\alpha\phi_\mathbf{q} = (D_\mathbf{q}/\sigma_\mathbf{q})'\partial_\alpha\phi_\mathbf{q}\partial_\beta\phi_\mathbf{q}$, we immediately arrive at the fundamental relation (3.18). Note that the C^2-differentiability of the response function $\psi_\mathbf{q}$ is a *natural* requirement for most physical solutions to this variational problem, though we cannot discard the possible existence of singular, non-differentiable solutions for $\psi_\mathbf{q}$ which would violate (3.18) at singular points. Note also that a weaker condition for $\psi_\mathbf{q}$ which nevertheless suffices to ensure the symmetry of its Hessian matrix is that all partial derivatives are themselves differentiable.

To better understand the tight constraints that Eq. (3.18) impose on the optimal current fields, it is important to realize that in all high-dimensional problems studied in literature up to now the dominant paths responsible of a current fluctuation, corresponding to the global extrema of the action S_τ in Eq. (3.12), always exhibit structure (if any) along a *principal direction*, that we denote here as $x_\parallel$ [18, 52, 176, 207–209]. This means in particular that $\phi_\mathbf{q}(\mathbf{r}, t) = \phi_\mathbf{q}(x_\parallel, t)$ and $\mathbf{j}_\mathbf{q}(\mathbf{r}, t) = \mathbf{j}_\mathbf{q}(x_\parallel, t)$. Examples include open systems subject to a boundary gradient, which develop structure along the gradient direction (irrespective of the external field) [176], see e.g. Fig. 3.1 above; or closed driven diffusive systems with periodic boundary conditions, for which different dynamic phase transitions appear to current regimes characterized by traveling waves with structure along one of the principal axes of the system of interest [52]. In all these cases, condition (3.18) leads to

$$\partial_\parallel\left(\frac{j_{\beta,\mathbf{q}}}{a_\beta\sigma_\mathbf{q}}\right) = 0 \qquad \forall\,\beta \neq \parallel\,, \tag{3.19}$$

which immediately implies that $j_{\beta,\mathbf{q}}(x_\parallel, t) = k_\beta\sigma[\phi_\mathbf{q}(x_\parallel, t)]\,\forall\beta \neq \parallel$, with k_β a direction-dependent constant which follows from the constraint (3.8) on the empirical current $\mathbf{q}$. Therefore we arrive at

$$j_{\beta,\mathbf{q}}(x_\parallel, t) = q_\beta\frac{\tau\sigma[\phi_\mathbf{q}(x_\parallel, t)]}{\displaystyle\int_0^\tau ds\int_0^1 dy\,\sigma[\phi_\mathbf{q}(y, s)]} \qquad \forall\,\beta \neq \parallel\,. \tag{3.20}$$

In this way the relation between the Jacobian matrix for $\chi_\mathbf{q}$ and the Hessian matrix of the response field $\psi_\mathbf{q}$, together with a natural analyticity condition for the latter, force the optimal current vector field $\mathbf{j}_\mathbf{q}$ to exhibit *non-trivial structure* along the dominant direction $\parallel$ in all its orthogonal components $\beta \neq \parallel$, and this structure is coupled to the optimal field $\phi_\mathbf{q}$ via the mobility transport coefficient $\sigma(\phi_\mathbf{q})$. Interestingly, this result makes manifest the *spatio-temporal nonlocality* of the current LDF (3.12) and the associated optimal trajectories, as the optimal current field at a given point of space and time depends explicitly on the space-time integral of the mobility of the optimal conserved field, see the denominator in Eq. (3.20). Note

also that conditions (3.18) and (3.20) become empty for $d = 1$, where structureless optimal current fields are still possible [40, 45, 173], evidencing the richness of the fluctuation landscape for $d > 1$ driven diffusive systems when compared with their one-dimensional counterparts.

3.4 Connection with previous results

We next explore how previous results on current fluctuations for both open and closed $d > 1$ driven diffusive systems fit into the above general result.

3.4.1 Open systems under a boundary drift

First we consider the case of open systems subjected to an external gradient along an arbitrary direction $x_\parallel$. For that we fix the field boundaries to $\phi(\mathbf{r}, t)|_{x_\parallel=0,1} = \phi_{0,1}$, which drive the system out of equilibrium as soon as $\phi_0 \neq \phi_1$, setting periodic boundary conditions for all other directions of space. This class of systems has been broadly studied during the last years, finding that a simplifying conjecture within MFT known as Additivity Principle (AP) allows to solve the problem of current statistics both for $d = 1$ [17, 18, 40, 45, 62, 170–174] and $d > 1$ [176, 207–209, 212, 213]. The AP, which offers explicit expressions for the current LDF and the optimal paths supporting a given fluctuation, establishes that the most probable trajectory to a current fluctuation is time-independent (apart from some initial and final transients of negligible weight for the current LDF). In this situation, the following general property is satisfied:

Property: *Consider the following boundary conditions for the optimal field*

$$\phi_{\mathbf{q}}(0, \boldsymbol{x}_\perp) = \phi_0 ; \quad \phi_{\mathbf{q}}(1, \boldsymbol{x}_\perp) = \phi_1 ;$$
$$\phi_{\mathbf{q}}(x_\parallel, \boldsymbol{x}_\perp + \hat{\boldsymbol{e}}_{\boldsymbol{i}}) = \phi_{\mathbf{q}}(x_\parallel, \boldsymbol{x}_\perp) , \qquad \forall i = 2, .., d , \qquad (3.21)$$

where we write $\mathbf{r} = (x_\parallel, \boldsymbol{x}_\perp)$ *with* $x_\parallel \in [0, 1]$ *and* $\boldsymbol{x}_\perp \in [0, 1]^{d-1}$*, being* $\hat{\boldsymbol{e}}_{\boldsymbol{i}}$ *the canonical unit vectors. If* $\phi_{\mathbf{q}}(\mathbf{r}) = \phi_{\mathbf{q}}(x_\parallel)$ *and* $j_{\mathbf{q}, \parallel}(\mathbf{r}) = j_{\mathbf{q}, \parallel}(x_\parallel)$*, with* $j_{\mathbf{q}, \parallel}$ *the component of the current in the principal direction* $x_\parallel$*, then the most probable current is of the form*

$$\mathbf{j}_{\mathbf{q}}(\mathbf{r}) = \left(q_\parallel, \boldsymbol{q}_\perp \frac{\sigma[\phi_{\mathbf{q}}(x_\parallel)]}{\int_0^1 dy \, \sigma[\phi_{\mathbf{q}}(y)]} \right) , \qquad (3.22)$$

where we have decomposed $\mathbf{q} = (q_\parallel, \boldsymbol{q}_\perp)$ *along the gradient* ($\parallel$) *and all other,* $(d - 1)$ *directions* ($\perp$).

Proof: The AP conjectures that the optimal paths associated to a current fluctuation are time-independent. Under this hypothesis, the set of equations for the most probable trajectories derived from variational problem (3.12) takes the form

$$H(\phi_{\mathbf{q}}) - \frac{\sigma_{\mathbf{q}}'}{2\sigma_{\mathbf{q}}^2}\mathbf{j_q} \cdot \hat{\mathcal{A}}^{-1}\mathbf{j_q} + \frac{\sigma_{\mathbf{q}}}{2}\mathbf{E} \cdot \hat{\mathcal{A}}\mathbf{E} = 0 \tag{3.23}$$

$$\mathbf{j_q} + \hat{D}_{\mathbf{q}}\mathbf{\nabla}\phi_{\mathbf{q}} - \hat{\sigma}_{\mathbf{q}}\mathbf{E} = \hat{\sigma}_{\mathbf{q}}\left(\boldsymbol{\lambda}_{\mathbf{q}} + \mathbf{\nabla}\psi_{\mathbf{q}}\right) \tag{3.24}$$

$$\mathbf{\nabla} \cdot \mathbf{j_q} = 0 \tag{3.25}$$

$$\mathbf{q} = \int_{\Lambda} d\mathbf{r}\, \mathbf{j_q} \,. \tag{3.26}$$

One can easily realize that Eq. (3.23), together with $\phi_{\mathbf{q}}(\mathbf{r}) = \phi_{\mathbf{q}}(x_{\parallel})$, leads to

$$\mathbf{j_q} \cdot \hat{\mathcal{A}}^{-1}\mathbf{j_q} = a_{\parallel}\, j_{\mathbf{q},\parallel}^2 + \sum_{\beta \neq \parallel} a_{\beta}\, j_{\mathbf{q},\beta}^2 = F(x_{\parallel}), \tag{3.27}$$

with $F(x_{\parallel})$ a function depending only on coordinate $x_{\parallel}$. Therefore, assuming $j_{\mathbf{q},\parallel}(\mathbf{r}) = j_{\mathbf{q},\parallel}(x_{\parallel})$, we can deduced from relation (3.18) of our theorem that

$$j_{\mathbf{q},\beta} = a_{\beta}\, C_{\beta}(\boldsymbol{x}_{\perp})\sigma[\phi_{\mathbf{q}}], \quad \forall \beta \neq \parallel, \tag{3.28}$$

where $C_{\beta}(\boldsymbol{x}_{\perp})$ is a function depending (at most) on the orthogonal coordinates $\boldsymbol{x}_{\perp}$. Using this expression in Eqs. (3.18), (3.27) and (3.25) we find

$$\partial_{\alpha}C_{\beta} = \partial_{\beta}C_{\alpha} \tag{3.29}$$

$$\sum_{\alpha} a_{\alpha}\, C_{\alpha}^2 = R \tag{3.30}$$

$$\sum_{\alpha} a_{\alpha}\, \partial_{\alpha}C_{\alpha} = W, \tag{3.31}$$

respectively, with R and W two constants. At this point, differentiating Eq. (3.30) with respect to x_{β}, and taking into account Eq. (3.29), it can be shown that

$$\sum_{\alpha} a_{\alpha}\, C_{\alpha}\partial_{\alpha}C_{\beta} = 0. \tag{3.32}$$

Differentiating again with respect to x_{β}, multiplying by a_{β} and summing over all β-coordinates, together with Eq. (3.29) and (3.31), we obtain

$$\sum_{\alpha}\sum_{\beta} a_{\alpha}\, a_{\beta}\, \left(\partial_{\alpha}C_{\beta}\right)^2 = 0, \tag{3.33}$$

which implies that $C_\beta(\boldsymbol{x}_\perp)$ is a constant. As a result, the most probable current field is of the form $\mathbf{j_q(r)} = \left(j_{\mathbf{q},\parallel}(x_\parallel), \boldsymbol{k}_\perp \sigma\right)$, with $\boldsymbol{k}_\perp$ a constant vector. Finally, considering Eqs. (3.25) and (3.26), finally leads to (3.22), as we want to proof. Note that in dimension $d = 2$ it can be proved that the optimal current field $\mathbf{j_q}$ is of the form (3.22) by only hypothesizing $\phi_\mathbf{q} = \phi_\mathbf{q}(x)$.

The structure of the most probable current field given by Eq. (3.22) corresponds exactly to the result obtained previously from the weak extension of Additivity Principle as applied to d-dimensional isotropic driven diffusive systems [176], starting from a variational problem for general but divergence-free current fields with structure along one dominant direction. Our general theorem (3.18) allows now to understand this structure as a direct consequence of the symmetry of the Jacobian matrix associated to the reduced excess current. Note that this result is not compatible with the straightforward extension to $d > 1$ of the $1d$-system solution (which considers the optimal current field to be constant [40, 45, 170, 173]), elucidating the dilemma exposed in Section 2.5.2. This situation will be study in depth in the next chapter, where our theorem and Eq.(3.22) will play a fundamental role.

3.4.2 Closed systems with periodic boundary conditions

To end this chapter, we consider current fluctuations in *closed* d-dimensional anisotropic driven diffusive systems under an external field $\mathbf{E}$ [52]. For that we set periodic boundary conditions along all directions of space. Due to the system periodicity, the total *mass* is conserved so $\phi_0 = \int_\Lambda \phi_\mathbf{q}(\mathbf{r}, t) d\mathbf{r}$ is constant in time, a further constraint that has to be taken care of in the MFT variational problem. A detailed analysis of the resulting MFT equations shows [18, 41, 52, 56, 57] that a 2nd-order *dynamic phase transition* (DPT) appears at a given critical current for this broad family of systems between a homogeneous fluctuation phase with Gaussian current statistics and constant, structureless optimal fields, $\phi_\mathbf{q}(\mathbf{r}, t) = \phi_0$ and $\mathbf{j_q}(\mathbf{r}, t) = \mathbf{q}$, and a symmetry-broken non-Gaussian phase characterized by the emergence of coherent traveling waves with structure along a dominant direction, $\phi_\mathbf{q}(\mathbf{r}, t) = \omega_\mathbf{q}(x_\parallel - vt)$ and $\mathbf{j_q}(\mathbf{r}, t) = \mathbf{j_q}(x_\parallel - vt)$, with v some velocity [52]. Interestingly, for mild or no anisotropy, different traveling-wave phases appear depending on the current separated by lines of 1st-order DPTs, a degeneracy which disappears beyond a critical anisotropy. This richness of the fluctuation phase diagram stems again from the relevance of structured current fields at the fluctuating level, a seemingly mathematical aspect which takes full significance at the light of our general result (3.18). In particular, the continuity equation $\partial_t \phi_\mathbf{q} + \boldsymbol{\nabla} \cdot \mathbf{j_q} = 0$ applied to the $1d$ traveling-wave structure implies that $\partial_\parallel[j_{\parallel,\mathbf{q}}(z_\parallel) - v\omega(z_\parallel)] = 0$,

where we have defined $z_\parallel \equiv x_\parallel - vt$, and this together with the constraint (3.8) on the empirical current leads to $j_{\parallel,\mathbf{q}}(z_\parallel) = q_\parallel - v[\phi_0 - \omega_\mathbf{q}(z_\parallel)]$. On the other hand, all orthogonal current components follow directly from our theorem above as $\mathbf{j}_{\perp,\mathbf{q}}(z_\parallel) = \mathbf{q}_\perp \sigma[\omega_\mathbf{q}(z_\parallel)] / \int_0^1 dy\, \sigma[\omega_\mathbf{q}(y)]$. This result, which is markedly different from the traveling-wave structure found in $1d$ models [41, 46, 57], will be broadly analyze in Chapter 5.

3.5 Conclusions

In summary, we have derived a fundamental relation which strongly constraints the structure of the optimal path sustaining a given current fluctuation. In particular, when a principal direction exists, the optimal current vector field is bounded to exhibit non-trivial structure along this dominant direction in all its orthogonal components, a structure coupled to the optimal conserved field via the mobility transport coefficient. This has been done by relating within macroscopic fluctuation theory the Jacobian matrix of the reduced optimal current field with the Hessian matrix of the response field associated to the continuity equation, and requiring analyticity for the latter. In this sense, we prove here that the structured optimal current fields predicted and observed by a number of recent works [52, 176, 209, 213] is indeed a fundamental requirement of any high-dimensional fluctuating theory, rather than a mathematical accident. Remarkably, our result also makes manifest the non-locality in space and time of the current large deviation function and the associated optimal trajectories. This result hence serves as a starting point in the study of fluctuations in complex d-dimensional systems, constraining the form of the optimal paths and thus aiding in the formulation of simplifying hypotheses to solve these complex variational problems in nonequilibrium statistical physics.

Chapter 4

Fluctuations of the empirical heat current on thermal conducting hydrodynamic systems

4.1 Introduction

The development of a theory of fluctuations in fluids has been a central object of study in statistical physics [117, 214]. A general framework to characterize fluctuations in thermodynamic equilibrium states was provided by Landau and Lifshitz [7, 109], and this program has been generalized with success to study small fluctuations for fluids in nonequilibrium steady states [110]. Nevertheless, understanding *arbitrary* fluctuations in fluids far from equilibrium still remains an open problem, and this is the focus of the present chapter. An interesting situation to analyze in this context is the problem of heat transport in a fluid subject to a thermal gradient, possibly one of the "simplest" and most studied cases of a nonequilibrium steady state [215]. Heat transport in this setting is governed by Fourier's law, which establishes the propotionality between the heat current and the local temperature gradient. The proportionality constant defines the heat conductivity κ, an intrinsic property of the fluid which could depend on the local temperature and density. Interestingly, while it is widely believed that Fourier's law is just a linear approximation to a more complex transport law, recent works have shown that, at least for some fluid models, this law holds locally far from equilibrium [216] and well beyond the linear transport regime. Numerous experimental works have studied the statistics of fluctuations of heat flux and temperature in this setting for a wide variety of systems, measuring the corresponding probability distributions [217–220], some low- and high-order cumulants [219–229] and the associated temperature profiles [221, 222, 224, 226, 229, 230]. In this case, Macro-

scopic Fluctuation Theory provides an suitable scheme to describe fluctuations of the corresponding relevant observables.

The aim of this chapter is to characterize within the MFT framework the statistics of fluctuations of the empirical heat current in an incompressible quiescent (i.e. at rest) d-dimensional model fluid subject to a boundary temperature gradient [110, 231]. In particular, we will focus on describing the optimal temperature field sustaining a given heat flux fluctuation in the long-time limit, determining its associated large deviation function controlling the probability distribution of the heat current and analizing its behaviour for small (near the steady state) and large fluctuations. Hence, in Section 4.2 we will describe the system at hand. Starting from the general balance laws describing fluid's evolution, we will deduce the diffusion equation controlling the dynamics of our model, which, at the mesoscopic level, will correspond to Eq. (2.10) for a diffusive system with no external drift. Then we will proceed, following the MFT scheme shown in Chapter 2, with the study of heat current statistics. In Section 4.3 we will obtain the most probable temperature fields minimizing the action of our system. As we will see, the theorem on the structure of the optimal current fields presented in the previous chapter will become an essential element, since the complex MFT variational problem will be solved under the conjecture established by the (weak) additivity principle [127, 176]. Once the optimal temperature fields are known, we will prove, in Section 4.4, that they can be gathered into families characterized by the same functional form (in terms of inverse Jacobi elliptic functions). This observation will allow us to classify all optimal trajectories in an infinite set of universal functions, providing a deeper understanding of their properties and structure. In Section 4.5 we will obtain the analytical form of the current LDF and analyze its behavior in limiting cases, both near the steady state and in the far tails of the distribution. While for small deviations from the stationary value, the current distribution can be properly approximated by a deformed Gaussian, its structure for large fluctuations exhibits an interesting logarithmic dependence which confirms the complex analytic behavior of the heat current LDF. We will further determine the cumulant generating function of the current distribution, from which analytical expressions for its cumulants follow, as well as interesting relations between them which open the door to further experimental research on this problem.

4.2 Heat current fluctuations in a quiescent incompressible fluid

We consider a d-dimensional fluid subject to a boundary temperature gradient in one direction, say $x \in [0, 1]$. The fluid is fully described at any instant of time by the mass density $\rho(\mathbf{r}, t)$, temperature $T(\mathbf{r}, t)$, pressure $p(\mathbf{r}, t)$ and local center-of-mass velocity $\mathbf{v}(\mathbf{r}, t)$ fields, with $\mathbf{r} \in \Lambda \equiv [0, 1]^d$ and $t \in [0, \tau]$ the spatial and temporal coordinates, respectively. The fluid's evolution at the macroscale is completely characterized by a set of $d + 2$ partial differential equations, called *balance equations*, which are derived from the local conservation laws together with the usual constitutive relations between the thermodynamic forces and the fluxes [214]. In particular, conservation of mass leads to the continuity equation

$$\partial_t \rho + \boldsymbol{\nabla} \cdot (\rho \mathbf{v}) = 0 \ , \tag{4.1}$$

while momentum conservation yields the Navier-Stokes equations

$$\rho \left[\partial_t \mathbf{v} + (\mathbf{v} \cdot \boldsymbol{\nabla}) \mathbf{v} \right] = -\boldsymbol{\nabla} \cdot p + \eta \boldsymbol{\nabla}^2 \mathbf{v} + \left(\zeta + \frac{1}{3}\eta \right) \boldsymbol{\nabla}(\boldsymbol{\nabla} \cdot \mathbf{v}) \ , \tag{4.2}$$

and conservation of energy results in

$$\partial_t \left(\frac{1}{2}\rho \mathbf{v}^2 + \rho \varepsilon \right) = -\boldsymbol{\nabla} \cdot \left[\rho \mathbf{v} \left(\frac{1}{2}\mathbf{v}^2 + \omega \right) + \boldsymbol{\Phi} + \mathbf{j_D} \right] \ . \tag{4.3}$$

In the above equations η and ζ are respectively the shear and bulk viscosity coefficients, ε is the internal energy per mass unit, ω is the enthalpy per mass unit, $\boldsymbol{\Phi}$ is the viscous dissipation function (proportional to the divergence of the velocity) and $\mathbf{j_D}$ is the local heat current [110, 214, 231]. In particular, the structure of the local heat current field is given by the well-known Fourier's law of heat conduction

$$\mathbf{j_D}(\mathbf{r}, t) = -\kappa(T)\boldsymbol{\nabla}T(\mathbf{r}, t) \ , \tag{4.4}$$

with $\kappa(T)$ the thermal conductivity. In this chapter we are interested in studying thermal transport in a *quiescent incompressible fluid* in contact with two boundary thermostats at temperatures T_0 and T_1 along the x-direction, with periodic boundary conditions along all perpendicular $(d - 1)$-directions, $\boldsymbol{x}_\perp$. Quiescence implies that $\mathbf{v}(\mathbf{r}, t) = 0 \, \forall \, \mathbf{r}, t$, while incompressibility implies that the fluid's mass density and pressure fields are constant across space, so the only relevant field in this case is the temperature field $T(\mathbf{r}, t)$, which then satisfies Fourier's heat equation [7, 109, 110, 214]

$$\partial_t T(\mathbf{r}, t) = \boldsymbol{\nabla} \cdot (D(T)\boldsymbol{\nabla}T(\mathbf{r}, t)) \ , \tag{4.5}$$

where $D = \frac{\kappa}{\rho c_p}$ is the *thermal diffusivity*, with c_p the specific heat at constant pressure. Finally, we further assume that the initial condition is such that the system relaxes to its steady state in a finite time scale.

The previous scheme is nothing more that the macroscopic description of a diffusive system characterized by one conservation law already presented in Chapter 2 (see in particular Eqs. (2.3), (2.4) and (2.10), identifying $\phi(\mathbf{r}, t) = T(\mathbf{r}, t)$. Therefore, as we are interested in analyzing macroscopic fluctuations of the heat current, we describe the mesoscopic evolution of our system by the Langevin equation (see Eq. (2.9))

$$\partial_t T(\mathbf{r}, t) + \boldsymbol{\nabla} \cdot [-D(T)\boldsymbol{\nabla} T(\mathbf{r}, t) + \boldsymbol{\xi}(\mathbf{r}, t)] = 0, \qquad (4.6)$$

where $\boldsymbol{\xi}(\mathbf{r}, t)$ is the Gaussian white noise vector field with

$$\langle \boldsymbol{\xi}(\mathbf{r}, t) \rangle = 0, \qquad (4.7)$$

$$\langle \xi_\alpha(\mathbf{r}, t)\xi_\beta(\mathbf{r}', t') \rangle = \frac{1}{\Omega}\sigma[T(\mathbf{r}, t)]\delta_{\alpha\beta}\delta(t - t')\delta(\mathbf{r} - \mathbf{r}'), \qquad (4.8)$$

and $\alpha, \beta \in [1, d]$. Note that this equation corresponds to Eq. (3.1) for an isotropic system. Consequently, the anisotropy matrix is equal to the identity, $\mathcal{A} = \mathbf{1}$, and both the diffusivity and mobility are scalar coefficients, $D[T(\mathbf{r}, t)]$ and $\sigma[T(\mathbf{r}, t)]$, respectively.

At this point, we can now proceed as in Section 3.2 and write the path probability of having a given trajectory $\{T(\mathbf{r}, t), \mathbf{j}(\mathbf{r}, t)\}_0^\tau$ as:

$$\mathbb{P}\left(\{T, \mathbf{j}\}_0^\tau\right) \asymp \exp\left(-\Omega\, \mathcal{S}_\tau[T, \mathbf{j}]\right), \qquad (4.9)$$

with

$$\mathcal{S}_\tau[T, \mathbf{j}] = \int_0^\tau dt \int_\Lambda d\mathbf{r}\, \frac{[\mathbf{j}(\mathbf{r}, t) + D[T(\mathbf{r}, t)]\boldsymbol{\nabla} T(\mathbf{r}, t)]^2}{2\sigma[T(\mathbf{r}, t)]}, \qquad (4.10)$$

and the temperature and current fields coupled via continuity equation:

$$\partial_t T(\mathbf{r}, t) + \boldsymbol{\nabla} \cdot \mathbf{j}(\mathbf{r}, t) = 0. \qquad (4.11)$$

Hence, the probability distribution of the space- and time-averaged current

$$\mathbf{q} \equiv \frac{1}{\tau}\int_0^\tau dt' \int_\Lambda d\mathbf{r}\, \mathbf{j}(\mathbf{r}, t'), \qquad (4.12)$$

takes the form:

$$P_\tau(\mathbf{q}) \propto \int \mathcal{D}T\, \mathcal{D}\mathbf{j}\, \mathcal{D}\psi\, d\boldsymbol{\lambda}\, P_{st}(T(\mathbf{r}, 0)) \exp\left(-\Omega S_\tau\left[T, \mathbf{j}, \psi, \boldsymbol{\lambda}\right]\right) \qquad (4.13)$$

with $P_{\rm st}$ the stationary distribution and where the modified action reads

$$
\begin{aligned}
S_\tau\left[T, \mathbf{j}, \psi, \boldsymbol{\lambda}\right] \;=\; & \int_0^\tau dt \int_\Lambda d\mathbf{r} \left[\frac{(\mathbf{j} + D[T]\boldsymbol{\nabla} T)^2}{2\sigma[T]} + \right. \\
& + \left. \psi(\mathbf{r}, t)\left(\partial_t T + \boldsymbol{\nabla}\cdot\mathbf{j}\right) + \boldsymbol{\lambda}\cdot(\mathbf{q} - \mathbf{j})\right].
\end{aligned}
\tag{4.14}
$$

Lagrange multipliers $\psi(\mathbf{r}, t)$ and $\boldsymbol{\lambda}$ ensure that constraints (4.11) and (4.12) are fulfilled, respectively. Furthermore, according to boundary conditions, the Lagrange multiplier associated to continuity equation satisfies:

$$
\psi(\mathbf{r}, t)\big|_{x=0,1} = 0, \quad \psi((x, \boldsymbol{x}_\perp + \hat{\boldsymbol{e}}_i), t) = \psi((x, \boldsymbol{x}_\perp), t), \forall i = 2, .., d, \tag{4.15}
$$

where we have decomposed the position vector $\mathbf{r} = (x, \boldsymbol{x}_\perp)$ along the gradient direction (x) and all other $(d-1)$ orthogonal directions $(\boldsymbol{x}_\perp)$, with $\hat{\boldsymbol{e}}_i$ the canonical unit vectors. In the long-time (and large scale separation Ω) limit, the probability density function (pdf) of the empirical current obeys a large deviation principle, scaling as $P_\tau(\mathbf{q}) \asymp \exp\left[-\Omega\tau G(\mathbf{q})\right]$, and the large deviation function takes the form:

$$
G(\mathbf{q}) = \lim_{\tau\to\infty}\left\{ \min_{T, \mathbf{j}, \psi, \boldsymbol{\lambda}} S_\tau\left[T, \mathbf{j}, \psi, \boldsymbol{\lambda}\right] \right\}. \tag{4.16}
$$

4.3 Most probable temperature and current fields

We next focus on solving the variational problem defined by (4.16). As we have seen, this analysis will lead to explicit predictions for the current statistics, as well as to a detailed knowledge of the properties of the optimal path associated to an arbitrary fluctuation. The set $(T_\mathbf{q}, \mathbf{j}_\mathbf{q}, \psi_\mathbf{q}, \boldsymbol{\lambda}_\mathbf{q})$ solution of (4.16) defines then the trajectory that the fluid follows in mesoscopic phase space to sustain a long-time current fluctuation. In this way, these optimals fields can be obtained by solving the following Euler-Lagrange equations

$$
\partial_t \psi_\mathbf{q} = -\frac{\sigma'_\mathbf{q}}{2\sigma_\mathbf{q}^2}\left(\mathbf{j}_\mathbf{q}^2 - D_\mathbf{q}^2(\boldsymbol{\nabla} T_\mathbf{q})^2\right) - \frac{D_\mathbf{q}}{\sigma_\mathbf{q}}\boldsymbol{\nabla}\cdot(\mathbf{j}_\mathbf{q} + D_\mathbf{q}\boldsymbol{\nabla} T_\mathbf{q}) \tag{4.17}
$$

$$
\mathbf{j}_\mathbf{q} + D_\mathbf{q}\boldsymbol{\nabla} T_\mathbf{q} = \sigma_\mathbf{q}\left(\boldsymbol{\nabla}\psi_\mathbf{q} + \boldsymbol{\lambda}_\mathbf{q}\right) \tag{4.18}
$$

$$
\partial_t T_\mathbf{q} + \boldsymbol{\nabla}\cdot\mathbf{j}_\mathbf{q} = 0 \tag{4.19}
$$

$$
\mathbf{q} = \frac{1}{\tau}\int_0^\tau dt \int_\Lambda d\mathbf{r}\, \mathbf{j}_\mathbf{q}(\mathbf{r}, t), \tag{4.20}
$$

with $D_{\mathbf{q}} = D[T_{\mathbf{q}}(\mathbf{r}, t)]$ and $\sigma_{\mathbf{q}} = \sigma[T_{\mathbf{q}}(\mathbf{r}, t)]$, and $\sigma_{\mathbf{q}}'$ the derivative of $\sigma_{\mathbf{q}}$ with respect to its argument, $T(\mathbf{r}, t)$. As a result, the current LDF takes the form

$$G(\mathbf{q}) = \frac{1}{\tau} \int_0^\tau dt \int_\Lambda d\mathbf{r} \, \frac{(\mathbf{j_q}(\mathbf{r}, t) + D_{\mathbf{q}} \boldsymbol{\nabla} T_{\mathbf{q}}(\mathbf{r}, t))^2}{2\sigma_{\mathbf{q}}} \,, \qquad (4.21)$$

in terms of the optimal temperature and current fields.

The general solution of the spatiotemporal problem (4.17)-(4.20) remains a major challenge in most cases [38, 55, 232, 233]. As we have seen in Section 2.5.2, a powerful conjecture known as Additivity Principle has been put forward to strongly simplify the variational problem at hand by assuming the optimal paths to be time-independent (except for initial and final transients of negligible statistical weight). We hence adopt the AP here and write $T_{\mathbf{q}}(\mathbf{r}, t) = T_{\mathbf{q}}(\mathbf{r})$ and $\mathbf{j_q}(\mathbf{r}, t) = \mathbf{j_q}(\mathbf{r})$. It is then straighforward to prove[1] that $\psi_{\mathbf{q}}(\mathbf{r}, t) = \psi_{\mathbf{q}}(\mathbf{r})$. Recalling the boundary conditions for the temperature field described in the previous section, we have that $T_{\mathbf{q}}(0, \boldsymbol{x}_\perp) = T_0$ and $T_{\mathbf{q}}(1, \boldsymbol{x}_\perp) = T_1$, together with

$$T_{\mathbf{q}}(x, \boldsymbol{x}_\perp + \hat{\boldsymbol{e}}_{\boldsymbol{i}}) = T_{\mathbf{q}}(x, \boldsymbol{x}_\perp) \quad \forall i = 2, .., d \,. \qquad (4.22)$$

These boundary conditions correspond to a fluid in contact with two plates at temperatures T_0 and T_1 at the x-boundaries at $x = 0$ and 1, respectively, and periodic boundary conditions on the perpendicular $(d-1)$-subspace. The symmetry of the boundary conditions leads to the natural assumption that the optimal temperature and x-component of the current fields will exhibit structure only along the x-direction, i.e. $T_{\mathbf{q}}(\mathbf{r}) = T_{\mathbf{q}}(x)$ and $j_{\mathbf{q},x}(\mathbf{r}) = j_{\mathbf{q},x}(x)$. We realize that the different hypothesis of the property for the structure of the optimal current field established in Section 3.4.1 are fulfilled. Consequently, the most probable current field exhibits the following non-trivial form:

$$\mathbf{j_q}(\mathbf{r}) = \left(q_x, \boldsymbol{q}_\perp \frac{\sigma[T_{\mathbf{q}}]}{A[T_{\mathbf{q}}]} \right) \,, \qquad (4.23)$$

with the decomposition $\mathbf{q} = (q_x, \boldsymbol{q}_\perp)$ and

$$A[T_{\mathbf{q}}] = \int_0^1 dy \, \sigma[T_{\mathbf{q}}(y)] \,. \qquad (4.24)$$

---

[1] Differentiating with respect to time both Eqs. (4.17) and (4.18) we see that $\partial_t^2 \psi_{\mathbf{q}} = 0$ and $\partial_t \boldsymbol{\nabla} \psi_{\mathbf{q}} = 0$ leading to $\partial_t \psi_{\mathbf{q}} = k$, with k a constant. Therefore, considering that boundary conditions (4.15) are satisty for all $t \in [0, \tau]$, we finally arrive to $k = 0$, which implies $\psi_{\mathbf{q}}(\mathbf{r}, t) = \psi_{\mathbf{q}}(\mathbf{r})$.

As a result, the probability $P_\tau(\mathbf{q})$ is completely characterized in terms of the optimal temperature profile $T_\mathbf{q}(x)$. Considering (4.17) and the previous assumptions, the most probable temperature field satisfies the ordinary differential equation [18]

$$\left(D[T_\mathbf{q}] \frac{dT_\mathbf{q}}{dx} \right)^2 = q_x^2 + K\sigma[T_\mathbf{q}] - \left(\frac{\sigma[T_\mathbf{q}]}{A[T_\mathbf{q}]} \right)^2 \mathbf{q}_\perp^2 \,, \qquad (4.25)$$

where K is an integration constant fixed by the boundary conditions, which are given by T_0 and T_1.

In order to proceed, we now need to specify the functional form of the thermal diffusivity and mobility transport coefficients, which completely define the model fluid we will study here. For an incompressible fluid under moderate boundary temperature gradients, the thermal conductivity can be considered a constant of the material, and hence the thermal diffusivity defined above will be a constant, that we take here to be $D = 1/2$. Furthermore, in this situation it can be proved using the fluctuation-dissipation theorem that the standard deviation of the fluctuating heat current (which is nothing but the mobility) scales as the local temperature squared [7,109,110], so we take $\sigma(T) = T^2$. Indeed, these two transport coefficients define a broadly studied transport model, the Kipnis-Marchioro-Presutti (KMP) model of heat conduction [126] which, as we see, captures the heat transport properties of a quiescent incompressible fluid. With these prescriptions, the differential equation (4.25) boils down to

$$\frac{dT_\mathbf{q}}{dx} = \pm 2 \left[q_x^2 + K T_\mathbf{q}^2 - \frac{T_\mathbf{q}^4}{A^2} \mathbf{q}_\perp^2 \right]^{1/2} \,. \qquad (4.26)$$

This equation can be solved in terms of Jacobi inverse elliptic functions, leading to the following reduced optimal temperature field

$$\tau_\mathbf{q}(x) \equiv \frac{T_\mathbf{q}(x)}{T_1} = \frac{\mathrm{cn}\left[-F_0 + (F_1 + F_0)x; k \right]}{\mathrm{cn}(F_1; k)} \,, \qquad (4.27)$$

where $\mathrm{cn}(u; k)$ is the cosine-amplitude Jacobi function with modulus k [234,235]. The reader could find in Appendix A a detailed resolution of Eq. (4.26), as well as a complete characterization of the optimal temperature fields. The value of the constant parameters $F_{0,1}$ and the modulus are fixed by the boundary conditions

and the clausure equation (4.24), namely

$$Q_x = \frac{\sqrt{1-k^2}(F_1 + F_0)}{2 \, \text{cn}(F_1; k)}, \tag{4.28}$$

$$Q_\perp = \frac{E_1 + E_0 - (1 - k^2)(F_1 + F_0)}{2k \, \text{cn}(F_1; k)}, \tag{4.29}$$

$$\tau_0 = \frac{\text{cn}(F_0; k)}{\text{cn}(F_1; k)}, \tag{4.30}$$

where we have defined $Q_x = |q_x|/T_1$, $Q_\perp = |\boldsymbol{q}_\perp|/T_1$, $\tau_0 = T_0/T_1$ and $E_{0,1} = E(\text{am}(F_{0,1}; k); k)$ with $\text{am}(u; k)$ the amplitude Jacobi function and $E(\theta; k)$ the Jacobi integral of the second kind [234, 235]. Note that, assuming without loss of generality that $T_0 \geq T_1$ so $\tau_0 \geq 1$, we have that $F_0 \in [-\mathbf{K}(k), \mathbf{K}(k)]$, $F_1 \in [\text{cn}^{-1}(\tau_0^{-1}; k), \mathbf{K}(k)]$ and $k \in [0, 1]$, with $F_1 \geq F_0$ and $\mathbf{K}$ the Jacobi complete elliptic integral of the first kind[2]

(using the notation of Gradshteyn & Ryzhik [234]). In this way, once the physical variables Q_x, $Q_\perp$ and τ_0 are fixed, we can obtain F_0, F_1 and k from Eqs. (4.28)-(4.30). Note also that, for a fixed value of the external gradient parameter τ_0, one can solve Eq. (4.30) to obtain

$$F_1 = \text{cn}^{-1}\left[\frac{1}{\tau_0}\text{cn}(F_0; k); k\right], \tag{4.31}$$

Therefore, substituting F_1 into Eqs. (4.28)-(4.29), we conclude that Q_x and $Q_\perp$ are just functions of F_0 and k.

4.4 Scaling, structure and universality of the optimal path

As shown above, the most probable reduced temperature profile $\tau_{\mathbf{q}}(x)$ is a continuous positive function written in terms of $\text{cn}(u; k)$, an even and periodic function of its argument $u = -F_0 + (F_1 + F_0)x$. Indeed, the cosine-amplitude Jacobi function presents only one positive maximum located at $u = 0$ [234, 235], i.e. $x_{max} = F_0/(F_0 + F_1)$, which implies that the optimal temperature field (defined in the spatial interval $x \in [0, 1]$) exhibits at most two possible typical behaviors, namely (i) a *single-maximum profile* for $F_0 > 0$, or (ii) a *monotonously decreasing profile* for $F_0 < 0$. The values of Q_x and $Q_\perp$ where the crossover happens can be found by setting $F_0 = 0$ and $F_1 = \text{cn}^{-1}(1/\tau_0; k)$ on Eqs. (4.28) and (4.29),
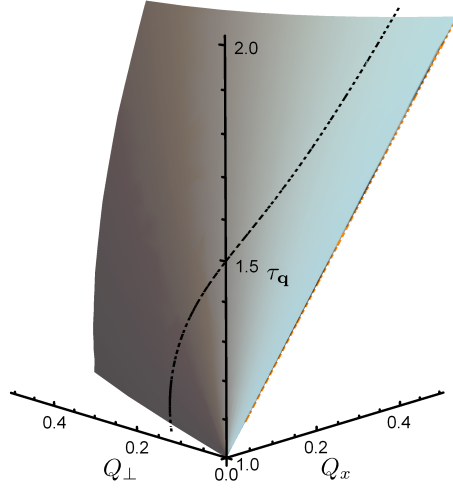
---

[2]See Appendix A.

Figure 4.1: Surface defined by the set of points $(\tau_0, Q_x, Q_\perp)$ with fixed modulus $k = 0.9$. Points in this surface have the same scaling form of the associated optimal reduced temperature field $\tau_{\mathbf{q}}(x)$ except for a linear transformation of the x-coordinate and a suitable amplitude factor, see Eq. (4.32). The black dashed line shows the set of points in this surface with the aditional constraint $F_1 + F_0 = 0.4$. Reduced optimal profiles along this curve present the same functional structure except for only a translation of the x-coordinate. The orange dashed line represents the stationary current values given by $(\tau_0, Q_x^{st}, Q_\perp^{st}) = (\tau_0, (\tau_0 - 1)/2, 0)$.

and are a function of the modulus $k \in [0, 1]$ and the external gradient parameter τ_0. This condition defines a limiting curve in the $(Q_x, Q_\perp)$ plane for each τ_0 separating both behaviors.

Interestingly, Eqs. (4.28)-(4.30) lead to a one-to-one correspondence between the set of physical variables $(\tau_0, Q_x, Q_\perp)$ and the parameters (k, F_0, F_1). The Jacobi-cosinus function $cn(u; k)$ defining the most probable temperature profile (4.27) is just a linear function of space, $u = -F_0 + (F_1 + F_0)x$, with constants fixed by $(\tau_0, Q_x, Q_\perp)$, while the modulus k captures the particular functional dependence on u (e.g. $cn(u; k = 0) = \cos u$ while $cn(u; k = 1) = \operatorname{sech} u$). In this way, the modulus k *parametrizes* in a natural way the topology of the optimal temperature field: all optimal profiles with the same modulus k share the same functional structure (after a linear transformation of the x-coordinate and a suitable amplitude factor). Therefore there exist a surface in $(\tau_0, Q_x, Q_\perp)$-space, defined by the constraint on constant k, whose optimal reduced temperature pro-
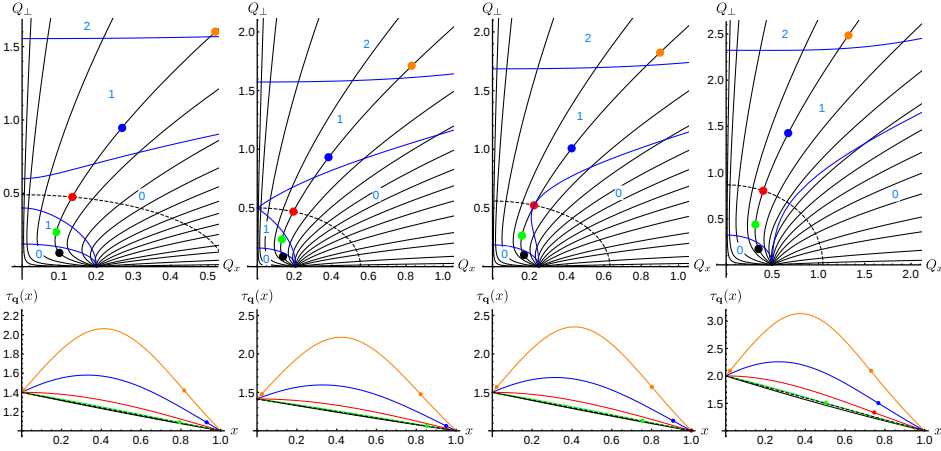
Figure 4.2: Top row: Current fluctuations exhibiting the same scaling form of the optimal reduced temperature profile. Each black solid line represents a uniparametric family of solutions $(Q_x(F_0), Q_\perp(F_0))$ of Eqs. (4.29)-(4.30) with varying F_0 and fixed k which share the same scaling form of the optimal profile. Each panel includes curves for $k = 0.001, 0.01, 0.05, 0.1, 0.2, 0.3,$ 0.4, 0.5, 0.6, 0.7, 0.8, 0.9, 0.95, 0.99, 0.999, 0.9999 (displayed counterclockwise). Each panel corresponds to a fixed external gradient parameter τ_0, with $\tau_0 = 1.4, \sqrt{2}, 1.5,$ and 2 from left to right. The dashed black line in each panel represents the crossover between monotonous (below the dashed line, $F_0 < 0$) and non-monotonous, single-maximum profiles (above the dashed line, $F_0 > 0$). Blue lines separate regions of profiles with 0, 1 and 2 inflection points. Bottom row: Optimal reduced temperature profiles associated to the different highlighted dots in upper panels. The dashed lines represents the stationary profile in each case, while the dots locate the corresponding inflection points (if any).

files follow the scaling function

$$\tau_{\mathbf{q}}(x) = A(\tau_0, Q_x, Q_\perp)\mathrm{cn}(u; k), \quad u = -F_0 + (F_0 + F_1)x. \qquad (4.32)$$

This defines a universal scaling behavior for the optimal temperature fields responsible for different current fluctuations in the quiescent incompressible fluid. Note in particular that the above scaling implies the existence of optimal profiles associated to different values of the external gradient parameter $\tau_0 = T_0/T_1$ with the same functional form. Fig. 4.1 shows an example of the surface of points $(\tau_0, Q_x, Q_\perp)$ having the same value of $k = 0.9$ and hence the same scaling behavior. We note that these surfaces are analytic at all points. Finally, one can define a stronger universal scaling by demanding that not only the modulus k is fixed, but also the slope $F_0 + F_1$ of the linear map in the scaling fundtion (4.32). This aditional contraint defines a curve within the $(\tau_0, Q_x, Q_\perp)$-surface of constant-

k along which the optimal temperature field for a heat current fluctuation has the same functional form except for a *translation* along the x-coordinate (see the black dashed line in Fig. 4.1).

The top row in Fig. 4.2 presents with black solid lines different families of current fluctuations which share the same scaling form of the optimal temperature field (i.e. have the same value of the modulus k) for different values of the external gradient parameter τ_0. Note that these curves are parametrized by F_0 for each fixed τ_0. Remarkably, we observe that all curves of current fluctuations converge to the stationary value $(Q_x^{\text{st}}, Q_\perp^{\text{st}}) = ((\tau_0 - 1)/2, 0)$ when $F_0 \to -\mathbf{K}(k)$, implying that around the nonequilibrium stationary state *all* family members have monotonous temperature profiles ($F_0 < 0$) and contribute to the fluctuating behavior of $\mathbf{q}$'s with a probability whose value will be study in the next section. In particular, we emphasize that all possible scaling structures of the optimal temperature profile are present when we consider infinitesimally small fluctuations around the steady state current, the dominant family being determined by the *orientation* of the infinitesimal current fluctuation vector.

Finally, we have also studied the convexity properties of the optimal temperature field by analyzing in detail the form of its second derivative, finding profiles with 0, 1 or 2 inflection points. This rich phenomenology is also displayed in Fig. 4.2 (top row), where we show for varying τ_0 the regions corresponding to profiles with different numbers of inflection points (blue solid lines and numbers). In addition, the particular shape of the most probable temperature fields for different values of $(\tau_0, Q_x, Q_\perp)$ signaled with points in the upper panels is also shown, see bottom row in Fig. 4.2. Important features to note here are the transition from *monotonous* to *single-maximum* profiles as the distance to the stationary state is increased (measured in terms of the current), as well as the change in the number of inflection points appearing in each one (identified with a dot). The evolution of the number of inflection points as we move away from the stationary current is non-trivial, and we notice the reentrant behavior of the curve delimiting the regime of current fluctuations whose optimal profiles have no inflection points. This reentrance changes as the external gradient parameter τ_0 is varied, disappearing for large enough τ_0. It is also interesting to stress that the curves delimiting the number of inflection points intersect with the curves defining the different scaling profile families for constant k, see top panels in Fig. 4.2, meaning that profiles within the same scaling family can exhibit a variable number of inflection points despite having the same overall functional form.

4.5 Heat current statistics

Once the optimal temperature profiles have been determined, we are now in position to study in detail the probability distribution $P_\tau(\mathbf{q})$ of the fluid's empirical heat current $\mathbf{q}$. As shown in Section 4.2 above, the pdf $P_\tau(\mathbf{q})$ obeys a large deviation principle for long times of the form $P_\tau(\mathbf{q}) \asymp \exp\left[-\tau\Omega G(\mathbf{q})\right]$, which defines the current LDF. In this way, $G(\mathbf{q})$ can be then written in terms of the optimal temperature and current fields as shown in Eq. (4.21). As a result, using the additivity principle [40] and taking into account the structure of the optimal temperature fields (4.27) and its relation with the optimal heat current (4.23), we arrive at the following expression for the current LDF

$$
\begin{aligned}
G(\mathbf{q}) &= \frac{q_x}{2}\left(\frac{1}{T_0} - \frac{1}{T_1}\right) + \frac{1}{8}(F_0 + F_1)^2 + \frac{1}{4}(F_0 + F_1)\left(\frac{\mathrm{sn}(F_1; k)\,\mathrm{dn}(F_1; k)}{\mathrm{cn}(F_1; k)}\right.\\
&+ \left.\frac{\mathrm{sn}(F_0; k)\,\mathrm{dn}(F_0; k)}{\mathrm{cn}(F_0; k)} - E_0 - E_1\right),
\end{aligned}
\tag{4.33}
$$

written in terms of the parameters (k, F_0, F_1) linked to the physical variables $(\tau_0, Q_x, Q_\perp)$ via Eqs. (4.28)-(4.30). From this expression, it is easy to check that the Gallavotti-Cohen fluctuation theorem [44, 48–51, 64], relating the probability of an arbitrary current fluctuation $\mathbf{q}$ with its time-reversed current $-\mathbf{q}$ (see Section 2.5.1 and Eq. (2.64)), holds in this case, namely

$$
G(\mathbf{q}) - G(-\mathbf{q}) = 2\varepsilon \cdot \mathbf{q} = 2|\varepsilon|q_x,
\tag{4.34}
$$

where $\varepsilon = \frac{1}{2}\left(T_0^{-1} - T_1^{-1}\right)\hat{\mathbf{x}}$ is the nonequilibrium driving force (with $\hat{\mathbf{x}}$ the unit versor along the gradient direction), related to the rate of entropy production in the nonequilibrium fluid appearing as a consequence of the boundary temperature gradient. Moreover, the symmetry of the problem implies that the LDF also satisfies $G(q_x, \mathbf{q}_\perp) = G(q_x, -\mathbf{q}_\perp)\ \forall q_x, \mathbf{q}_\perp$.

To better understand the fluid's heat current statistics, it is interesting to analyze the behaviour of $G(\mathbf{q})$ in two opposing limits, i.e. for small current fluctuations around the stationary state defined by $\mathbf{q}_{\mathbf{st}} = \left(q_x^{\mathrm{st}} = T_1(\tau_0 - 1)/2, \mathbf{q}_\perp^{\mathrm{st}} = 0\right)$, and its behavior in the far tails of the distribution.

4.5.1 Fluctuations around the stationary state

In the following lines we will describe in brief how to deduce the structure of the current LDF for small devations about the stationary state. For a fixed k, it is easy to show that the convergence to the stationary value $\mathbf{Q}^{\mathbf{st}} = ((\tau_0 - 1)/2, 0)$ takes

place when $F_0 \to -\mathbf{K}(k)$ (see Section 4.4). As a consequence, the behaviour near $\mathbf{Q}^{\text{st}}$ can be analyze by fixing $F_0 = -\mathbf{K}(k) + \delta$ for small values of δ and any k-value. We can now introduce the excess reduced current vector $\tilde{\mathbf{Q}} = (\tilde{Q}_1, \tilde{Q}_\perp)$, with the definitions

$$\tilde{Q}_x \equiv Q_x - |q_x^{\text{st}}|/T_1\,, \quad \tilde{Q}_\perp \equiv Q_\perp - |q_\perp^{\text{st}}|/T_1\,. \tag{4.35}$$

Expanding Eqs. (4.28) and (4.29) around $\delta = 0$ we realize that they have the structure $\tilde{Q}_\alpha = Q_\alpha - Q_\alpha^{\text{st}} = a_0 \delta^2 (1 + a_1 \delta^2 + \ldots)$, with $\alpha = x, \perp$. It hence seems reasonable to parameterize $\tilde{Q}_x = R \sin\theta$ and $\tilde{Q}_\perp = R \cos\theta$ and rewrite both (4.28) and (4.29) as functions of R and θ. Afterwards, we expand $\tilde{Q}_x/\tilde{Q}_\perp = \tan\theta$ in terms of δ and look for the k-expansion on δ compatible with such expansion and whose coefficients are functions of $\tan\theta$. Then we substitute the k-expansion on the $\tilde{Q}_x$ expansion and invert the series to find δ^2 and k^2 as a series expansion on R. In particular, we find

$$
\begin{aligned}
k^2 &= \frac{1}{2}(1 - \sin\theta) + \frac{9(1 + \tau_0 + \tau_0^2 + \tau_0^3 + \tau_0^4)}{10(\tau_0 - 1)(1 + \tau_0 + \tau_0^2)^2} R \cos^2\theta + \mathcal{O}(R^2) \tag{4.36} \\
\delta^2 &= \frac{12\tau_0^2}{\tau_0^3 - 1} R - \frac{12\tau_0^2(27 + 27\tau_0 + 7\tau_0^2 + 7\tau_0^3 + 7\tau_0^4)}{5(\tau_0 - 1)^2(1 + \tau_0 + \tau_0^2)^3} R^2 \sin\theta \\
&\quad + \mathcal{O}(R^3)\,, \tag{4.37}
\end{aligned}
$$

Note that the expansions are well defined whenever $R/(\tau_0 - 1) < 1$, implying the equilibrium limit ($\tau_0 \to 1$) is singular and cannot be studied by an analytical continuation of the nonequilibrium steady state using Eqs. (4.37). Therefore, near the stationary state, the current LDF can be approximated by:

$$
\begin{aligned}
G(\tilde{\mathbf{Q}}) &= G_{\text{gauss}}(\tilde{\mathbf{Q}}) - \frac{3(\tilde{Q}_x^2 + \tilde{Q}_\perp^2)}{2(1 + \tau_0 + \tau_0^2)} \left[\frac{2(\tau_0 - 1)(4 + 7\tau_0 + 4\tau_0^2)}{5(1 + \tau_0 + \tau_0^2)^2} \tilde{Q}_x \right. \\
&\quad + \frac{9}{175(1 + \tau_0 + \tau_0^2)^4} \left(-5(4 + 2\tau_0 - 30\tau_0^2 - 57\tau_0^3 - 30\tau_0^4 + 2\tau_0^5 \right. \\
&\quad + 4\tau_0^6)(\tilde{Q}_x^2 + \tilde{Q}_\perp^2) + 2(\tau_0 - 1)^2(16 + 61\tau_0 + 91\tau_0^2 + 61\tau_0^3 \\
&\quad + \left. 16\tau_0^4)(\tilde{Q}_\perp^2 - \tilde{Q}_x^2) \right) + \left. \mathcal{O}(\tilde{\mathbf{Q}}^3) \right]\,, \tag{4.38}
\end{aligned}
$$

where

$$G_{\text{gauss}}(\tilde{\mathbf{Q}}) = \frac{3(\tilde{Q}_x^2 + \tilde{Q}_\perp^2)}{2(1 + \tau_0 + \tau_0^2)} \tag{4.39}$$

captures the Gaussian fluctuations around the steady state expected from the central limit theorem. In Fig. 4.3 we represent the exact $G(\mathbf{q})$ of Eq. (4.33) (dark
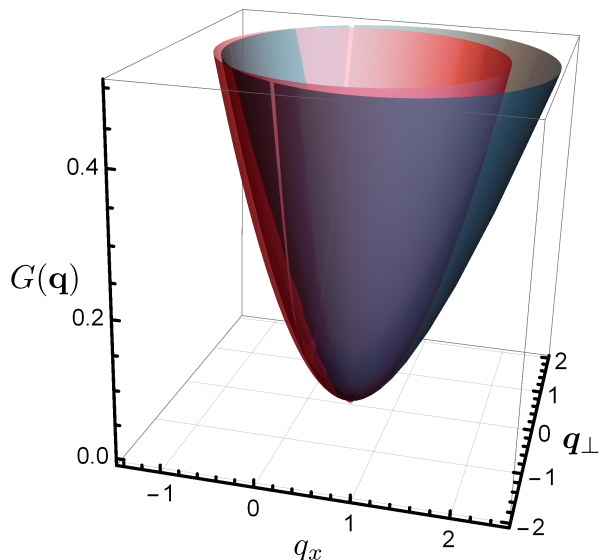
Figure 4.3: The dark (outer) surface represents the exact current LDF $G(\mathbf{q})$ for $T_0 = 2$ and $T_1 = 1$ (so $\tau_0 = 2$), see Eq. (4.33). The red (inner) surface corresponds to Gaussian approximation $G_{\text{gauss}}(\mathbf{q})$ around the stationary state for the same parameters, see Eq. (4.39). The red point at the bottom represents the stationary state.

outer surface) for $\tau_0 = 2$, together with the Gaussian part of the expansion (4.38), G_{gauss}, (red inner surface). We stress here the non-gaussian, asymmetric structure of the exact $G(\mathbf{q})$, which can be however approximated by a deformed Gaussian on both axis at least for moderate current fluctuations. The dominant corrections of the optimal reduced temperature field beyond the steady-state (linear) profile can be also computed to first order in $\tilde{\mathbf{Q}}$, leading to

$$\tau_{\mathbf{q}}(x) = \tau_0 - x(\tau_0 - 1) + \frac{2(\tau_0 - 1)}{1 + \tau_0 + \tau_0^2} x(1 - x)(1 + 2\tau_0 - x(\tau_0 - 1))\tilde{Q}_x + O(\tilde{\mathbf{Q}}^2),$$
(4.40)

i.e. a polynomial deformation of the linear stationary profile.

4.5.2 Far tails of the current LDF

We are also interested on the leading behavior of $G(\mathbf{q})$ for currents far from stationary state behavior. This can be studied in detail by focusing on two different limits, namely $\left(|q_x| \gg q_x^{st}, \boldsymbol{q}_\perp = 0\right)$ and $(q_x = 0, |\boldsymbol{q}_\perp| \gg 0)$.

The behavior in the first situation, $\left(|q_x| \gg q_x^{st}, \boldsymbol{q}_\perp = 0\right)$, can be obtained by plugging $k = 0$ into Eq. (4.33) and expanding the expression around its maximum value using $F_0 = \pi/2 - \delta$, which for $q_x > 0$ results in

$$G(q_x, 0) \simeq \frac{\pi}{2\delta} - \frac{4 + \tau_0(\pi^2 + 4)}{8\tau_0} + \frac{\pi(3 + 5\tau_0)}{24\tau_0}\delta + \mathcal{O}(\delta^2)\,, \qquad (4.41)$$

with

$$\tilde{Q}_x = Q_x - Q_x^{st} = \frac{\pi\tau_0}{2\delta}\left(1 - \frac{2\delta}{\pi} + \frac{\delta^2}{6} + O(\delta^3)\right)\,. \qquad (4.42)$$

Inverting this series we obtain

$$\delta = \frac{\pi\tau_0}{2\tilde{Q}_x} - \frac{\pi\tau_0^2}{2\tilde{Q}_x^2} + \frac{\pi(24 + \pi^2)\tau_0^3}{48\tilde{Q}_x^3} + O(\tilde{Q}_x^{-4})\,, \qquad (4.43)$$

which finally leads to

$$G(q_x, 0) = \frac{q_x}{T_0} - \frac{\pi^2}{8} + \frac{\pi^2(1 + \tau_0)T_1}{16q_x} + O(q_x^{-2})\,, \qquad (4.44)$$

In order to find the behavior for $-q_x$ we employ the Gallavotti-Cohen relation $G(\mathbf{q}) - G(-\mathbf{q}) = 2|\varepsilon|q_x$:

$$G(-q_x, 0) = \frac{q_x}{T_1} - \frac{\pi^2}{8} + \frac{\pi^2(1 + \tau_0)T_1}{16q_x} + O(q_x^{-2})\,, \quad q_x > 0\,. \qquad (4.45)$$

This implies in particular that large current fluctuations along the gradient direction decay exponentially in the current, rather than in a Gaussian manner as a naive central-limit analysis would suggest. Note also that the asymptotic slopes of $G(q_x, 0)$ for positive and negative values of the currents q_x are just the inverse temperatures of the left and right reservoirs, respectively.

The second limit, $(q_x = 0, |\boldsymbol{q}_\perp| \gg 0)$, corresponds to $k^2 \to 1$ and $F_0 \to \pi/2$, leading to

$$G(0, |\boldsymbol{q}_\perp|) = \frac{1}{8}\left(F_0 + F_1\right)^2\,, \qquad (4.46)$$

with

$$Q_x = 0\,, \quad Q_\perp = \cosh F_1(\tanh F_0 + \tanh F_1)/2\,, \quad \tau_0 = \cosh F_1/\cosh F_0\,. \qquad (4.47)$$

Expanding these expressions for large values of $|\boldsymbol{q}_\perp|$, we obtain the following
asymptotic form for the LDF

$$G(0, |\boldsymbol{q}_\perp|) = \frac{1}{8} \ln \left(\frac{4|\boldsymbol{q}_\perp|^2 T_1^3}{T_0} \right) \left[\ln \left(\frac{4|\boldsymbol{q}_\perp|^2 T_1^3}{T_0} \right) + \frac{1 + \tau_0^2}{T_1^2 |\boldsymbol{q}_\perp|^2} + O(|\boldsymbol{q}_\perp|^{-4}) \right].$$

(4.48)

This result is even more relevant, since it shows that the statistics of large current
fluctuations *orthogonal* to the thermal gradient exhibit a remarkable logarithmic
behaviour, which makes these rare fluctuations much more probable than antici-
pated within the Gaussian approximation. This interesting behaviour points out
once again to the complex analytic behavior of the heat current LDF, in contrast
with the apparent smooth and simple structure shown in Fig. 4.3 for moderate
current fluctuations.

4.5.3 Cumulants of the heat current distribution

Finally, we proceed to compute the first low-order cumulants of the heat current
distribution. With this aim in mind, we calculate the scaled cumulant generating
function (sCGF) $\mu(\boldsymbol{\lambda})$ of such a probability distribution (see Section 2.4.2):

$$\mu(\boldsymbol{\lambda}) = \lim_{\tau \to \infty} \frac{1}{\tau \Omega} \ln \langle e^{-\tau \Omega \boldsymbol{\lambda} \cdot \boldsymbol{q}} \rangle.$$

(4.49)

Thus, considering the form of $G(\mathbf{q})$ near the stationary state (4.38) and that, as
we have shown (see Eq. (2.60)), both LDF and sCGF are related via a Legendre-
Fenchel transform [19, 24, 37], the sCGF can be expanded as

$$
\begin{aligned}
\mu(\boldsymbol{\lambda}) &= \frac{1}{2}(T_0 - T_1)\lambda_x + (\lambda_x^2 + \boldsymbol{\lambda}_\perp^2) \left[\frac{1}{6}(T_0^2 + T_0 T_1 + T_1^2) \right. \\
&+ \frac{1}{45}(T_0 - T_1)(4T_0^2 + 7T_0 T_1 + 4T_1^2)\lambda_x \\
&+ \frac{9}{1890}(12T_0^4 + 8T_0^3 T_1 - 5T_0^2 T_1^2 + 8T_0 T_1^3 + 12T_1^4)\lambda_x^2 \\
&+ \frac{1}{1890}(44T_0^4 + 76T_0^3 T_1 + 75T_0^2 T_1^2 + 76T_0 T_1^3 + 44T_1^4)\boldsymbol{\lambda}_\perp^2 \left. \right] \\
&+ \mathcal{O}(\boldsymbol{\lambda}^5),
\end{aligned}
$$

(4.50)

where we have decomposed $\boldsymbol{\lambda} = (\lambda_x, \boldsymbol{\lambda}_\perp)$ along the gradient (λ_x) and all or-
thogonal ($\boldsymbol{\lambda}_\perp$) directions. We are now in position to compute the lower-order
cumulants by differentiating with respect to the components of the $\boldsymbol{\lambda}$-vector, see

Eq. (2.62). The first derivatives yield the steady state value of the current components, $\langle q_x \rangle = q_x^{\text{st}} = (T_0 - T_1)/2$ and $\langle \boldsymbol{q}_\perp \rangle = 0$. The next few cumulants for arbitrary boundary temperatures T_0 and T_1 compatible with the perturbation expansions ($\tau_0 > 1$) can be written as

$$
\begin{aligned}
\lim_{\tau \to \infty} \tau \Omega \langle (q_s - q_s^{\text{st}})^2 \rangle &= \frac{1}{3}(T_0^2 + T_0 T_1 + T_1^2) \\
\lim_{\tau \to \infty} (\tau \Omega)^2 \langle (q_x - q_x^{\text{st}})^3 \rangle &= \frac{2}{15}(T_0 - T_1)(4T_0^2 + 7T_0 T_1 + 4T_1^2) \\
\lim_{\tau \to \infty} (\tau \Omega)^2 \langle (q_x - q_x^{\text{st}}) q_\alpha^2 \rangle &= \frac{2}{45}(T_0 - T_1)(4T_0^2 + 7T_0 T_1 + 4T_1^2) \\
\lim_{\tau \to \infty} (\tau \Omega)^3 \langle (q_x - q_x^{\text{st}})^4 \rangle &= \frac{4}{35}(12T_0^4 + 8T_0^3 T_1 - 5T_0^2 T_1^2 + 8T_0 T_1^3 + 12T_1^4) \\
\lim_{\tau \to \infty} (\tau \Omega)^3 \langle (q_x - q_x^{\text{st}})^2 q_\alpha^2 \rangle &= \frac{2}{945}(76T_0^4 + 74T_0^3 T_1 + 15T_0^2 T_1^2 + 74T_0 T_1^3 \\
&\quad + 76T_1^4) \\
\lim_{\tau \to \infty} (\tau \Omega)^3 \langle q_\alpha^4 \rangle &= \frac{4}{315}(44T_0^4 + 76T_0^3 T_1 + 75T_0^2 T_1^2 + 76T_0 T_1^3 \\
&\quad + 44T_1^4) \\
\lim_{\tau \to \infty} (\tau \Omega)^3 \langle q_\alpha^2 q_\beta^2 \rangle &= \frac{4}{945}(44T_0^4 + 76T_0^3 T_1 + 75T_0^2 T_1^2 + 76T_0 T_1^3 \\
&\quad + 44T_1^4),
\end{aligned}
\tag{4.51}
$$

where $s \in [1, d]$ and $\alpha \neq \beta$ corresponding to any pair of different coordinates in the subspace orthogonal to x. Interestingly, remarkable relations between different cumulants can be now derived from (4.51). In particular

$$
\begin{aligned}
3 \lim_{\tau \to \infty} \tau^2 \langle (q_x - q_x^{\text{st}}) q_\alpha^2 \rangle &= \lim_{\tau \to \infty} \tau^2 \langle (q_x - q_x^{\text{st}})^3 \rangle \\
3 \lim_{\tau \to \infty} \tau^3 \langle q_\alpha^2 q_\beta^2 \rangle &= \lim_{\tau \to \infty} \tau^3 \langle q_\alpha^4 \rangle.
\end{aligned}
\tag{4.52}
$$

Indeed, recalling the definition (4.12) of the empirical current vector $\mathbf{q}$, these equations establish interesting and unforeseeing integral relations between different n-point correlators of the current field [18] for arbitrary values of the driving thermal baths T_0 and T_1.

4.6 Conclusions

In summary, we have delved into the heat current statistics of an incompressible quiescent d-dimensional fluid subject to a boundary temperature gradient in one

direction. This analysis has been carried out within the framework of fluctuating hydrodynamics, using tools borrowed from large deviation theory and macroscopic fluctuation theory. This framework provides powerful techniques to determine the full heat current probability distribution, based on the computation of the most probable trajectories and the current large deviation function. In this way, under the well-established additivity conjecture (which considers the optimal paths sustaining atypical values of the current to be time-independent), we have determined the explicit form of the most probable temperature fields. We have analyzed their topological properties as a function of the external baths temperatures (T_0, T_1) and the desired empirical current $\mathbf{q}$, defining different regimes where temperature profiles exhibit varying behaviors. Interestingly, our solution to the fluctuation problem shows that optimal temperature fields can be naturally classified in an infinite set of curves, each set sharing the same mathematical structure, parametrized in terms of the modulus k of a Jacobi inverse elliptic function.

Such characterization of the optimal temperature fields opens the door to the computation of the full heat current probability distribution, as codified in the current large deviation function. In particular, we have obtained the exact analytical form of the heat current LDF, analyzing its behavior both for small fluctuations around the nonequilibrium steady state, and in the far tails of the distribution. We observe that near the stationary state corrections to Gaussian behavior are small, and the heat current distribution can be well approximated by a deformed Gaussian along all directions. On the other hand, the behavior of current LDF for large values of the current is far more complex, pointing out to the intricateness of fluctuations far from equilibrium. In particular, we find remarkable logarithmic tails in the current LDF for large fluctuations orthogonal to the thermal gradient, showing that these fluctuations are far more probable than previously anticipated. Finally, reformulating the statistical problem in terms of the associated cumulant generating function, we have obtained analytic formulas for the first few cumulants of the heat current distribution. These results allow us to find remarkable new relations between some of this cumulants, which imply integral relations between different correlators of the heat current field. This finding opens the door to further experimental research to test these results, as the lower-order cumulants of the empirical heat current can be readily measured in actual experiments.

Chapter 5

Order and symmetry-breaking in the fluctuations of driven systems

5.1 Introduction

The theory of critical phenomena is a cornerstone of modern theoretical physics [236, 237]. Indeed, phase transitions of all sorts appear ubiquitously in most domains of physics, from cosmological scales to the quantum world of elementary particles. As we have shown in Section 2.5.4, in a typical 2nd-order phase transition order emerges *continuously* at some critical point, as captured by an order parameter, signaling the spontaneous breaking of a symmetry and an associated non-analyticity of the relevant thermodynamic potential. Conversely, 1st-order transitions are characterized by an *abrupt* jump in the order parameter and a co-existente of different phases [236, 237]. In the last years, a number of works has brought to light the existence of dynamical phase transitions at a fluctuating level in many different situations where the previous features and elements typical from standard critical behaviour have been now analyzed. When considering the large-deviation scaling of the stationary distribution in the weak-noise (large Ω) limit, the appearance of dynamical phase transitions as singularities (non-differentiabilities) in the quasi-potential of non-equilibrium dynamics has been observed [238–240]. Another type of DPTs has been reported when conditioning a system to have a fixed value (typical or rare) of some time-integrated observable, as e.g. the current or the activity [16–18, 41, 52, 55–59, 61, 62, 88, 177–179, 181–196, 241, 242]. These class of DPTs are the ones we are interested in. In this case, the different dynamical phases then correspond to different types of trajectories adopted by the system to sustain atypical values of this observable and the points at which the

transition between them takes place corresponds to non-analicity of the associated large deviation funcion. In this scheme, events such as the spontaneous breaking of a symmetry, dynamical phase coexistence or emergence of ordered structures enhancing the probability of observing a given fluctuation [18, 60] appear, opening the door to the discovery of a whole new, rich and complex phenomenology.

Apart from their conceptual importance, DPTs has acquired great relevance in practical situations. As we have seen in Introduction, recent breakthroughs have shown that fluctuations admit a control-theory (or active) interpretation [16, 75, 243]: among the external control fields that drive the system to the desired fluctuation, the one minimizing the dissipated energy is univocally related to the typical trajectory for the spontaneous emergence of such fluctuation [16]. In this way, a DPT at the trajectory level corresponds to a singular change in the optimal control field, and this can be observed in actual experiments. However, up to now most works on DPTs have focused on toy $1d$ models [18, 56–59, 62, 179, 181–185] or fluctuations of *scalar* ($1d$) observables in $d > 1$ [61, 186–194, 242], and the goal is to understand DPTs in the fluctuations of fully vectorial observables in d-dimensions and how they are affected by the (possible) system anisotropy for realistic $d > 1$ systems amenable to control for technological applications

In this chapter we address this challenge and report compelling evidences of a rich DPT and new physics in the statistics of vectorial currents in an archetypal $2d$ driven diffusive system, the weakly asymmetric simple exclusion process (WASEP) [244]. To crack this problem, we use massive cloning Monte Carlo simulations for rare event statistics [153–155], together with macroscopic fluctuation theory (MFT) to understand the fluctuation phase diagram [16]. We find a 2nd-order DPT between a homogeneous fluctuation phase with structureless trajectories and Gaussian current statistics, and a symmetry-broken non-Gaussian phase for small currents characterized by the emergence of coherent jammed states in the form of traveling-wave trajectories. Such jammed states, which are surprisingly extended and non-compact, hamper particle flow enhancing the probability of low-current fluctuations [57]. Interestingly, for mild or no anisotropy different symmetry-broken phases appear depending on the current separated by lines of 1st-order DPTs, a degeneracy which disappears beyond a critical anisotropy. Dynamical coexistence of the different traveling-wave phases appears along these 1st-order lines.

The chapter is organized as follows. In Section 5.2 we will study the vectorial current fluctuations in arbitrary periodic driven diffusive systems under the scheme of MFT. We will observe that for small fluctuations, the most probable paths are constant and homogeneus. We will deduce that such optimal profiles become un-

stable for low values of the current pointing out the existence of a dynamical phase transitions. Furthermore, we will show that the optimal trajectories minimizing the action inmediately after the transtion line present a traveling-wave structure, and we will characterize its properties. In Section 5.3, we will particularize these results to the 2d-WASEP. We will present the dynamical phase diagram the system exhibits at a fluctuating level. Moreover, we will study the nature of the different DPTs, finding non-analiticities of both 1$^{\text{st}}$- and 2$^{\text{nd}}$-order in the sCGF. Finally, in Section 5.4 we will compare this theoretical scheme with numerical results obtained from extensive cloning simulations. We will observe how the sCGF beyond the transition line deviates from the quadratic behaviour typical of Gaussian fluctuations and converges to the MFT predictions on the dynamical free energy in the symmetry-broken phase. Finally, to fully understand this 2$^{\text{nd}}$-order phase transition and its associated symmetry-breaking, we will define a microscopic order parameter which will characterize the behaviour of the system beyond the critical line.

5.2 Current fluctuations in periodic driven diffusive systems

We aim to analyze the equations of macroscopic fluctuation theory for the current vector statistics of arbitrary driven diffusive systems, with special emphasis on the MFT predictions regarding the existence and nature of dynamic phase transitions in some regimes of current fluctuations. In this way, our system of interest is the d-dimensional anisotropic driven diffusive system characterized by the (locally-conserved) particle density field $\rho(\mathbf{r}, t)$, with $\mathbf{r} \in \Lambda \equiv [0, 1]^d$ and $t \in [0, \tau]$. As we have studied in Section 2.2.1, its evolution is govern by the Langevin equation[1]

$$\partial_t \rho(\mathbf{r}, t) + \boldsymbol{\nabla} \cdot \left(-\hat{D}[\rho] \boldsymbol{\nabla} \rho(\mathbf{r}, t) + \hat{\sigma}(\rho) \mathbf{E} + \boldsymbol{\xi}(\mathbf{r}, t) \right) = 0 \,, \qquad (5.1)$$

with $\mathbf{E}$ the external field driving the system out of equilibrium, and where the field $\mathbf{j}(\mathbf{r}, t) \equiv -\hat{D}[\rho] \boldsymbol{\nabla} \rho(\mathbf{r}, t) + \hat{\sigma}(\rho) \mathbf{E} + \boldsymbol{\xi}(\mathbf{r}, t)$ is the fluctuating current. Following the scheme exposed in Section 3.2, both $\hat{D}[\rho] \equiv D[\rho]\hat{\mathcal{A}}$ and $\hat{\sigma}(\rho) = \sigma[\rho]\hat{\mathcal{A}}$ are the diffusivity and mobility matrices, respectively, related via the local Einstein relation, with $\hat{\mathcal{A}}$ a diagonal anisotropy matrix with components $\hat{\mathcal{A}}_{\alpha\beta} = a_\alpha \delta_{\alpha\beta}$, $\alpha, \beta \in [1, d]$. The term $\boldsymbol{\xi}(\mathbf{r}, t)$ is a Gaussian white noise with average and variance given by (3.2)-(3.3), where in this case $\phi(\mathbf{r}, t) = \rho(\mathbf{r}, t)$. Finally, to completely

---

[1]Once again, to facilitate reading we recall some concepts already presented in previous chapters.

define the problem, the evolution equation (5.1) must be supplemented with appropriate boundary conditions, which in this situation are simply periodic along all d directions, i.e.

$$\rho(\mathbf{r} + \hat{\boldsymbol{e}_i}, t) = \rho(\mathbf{r}, t), \quad \forall i \in [1, d], \tag{5.2}$$

with $\hat{\boldsymbol{e}_i}$ the already presented canonical unit vectors.

We are now in position to study the current distribution under the framework of MFT. Indeed, proceeding as in Section 2.4.2, the probability of observing a given trajectory $\{\rho(\mathbf{r}, t), \mathbf{j}(\mathbf{r}, t)\}_0^\tau$ can be writen as

$$\mathbb{P}\left(\{\rho, \mathbf{j}\}_0^\tau\right) \asymp \exp\left(-\Omega \mathcal{S}_\tau\left[\rho, \mathbf{j}\right]\right), \tag{5.3}$$

with

$$
\begin{aligned}
\mathcal{S}_\tau\left[\rho, \mathbf{j}\right] &= \int_0^\tau dt \int_\Lambda d\mathbf{r} \frac{1}{2\sigma[\rho]} \left(\mathbf{j} + D[\rho]\hat{\mathcal{A}}\boldsymbol{\nabla}\rho - \sigma[\rho]\hat{\mathcal{A}}\mathbf{E}\right) \\
&\qquad \cdot \hat{\mathcal{A}}^{-1} \left(\mathbf{j} + D[\rho]\hat{\mathcal{A}}\boldsymbol{\nabla}\rho - \sigma[\rho]\hat{\mathcal{A}}\mathbf{E}\right),
\end{aligned}
\tag{5.4}
$$

and where the fields $\rho(\mathbf{r}, t)$ and $\mathbf{j}(\mathbf{r}, t)$ are coupled via the continuity equation (see Eq. (5.1))

$$\partial_t \rho(\mathbf{r}, t) + \boldsymbol{\nabla} \cdot \mathbf{j}(\mathbf{r}, t) = 0. \tag{5.5}$$

Interestingly, for any other trajectory not obeying (5.5), $\mathcal{S}_\tau\left[\rho, \mathbf{j}\right] \to \infty$. At this point, an additional constraint (already introduced in Section 3.4.2) needs to be imposed as a consequence of considering the boundary conditions to be periodic. Indeed, the system of interest is now isolated so the total mass is conserved, leading to:

$$\rho_0 = \int_\Lambda d\mathbf{r}\, \rho(\mathbf{r}, t). \tag{5.6}$$

Therefore, the probability $P_\tau(\mathbf{q})$ of observing a space- and time-averaged empirical current vector $\mathbf{q}$, defined as

$$\mathbf{q} = \frac{1}{\tau} \int_0^\tau dt \int_\Lambda d\mathbf{r}\, \mathbf{j}(\mathbf{r}, t), \tag{5.7}$$

scales for long times as $P_\tau(\mathbf{q}) \asymp \exp[-\tau\Omega G(\mathbf{q})]$, and the current large deviation function $G(\mathbf{q})$ can be related to $\mathcal{S}_\tau[\rho, \mathbf{j}]$ via a simple saddle-point calculation in the long-time limit,

$$G(\mathbf{q}) = \lim_{\tau \to \infty} \left\{ \frac{1}{\tau} \min_{\{\rho, \mathbf{j}\}_0^\tau} \mathcal{S}_\tau[\rho, \mathbf{j}] \right\}, \tag{5.8}$$

subjected to constraints (5.5), (5.6) and (5.7)[2] The optimal paths $\rho_{\mathbf{q}}(\mathbf{r}, t)$, $\mathbf{j}_{\mathbf{q}}(\mathbf{r}, t)$ solution of (5.8) may be in general time-dependent, and, as we have seen, the associated general variational problem is remarkably hard.

5.2.1 Uniform optimal fields and local stability analysis

The problem (5.8) becomes simpler however in different limiting cases. For instance, in the steady state the system exhibits translation symmetry with an homogeneous stationary density profile $\rho_{\mathrm{st}}(\mathbf{r}) = \rho_0$ and a constant average current $\mathbf{j}_{\mathrm{st}}(\mathbf{r}) = \langle \mathbf{q} \rangle = \sigma_0 \hat{A} \mathbf{E}$, where we have defined $\sigma_0 \equiv \sigma[\rho_0]$. Now, one can argue that small fluctuations of the empirical current $\mathbf{q}$ away from the average behavior $\langle \mathbf{q} \rangle$ will typically result from weakly-correlated local events in different parts of the system which add up incoherently to yield the desired $\mathbf{q}$, so the most probable trajectories associated to these small fluctuations are still homogeneus and time-independent, as the stationary ones [41, 56]. Thus, according to Eqs. (5.6) and (5.7), the optimal density and current fields takes the form:

$$\rho_{\mathbf{q}}(\mathbf{r}, t) = \rho_0 \quad \mathbf{j}_{\mathbf{q}}(\mathbf{r}, t) = \mathbf{q}, \tag{5.9}$$

for $|\mathbf{q} - \langle \mathbf{q} \rangle| \ll 1$, leading to a quadratic current LDF corresponding to Gaussian current statistics,

$$G_{\mathrm{G}}(\mathbf{q}) = \frac{1}{2\sigma_0} \left(\mathbf{q} - \sigma_0 \hat{A} \mathbf{E} \right) \cdot \hat{A}^{-1} \left(\mathbf{q} - \sigma_0 \hat{A} \mathbf{E} \right), \tag{5.10}$$

as it was predicted by Central Limit Theorem. Indeed, this result has been corroborated in simulations for a broad range of $\mathbf{q}$'s [52]. As an interesting by-product, note that current fluctuations in this Gaussian regime obey an anisotropic version of the Isometric Fluctuation Theorem [46, 67, 70], which links in simple terms the probability of two different but $\hat{A}$-isometric current vector fluctuations (see Section 2.5.3). In particular,

$$\lim_{\tau \to \infty} \frac{1}{\tau \Omega} \ln \left[\frac{P_\tau(\mathbf{q})}{P_\tau(\mathbf{q}')} \right] = \mathbf{E} \cdot (\mathbf{q} - \mathbf{q}'), \tag{5.11}$$

$\forall \mathbf{q}, \mathbf{q}'$ in the Gaussian regime such that $\mathbf{q} \cdot \hat{A} \mathbf{q} = \mathbf{q}' \cdot \hat{A} \mathbf{q}'$.

The above ansatz with the associated *flat* profiles remains a solution of the full variational problem (5.8) for all $\mathbf{q}$, but the question remains as to whether other solutions with more complex spatiotemporal structure may yield a better minimizer

---

[2]Note that this problem is equivalent to define a modified action by introducing constraints (5.5), (5.6) and (5.7) with the corresponding Lagrange multipliers, as we have done in previous chapters.

of the MFT action (5.4) for certain values of the current. To address this question, we now perturb the above flat solution with small but otherwise arbitrary functions of space and time, and study the local stability of the homogeneous solution against such perturbations. In particular, we ask whether the perturbed fields yield in some case a smaller $G(\mathbf{q})$. With this aim in mind, we write

$$\bar{\rho}(\mathbf{r},t) = \rho_0 + \delta\rho(\mathbf{r},t), \quad \bar{\mathbf{j}}(\mathbf{r},t) = \mathbf{q} + \delta\mathbf{j}(\mathbf{r},t), \tag{5.12}$$

where both $\bar{\rho}(\mathbf{r},t)$ and $\bar{\mathbf{j}}(\mathbf{r},t)$ remain constrained by Eqs. (5.5), (5.6) and (5.7). Inserting these expressions in Eq. (5.8) and expanding to second order in the perturbations, we obtain the leading correction to the quadratic form $G_{\mathrm{G}}(\mathbf{q})$ of Eq. (5.10), denoted here by $O2$:

$$
\begin{aligned}
O2 &= \frac{1}{2\tau} \int_0^\tau dt \int_\Lambda d\mathbf{r} \left\{ A(\rho_0, \mathbf{q})\delta\rho^2 + \boldsymbol{\nabla}\delta\rho \cdot \hat{B}(\rho_0)\boldsymbol{\nabla}\delta\rho + \delta\mathbf{j} \cdot \hat{C}(\rho_0)\delta\mathbf{j} \right. \\
&\quad + \left. \delta\mathbf{j} \cdot \mathbf{F}(\rho_0, \mathbf{q})\delta\rho \right\},
\end{aligned}
\tag{5.13}
$$

where we have defined

$$A(\rho_0, \mathbf{q}) = \left(\frac{\sigma_0'^2}{\sigma_0^3} - \frac{\sigma_0''}{2\sigma_0^2} \right) \mathbf{q} \cdot \hat{\mathcal{A}}^{-1}\mathbf{q} + \sigma_0''\mathbf{E} \cdot \hat{\mathcal{A}}\mathbf{E},$$

$$\hat{B}(\rho_0) = \frac{D_0^2}{\sigma_0}\hat{\mathcal{A}}, \quad \hat{C}(\rho_0) = \frac{\hat{\mathcal{A}}^{-1}}{\sigma_0}, \quad \mathbf{F}(\rho_0, \mathbf{q}) = -\frac{\sigma_0'}{\sigma_0^2}\hat{\mathcal{A}}^{-1}\mathbf{q}, \tag{5.14}$$

with $'$ denoting derivative with respect to the argument, and $D_0 \equiv D[\rho_0]$. We next expand the perturbations $\delta\rho(\mathbf{r},t)$ and $\delta\mathbf{j}(\mathbf{r},t)$ in Fourier series, taking advantage of the spatial periodic boundary conditions, and imposing explicitly along the way the constraints (5.5), (5.6) and (5.7). For simplicity we particularize hereafter our results for dimension two, $d = 2$, though the generalization to arbitrary d is straightforward. In this way, perturbations take the form[3]

$$\delta\rho(\mathbf{r},t) = \sum_\nu \frac{1}{\nu}\left[-\boldsymbol{\nabla} \cdot \boldsymbol{\gamma}_{1,\nu}(\mathbf{r})\sin(\nu t) + \boldsymbol{\nabla} \cdot \boldsymbol{\gamma}_{2,\nu}(\mathbf{r})\cos(\nu t) \right], \tag{5.15}$$

$$\delta\mathbf{j}(\mathbf{r},t) = \sum_\nu \left[\boldsymbol{\gamma}_{1,\nu}(\mathbf{r})\cos(\nu t) + \boldsymbol{\gamma}_{2,\nu}(\mathbf{r})\sin(\nu t) \right], \tag{5.16}$$

---

[3]Note that the form of the density and current fields at initial and final times are not fixed. Consequently, we use the complete Fourier basis $\{\sin(\nu t), \cos(\nu t)\}$ in the expansions of the perturbations.

where the first equation follows from the second expansion after imposing the continuity constraint (5.5), with

$$
\begin{aligned}
\boldsymbol{\gamma}_{1,\nu}(\mathbf{r}) \;=\;& \frac{1}{4}\mathbf{a}_{\nu00} + \frac{1}{2}\sum_{k_1 \neq 0}\left(\mathbf{a}_{\nu k_1 0}\cos k_1 x + \mathbf{c}_{\nu k_1 0}\sin k_1 x\right) \\
& + \;\frac{1}{2}\sum_{k_2 \neq 0}\left(\mathbf{a}_{\nu 0 k_2}\cos k_2 y + \mathbf{b}_{\nu 0 k_2}\sin k_2 y\right) \\
& + \;\sum_{k_1, k_2 \neq 0}\left(\mathbf{a}_{\nu k_1 k_2}\cos k_1 x\cos k_2 y + \mathbf{b}_{\nu k_1 k_2}\cos k_1 x\sin k_2 y\right. \\
& + \;\left.\mathbf{c}_{\nu k_1 k_2}\sin k_1 x\cos k_2 y + \mathbf{d}_{\nu k_1 k_2}\sin k_1 x\sin k_2 y\right) \qquad (5.17)
\end{aligned}
$$

$$
\begin{aligned}
\boldsymbol{\gamma}_{2,\nu}(\mathbf{r}) \;=\;& \frac{1}{4}\mathbf{s}_{\nu00} + \frac{1}{2}\sum_{k_1 \neq 0}\left(\mathbf{s}_{\nu k_1 0}\cos k_1 x + \mathbf{u}_{\nu k_1 0}\sin k_1 x\right) \\
& + \;\frac{1}{2}\sum_{k_2 \neq 0}\left(\mathbf{s}_{\nu 0 k_2}\cos k_2 y + \mathbf{t}_{\nu 0 k_2}\sin k_2 y\right) \\
& + \;\sum_{k_1, k_2 \neq 0}\left(\mathbf{s}_{\nu k_1 k_2}\cos k_1 x\cos k_2 y + \mathbf{t}_{\nu k_1 k_2}\cos k_1 x\sin k_2 y\right. \\
& + \;\left.\mathbf{u}_{\nu k_1 k_2}\sin k_1 x\cos k_2 y + \mathbf{v}_{\nu k_1 k_2}\sin k_1 x\sin k_2 y\right) \qquad (5.18)
\end{aligned}
$$

where $\mathbf{a}_{\nu ij}$, $\mathbf{b}_{\nu ij}$, $\mathbf{c}_{\nu ij}$, $\mathbf{d}_{\nu ij}$, $\mathbf{s}_{\nu ij}$, $\mathbf{t}_{\nu ij}$, $\mathbf{u}_{\nu ij}$, $\mathbf{v}_{\nu ij}$ are the coefficients of the Fourier series. Remarkably, the previous expansion has been divided into first the only-temporal modes, then all $1+1$ spatiotemporal modes along each direction of space, and finally the fully $2 + 1$ spatiotemporal modes. The $O2$ correction (5.13) is of course a quadratic form of the perturbations with constant coefficients, which, together with the orthonormality properties of Fourier basis, imply that the different Fourier modes decouple simplifying the problem. In this way the stability analysis melts down as usual to an eigenvalue problem, which in this case splits into different problems for only temporal modes, spatiotemporal modes with structure along just one dimension, x or y, and $2d$ spatiotemporal modes, which can be analyzed separately. This straightforward but lengthy calculation leads to the following conclusion: the flat solution corresponding to Gaussian current statistics remains stable (i.e. the $O2$ correction is positive) whenever the following condi-

tions hold,

$$a_{\min}k_n^2 \frac{D_0^2}{\sigma_0} \quad + \quad H(\mathbf{E}, \mathbf{q}) > 0$$

$$a_{\max}k_m^2 \frac{D_0^2}{\sigma_0} \quad + \quad H(\mathbf{E}, \mathbf{q}) > 0 \tag{5.19}$$

$$\left(a_{\min}k_n^2 + a_{\max}k_m^2\right) \frac{D_0^2}{\sigma_0} \quad + \quad H(\mathbf{E}, \mathbf{q}) > 0,$$

with $k_n = 2\pi n$ and $k_m = 2\pi m$ the different spatial modes associated to each perturbation along either direction, $a_{\min} = \min\{a_\alpha, \alpha \in [1, d]\}$ and $a_{\max} = \max\{a_\alpha, \alpha \in [1, d]\}$, and

$$H(\mathbf{E}, \mathbf{q}) = \frac{\sigma_0''}{2} \left(\mathbf{E} \cdot \hat{\mathcal{A}}\mathbf{E} - \sigma_0^{-2}\mathbf{q} \cdot \hat{\mathcal{A}}^{-1}\mathbf{q}\right) \tag{5.20}$$

A number of important conclusions can be directly derived from this set of conditions, namely:

  (i) The first mode to become unstable (if any) is always the fundamental mode $k_1 = 2\pi$.

  (ii) For any value of the anisotropy, the first perturbations to become unstable are those with structure along one spatial dimension, x or y.

  (iii) For anisotropic systems, $a_{\min} < a_{\max}$, the leading unstable perturbation has structure in the direction of minimum anisotropy.

  (iv) For isotropic systems, $a_{\min} = a_{\max} \equiv a$, both one-dimensional perturbations trigger the instability of the flat solution at the same point. In this case, the orientation of the current vector $\mathbf{q}$ determines the most probable profile immediately after the instability kicks in, with structure only along the x- or y-direction, as dictated by the term proportional to $\mathbf{F}(\rho_0, \mathbf{q})$ in the $O2$ correction, see Eq. (5.13).

Therefore there exists a line of critical values for the current $\mathbf{q}_c$ at which the instability appears, given by

$$\mathbf{q}_c \cdot \hat{\mathcal{A}}^{-1}\mathbf{q}_c = \sigma_0^2 \Xi_c, \tag{5.21}$$

where

$$\Xi_c \equiv \left(\mathbf{E} \cdot \hat{\mathcal{A}}\mathbf{E} + 8\pi^2 a_{\min} \frac{D_0^2}{\sigma_0 \sigma_0''}\right) \tag{5.22}$$

For systems with $\sigma_0'' > 0$ (as e.g. the Kipnis-Marchioro-Presutti model of heat transport [18,46,126]), the instability appears always, regardless of the value of the external field (even for $\mathbf{E} = 0$), separating a regime of Gaussian current statistics for $\mathbf{q} \cdot \hat{\mathcal{A}}^{-1}\mathbf{q} \leq \sigma_0^2 \Xi_c$ and a non-Gaussian region for $\mathbf{q} \cdot \hat{\mathcal{A}}^{-1}\mathbf{q} > \sigma_0^2 \Xi_c$. On the other hand, for systems with $\sigma_0'' < 0$ (as the weakly asymmetric simple exclusion process, WASEP, that we will study in this chapter [41,57,244]) a line of critical values of the external field exists, defined by

$$\mathbf{E}_c \cdot \hat{\mathcal{A}}\mathbf{E}_c = 8\pi^2 a_{\min}\frac{D_0^2}{\sigma_0|\sigma_0''|} \equiv |\Sigma_c| \,. \tag{5.23}$$

beyond which the instability appears, $\mathbf{E} \cdot \hat{\mathcal{A}}\mathbf{E} \geq |\Sigma_c|$. In this strong field case, Gaussian statistics are expected for all currents except for a region around $\mathbf{q} = 0$, defined by $\mathbf{q} \cdot \hat{\mathcal{A}}^{-1}\mathbf{q} \leq \sigma_0^2 \Xi_c$, where current fluctuations are non-Gaussian[4]. For weak external fields, $\mathbf{E} \cdot \hat{\mathcal{A}}\mathbf{E} < |\Sigma_c|$, only Gaussian statistics are observed. Consequently, the existence of the instability reveals the fact that a dynamical phase transition is taken place along this line.

Whenever the instability emerges, the first two frequencies to become unstable are

$$\nu_c^{\pm} = \pm 2\pi q_{\parallel}\frac{\sigma_0'}{\sigma_0} \,, \tag{5.24}$$

with $q_{\parallel}$ the component of the current vector along the direction of structure formation (that we denote here as $x_{\parallel}$). Considering that the first unstable spatial mode correspond to $k_{\perp} = 0$, $k_{\parallel} = 2\pi$, the resulting leading perturbations simplify to

$$
\begin{aligned}
\delta\rho_{\pm}(\mathbf{r}, t) &= \frac{\pi}{\nu_c^{\pm}}\left(a_{\nu_c^{\pm}01}^{(2)}\sin 2\pi x_{\parallel} - b_{\nu_c^{\pm}01}^{(2)}\cos 2\pi x_{\parallel}\right)\sin\nu_c^{\pm}t \\
&+ \left(-s_{\nu_c^{\pm}01}^{(2)}\sin 2\pi x_{\parallel} + t_{\nu_c^{\pm}01}^{(2)}\cos 2\pi x_{\parallel}\right)\cos\nu_c^{\pm}t
\end{aligned}
\tag{5.25}
$$

$$
\begin{aligned}
\delta\mathbf{j}_{\pm}(\mathbf{r}, t) &= \frac{1}{2}\left(\mathbf{a}_{\nu_c^{\pm}01}\cos 2\pi x_{\parallel} + \mathbf{b}_{\nu_c^{\pm}01}\sin 2\pi x_{\parallel}\right)\cos\nu_c^{\pm}t \\
&+ \left(\mathbf{s}_{\nu_c^{\pm}01}\cos 2\pi x_{\parallel} + \mathbf{t}_{\nu_c^{\pm}01}\sin 2\pi x_{\parallel}\right)\sin\nu_c^{\pm}t
\end{aligned}
\tag{5.26}
$$

with

$$
\begin{aligned}
\mathbf{a}_{\nu_c^{\pm}01} &= (a_{\nu_c^{\pm}01}^{(1)}, a_{\nu_c^{\pm}02}^{(2)}), \quad \mathbf{b}_{\nu_c^{\pm}01} = (b_{\nu_c^{\pm}01}^{(1)}, b_{\nu_c^{\pm}02}^{(2)}), \\
\mathbf{s}_{\nu_c^{\pm}01} &= (s_{\nu_c^{\pm}01}^{(1)}, s_{\nu_c^{\pm}02}^{(2)}), \quad \mathbf{t}_{\nu_c^{\pm}01} = (t_{\nu_c^{\pm}01}^{(1)}, t_{\nu_c^{\pm}02}^{(2)}),
\end{aligned}
\tag{5.27}
$$

[4]Note that the sign of σ_0'' is a crucial element to fully undertstand the phenomenology associated to this analysis. Indeed, for $\sigma_0'' > 0$ the non-Gaussian region appears above the critical line $\mathbf{q} \cdot \hat{\mathcal{A}}^{-1}\mathbf{q} > \sigma_0^2 \Xi_c$, while for $\sigma_0'' < 0$ the situation is reversed and the non-Gaussian region takes place (if any) below the critical line $\mathbf{q} \cdot \hat{\mathcal{A}}^{-1}\mathbf{q} < \sigma_0^2 \Xi_c$.

the coefficients of the Fourier series corresponding to that mode. Introducing these perturbations in (5.13) and imposing $O2 < 0$ [41], we arrive at a relation between the different coefficients, $a_{01}^{(2)} = \pm t_{01}^{(2)}$, $b_{01}^{(2)} = \mp s_{01}^{(2)}$ for $\nu_c^{\pm}$. As a result, the dominant perturbation of the density profile once the instability is triggered takes the form of a one-dimensional traveling wave

$$\delta\rho(x_{\|}, t) = A\sin\left[2\pi\left(x_{\|} - x_{\|}^0 - \frac{q_{\|}\sigma_0'}{\sigma_0}t\right)\right],\tag{5.28}$$

with A and $x_{\|}^0$ two arbitrary constants.

5.2.2 Coherent jammed states: one-dimensional traveling-wave solutions

With the previous result in mind, we consider now that the relevant density fields well below the instability conserve a traveling-wave structure, i.e. $\rho(\mathbf{r}, t) \equiv \omega(\mathbf{r} - \mathbf{v}t)$, with $\mathbf{v}$ some velocity vector to be determined in the variational problem. Taking now into account the continuity constraint Eq. (5.5) we have that

$$\boldsymbol{\nabla}_{\mathbf{r}'} \cdot \mathbf{j}(\mathbf{r}') = \mathbf{v} \cdot \boldsymbol{\nabla}_{\mathbf{r}'}\omega(\mathbf{r}'),\tag{5.29}$$

with the definition $\mathbf{r}' = \mathbf{r} - \mathbf{v}t$. Integrating the previous expression leads to

$$\mathbf{j}(\mathbf{r}, t) = \mathbf{v}\omega(\mathbf{r} - \mathbf{v}t) + \boldsymbol{\Phi}(\mathbf{r} - \mathbf{v}t),\tag{5.30}$$

where $\boldsymbol{\Phi}(\mathbf{r} - \mathbf{v}t)$ is an arbitrary divergence-free vector field. To explicitly account for the constraint (5.7) on the empirical current, we now split the field $\boldsymbol{\Phi}$ into two terms, $\boldsymbol{\Phi}(\mathbf{r} - \mathbf{v}t) = \mathbf{k} + \boldsymbol{\varphi}(\mathbf{r} - \mathbf{v}t)$, where $\mathbf{k} = \mathbf{q} - \mathbf{v}\rho_0$ is a constant vector fixed by constraints (5.6) and (5.7), and $\boldsymbol{\varphi}(\mathbf{r} - \mathbf{v}t)$ is now an arbitrary divergence-free field with zero integral, see Eqs. (5.36)-(5.37) below, defining another degree of freedom (a sort of *gauge field*) to be determined in the variational problem. The resulting traveling-wave form of the current field is

$$\mathbf{j}(\mathbf{r}, t) = \mathbf{q} - \mathbf{v}\left[\rho_0 - \omega(\mathbf{r} - \mathbf{v}t)\right] + \boldsymbol{\varphi}(\mathbf{r} - \mathbf{v}t).\tag{5.31}$$

Interestingly, the system uses this kind of *gauge freedom* to optimize a given current fluctuation in the symmetry-broken phase, selecting among all possible *gauges* a particular, non-trivial one which maximizes the probability of this event. This sort of gauge freedom is precisely the key feature responsible of the richness of the fluctuation phase diagram for $d > 1$.

In this way, under the above traveling-wave assumptions, the current LDF of Eq. (5.8) can now be written, after a change of variables $(\mathbf{r} - \mathbf{v}t) \to \mathbf{r}$, as

$$G(\mathbf{q}) = \min_{\omega,\varphi,\mathbf{v}} \int_{\Lambda} d\mathbf{r} \, \mathcal{G}_{\mathbf{q}}(\omega,\varphi,\mathbf{v}), \tag{5.32}$$

with the definitions

$$\mathcal{G}_{\mathbf{q}}(\omega,\varphi,\mathbf{v}) \equiv \frac{1}{2\sigma[\omega]} \boldsymbol{\mathcal{J}}_{\mathbf{q}}(\omega,\varphi,\mathbf{v}) \cdot \hat{\mathcal{A}}^{-1} \boldsymbol{\mathcal{J}}_{\mathbf{q}}(\omega,\varphi,\mathbf{v}), \tag{5.33}$$

$$\boldsymbol{\mathcal{J}}_{\mathbf{q}}(\omega,\varphi,\mathbf{v}) \equiv \mathbf{q} - \mathbf{v}(\rho_0 - \omega) + \varphi + D[\omega]\hat{\mathcal{A}}\boldsymbol{\nabla}\omega - \sigma[\omega]\hat{\mathcal{A}}\mathbf{E}, \tag{5.34}$$

and with the additional constraints

$$\rho_0 = \int_{\Lambda} \omega(\mathbf{r}) \, d\mathbf{r} \tag{5.35}$$

$$\int_{\Lambda} \varphi(\mathbf{r}) \, d\mathbf{r} = 0 \tag{5.36}$$

$$\boldsymbol{\nabla} \cdot \varphi(\mathbf{r}) = 0 \tag{5.37}$$

To account for these constraints, we employ the method of Lagrange multipliers. In particular, we write

$$G(\mathbf{q}) = - \min_{\substack{\omega,\varphi,\mathbf{v} \\ \zeta,\kappa,\Psi}} \int_{\Lambda} d\mathbf{r} \, \tilde{\mathcal{G}}_{\mathbf{q}}(\omega,\varphi,\mathbf{v},\zeta,\kappa,\Psi), \tag{5.38}$$

where the modified functional to minimize is

$$\tilde{\mathcal{G}}_{\mathbf{q}}(\omega,\varphi,\mathbf{v},\zeta,\kappa,\Psi) \equiv \mathcal{G}_{\mathbf{q}}(\omega,\varphi,\mathbf{v}) + \zeta\left[\rho_0 - \omega(\mathbf{r})\right] + \kappa \cdot \varphi(\mathbf{r}) + \Psi(\mathbf{r})\boldsymbol{\nabla} \cdot \varphi(\mathbf{r}), \tag{5.39}$$

and ζ, κ and $\Psi(\mathbf{r})$ are the Lagrange multipliers associated to the constraints (5.35), (5.36) and (5.37), respectively. Standard variational calculus shows now that the optimal fields and velocity solution of this complex variational problem, denoted as $\omega_{\mathbf{q}}(\mathbf{r})$, $\varphi_{\mathbf{q}}(\mathbf{r})$, and $\mathbf{v}_{\mathbf{q}}$, obey the following system of coupled equations,

$$\mathbf{M_1} \cdot \hat{\mathcal{A}}^{-1}\mathbf{j}_{\mathbf{q}} - \mathbf{M_2} \cdot \hat{\mathcal{A}}\boldsymbol{\nabla}\omega_{\mathbf{q}} + \frac{1}{2}\sigma'[\omega_{\mathbf{q}}]\mathbf{E} \cdot \hat{\mathcal{A}}\mathbf{E} - \zeta = 0 \tag{5.40}$$

$$D[\omega_{\mathbf{q}}]\boldsymbol{\nabla}\omega_{\mathbf{q}} + \hat{\mathcal{A}}^{-1}\mathbf{j}_{\mathbf{q}} + \sigma[\omega_{\mathbf{q}}]\left[\kappa - \boldsymbol{\nabla}\Psi\right] = 0, \tag{5.41}$$

$$\int_{\Lambda} d\mathbf{r}\left(\frac{\omega_{\mathbf{q}} - \rho_0}{\sigma[\omega_{\mathbf{q}}]}\right)\hat{\mathcal{A}}^{-1}\mathbf{j}_{\mathbf{q}} = 0, \tag{5.42}$$

together with constraints (5.35), (5.36) and (5.37), where we have defined $\mathbf{j_q(r)} \equiv \mathbf{q} - \mathbf{v_q}\left[\rho_0 - \omega_\mathbf{q}(\mathbf{r})\right] + \boldsymbol{\varphi_q(r)}$ and

$$\mathbf{M_1} \equiv \left[\frac{\mathbf{v_q}}{\sigma[\omega_\mathbf{q}]} - \frac{\sigma'[\omega_\mathbf{q}]}{2\sigma[\omega_\mathbf{q}]^2}\mathbf{j_q}\right] \; , \quad \mathbf{M_2} \equiv \left[\left(\frac{D[\omega_\mathbf{q}]^2}{2\sigma[\omega_\mathbf{q}]}\right)' \boldsymbol{\nabla}\omega_\mathbf{q} + \frac{D[\omega_\mathbf{q}]^2}{\sigma[\omega_\mathbf{q}]}\boldsymbol{\nabla}\right] \tag{5.43}$$

for simplicity in notation.

As discussed above, our local stability analysis shows that whenever the transition is unleashed, the leading instability is a density wave with structure in one dimension only, determined either by the minimum-anisotropy direction, see condition (iii) above, or by the orientation of the current vector for isotropic systems, see (iv). Such a $1d$ traveling wave will dominate the optimal solution of our variational problem *at least* in a finite region below the transition line, so we now assume $1d$ optimal traveling-wave fields of the form $\omega_\mathbf{q}(x_\parallel)$ and $\boldsymbol{\varphi_q}(x_\parallel)$ (recall that we denote as $x_\parallel$ the direction of structure formation, and $x_\perp$ the orthogonal, structureless direction). Let us show the implications of such an ansatz in the system of equations (5.35)-(5.37), (5.40)-(5.42) and on the form of the optimal traveling-wave trajectories. First, we focus on the most probable current field. We decompose the optimal vector field $\boldsymbol{\varphi_q}$ along the $\parallel$- and $\perp$-directions, $\boldsymbol{\varphi_q}(x_\parallel) = [\varphi_\mathbf{q}^\parallel(x_\parallel), \varphi_\mathbf{q}^\perp(x_\parallel)]$. The divergence-free constraint (5.37) on $\boldsymbol{\varphi_q}(x_\parallel)$ immediately implies that $\varphi_\mathbf{q}^\parallel$ is in fact a constant, while the zero-integral constraint (5.36) sets this constant to zero, resulting in a simplfied form of the vector field $\boldsymbol{\varphi_q}(x_\parallel) = (0, \varphi_\mathbf{q}^\perp(x_\parallel))$. This in turn implies that

$$j_\mathbf{q}^\parallel(x_\parallel) = q_\parallel - v_\parallel[\rho_0 - \omega_\mathbf{q}(x_\parallel)] \, . \tag{5.44}$$

Now, by differentiating the $\perp$-component of Eq. (5.41) with respect to $x_\perp$, it is straightforward to see that $\partial_\perp \Psi$ is a function of $x_\parallel$ at most. Moreover, doing the same differentiation on the $\parallel$-component of (5.41), we obtain that $\partial_\parallel \partial_\perp \Psi = 0$, which together with the previous observation implies that $\partial_\perp \Psi$ is indeed a constant. Using this information in the $\perp$-component of Eq. (5.41), together with constraint (5.7) on the empirical current, we obtain that

$$j_\mathbf{q}^\perp(x_\parallel) = q_\perp \frac{\sigma[\omega_\mathbf{q}(x_\parallel)]}{\int_0^1 \sigma[\omega_\mathbf{q}(x_\parallel)]dx_\parallel} \, , \tag{5.45}$$

which is nothing more that the natural consequence derived from the application of our theorem on the structure of the optimal current fields exposed in Chapter 3 to

this problem (see Eq. (3.20)). Summarising, the combined action of Eqs. (5.36), (5.37) and (5.41) lead to an optimal current vector field of the form:

$$
\mathbf{j_q}(x_\parallel) = \left(q_\parallel - v_\parallel[\rho_0 - \omega_\mathbf{q}(x_\parallel)], q_\perp \frac{\sigma[\omega_\mathbf{q}(x_\parallel)]}{\int_0^1 \sigma[\omega_\mathbf{q}(x_\parallel)]dx_\parallel} \right) \tag{5.46}
$$

We next focus on Eq. (5.40). Multiplying this equation by $\omega'_\mathbf{q}(x_\parallel)$, using that $dF[\omega_\mathbf{q}(x_\parallel)]/dx_\parallel = F'[\omega_\mathbf{q}]\,\omega'_\mathbf{q}(x_\parallel)$ for any arbitrary functional $F[\omega_\mathbf{q}]$, and the identity

$$
\frac{d\mathbf{j_q}(x_\parallel)}{dx_\parallel} = \mathbf{v_q}\omega'_\mathbf{q}(x_\parallel) + \frac{d\boldsymbol{\varphi}_\mathbf{q}(x_\parallel)}{dx_\parallel} \tag{5.47}
$$

Eq. (5.40) can be rewritten as

$$
\frac{d}{dx_\parallel} \left[\frac{1}{2\sigma[\omega_\mathbf{q}]}\mathbf{j_q} \cdot \hat{\mathcal{A}}^{-1}\mathbf{j_q} - a_{\min}\frac{D[\omega_\mathbf{q}]^2}{2\sigma[\omega_\mathbf{q}]}\left(\frac{d\omega_\mathbf{q}}{dx_\parallel}\right)^2 + \frac{1}{2}\sigma[\omega_\mathbf{q}]\mathbf{E} \cdot \hat{\mathcal{A}}\mathbf{E} \right]
$$

$$
- \frac{1}{a_{\max}\sigma[\omega_\mathbf{q}]}\frac{d\varphi_\mathbf{q}^\perp(x_\parallel)}{dx_\parallel}j_\mathbf{q}^\perp(x_\parallel) - \zeta\omega'_\mathbf{q}(x_\parallel) = 0. \tag{5.48}
$$

Integrating this equation once and taking into account the form of $\mathbf{j_q}(x_\parallel)$, see Eq. (5.46), we arrive at a differential equation for the optimal traveling-wave profile

$$
X[\omega_\mathbf{q}]\left(\frac{d\omega_\mathbf{q}}{dx_\parallel}\right)^2 - Y[\omega_\mathbf{q}] + \tilde{K}\omega_\mathbf{q}(x_\parallel) - K = 0, \tag{5.49}
$$

with K and $\tilde{K}$ two constants which comprise the Lagrange multiplier ζ, the wave velocity $\mathbf{v_q}$, and information on the boundary conditions, and where we have defined

$$
X[\omega] \equiv \frac{D[\omega]^2}{2\sigma[\omega]}a_{\min}, \tag{5.50}
$$

$$
Y[\omega] \equiv \frac{\sigma[\omega]}{2}\left(\mathbf{E} \cdot \hat{\mathcal{A}}\mathbf{E} + \frac{[q_\parallel - v_\parallel(\rho_0 - \omega)]^2}{a_{\min}\sigma[\omega]^2} - \frac{q_\perp^2}{a_{\max}(\int_0^1 \sigma[\omega]dx_\parallel)^2}\right). \tag{5.51}
$$

Finally, two additional equations follow from the $\parallel$-component of Eq. (5.42) and constraint (5.35)

$$
\int_0^1 dx_\parallel \frac{[\omega_\mathbf{q}(x_\parallel) - \rho_0]}{a_{\min}\sigma[\omega_\mathbf{q}]}\left[q_\parallel - v_\parallel(\rho_0 - \omega_\mathbf{q}(x_\parallel))\right] = 0, \tag{5.52}
$$

$$
\rho_0 = \int_0^1 \omega_\mathbf{q}(x_\parallel)\,dx_\parallel. \tag{5.53}
$$

Therefore, the set (5.49), (5.52) and (5.53), supplemented by periodic boundary conditions, constitutes the system of coupled integro-differential equations for the optimal fields.

In order to solve this system, we now introduce a reparametrization which simplifies the numerical evaluation of the optimal $1d$ density wave profile and thus of the current LDF $G(\mathbf{q})$. First note that, in our geometry, Eq. (5.49) leads to a periodic optimal profile *symmetric* around $x_\parallel = 1/2$ (recall that $x_\parallel \in [0,1]$), i.e. with reflection symmetry $x_\parallel \to 1 - x_\parallel$. Next we consider the possible maxima and minima of the optimal density wave. For models with a quadratic mobility transport coefficient $\sigma[\omega]$, as the WASEP and KMP models typically studied in literature, the number of possible maxima ω_+ and minima ω_- of the curve $\omega_\mathbf{q}(x_\parallel)$ is rather restricted (see Eq. (5.49) once particularized for $\omega'_\mathbf{q}(x_\parallel) = 0$). In the simplest case [18, 57], a single maximum $\omega_+ = \omega_\mathbf{q}(x_\parallel^+)$ and minimum $\omega_- = \omega_\mathbf{q}(x_\parallel^-)$ will appear, such that the position of two consecutive extrema $x_\parallel^+$ and $x_\parallel^-$ is such that $|x_\parallel^+(k) - x_\parallel^-(k)| = 1/2n$, with n the number of cycles in the unit interval. One can then study numerically the dependence of the current LDF on the number n of cycles, finding that $n = 1$ is the optimal case. We hence restrict hereafter to $1d$ density waves with a single maximum and minimum with $n = 1$. As a result, we can express now the constants $\tilde{K}$ and K of Eq. (5.49) in terms of these extrema

$$Y(\omega_\pm) = \tilde{K}\omega_\pm - K \,. \tag{5.54}$$

The values of these extrema $\omega_\pm$ can be obtained from the constraints on the distance between them and the total density of the system. In particular, the first constraint leads to the following equation,

$$1 = \int_0^1 dx_\parallel = 2 \int_{\omega_-}^{\omega_+} \frac{d\omega_\mathbf{q}}{\omega'_\mathbf{q}} = 2 \int_{\omega_-}^{\omega_+} f(\omega_\mathbf{q}) \, d\omega_\mathbf{q} \tag{5.55}$$

with

$$f(\omega_\mathbf{q}) \equiv \sqrt{\frac{X(\omega_\mathbf{q})}{Y(\omega_\mathbf{q}) - \tilde{K}\omega_\mathbf{q} + K}} \tag{5.56}$$

as derived from Eq. (5.49), while the constraint on the total density leads to

$$\rho_0 = \int_0^1 \omega_\mathbf{q}(x_\parallel) \, dx_\parallel = 2 \int_{\omega_-}^{\omega_+} \frac{\omega_\mathbf{q}}{\omega'_\mathbf{q}} d\omega_\mathbf{q} = 2 \int_{\omega_-}^{\omega_+} \omega_\mathbf{q} f(\omega_\mathbf{q}) \, d\omega_\mathbf{q} \,. \tag{5.57}$$

Note that the unknown variables $\omega_\pm$ appear as integration limits in Eqs. (5.55) and (5.57), difficulting the numerical solution of this problem. However, a suitable

change of variables in ω-space allows to drop this dependence. In particular, we write now $\omega_{\mathbf{q}} \equiv \omega_- + \Omega(\omega_+ - \omega_-)$, with $\Omega \in [0, 1]$, and define $h(\Omega) \equiv (\omega_+ - \omega_-)f[\omega_- + \Omega(\omega_+ - \omega_-)]$. With this choice, constraints (5.55) and (5.57), together with Eq. (5.52) for the velocity, now read

$$\frac{1}{2} = \int_0^1 h(\Omega)\, d\Omega \,, \tag{5.58}$$

$$\frac{\rho_0}{2} = \int_0^1 \omega_{\mathbf{q}}(\Omega)h(\Omega)\, d\Omega \,, \tag{5.59}$$

$$\int_0^1 h(\Omega)\frac{[\omega_{\mathbf{q}}(\Omega) - \rho_0]}{a_{\min}\sigma[\omega_{\mathbf{q}}(\Omega)]} \left[q_\parallel - v_\parallel(\rho_0 - \omega_{\mathbf{q}}(\Omega))\right]\, d\Omega = 0 \,. \tag{5.60}$$

The solution of this three integral equations for a particular model and a given current vector $\mathbf{q}$ leads to particular values of the parameters ω_-, ω_+ and $v_\parallel$, which can be used in turn to obtain the constants K and $\tilde{K}$ from Eq. (5.54) needed to solve numerically the differential equation (5.49) for the optimal density wave profile [18, 57] and thus obtain the current LDF $G(\mathbf{q})$.

5.2.3 Scaled Cumulant Generating Function

As we have shown, a related, interesting function is the scaled cumulant generating function $\mu(\boldsymbol{\lambda})$ associated to the current probability distribution $P_\tau(\mathbf{q})$, also called dynamical free energy since it plays a role akin to free energy out of equilibrium. We recall here some definitions and we refer to Section 2.4.2 for further details. Indeed, the sCGF is defined as:

$$\mu(\boldsymbol{\lambda}) \equiv \lim_{\tau \to \infty} \frac{1}{\tau\Omega} \ln \Pi_\tau(\boldsymbol{\lambda}) \,, \tag{5.61}$$

with $\Pi_\tau(\boldsymbol{\lambda}) = \langle e^{-\tau\Omega\boldsymbol{\lambda}\cdot\mathbf{q}} \rangle$ the generating function, also known as dynamical partition function. The Gärtner-Ellis theorem [19, 24, 37] related both the sCGF and LDF via the Legendre-Fenchel transform

$$\mu(\boldsymbol{\lambda}) = \max_{\mathbf{q}}[G(\mathbf{q}) + \tau\Omega\boldsymbol{\lambda} \cdot \mathbf{q}] \,, \tag{5.62}$$

where we can see that $\boldsymbol{\lambda}$ and $\mathbf{q}$ are *conjugated* vectors. In this way, fixing $\boldsymbol{\lambda}$ is equivalent to conditioning the system to have an empirical current $\mathbf{q}_{\boldsymbol{\lambda}} \equiv \mathbf{Q}_{\boldsymbol{\lambda}}/t = \nabla_{\boldsymbol{\lambda}}\mu(\boldsymbol{\lambda})$, so it is expected that by varying $\boldsymbol{\lambda}$ one can explore the different regimes presented in the previous section.

Certainly, the above MFT analysis of the dynamic phase transition can be developed also in terms of $\mu(\boldsymbol{\lambda})$, which will provide a direct comparison with the results of numerical experiments based on the cloning Monte Carlo method (see Section 5.4 below). In particular, defining $\mathbf{z} \equiv \boldsymbol{\lambda} + \mathbf{E}$, it can be shown that a line of critical values $\mathbf{z}_c$ exists at which the instability appears, defined by the equation $\mathbf{z}_c \cdot \hat{\mathcal{A}} \mathbf{z}_c = \Xi_c$, with Ξ_c the critical threshold defined in Eq. (5.22). This critical line separates a phase of Gaussian current statistics and homogeneous optimal profiles, corresponding to a quadratic sCGF $\mu_G(\mathbf{z}) = \sigma_0 (\mathbf{z} \cdot \hat{\mathcal{A}} \mathbf{z} - \mathbf{E} \cdot \hat{\mathcal{A}} \mathbf{E})/2$, see Eq. (5.10), and the non-Gaussian, traveling-wave phase. As before, for systems with $\sigma_0'' > 0$ (as the KMP model) the Gaussian regime dominates for $\mathbf{z} \cdot \hat{\mathcal{A}} \mathbf{z} \leq \Xi_c$ while the traveling-wave region appears for $\mathbf{z} \cdot \hat{\mathcal{A}} \mathbf{z} > \Xi_c$ and for all $\mathbf{E}$. On the other hand, for systems with $\sigma_0'' < 0$ (as the WASEP studied here) a line of critical values of the external field exist, defined by Eq. (5.23), beyond which the instability appears, $\mathbf{E} \cdot \hat{\mathcal{A}} \mathbf{E} \geq |\Sigma_c|$. In this strong field case, Gaussian statistics are expected for all $\mathbf{z}$-values except for a region defined by $\mathbf{z} \cdot \hat{\mathcal{A}} \mathbf{z} \leq \Xi_c$, where current fluctuations are non-Gaussian.

5.3 Dynamical phase transitions in the current vector statistics from MFT

Our goal now is to characterize the different dynamical phase transitions observed in the previous section when analyzing the current vector statistics. With this idea in mind and the aim of establishing a comparision between this theoretical scheme and numerical predictions, we will focus on a paradigmatic example of anisotropic driven diffusive system: the weakly asymmetric simple exclusion process (WASEP).

5.3.1 Two-dimensional Weakly Asymmetric Simple Exclusion Process (WASEP)

The $2d$-WASEP belongs to a broad family of driven diffusive systems of fundamental and technological interest [16–18]. Microscopically, this model is defined on a $2d$ square lattice of size $N = L \times L$ with periodic boundaries where $M \leq N$ particles evolve, so the global density is $\rho_0 = M/N$. Each lattice site may contain at most one particle, which performs stochastic jumps to neighboring empty sites along the $\pm \alpha$-direction ($\alpha = x, y$) at a rate $r_{\pm}^{\alpha} \equiv \exp[\pm E_{\alpha}/L]/2$, with $\mathbf{E} = (E_x, E_y)$ an external field, see Fig. 5.1. These rates converge for large L to the standard ones found in literature [17, 41], namely $\frac{1}{2}(1 \pm E_{\alpha}/L)$, but avoid

problems that the last ones could originate with negative rates for small L. Indeed, the hydrodynamic description of both variants of the model is identical in the thermodynamic limit. However, for finite, moderate values of L and large $\mathbf{E}$ the field per unit length ($\mathbf{E}/L$) is strong enough to induce an *effective anisotropy* in the system. In fact, by expanding the microscopic transition rate $r_{\pm}^{\alpha}$ to second order in the field per unit length, i.e. $r_{\pm}^{\alpha} \approx \frac{1}{2}[1 \pm E_{\alpha}/L + \frac{1}{2}(E_{\alpha}/L)^2] + \mathcal{O}[(E_{\alpha}/L)^3]$, it is easy to show using a simple random walk argument that the second-order perturbation results in an effective enhancing of diffusivity and mobility along the field direction, and an associated decrease in the orthogonal direction.

It can be proved [124, 245] that, for large enough L, this model is defined, at a mesoscopic level, by a diffusivity and mobility matrices $\hat{D}[\rho] = D[\rho]\hat{\mathcal{A}}$ and $\hat{\sigma}(\rho) = \sigma[\rho]\hat{\mathcal{A}}$, respectively, with

$$D[\rho] = 1/2, \quad \sigma[\rho] = \rho(1 - \rho) \tag{5.63}$$

(note that $\sigma''(\rho) < 0$). The diagonal anisotropy matrix $\hat{\mathcal{A}}$ has components $\hat{\mathcal{A}}_{\alpha\beta} = a_{\alpha}\delta_{\alpha\beta}$, with $\alpha, \beta = x$ or y. For simplicity, we can assume that the external field is applied only in the x-direction, with no loss of generality. In this case, we consider systems such that $a_x = 1 + \varepsilon$ and $a_y = 1 - \varepsilon$, with ε an anisotropy parameter accounting for the microscopic effective anisotropy previosly described. Indeed, such an effect is modeled in our case with a parameter $\varepsilon \geq 0$ so that the direction of minimum anisotropy (if any) is y. Interestingly, the reason behind this choice is that the finite lattice systems which we can simulate effectively using the cloning method (see Section 5.4 below) present a moderate size L and strong external field $\mathbf{E}$, inducing an increase on the diffusivity and mobility along the field direction.

Using these definitions, one can particularize the theoretical framework described in Section 5.2 for the $2d$ anisotropic WASEP and proceed to solve numerically the variational problem for the current sCGF $\mu(\boldsymbol{\lambda})$ and the optimal profiles.

5.3.2 Order and symmetry-breaking at the fluctuating level: dynamical phase diagram

The solution of the MFT problem shows that the interplay among the external field, the two-dimensional current vector and the anisotropy leads to a rich phase diagram for current fluctuations. Fig. 5.2.a-c. shows $\mu(\boldsymbol{\lambda})$, as derived from our MFT calculations, for three different values of the anisotropy ε as well as the projections of the corresponding dynamical phase diagrams, while Fig. 5.2 shows raster plots sketching typical configuration trajectories for WASEP in the Gaussian current fluctuation phase, Fig. 5.2.d, and in the two different non-Gaussian symmetry-broken phases which appear for low currents, Figs. 5.2.e-f. As we have
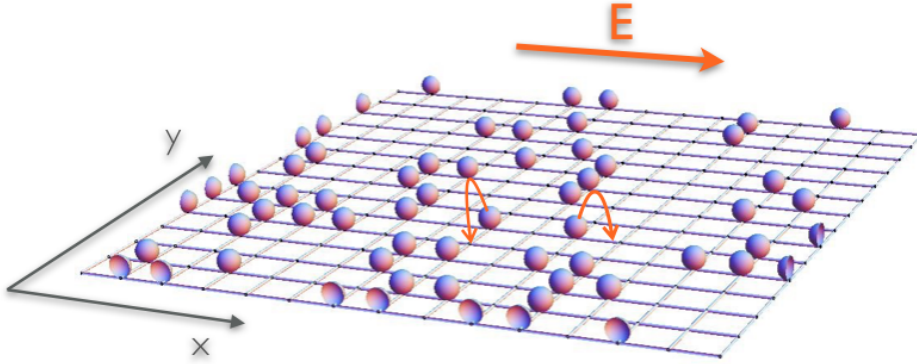
Figure 5.1: Sketch of the $2d$ weakly asymmetric simple exclusion process (WASEP) with an external field in the x-direction, i.e. $\mathbf{E} = (E, 0)$.

seen, small current fluctuations ($|\mathbf{q} - \langle \mathbf{q} \rangle| \ll 1$ or $|\boldsymbol{\lambda}| \approx 0$) typically result from the random superposition of mostly-independent local jumps which sum incoherently to yield the desired current, so the typical trajectories are homogeneous. This flat phase is depicted in light gray in Fig. 5.2. For WASEP, the local stability analysis then shows that this Gaussian, homogeneous regime eventually becomes unstable for $\mathbf{q} \cdot \hat{\mathcal{A}}^{-1} \mathbf{q} = \sigma_0^2 \Xi_c$, or equivalently $\mathbf{z} \cdot \hat{\mathcal{A}} \mathbf{z} = \Xi_c$, where Ξ_c is the critical threshold defined in Eq. (5.22), revealing the existence of a dynamical phase transition between the Gaussian and non-Gaussian (dark colors) phases, see black eliptical lines in Fig. 5.2.a-c.

Immediately after the instability kicks in, the dominant trajectory takes the form of a traveling density wave with structure only along one-dimension ($1d$), either x (red) or y (blue), see Figs. 5.2.e-f. This collective rearrangement breaks the system spatiotemporal translation symmetry by localizing particles in a jammed region to facilitate a low-current fluctuation. This solution can be extended to all currents below the critical line, and we find numerically that different traveling wave structures dominate different parts of the symmetry-broken, non-Gaussian phase, see Fig. 5.2.a-c. For isotropic systems, $\varepsilon = 0$, the optimal density traveling wave for subcritical vectors $\mathbf{z} = (z_x, z_y)$ with $|z_x| > |z_y|$ ($|z_x| < |z_y|$) has structure along the y-direction (x-direction), preserving deep into the non-Gaussian phase the result derived from our local stability analysis right below the transition line, see conclusion (iv) derived from the local stability analysis presented above. On the other hand, for anisotropic systems ($\varepsilon > 0$) the transition triggers the formation of a density traveling wave with structure only along the minimum anisotropy, y-direction, see Figs. 5.2.b-c,e. , in agreement with conclusion (iii) above. However,
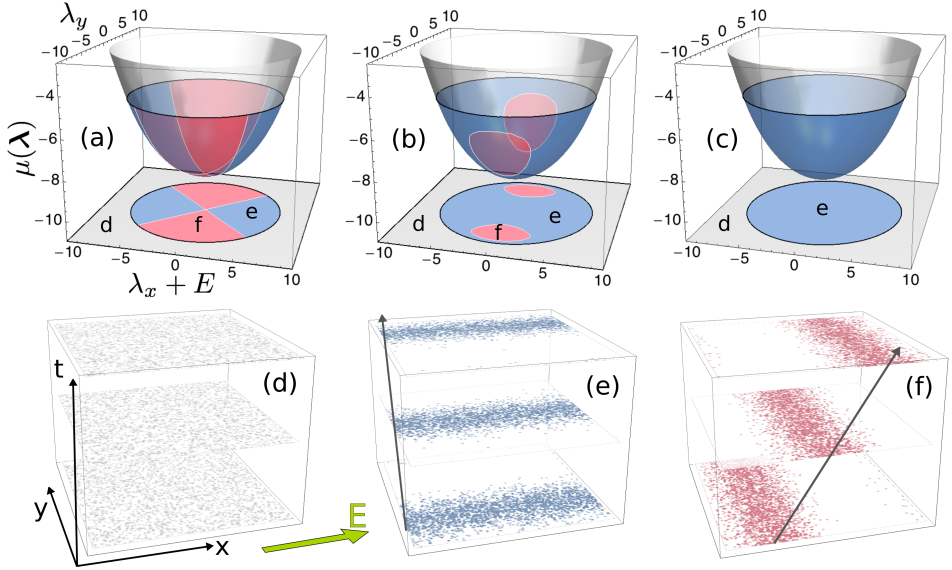
Figure 5.2: Top: Dynamical free energy of the current for the $2d$-WASEP in an external field $\mathbf{E} = (10, 0)$ along the x-direction, as derived from MFT in the case of (a) no anisotropy, $\varepsilon = 0$, (b) mild anisotropy, $0 < \varepsilon < \varepsilon_c$, and (c) strong anisotropy, $\varepsilon > \varepsilon_c$. A DPT appears between a Gaussian phase (light gray) with homogeneous optimal pathways, see sketch (d), representing a typical configuration trajectory in this case, and two different non-Gaussian symmetry-broken phases for low currents characterized by traveling-wave jammed states. The first DPT is 2nd-order while the two symmetry-broken phases are separated by lines of 1st-order DPTs, see Fig. 5.4 below. Bottom: Raster plots of typical configuration trajectories for the anisotropic $2d$ WASEP in the Gaussian current fluctuation phase (d), and in the two different non-Gaussian symmetry-broken phases for low currents, (e) and (f). These two novel phases are characterized by traveling density waves which jam particle flow along the field direction, (b) and blue phase in (a)-(c), or along the direction orthogonal to $\mathbf{E}$, (c) and red phase in (a)-(c).

for mild anisotropy we find deep into the non-Gaussian regime two pockets of the second symmetry-broken phase, i.e. the one with structure along the maximum anisotropy axis, see Figs. 5.2.b,f. These two patches decrease with increasing ε, up to a critical anisotropy $\varepsilon_c \approx 0.035$ beyond which only the minimum-anisotropy density wave appears in the non-Gaussian regime, see Figs. 5.2.c. Interestingly, in Fig. 5.3 swe show the phase diagrams for current fluctuations for the different anisotropy parameters (corresponding to the bottom projections of Fig. 5.2), to illustrate such a rich and complex phenomenology.

Next, we investigate the order of the different DPT's showing up in the current statistics of this model. We first focus on the DPT from the Gaussian to the
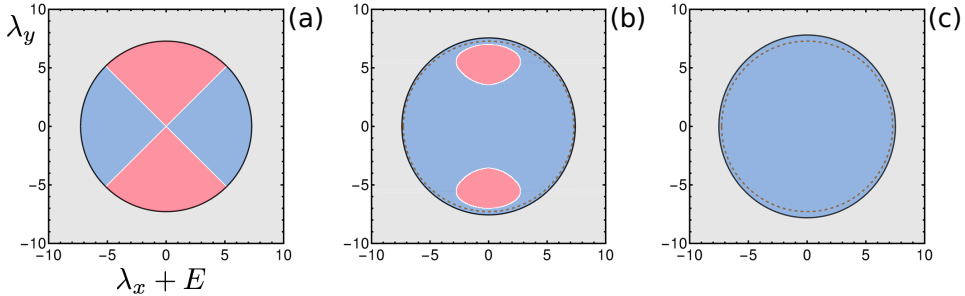
Figure 5.3: A closer look at the phase diagrams for current fluctuations in the case of (a) no anisotropy, $\varepsilon = 0$, (b) mild anisotropy, $0 < \varepsilon < \varepsilon_c$, and (c) strong anisotropy, $\varepsilon > \varepsilon_c$, corresponding to the bottom projections in Fig. 5.2. The 2nd-order DPT between the Gaussian phase (light gray) and the two different traveling-wave, non-Gaussian phases (dark blue and red) corresponds to the black thick line, while the 1st-order DPT separating both symmetry-broken non-Gaussian phases is depicted as a white thin line. Panels (b) and (c) also include a dashed line which corresponds to the 2nd-order DPT line for $\varepsilon = 0$. This shows that the shape of this critical line does change as the anisotropy parameter ε increases.

non-Gaussian phase at $\mathbf{z}_c \cdot \hat{\mathcal{A}} \mathbf{z}_c = \Xi_c$. Left panel in Fig. 5.4 shows $\mu(\mathbf{z})$ as a function of $z = |\mathbf{z}|$ for a current angle $\phi = 0$ in the isotropic case ($\varepsilon = 0$), as well as its first and second partial derivatives with respect to z at constant ϕ. Clearly, the dynamical free energy exhibits a kink in its first derivative and a related discontinuity in the second derivative, a hallmark of a second-order phase transition. Similar discontinuities in $\partial_z^2 \mu(z, \phi)$ appear at $z_c(\phi) \; \forall \phi \in [0, 2\pi]$. Therefore, as happens also in the simpler DPT's already described and observed in $1d$ oversimplified transport models [56, 57], the DPT from the Gaussian, homogeneous phase and the non-Gaussian, traveling-wave phases is of second order type.

On the other hand, the DPT between different symmetry-broken phases for $\mathbf{z}_c \cdot \hat{\mathcal{A}} \mathbf{z}_c < \Xi_c$ and mild or no anisotropy, see Fig. 5.2.a-b, is clearly discontinuous. Indeed, right panel in Fig. 5.4 shows $\mu(\mathbf{z})$ as a function of the angle $\phi \in [0, \pi/2]$ for $z = 3$ (deep into the symmetry-broken phase) in the isotropic case $\varepsilon = 0$, see Fig. 5.2.a, as well as its first derivative with respect to ϕ at constant z. The vertical dotted line in this plot signals the DPT separating the two distinct non-Gaussian symmetry-broken phases with traveling jammed states along the field direction ($\phi < \pi/4$) or orthogonal to it ($\phi > \pi/4$). While $\mu(z = 3, \phi)$ is continuous across the transition, it exhibits a kink at $\phi_c = \pi/4$ and an associated discontinuity in $\partial_\phi \mu(z = 3, \phi)$, signaling the first-order character of this DPT between the two traveling density wave phases. Something similar happens for all other subcritical z and $\varepsilon < \varepsilon_c$. Interestingly, the current $\mathbf{q}_{\boldsymbol{\lambda}} = \boldsymbol{\nabla}_{\boldsymbol{\lambda}} \mu(\boldsymbol{\lambda})$ corresponding to a given $\boldsymbol{\lambda}$ jumps discontinuously at these lines. In this way the 1st-order DPT lines in $\boldsymbol{\lambda}$-space
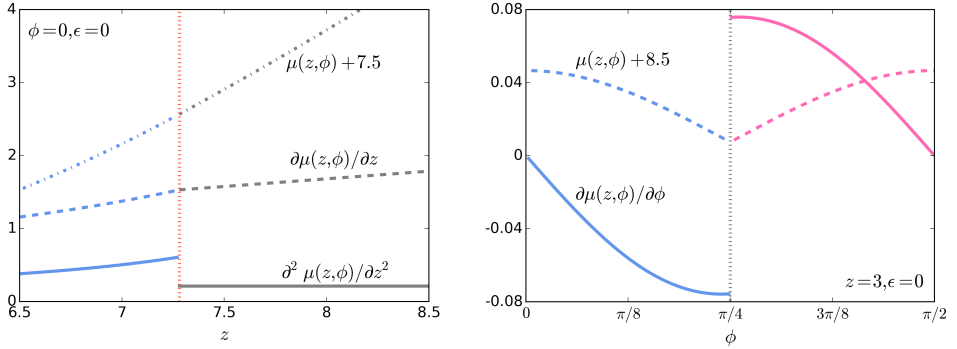
Figure 5.4: Left: Dynamical free energy for the current $\mu(z, \phi)$, with $\mathbf{z} = \boldsymbol{\lambda} + \mathbf{E}$, as a function of $z = |\mathbf{z}|$ for $\phi = 0$ in the isotropic case ($\varepsilon = 0$), see Fig. 5.2.a, as well as its first and second partial derivative with respect to z. Note that $\mu(z, \phi)$ has been shifted vertically for the sake of clarity. The vertical dotted line signals the DPT between the Gaussian, homogeneous current fluctuation phase ($z > z_c(\phi)$) and the non-Gaussian, symmetry broken phase ($z < z_c(\phi)$) with jammed density waves along the field direction, see Fig. 5.2.e. The dynamical free energy exhibits a kink in its first derivative and an associated discontinuity in the second derivative, a hallmark of a second-order phase transition. Similar discontinuities in $\partial_z^2 \mu(z, \phi)$ appear at $z_c(\phi)$ $\forall \phi \in [0, 2\pi]$. Right: $\mu(z, \phi)$ vs ϕ for $\phi \in [0, \pi/2]$ and $z = 3$ in the isotropic case ($\varepsilon = 0$), see Fig. 5.2.a, as well as its first derivative with respect to ϕ. As before, $\mu(z, \phi)$ has been shifted vertically for clarity. The vertical dotted line signals the DPT separating the two distinct non-Gaussian symmetry-broken phases with jammed states along the field direction ($\phi < \pi/4$) or orthogonal to it ($\phi > \pi/4$). While $\mu(z = 3, \phi)$ is continuous across the transition, it exhibits a kink at $\phi_c = \pi/4$ and an associated discontinuity in $\partial_\phi \mu(z = 3, \phi)$, signaling the first-order character of this DPT between the two symmetry-broken non-Gaussian phases.

correspond to regions in $\mathbf{q}$-space where *dynamical coexistence* emerges between the two symmetry-broken non-Gaussian phases, see Fig. 5.5.a-c. This means that if we were to observe an atypical current $\mathbf{q}$ sitting in one of these regions, either by an unlikely spontaneous fluctuation or by an active control of the current with an optimal field, we would observe dynamical coexistence of the two different traveling density waves.

To end this section we note that, even though our local stability analysis shows that the dominant perturbations immediately beyond the instability line are one-dimensional traveling waves, in principle one could expect more complex two-dimensional (traveling-wave) patterns to emerge deeper into the symmetry-broken phase. In this case, the equations defining the form of the optimal profiles are partial differential equations, see e.g. Eq. (5.40), and the uniqueness of their solution is in general unknown. However, one can find some particular solutions which are *local* maximizers of the MFT action for currents. The particular 2d solutions
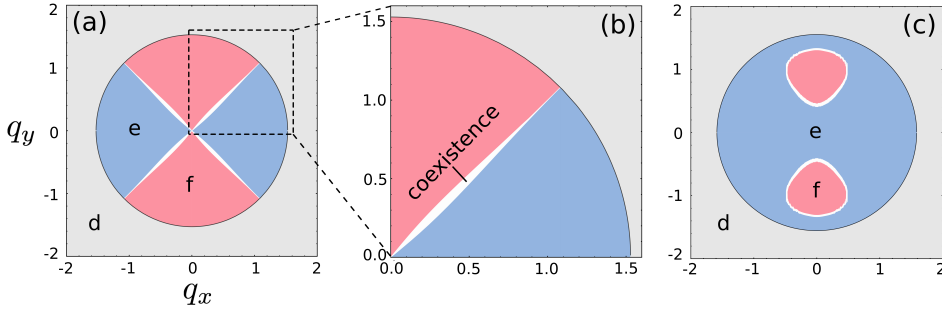
Figure 5.5: Dynamical phase diagram for fluctuations of the current in **q**-space for anisotropy $\varepsilon = 0$ (a,b), and $0 < \varepsilon < \varepsilon_c$ (c). The two symmetry-broken phases are separated by lines of 1st-order DPTs, and the coexistence regions (white) are apparent.

we have explored numerically do not improve the current LDF when compared to their $1d$ counterparts described above. This is surprising, as one would naively expect the system to minimize the interface between the high- and low-density regions while developing a macroscopic jam to sustain a low-current fluctuation. In any case, we cannot discard exotic $2d$ solutions not yet explored, though our simulation results, as we will see in the next section, strongly support that $1d$ traveling waves are the global optimal solutions in all cases.

5.4 Comparision with numerical predictions

The previous results call for independent empirical microscopic verification, as they derive from an effective mesoscopic theory which relies on a few hypotheses [16]. To search for this DPT, we explored the current statistics of the $2d$-WASEP using massive cloning Monte Carlo simulations [153–155]. In particular, we simulated systems with density $\rho_0 = 0.3$, several system sizes up to $N = 144$, and a strong external field $\mathbf{E} = (10, 0)$. The cloning Monte Carlo method relies on a controlled modification of the system stochastic dynamics such that the rare events responsible for a given fluctuation are no longer rare, and involves the parallel simulation of multiple copies of the system [153–155]. The number of clones needed to observe a given rare event grows exponentially with the system size, all the more the rarer the event is [246, 247]. In particular, to pick up and characterize reliably the DPT in the $2d$-WASEP we needed the extraordinary number of $N_c = 5.12 \times 10^5$ clones evolving in parallel for a long time.

5.4.1 Dynamical free energy across the DPT

According to MFT, Gaussian current statistics corresponding to a quadratic dFE $\mu_{G}(\mathbf{z})$ are expected for $\mathbf{z} \cdot \hat{\mathcal{A}}\mathbf{z} \geq \Xi_c$, see Fig. 5.2 and discussion above. This is fully confirmed in Fig. 5.6, which shows the measured $\mu(\mathbf{z})$ for $N = 144$ as a function of $z = |\mathbf{z}|$ for different current orientations ϕ. This corroborates that mild current fluctuations stem from the random superposition of weakly-correlated, localized events which sum up incoherently to yield Gaussian statistics, leading to flat profiles. Interestingly, we find a weak dependence of $\mu(\mathbf{z})$ on ϕ in this Gaussian regime, a clear hallmark of the effective anisotropy mentioned above. Indeed, this ϕ-dependence can be used to estimate that $\varepsilon \approx 0.038$ properly describes the observed weak anisotropy, see inset in Fig. 5.7. This effective anisotropy is slightly larger than the critical anisotropy $\varepsilon_c \approx 0.035$ beyond which a single symmetry-broken phase dominates the non-Gaussian regime, see Fig. 5.2.c, an observation consistent with additional results below. The Gaussian, incoherent fluctuation regime ends up for $\mathbf{z} \cdot \hat{\mathcal{A}}\mathbf{z} < \Xi_c$, where clear deviations from the quadratic form $\mu_{G}(\mathbf{z})$ become apparent, see Fig. 5.6. This change of behavior, in excellent agreement with MFT predictions, signals the onset of the DPT to a symmetry-broken phase characterized by non-Gaussian current fluctuations and traveling density wave trajectories. A clear convergence to the MFT prediction is observed in the Gaussian and non-Gaussian regimes as both N and the number of clones N_c increase, see inset in Fig. 5.6.

5.4.2 An order parameter for the dynamic phase transition

The smoking gun of any continuous phase transition, such as the 2nd-order DPT here reported, is a smooth but apparent change in an order parameter [236]. In our situation, we expect order to emerge across the DPT in the form of $1d$ coherent traveling waves which jam particle flow along one direction, thus facilitating low-current deviations. The interplay described above among the external field, anisotropy and currents opens the door to different, competing symmetry-broken phases, see Fig. 5.2.e-f., and our aim here will be to determine which ones do emerge in our simulations. To do so, we introduce now a novel *structural* order parameter, capable of discerning the jam direction (if any), which characterize the onset of the 2nd-order DPT predicted by MFT from a microscopic point of view. In this way, to define such an appropriate order parameter we perform now a *tomographic analysis* by taking $1d$ sections of our $2d$ system. In particular we consider a microscopic particle configuration $\mathbf{n}$ and slice it along one of the principal axes, say x, defining the j-slice configuration $\mathbf{n}_j \equiv \{n_{ij}; i \in [1, L]\}$, with
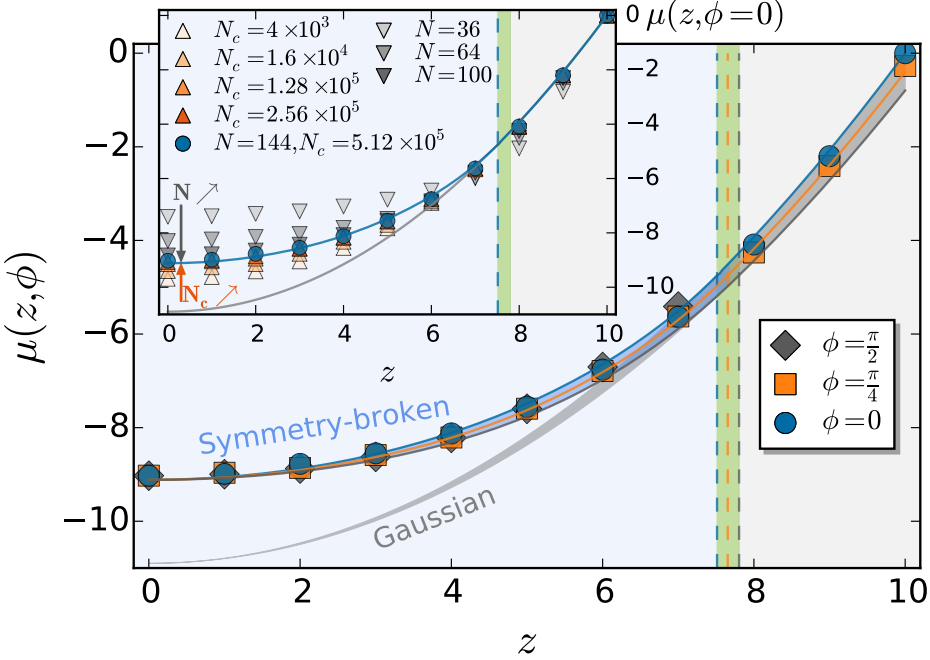
Figure 5.6: Main: $\mu(\boldsymbol{\lambda})$ vs $z = |\boldsymbol{\lambda}+\mathbf{E}|$ as obtained in simulations for $N = 144$, $N_c = 5.12 \times 10^5$ and different $\phi = \tan^{-1}(z_y/z_x)$, together with MFT predictions for anisotropy $\varepsilon = 0.038$. A DPT from a Gaussian regime (light-gray ribbon) to a symmetry-broken, non-Gaussian phase (blue ribbon) is apparent upon crossing $z_c(\phi)$, with $\mathbf{z}_c \cdot \hat{\mathcal{A}}\mathbf{z}_c = \Xi_c$ (green vertical stripe). Different ϕ correspond to different MFT lines within the shaded ribbons. Inset: Convergence to the $\phi = 0$ MFT prediction (blue line) for $N = 144$ as N_c increases ($\triangle$) and for optimal N_c as N increases ($\triangledown$).

$M_j = \sum_{i=1}^{L} n_{ij}$ the total number of particles in this slice and $M = \sum_{j=1}^{L} M_j$, see e.g Figs. 5.7.a,d. To properly take into account the periodic boundaries (i.e. the system torus topology, see Figs. 5.7.b,e), we consider each j-slice as a $1d$ ring of fixed radius embedded in $2d$ where each site $i \in [1, L]$ is assigned an angle $\theta_i = 2\pi i/L$, and compute the angular position of the center of mass for the j-slice, $\theta_{\text{cm}}^{(j)}$. This is defined as

$$\theta_{\text{cm}}^{(j)} \equiv \tan^{-1}\left(\frac{S_j}{C_j}\right) \qquad (5.64)$$
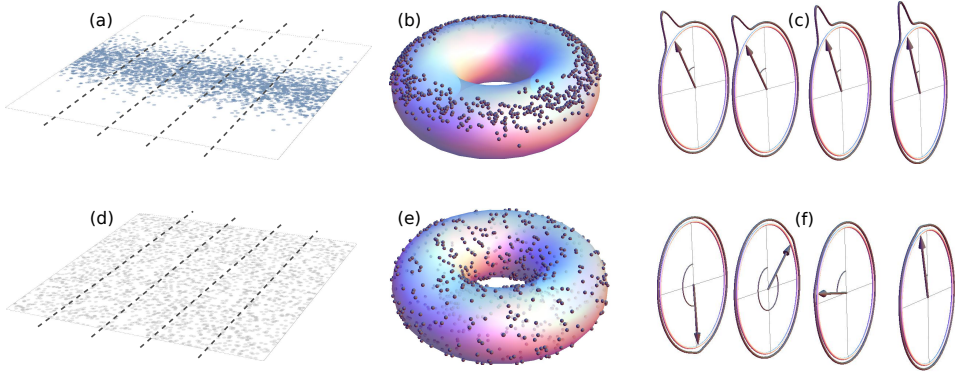
Figure 5.7: Tomographic analysis to define an order parameter for the DPT. Order is expected to emerge across the DPT in the form of $1d$ coherent traveling waves (a) which jam particle flow along one direction. To detect these jams, we slice microscopic configurations along principal axes (see dashed lines in (a)). Due to the periodic boundaries, the systemÕs topology is in fact that of a torus, as in (b), so each slice can be considered as a 1d ring of fixed radius embedded in 2d, with a given angular mass distribution (c) depending on the positions of the particles in the slice. A small dispersion σ_x^2 of the angular centers of mass across the different slices, (c), will signal the formation of a coherent jam along the x-direction and the associated density wave in the orthogonal direction, see (a). A similar analysis in the homogeneous, Gaussian phase leads to a typically large dispersion σ_x^2, see (d)-(f).

with the additional definitions

$$S_j \quad \equiv \quad \frac{1}{M_j} \sum_{i=1}^{L} n_{ij} \sin \theta_i \,, \tag{5.65}$$

$$C_j \quad \equiv \quad \frac{1}{M_j} \sum_{i=1}^{L} n_{ij} \cos \theta_i \,. \tag{5.66}$$

Clearly, a small dispersion of the angular centers of mass across the different slices will signal the formation of a coherent jam along the x-direction and the associated density wave in the orthogonal direction, see Fig. 5.7.c. On the other hand, a large dispersion of $\theta_{\text{cm}}^{(j)}$ across the different $j \in [1, L]$ is the typical signature of a structureless, homogeneous random configuration, see Figs. 5.7.d,f. In this way, we write

$$\sigma_x^2 \equiv \langle (\theta_{\text{cm}}^{(j)})^2 \rangle_x - \langle \theta_{\text{cm}}^{(j)} \rangle_x^2 \,, \tag{5.67}$$

where we have defined

$$\langle f_j \rangle_x \equiv \frac{1}{L} \sum_{j=1}^{L} f_j \,, \tag{5.68}$$
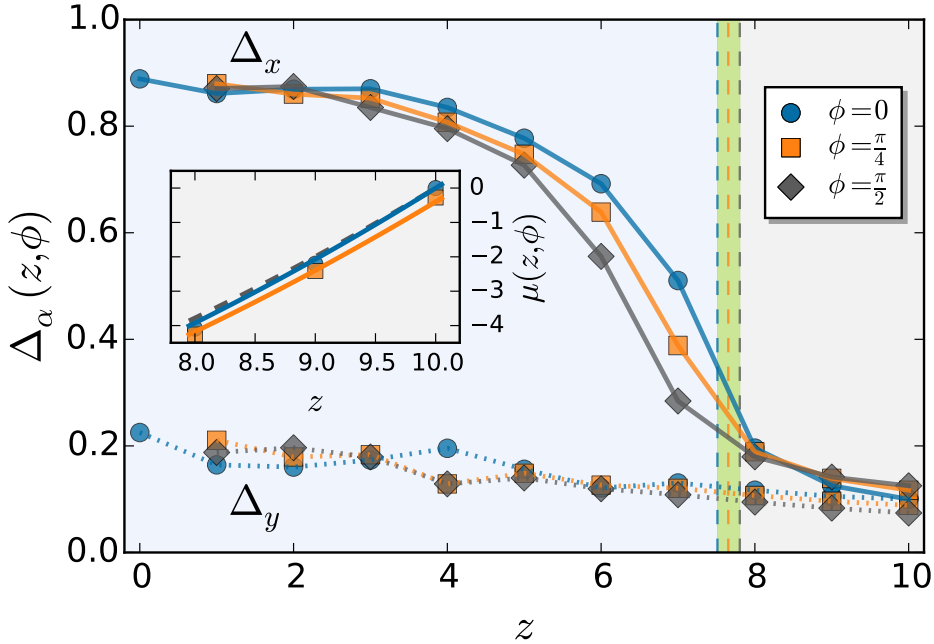
Figure 5.8: Tomographic α-coherences, with $\alpha = x, y$, as a function of z for different current angles ϕ measured for $N = 100$ and $\mathbf{E} = (10, 0)$. Inset: dFE $\mu(\mathbf{z})$ vs z in the Gaussian regime for $\phi = 0, \pi/4$, see Fig. 5.6. Full (dashed) lines are MFT predictions with anisotropy $\varepsilon = 0.038$ ($\varepsilon = 0$).

for any arbitrary local observable f_j, and define the *tomographic x-coherence* as

$$\Delta_x(\boldsymbol{\lambda}) \equiv 1 - \langle \sigma_x^2 \rangle_{\boldsymbol{\lambda}}, \tag{5.69}$$

where the average $\langle \cdot \rangle_{\boldsymbol{\lambda}}$ is taken over the biased $\boldsymbol{\lambda}$-ensemble, i.e. over all trajectories statistically relevant for a rare event of fixed $\boldsymbol{\lambda}$ [17, 18, 41]. We can define in an equivalent way the tomographic y-coherence $\Delta_y(\boldsymbol{\lambda})$ to detect particle jams along the y-direction, and Fig. 5.8 shows these two order parameters measured across the DPT as a function of $z = |\mathbf{z}|$, with $\mathbf{z} \equiv \boldsymbol{\lambda} + \mathbf{E}$.

Remarkably, $\Delta_x(z)$ increases steeply for $\mathbf{z} \cdot \hat{\mathcal{A}} \mathbf{z} \leq \Xi_c$ and *all angles* ϕ of the current vector, while $\Delta_y(z)$ remains small and does not change appreciably across the DPT, clearly indicating that a coherent particle jam emerges along the x-direction in all cases, as in the sketch of Fig. 5.7.a above. This means that only one of the two possible symmetry-broken phases appear in our simulations (regardless of the current vector orientation), as expected from MFT in the super-
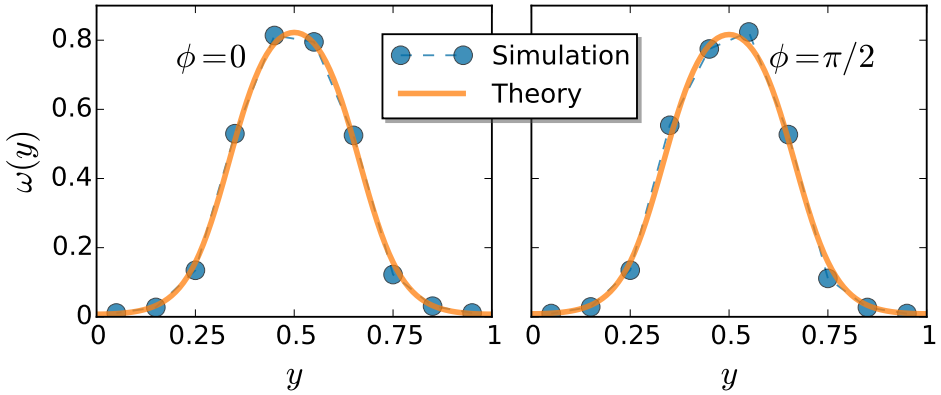
Figure 5.9: Density wave profile along the y-direction for $z = 2$ and $\phi = 0, \pi/2$, measured for $N = 100$ and $\mathbf{E} = (10, 0)$. Lines correspond to MFT predictions.

critical anisotropy regime $\varepsilon > \varepsilon_c$, see Fig. 5.2.c, and consistent with the measured effective anisotropy $\varepsilon \approx 0.038 > \varepsilon_c$, see inset in Fig. 3.d of the main text. Note also that the behavior of both Δ_α ($\alpha = x, y$) across the DPT is consistent with the emergence of a traveling wave with structure in $1d$ and not in $2d$, as in the latter case both Δ_α should increase upon crossing $z_c(\phi)$. Moreover, the acute but continuous change of $\Delta_x(\mathbf{z})$ across the DPT is consistent with a second-order transition, in agreement with the MFT prediction.

Finally, we have also measured the average density profile along the y-direction, i.e. orthogonal to the jam direction, associated to a given current fluctuation deep into the symmetry broken phase, see Fig. 5.9. In order not to blur away the structure of the moving density wave, we performed profile averages around the instantaneous angular center of mass, shifting it to the origin before averaging. Fig. 5.9 shows the highly-nonlinear density profile $\omega(y)$ of the traveling wave so obtained for current fluctuations with $z = 2$ and $\phi = 0, \pi/2$, together with MFT predictions, and the agreement is remarkable in both cases. In particular, note that the traveling wave has structure along the y-axis in both cases, as expected from the analysis of Fig. 5.8 and consistent with the supercritical anisotropy scenario $\varepsilon > \varepsilon_c$, see Fig. 5.2.c,e.

5.5 Conclusions

We have presented compelling evidences of a complex dynamic phase transition in the current vector statistics of a paradigmatic model of transport in $2d$, charac-

terizing its properties with the tools of macroscopic fluctuation theory. Our analysis of MFT equations predicts a rich phase diagram, with non-analiticities of 1st- and 2nd-order type in the current dynamical free energy, accompanied by emergent order in different symmetry-broken phases characterized by traveling density waves. This richness is aided by the complex interplay among anisotropy, external field and vector currents in $d > 1$, key features missing in the simpler models studied in the past. First, by considering *vectorial currents* it becomes apparent that current rotations can trigger 1st-order transitions between different symmetry-broken jammed dynamical phases. This is certainly not present in simpler $1d$ models [18,56–59,62,179,181–185] and cannot show up when studying fluctuations of scalar observables in $d > 1$ [61, 186–194, 242]. Second, by including *anisotropy* in our analysis (a main feature of many realistic $d > 1$ systems not considered before), it becomes clear its strong effect on the relative shape and position of the different jammed phases, see Fig. 5.2.a-c. Interestingly, our results show that order and coherence may emerge out of an unlikely fluctuation, proving the deep connection between rare events and self-organized structures which enhance their probability. This is expected to be a general feature of many complex dynamical systems [60]. The mapping between exclusion processes and dual quantum spin systems [248–251] suggests a connection between the DPT here uncovered and a rich quantum phase transition yet to be explored. It would be also interesting to determine the universality class of this DPT, and the dynamical exponents of the different fluctuation phases [177, 182].

Chapter 6

Dynamic phase transition in the one-dimensional Landau-Ginzburg model

6.1   Introduction

In its origin, Macroscopic Fluctuation Theory was formulated to understand the behaviour of macroscopic fluctuations in general driven diffusive systems [16, 38, 53–55]. In this context, MFT has provided a very powerful framework to characterize the distribution of fluctuations in these situations, and a huge number of results, including all that we have presented in this Thesis up to now, has been derived in the light of this scheme. However, it has been shown that this theory could be extended to other classes of systems [112]. In this chapter we will describe techniques to study macroscopic fluctuations in dissipative systems with no conservation laws following a similar mechanism to the one developed in MFT.

As we have seen, an interesting phenomena taking place in fluctuations and broadly studied under the framework of MFT are the dynamic phase transitions. In this way, the well-known Mermin-Wagner theorem [252] establishes that continuous symmetries cannot spontaneously breaking in systems with short interactions in dimension $d \leq 2$. However, recent works have shown that this theorem does not satisfy at fluctuating level, finding remarkble DPTs when studying the statistics of fluctuations of space- and time-integrated observables in one-dimensional driven diffusive systems [41, 57, 175]. In the following lines we will see that this fact is not exclusive for systems with conservation laws, but on the contrary we can observe DPTs in systems with non-locallly conserved dynamics in fluctuations. This outcome could open the door to the formulation of general results in dynamic phase transtions at a fluctuating level.

With these ideas in mind, in this chapter we will focus on the study of fluctuations of the space- and time-integrated magnetization in a paradigmatic dissipative system: the stochastic one-dimensional perdiodic Landau-Ginzburg model [236]. The values of the parameters characterizing such a model completely define its behaviour. Indeed, the Ginzburg-Landau potential associated to this system can exhibit (i) one global minimum (one equilibrium state) or (ii) two symmetric global minima (two different equilibrium states). We will find that such a model presents a DPT for low values of the magnetization if the system is in the "double well" regime, i.e. if the potential has two different minima. Furthermore, we will analyze the form of the perturbation inmediately after the transition point, observing that two different dynamic phase transitions can take place depending on the system parameters: (a) a DPT between an uniform dynamical phase and a homogeneus time-dependent phase or (b) a DPT between an uniform phase and a spatio-temporal structured phase. Finally, we will find an exotic homogeneus time-periodic optimal magnetization field and we will characterize its structure and associated LDF.

6.2 Space- and time-integrated magnetization fluctuations in one-dimensional periodic Landau-Ginzburg model

Consider a system characterized by a scalar field (called magnetization) $\phi(x,t)$ with $x \in [0,1]$ and $t \in [0,\tau]$, which evolves according to the Langevin equation [93]:

$$\partial_t \phi(x,t) = -\frac{1}{2}\frac{\delta \mathcal{H}_{LG}[\phi(x,t)]}{\delta \phi(x,t)} + \varpi(x,t)\,, \qquad (6.1)$$

with:

$$\mathcal{H}_{LG} = \int_0^1 dx \left\{ \frac{1}{2}\partial_x \phi^2 + \frac{1}{2}\mu^2 \phi^2 + \frac{1}{4!}\lambda \phi^4 \right\} \qquad (6.2)$$

the Landau-Ginzburg Hamiltonian [236] and $\varpi(x,t)$ a Gaussian white noise with:

$$\langle \varpi(x,t) \rangle = 0 \qquad (6.3)$$

$$\langle \varpi(x,t)\varpi(x',t') \rangle = \frac{1}{\Omega}\delta(x-x')\delta(t-t')\,. \qquad (6.4)$$

Note that the dynamics of the system at hand is a particular case of the one presented in Section 2.6.1, with $F[\phi] = -\frac{1}{2}\frac{\delta \mathcal{H}_{LG}[\phi(x,t)]}{\delta \phi(x,t)}$ and $G[\phi] = 1$. Interestingly, the Langevin equation (6.1) corresponds to the well-known Hohenberg-Halperin

model A [93]. The functional derivative $\delta/\delta\phi$ of a certain functional of the form $R[\phi] = \int_0^1 dx\, r[\phi]$ is defined as:

$$\frac{\delta R[\phi(x,t)]}{\delta \phi(x,t)} = \frac{\partial r[\phi(x,t)]}{\partial \phi(x,t)} - \partial_x \cdot \frac{\partial r[\phi(x,t)]}{\partial(\partial_x \phi(x,t))} , \tag{6.5}$$

so the Langevin evolution equation (6.1) takes form:

$$\partial_t \phi(x,t) = \frac{1}{2}(\partial_x^2 \phi(x,t) - V'_{LG}[\phi(x,t)]) + \varpi(x,t) , \tag{6.6}$$

where

$$V_{LG}[\phi] = \frac{1}{2}\mu^2 \phi^2 + \frac{1}{4!}\lambda\phi^4 , \tag{6.7}$$

and $'$ stands for derivative with respect to the argument. To completely define the system at hand, Eq. (6.6) needs to be supplemented by appropiated boundary condition, which in this case is periodic, i.e.

$$\phi(x,t) = \phi(x+1,t) . \tag{6.8}$$

Note that both (6.6) and (6.8) describe a system which, after a time transient, evolve to an equilibrium state.

As we have shown in Section 2.6.1, we can write the mesoscopic evolution of this system in terms of a path integral representation. Indeed, in the large Ω limit, the weight of a given trajectory $\{\phi\}_0^\tau$ takes the form (see Eqs.(2.71) and (2.72))

$$\mathbb{P}(\{\phi\}_0^\tau) \propto \exp\left[-\Omega \mathcal{S}_\tau^{nc}[\phi]\right] , \tag{6.9}$$

with

$$\mathcal{S}_\tau^{nc}[\phi] = \frac{1}{2}\int_0^\tau dt \int_0^1 dx \left(\partial_t \phi - \frac{1}{2}(\partial_x^2 \phi - V'_{LG}[\phi])\right)^2 . \tag{6.10}$$

We are now in position to study fluctuations of the space- and time-integrated magnetization, namely

$$m = \frac{1}{\tau}\int_0^\tau dt \int_0^1 dx\, \phi(x,t) . \tag{6.11}$$

In this way, the probability of observing a given value of this observable is

$$P_\tau(m) = \int \mathcal{D}\phi\, P_{\text{st}}(\phi(\mathbf{r},0))\mathbb{P}\left(\{\phi\}_0^\tau\right)\delta\left(m - \frac{1}{\tau}\int_0^\tau dt \int_0^1 dx\, \phi(x,t)\right) , \tag{6.12}$$

103

where the initial condition is chosen from $P_{st}(\phi(\mathbf{r}, 0))$. The large deviation principle establishes that this probability scales as $P_\tau(m) \asymp \exp[-\tau\Omega G(m)]$, with $G(m)$ the large deviation function. According to Eq. (2.54), in the large time limit, the LDF can be written as

$$G(m) = \lim_{\tau\to\infty} \left\{ \frac{1}{\tau} \min_{\{\phi,\nu\}} S_\tau^{nc}[\phi, \nu] \right\}, \qquad (6.13)$$

with

$$S_\tau^{nc}[\phi, \nu] = \frac{1}{2} \int_0^\tau dt \int_0^1 dx \left[\left(\partial_t\phi - \frac{1}{2}(\partial_x^2\phi - V_{LG}'[\phi]) \right)^2 - \nu\phi \right], \qquad (6.14)$$

and ν the Lagrage multiplier guaranteeing that Eq. (6.11) is satisfied.

6.3 Uniform magnetization field and instability analysis

A trivial solution of the previous variational problem is consider the optimal field to be homogeneus and constant. In this way, according to (6.11), the most probable magnetization field is

$$\phi(x, t) = m, \qquad (6.15)$$

leading to a LDF of the form

$$G_U(m) = \frac{1}{2}V_{LG}'^2(m) = \frac{1}{8} \left(\mu^2 m + \frac{1}{3!}\lambda m^3 \right)^2. \qquad (6.16)$$

In Fig. 6.1 we show the form of the LDF for $\mu^2 = -1$ and $\lambda = 1$.

At this point, we can ask whether we can find other solutions of the variational problem (6.13) with more complex spatio-temporal structure which better minimize the action. To answer this question, we perturb the above uniform field with a small but arbitrary function of space and time, and study the local stability of flat solutions. Consequently, we write

$$\bar{\phi}(x, t) = m + \delta\phi(x, t). \qquad (6.17)$$

Inserting this expression in (6.13), and expanding to second order in the perturbation, we obtain the leading correction to $G_U(m)$, namely $O2$:

$$
\begin{aligned}
O2 &= \frac{1}{2\tau} \int_0^\tau dt \int_0^1 dx \left\{ \left[\frac{1}{4}V_{LG}''^2 + \frac{1}{2} \left(\partial_t\phi + \frac{1}{2}V_{LG}' - \frac{1}{2}\partial_x^2\phi \right) V_{LG}''' \right] \delta\phi^2 \right. \\
&\quad \left. + (\partial_t\delta\phi)^2 + \frac{1}{4}(\partial_x^2\delta\phi)^2 + V_{LG}''\delta\phi\partial_t\delta\phi - \frac{1}{2}V_{LG}''\delta\phi\partial_x^2\delta\phi \right\}. \qquad (6.18)
\end{aligned}
$$

Figure 6.1: Large deviation function $G_U(m)$ associated to uniform optimal field, with $\mu^2 = -1$ and $\lambda = 1$.

We now expand the perturbation $\delta\phi(x, t)$ in Fourier series, taking the advantage of the spatial periodic boundary condition, obtaining:

$$\delta\phi = \frac{1}{2}\alpha_0(x) + \sum_\omega \left(\alpha_\omega(x)\cos\omega t + \beta_\omega(x)\sin\omega t\right) , \qquad (6.19)$$

with:

$$\alpha_0(x) = \sum_{k_1} \left(a_{0k_1}\cos k_1 x + b_{0k_1}\sin k_1 x\right) , \qquad (6.20)$$

$$\alpha_\omega(x) = \frac{1}{2}a_{\omega 0} + \sum_{k_1} \left(a_{\omega k_1}\cos k_1 x + b_{\omega k_1}\sin k_1 x\right) , \qquad (6.21)$$

$$\beta_\omega(x) = \frac{1}{2}c_{\omega 0} + \sum_{k_1} \left(c_{\omega k_1}\cos k_1 x + d_{\omega k_1}\sin k_1 x\right) . \qquad (6.22)$$

Following the same procedure that we have shown in Section 5.2.1, we realize that, when we introduce these expasions in (6.18), the different modes decoupled as a consequence of the orthonormality property of Fourier basis. After a lenghty computation, it can be proved that the flat solution remains stable whenever the following conditions hold:

$$(V''_{LG})^2 + V'_{LG}V'''_{LG} > 0 \qquad (6.23)$$
$$(V''_{LG})^2 + V'_{LG}V'''_{LG} + k_n^2(k_n^2 + 2V''_{LG}) > 0 , \qquad (6.24)$$

105

where the potential V_{LG} is evaluated in m. Interestingly, one can see that

$$4G''_U = (V''_{LG})^2 + V'_{LG}V'''_{LG}, \tag{6.25}$$

so the previous conditions takes the form

$$G''_U > 0 \tag{6.26}$$
$$4G''_U + k_n^2(k_n^2 + 2V''_{LG}) > 0, \tag{6.27}$$

These solutions lead to some conclusions:

(i) The uniform solution is always stable if $\mu^2 > 0$, i.e. in the "single well" regime of the potential.

(ii) The first spatial mode to become unstable (if any) is the fundamental mode $k_1 = 2\pi$.

(iii) The interplay between $4G'''_U$ and $k_1^2(k_1^2 + 2V''_{LG})$ defines if the leading unstable perturbation has only temporal structure (associated to condition (6.26)) of spatio-temporal structure (associated to condition (6.26)).

Therefore, after comparing both $4G'''_U$ and $k_1^2(k_1^2 + 2V''_{LG})$, it can be proved that the system exhibits the following phenomenology:

- If $\mu^2 > 0$, the flat field $\phi(x,t) = m$ is stable for all m.

- If $\mu \in [-2\pi^2, 0]$, the flat field becomes unstable for $m < m_c$, with m_c being the solution of

$$G''_U(m_c) = 0. \tag{6.28}$$

  Furthemore, the most probable field inmediately after the transition point has only temporal structure, i.e. $\phi(x,t) = \phi(t)$.

- If $\mu < -2\pi^2$, the flat field becomes unstable for $m < \bar{m}_c$, with $\bar{m}_c$ being the solution of

$$4G''_U(\bar{m}_c) + (2\pi)^2((2\pi)^2 + 2V''_{LG}(\bar{m}_c)) = 0. \tag{6.29}$$

  Moreover, the most probable field inmediately after the transition point has spatio-temporal structure $\phi(x,t)$.

6.4 Time-periodic homogeneus magnetization field

In this Section we are going to focus on one particular solution of the variational problem (6.13): the time-periodic homogeneus magnetization field. The Euler-Lagrange equation derived from (6.13) for this solution takes the form:

$$\partial_t^2 \phi = \frac{1}{4} V'_{LG} V''_{LG} - \nu \,. \tag{6.30}$$

Integrating this equation we obtain

$$(\partial_t \phi)^2 = \frac{1}{4} V'^2_{LG} - \nu\phi + K \,, \tag{6.31}$$

with K a constant which encodes information about initial conditions. We can now reparametrize the field ϕ by

$$\phi = \bar{m}\bar{\phi} \,, \tag{6.32}$$

with $\bar{m}$ the positive minimum of the Landau-Ginzburg potential V_{LG}, that is

$$\bar{m} = \sqrt{\frac{3!|\mu^2|}{\lambda}} \,. \tag{6.33}$$

Hence, the equation for the optimal magnetization field (6.31) takes the form

$$(\partial_t \bar{\phi})^2 = f[\bar{\phi}] \,, \tag{6.34}$$

with

$$f[\bar{\phi}] = \frac{1}{\bar{m}^2} \left[\frac{1}{4} V'^2_{LG}[\bar{m}\bar{\phi}] - \nu\bar{m}\bar{\phi} + K \right] \,. \tag{6.35}$$

Let us assume the simplest case in which the optimal magnetization fields exhibits only a single minimum $\bar{\phi}_-$ and maximum $\bar{\phi}_+$. According to (6.34), these values are the solution of the equation $f[\bar{\phi}_\pm] = 0$. In this way, it can be proved that the period of the most probable magnetization field is

$$T = 2 \int_{\bar{\phi}_-}^{\bar{\phi}_+} \frac{d\bar{\phi}}{\sqrt{f[\bar{\phi}]}} \,, \tag{6.36}$$

and constraint (6.11) transforms into

$$m = \frac{2\bar{m}}{T} \int_{\bar{\phi}_-}^{\bar{\phi}_+} d\bar{\phi} \frac{\bar{\phi}}{\sqrt{f[\bar{\phi}]}} \,. \tag{6.37}$$

Finally, introducing this expressions in (6.13), we obtain the following expression for the large deviation function of the space- and time-integrated magnetization associated to a time-periodic homogeneus optimal field:

$$G_{\text{TP}}(\bar{\phi}) = \frac{1}{T} \int_{\bar{\phi}_-}^{\bar{\phi}_+} d\bar{\phi} \left\{ 2\bar{m}^2 \sqrt{f[\bar{\phi}]} + \frac{V_{LG}^{'2}[\bar{m}\bar{\phi}]}{2\sqrt{f[\bar{\phi}]}} \right\} . \qquad (6.38)$$

6.5 Conclusions

In this chapter we have studied the effects of fluctuations in dissipative systems with no conservation laws. In particular, by using similar tools that those provides by MFT, we have analyzed the distribution of fluctuations of the space- and time-integrated magnetization in the one-dimensional periodic stochastic Landau-Ginzburg model, with a dynamics given by the Hohenberg-Halperin model A. We have deduced the existence of a dynamic phase transition for low values of the magnetization by studying the stability of an uniform magnetization fields against spatio-temporal pertubations. We have observed that the DPT only takes place for $\mu^2 < 0$, which corresponds to the case in which the system presents two equilibrium states. Furthermore, we have seen the optimal trajectory inmediately beyond the transtion can exhibits only temporal or both spatio-temporal structures, depending on the value of μ^2 characterizing the system at hand. This results is of special relevance, since opens the door to the discovery of new phenomenology related to the appearance of DPTs in one-dimensional dissipative systems at a fluctuating level. Finally, we have found a new exotic dynamic phase beyond the transition. Indeed, for low values of the magnetization, the system evolve in time in a periodic way with no spatial structure. We have completely characterized the properties of this optimal trajectory and determined its associated LDF controlling the statistics of magnetization fluctuations.

Effective driven dynamics for one-dimensional conditioned Langevin processes in the weak-noise limit

7.1   Introduction

Traditional approaches in statistical physics are based on the study of the probability distribution of microscopic configurations at a given time [253]. Although such approaches have been very successful at equilibrium where configurations with the same energy are distributed uniformly in an isolated system, one is faced with difficulties when considering the statistics of configurations in non-equilibrium steady-states, as this statistics is in general non-uniform and unknown (see Introduction). It has been realised in the last decades that a more general space-time formulation, which deals with the statistics of full trajectories (that is, configurations as a function of time on a large time window) could be formulated in a quite general way, even for non-equilibrium systems [104, 254]. Moreover, the large-deviation formalism provides an efficient framework to formulate the problem [16, 139–142]. Along this Thesis we have shown that the large-deviation formalism is particularly useful for instance to evaluate the statistics of time-integrated observables (*e.g.*, particle current or dynamical activity), which are natural observables when characterising the statistics of trajectories [16–18, 55, 142, 147, 150, 255–257]. One can for instance consider a modified equilibrium statistics of trajectories conditioned to a given value of a time-integrated observable, like the average particle current. It is then of interest to ask whether this artificial, biased dynamics shares some similarities with (or even could be mapped to) a 'real' non-equilibrium dynamics. In other words, does a physical force which drives a system into a non-equilibrium state (and thus generates a given current) select all trajectories having a given average

current in a least-biased way?

In practice, fixing a given average value of an integrated observable is done by introducing a conjugated Lagrange multiplier (see Section 2.4.2), in the same way as, at equilibrium, temperature fixes the average energy in the canonical ensemble [16]. This Lagrange multiplier enters the definition of a "deformed" Markov operator that describes the biased dynamics. A well-know difficulty is that this deformed Markov operator no longer conserves probability, and cannot straightforwardly be interpreted as describing a *bona fide* probability-preserving dynamics. It has however been shown [72,73,76,258] how a relatively simple but abstract transformation of the deformed Markov operator allows one to define a closely related probability-conserving Markov operator, which defines an effective dynamics that is *asymptotically equivalent* at large times to the biased dynamics and the conditional dynamics [76,79,259] after proper normalisation. Under this new dynamics, the rare trajectories taking place in the original becomes now typical. Determining and characterizing such an effective dynamics will be the main goal of this chapter.

With these ideas in mind, the results we next expose are the following: focusing on the example of a particle diffusing in a periodic potential in one-dimension, we make analytical progress in the determination of large-deviation functions (LDF) quantifying the distribution of generic additive observables. We show that, in this case, the two asymptotic regimes we are considering, namely, the large-time and small-noise (i.e. large Ω) ones, can be taken in any order. A standard variational principle arising from a weak-noise, Wentzel–Kramers–Brillouin (WKB) [260] type asymptotic analysis is partially solved analytically and replaced by a much simpler one. This allows us to obtain an explicit form of the effective dynamics, and to study the occurrence of a singularity of the LDF, which corresponds to a dynamical phase transition separating different regimes of fluctuations.

LDFs of the distribution of additive observables in such periodic one-dimensional diffusive problems have been the subject of a number of studies in the past years, but the actual derivation of LDFs were mostly limited to peculiar additive observables, such as the entropy production [261–263] or the current [85, 264, 265], and were not fully explicit analytically. In this chapter, we extend a recent work in which the large deviations of the current were studied in the weak-noise asymptotics [85] to the case of generic time-integrated observables[1]. Instead of relying on an a numerical analysis of a truncated Fourier–Bloch decomposition of a spectral problem underlying the LDF problem (as done in [85, 262]), our work

---

[1]Remarkably, two recent works show similar approaches [266, 267]. The results of [266] are complementary to those we will present here and elucidate interesting finite-time behaviours in the initial and final times of the observation window $[0, \tau]$. In [267], the authors determine the non-zero temperature behaviour of the sCGF, for a periodic potential with no local minima.

is based on an analytical study of the the variational problem that governs the value of LDFs, using a different approach than the one presented in [264, 265] (a detailed comparison is provided when presenting our results). In this process, we find the optimal trajectories minimising the action (in analogy with Lagrangian mechanics); such trajectories are indexed by a conserved quantity (the energy) which, in our LDF problem, also has to be optimised over, in contrast to other physical situations where the energy is given. We show that the value of the action for the trajectory with optimal energy takes a very special form that simplifies the actual computation of the LDF, and that could prove useful in other contexts where variational principles fit in the framework of Lagrangian mechanics.

As we have repeatedly shown along this Thesis (see Section 2.5.4 and Chapter 5), when studying fluctuations of time-integrated observables, the existence of dynamical phase transitions are reflected as singularities (non-analiticities) of the large deviation functions. While the occurrence of dynamical phase transitions in periodic 1D diffusion problems has been analysed in previous studies [85, 263, 264], we provide in this chapter a thorough analysis of the competition between time-dependent and time-independent typical trajectories on both sides of the transition, together with a complete analysis of the LDF singularity (which takes the form of a first-order transition with a logarithmic prefactor that makes it continuous instead of discontinuous). The occurrence of transitions of such form is of special interest since, to our knowledge, they had not been previously determined in this context.

In this way, the chapter is organised as follows. In Section 7.2, we define the Langevin dynamics and reformulate it in a path-integral framework, to be able to bias the dynamics by a given value of the integrated additive observable considered. We also introduce the large deviation form of the action at large time, leading to the definition of the scaled cumulant generating function. In Section 7.3, we show how the scaled cumulant generating function can be evaluated explicitly, in the small noise limit, using a saddle-point calculation. Finally, in Section 7.4, we use the knowledge of the scaled cumulant generating function to derive an effective physically driven dynamics that leads to the same statistics of trajectories (after normalisation), and discuss its interpretation.

7.2 Rare trajectories: conditioning or biasing the dynamics

We present in this section the class of systems we focus on, and the type of the observables whose distribution we are interested in. We refer the reader to existing

reviews [142, 144] for generalisations for instance to mixed Langevin and Markov jump processes.

7.2.1 Langevin dynamics and additive observables

Consider a particle of position $x(t)$ at time t subjected to a force $F(x)$ and a thermal noise $\zeta(t)$. In the overdamped limit, the evolution of its position is described by the Langevin equation

$$\dot{x}(t) = F[x(t)] + \sqrt{\varepsilon}\,\zeta(t) \ , \tag{7.1}$$

where $\zeta(t)$ is a Gaussian white noise of average $\langle \zeta(t) \rangle = 0$ and correlation function $\langle \zeta(t)\zeta(t') \rangle = \delta(t - t')$. Note that this is a particular case of the class of systems presented in Section 2.6.2, identifying $G[x(t)] = 1$ and $\varepsilon = \Omega^{-1}$ (this last one equivalence implies that the weak-noise limit corresponds now to $\varepsilon \to 0$). Our interest goes to observables depending on the trajectory on a time window $[0, \tau]$ and taking the form[2]

$$A_\tau = \int_0^\tau h(x(t))\,dt + \int_0^\tau g(x(t))\,\dot{x}(t)\,dt \ . \tag{7.2}$$

Examples of such an *additive* observable encompass time-integrated current, work, entropy production, or activity for specific choices of the functions $h(x)$ and $g(x)$[3] (see [144] for examples). Contributions involving the function h are termed to be of 'density-type' while the ones involving g are of the 'current-type'. We are interested in the distribution $P_\tau(A_\tau)$ of the observable A_τ at time τ, in the weak-noise and/or the large-time limit. Under these assumptions, Large Deviation Theory provides a description of the scaling form of $P_\tau(A_\tau)$ [139–144]. In Section 2.4.2 we have developed the different techniques used to study macroscopic fluctuations of space- and time-integrated observables in systems characterized by a locally-conserved dynamics in the LDT (or MFT) formalism. In the following lines we will present an analogous approach for this new situation, starting from the path integral representation of previously defined dynamics. We will observe deep similarities between both schemes, laying bare the power and general nature of this mathematical framework.

---

[2]The stochastic integral in 7.2 is taken in the Stratonovich convention (see *e.g.* [268] for a review on stochastic integrals).

[3]In the following, for simplicity we will write the explicit dependency of functionals on the corresponding functions with () instead of [], that is $f[x] = f(x)$.

The Langevin equation (7.1) is equivalently described (see Section 2.6.2) by the Onsager–Machlup weight of a trajectory $\{x(t)\}_0^\tau$ of duration τ

$$\mathbb{P}(\{x(t)\}_0^\tau) \propto \exp\left[-\frac{1}{2\varepsilon}\int_0^\tau (\dot{x}-F)^2\, dt\right] \tag{7.3}$$

(valid in the weak-noise asymptotics $\varepsilon \to 0$) or by the Fokker–Planck equation for the evolution of the probability $P(x,t)$ of finding the particle at a position x at time t, which takes the form

$$\partial_t P(x,t) = \mathbb{W}P(x,t)\,. \tag{7.4}$$

The Fokker–Planck operator $\mathbb{W}$ reads:

$$\mathbb{W}\cdot = -\partial_x(F(x)\cdot) + \frac{1}{2}\varepsilon\partial_x^2\cdot\,. \tag{7.5}$$

Note that the conservation of probability reads $\langle-|\mathbb{W}=0$ where $\langle-|$ is the flat vector with all components equal to 1 (*i.e.* $\langle-|x\rangle = 1$ for all x)[4]. In other words, $\langle-|$ is a left eigenvector of $\mathbb{W}$ of eigenvalue 0. We now recall how, by studying the generating function of the observable A_τ, one can extend the operator approach we just presented in order to study the distribution of A_τ.

7.2.2 Path-integral and Fokker–Planck representations of the biased dynamics

We aim at characterising the physical features of trajectories $\{x(t)\}_0^\tau$ presenting an arbitrary (for instance, atypical) value of the observable A_τ. One way to proceed is to determine the probability $P_\tau(x,A)$ of the particle to be in position x at time τ, while having observed a value A of the additive observable (7.2) on the time window $[0,\tau]$. It reads as follows

$$P_\tau(x,A) = \left\langle \int_{x(0)}^{x(\tau)=x} \mathcal{D}x\, \delta(A-A_\tau)\, \exp\left[-\frac{1}{2\varepsilon}\int_0^\tau (\dot{x}-F)^2\, dt\right]\right\rangle_{x(0)} \tag{7.6}$$

where the notation $\langle \dots \rangle_{x(0)}$ indicates an average over the initial position $x(0)$ with a stationary distribution $P_{\mathrm{st}}(x)$. We implicitly assume that $x(0)$ is distributed with $P_{\mathrm{st}}(x)$ in the following, except otherwise indicated.

---

[4]Here we use a bra-ket notation to describe the vector space on which operators such as $\mathbb{W}$ act, with $|x\rangle$ the state representing the particle at position x and $\langle x|$ its transpose. These define the canonical scalar product $\langle x|x'\rangle = \delta(x-x')$.

It is difficult in general to determine $P_\tau(x, A)$ or even to write a closed equation for this 'microcanonical' probability. Following Varadhan [269], one performs a Laplace transform and introduces the following generating function (and its associated *biased* ensemble)

$$\Pi_\tau(x, \lambda) = \int e^{-\frac{\lambda}{\varepsilon}A} P_\tau(x, A) \, dA \tag{7.7}$$

$$= \left\langle \int_{x(0)}^{x(\tau)=x} \mathcal{D}x \, \exp\left[-\frac{1}{\varepsilon}\left[\lambda A_\tau + \frac{1}{2}\int_0^\tau (\dot{x} - F)^2 \, dt\right]\right]\right\rangle_{x(0)}$$

$$\equiv \left\langle \int_{x(0)}^{x(\tau)=x} \mathcal{D}x \, \exp\left[-\frac{1}{\varepsilon}S_\tau^\lambda[x(t)]\right]\right\rangle_{x(0)} \tag{7.8}$$

where $S_\tau^\lambda[x(t)]$ is defined as

$$S_\tau^\lambda[x(t)] = \lambda A_\tau + \frac{1}{2}\int_0^\tau (\dot{x} - F)^2 \, dt = \int_0^\tau \left\{\frac{1}{2}(\dot{x} - F)^2 + \lambda(h + \dot{x}g)\right\} dt \tag{7.9}$$

with $F \equiv F(x(t))$, $g \equiv g(x(t))$ and $h \equiv h(x(t))$ to lighten notations. As we have shown, in analogy with thermodynamics, this defines a 'canonical' version of the problem, where trajectories are biased by an exponential factor $\exp\left[-\frac{\lambda}{\varepsilon}A_\tau\right]$ on the time window $[0, \tau]$. In the large τ limit, as detailed below, the joint distribution corresponding to (7.6) and the generating function (7.7) present the same LDF scaling provided that the value of λ is well chosen as a function of A, as in any change of ensemble[5] (see *e.g.* [142] for a review). It is known that the evolution in time of $\Pi_\tau(x, \lambda)$ reads $\partial_t \Pi_t = \mathbb{W}_\lambda \Pi_t$ with a biased Fokker–Planck operator given by a generalised Feynman–Kac formula [79, 259]

$$\mathbb{W}_\lambda \cdot = -\partial_x\big((F - \lambda g) \cdot\big) + \frac{1}{2}\varepsilon \partial_x^2 \cdot + \frac{\lambda}{\varepsilon}\left(\frac{\lambda}{2}g^2 - gF - h\right)\mathbf{1} \cdot . \tag{7.10}$$

We provide here for completeness an alternative derivation based on path integrals, as it also sheds light on how one can jointly change process and LDF observable while keeping the same action. The starting point consists in remarking that the biased action $S_\tau^\lambda[x(t)]$ in 7.9 is equivalently written as:

$$S_\tau^\lambda[x(t)] = \int_0^\tau \frac{1}{2}(\dot{x} - F + \lambda g)^2 \, dt \;-\; \int_0^\tau \lambda\left(\frac{\lambda}{2}g^2 - gF - h\right) dt . \tag{7.11}$$

---

[5]This implies some requirement on the convexity of a large deviation function, as we explain below.

This rewriting (7.11) of the action (7.9) is only the factorisation of the $\lambda \dot{x} g$ contribution into the square term of the action. The action given in Eq. (7.11) can be interpreted as follows. The first integral in (7.11) is the action of a modified process[6] $x(t)$ obeying a Langevin equation

$$\dot{x} = F(x) - \lambda g(x) + \sqrt{\varepsilon}\, \zeta \,. \tag{7.12}$$

The second integral in (7.11) corresponds to a trajectorial reweighting

$$\exp\left\{ \int_0^\tau \frac{\lambda}{\varepsilon} \left[\frac{\lambda}{2} g(x(t))^2 - g(x(t)) F(x(t)) - h(x(t)) \right] dt \right\} \,. \tag{7.13}$$

Hence, the path integral over $x(t)$ of the full weight $\exp\left[-\frac{1}{\varepsilon} S_\tau^\lambda \right]$ is read as the average of the trajectorial reweighting (7.13) over the realisations of a process $x(t)$ obeying the modified Langevin equation (7.12). Since the integrand in (7.13) does not involve any time derivative, one can use the classical Feynman–Kac formula to finally infer the form of the biased operator (7.10) as follows: in this expression, the Fokker–Planck contribution $-\partial_x\big((F - \lambda g)\,\cdot\,\big) + \frac{1}{2}\varepsilon\partial_x^2\cdot$ corresponds to the modified process (7.12) and the diagonal part $\frac{\lambda}{\varepsilon}\big(\frac{\lambda}{2} g^2 - gF - h\big)\mathbf{1}$ corresponds to the integrand in (7.13).

Formally, the procedure we have just presented amounts to reinterpreting the biased operator (7.10), that describes LDFs for combination of current-type and density-type additive observables, into a biased operator for a purely density-type observable (since the integrand of (7.13) is independent of $\dot{x}$) but for a *different* process, Eq. (7.12) instead of Eq. (7.1). This procedure is the analogue for diffusions of a similar one that can be devised for Markov jump processes (see *e.g.* the Appendix B of [270]).

From a more physical viewpoint, the exposed procedure shows that even if the biasing resulting from the parameter λ can be partly reabsorbed into the force by changing $F(x)$ into $F(x) - \lambda g(x)$, the Langevin dynamics defined by Eq. (7.12) is not equivalent to the biased dynamics defined by the action Eq. (7.9), because of the remaining exponential reweighting given in Eq. (7.13). This remains true even in the simple case when A is the integrated current (or position of the particle), corresponding to $h(x) = 0$ and $g(x) = 1$. We will explain in the next sections how an effective probability-preserving dynamics, equivalent (in a sense that will be specified) to the biased dynamics defined by the action Eq. (7.9), can however be defined using a transformation of the operator $\mathbb{W}_\lambda$.

---

[6]The process described by Eq. (7.12) is not related to the effective process in general.

7.2.3 Large-deviation principle at large time

We now turn to the study of the large-time and weak-noise scaling behaviour of the distributions at hand. One first remarks from (7.10) that the biased operator $\mathbb{W}_\lambda$ does not preserve probability (at odds with $\mathbb{W}$, $\langle-|$ is not a left eigenvector of $\mathbb{W}_\lambda$ of eigenvalue 0). In fact, the Perron–Frobenius theorem[7] ensures that the maximal eigenvalue $\varphi_\varepsilon(\lambda)$ of $\mathbb{W}_\lambda$ is real and unique. We now assume that this operator has a gap (this is the case in general if the force is confining or if the space is compact); this ensures that at large time one has

$$e^{\tau \mathbb{W}_\lambda} \underset{t\to\infty}{\sim} e^{\tau\,\varphi_\varepsilon(\lambda)} |R\rangle\langle L| \qquad \text{with} \quad \varphi_\varepsilon(\lambda) = \max \mathrm{Sp}\ \mathbb{W}_\lambda \qquad (7.14)$$

where $\langle L|$ and $|R\rangle$ are the corresponding left and right eigenvectors of $\mathbb{W}_\lambda$, normalised as $\langle L|R\rangle = 1$ and $\langle-|R\rangle = 1$. Then, the formal solution $|\Pi_\tau\rangle = e^{\tau \mathbb{W}_\lambda}|P_{\mathrm{st}}\rangle$ of the evolution equation $\partial_t \Pi_t = \mathbb{W}_\lambda \Pi_t$ implies that

$$\Pi_\tau(x, \lambda) \underset{\tau\to\infty}{\asymp} e^{\tau\,\varphi_\varepsilon(\lambda)} R(x)\,. \qquad (7.15)$$

Integrating (7.7) over x, this implies that, at large time, the moment generating function behaves as

$$\left\langle e^{-\frac{\lambda}{\varepsilon} A_\tau} \right\rangle \underset{\tau\to\infty}{\asymp} e^{\tau\,\varphi_\varepsilon(\lambda)}\,. \qquad (7.16)$$

This result is an instance of a large deviation function (LDF) exponential scaling [20]: it indicates that the scaled cumulant generating function (sCGF) $\Phi_\varepsilon(\lambda, \tau)$ defined as

$$\left\langle e^{-\frac{\lambda}{\varepsilon} A_\tau} \right\rangle = e^{\tau\,\Phi_\varepsilon(\lambda,\tau)} \qquad (7.17)$$

goes to a constant at large τ: $\lim_{\tau\to\infty} \Phi_\varepsilon(\lambda, \tau) = \varphi_\varepsilon(\lambda)$. In other words, all cumulants of the observable A_τ behave linearly in τ at large τ.

Such LDF scaling can be translated into a large-time behaviour of the distribution of A: integrating (7.7) over x one gets from (7.17) that

$$e^{\tau\,\Phi_\varepsilon(\lambda,\tau)} = \int e^{-\frac{\lambda}{\varepsilon} A}\, P_\tau(A)\, dA\,. \qquad (7.18)$$

Since the l.h.s. behaves exponentially in τ at large τ, this is compatible with a distribution $P_\tau(A \simeq a\tau)$ obeying the following scaling

$$P_\tau(A \simeq a\tau) \underset{\tau\to\infty}{\asymp} e^{\tau\,\pi_\varepsilon(a)}\,, \qquad (7.19)$$

---

[7]We assume that its conditions of validity are satisfied.

with φ_ε and π_ε related through

$$\varphi_\varepsilon(\lambda) = \sup_a \left\{ \pi_\varepsilon(a) - \frac{\lambda}{\varepsilon} a \right\}. \tag{7.20}$$

This is an example of large deviation principle, obtained here through a saddle-point analysis of the integral in (7.18) through the Gärtner–Ellis theorem [145, 146]. It indicates that, in the scaling $A \simeq a\tau$, the distribution of A concentrates exponentially around the most probable value(s) of a, located at the maxima of the function $\pi_\varepsilon(a)$. If $\pi_\varepsilon(a)$ is a concave function of a, then one can invert the Legendre–Fenchel transformation appearing in (7.20) and obtain

$$\pi_\varepsilon(a) = \inf_\lambda \left\{ \varphi_\varepsilon(\lambda) - \frac{\lambda}{\varepsilon} a \right\}. \tag{7.21}$$

These two Legendre–Fenchel transformations describe the change of ensemble between the microcanonical (fixed a) and canonical (fixed λ) descriptions, at fixed ε. The correspondence (7.21) can be extended at the level of trajectories: under the same convexity hypothesis, the trajectories conditioned to present a given value of $a = A_\tau/\tau$ and the trajectories weighted by $\exp\left[-\frac{1}{\varepsilon} S_\lambda\right]$ present an asymptotically equivalent distribution as $\tau \to \infty$, in a sense defined and studied in great depth by Chétrite and Touchette [79, 259], provided that the value of λ is the one which realises the infimum in (7.21).

7.2.4 Large-deviation principle in the weak-noise asymptotics $\varepsilon \to 0$

We now consider the opposite order of limits, by keeping the duration τ finite and sending first the noise amplitude to 0. Note that this order of limits is the one that we have presented in Chapter 2 and used along this Thesis. In this way, we can now focus on the path-integral representation (7.8) in order to study the weak-noise asymptotics of the distributions. By a saddle-point evaluation in the $\varepsilon \to 0$ limit, one sees from the definition (7.17) that, integrating (7.8) over x, the sCGF behaves as

$$\Phi_\varepsilon(\lambda, \tau) \underset{\varepsilon \to 0}{\sim} \frac{1}{\varepsilon} \mu_\tau(\lambda) \qquad \text{with} \quad \mu_\tau(\lambda) = -\frac{1}{\tau} \inf_{x(t)} S_\tau^\lambda[x(t)] \tag{7.22}$$

where the action $S_\tau^\lambda[x(t)]$ is defined in (7.9). The optimisation is performed over trajectories $\{x(t)\}_0^\tau$ of duration τ, whose initial position $x(0)$ is sampled according to the initial stationary distribution $P_{\rm st}$ (the simplest case is when $x(0)$ takes a fixed value), and whose final position $x(\tau)$ is optimised over in the $\inf$ of (7.22). The

function $\mu_\tau(\lambda)$ is a sCGF. Since $\Phi_\varepsilon(\lambda, \tau)$ converges to $\varphi_\varepsilon(\lambda)$ as $\tau \to \infty$ for all ε (see (7.16)), one expects that

$$\lim_{\tau \to \infty} \mu_\tau(\lambda) = \mu(\lambda) \qquad \text{with} \quad \varphi_\varepsilon(\lambda) \underset{\varepsilon \to 0}{\sim} \frac{1}{\varepsilon} \mu(\lambda). \qquad (7.23)$$

Situations where noise-dependent LDFs (here, $\varphi_\varepsilon(\lambda)$) scale as one over the noise strength were for instance considered in [85, 271]. In all, the saddle-point asymptotics provides the following optimisation principle for the sCGF $\mu(\lambda)$ as:

$$\mu(\lambda) = -\lim_{\tau \to \infty} \left\{ \frac{1}{\tau} \inf_{x(t)} S_\tau^\lambda[x(t)] \right\}. \qquad (7.24)$$

Hence, the determination of $\mu(\lambda)$ requires the knowledge of the optimal trajectories in the weak-noise limit[8]. This is the topic of the next section.

It is not obvious that the large-time and the weak-noise commute, *i.e.* that the sCGF $\mu(\lambda)$ given in (7.24) by first taking $\varepsilon \to 0$ and then $\tau \to \infty$ is the same as the $\varepsilon \to 0$ asymptotics $\mu(\lambda) = \lim_{\varepsilon \to 0}[\varepsilon\,\varphi_\varepsilon(\lambda)]$ (see 7.23) of the CGF $\varphi_\varepsilon(\lambda)$ obtained from spectral considerations by first taking the $\tau \to \infty$ limit, as done in (7.16). We will show in Sections 7.3 and 7.4 that these two definitions coincide for periodic systems, *i.e.* that one can take the large-time and the weak-noise limits in whichever order one prefers.

7.3 Determination of the sCGF $\mu(\lambda)$ for spatially periodic systems

7.3.1 Optimal trajectories in the weak-noise limit

We now aim at computing the scaled cumulant generating function $\mu(\lambda)$ by minimising the action $S_\tau^\lambda[x(t)]$ according to Eq. (7.24). The saddle-point equation for the optimal path sustaining a given fluctuation is obtained from the optimisation principle (7.22) and reads

$$\ddot{x} - F(x)F'(x) - \lambda h'(x) = 0, \qquad (7.25)$$

where the prime denotes a derivative with respect to x. We note that it does not depend on the function $g(x)$ since the term $\dot{x}(t)\,g(x(t))$ in the integrand of the action (7.9) is a total derivative, but of course the function $g(x)$ still plays a role

---

[8]Note that this definition of the sCGF coincides with the one we have used along this Thesis just by a change of sign.

because it appears in the expression of the action whose value is to be minimised. It represents the conservative dynamics of a particle of unit mass in a potential

$$\mathcal{V}(x) = -\frac{1}{2}F(x)^2 - \lambda h(x). \tag{7.26}$$

As a result, the energy

$$\mathcal{E}(\dot{x}, x) = \frac{1}{2}\dot{x}^2 + \mathcal{V}(x) \tag{7.27}$$

is conserved along an optimal trajectory. Let us recall, however, that while optimal trajectories obey a deterministic conservative dynamics in the potential $\mathcal{V}(x)$ given by Eq. (7.26), the original dynamics of the problem obeys an overdamped Langevin dynamics, with a deterministic force $F(x)$ that may derive or not from a potential — see Eq. (7.1). Note that since $x(t)$ satisfies the second-order differential equation (7.25), it is uniquely specified in general only when one specifies a set of two parameters. It is convenient to choose for these two parameters the energy $\mathcal{E}$ and the initial position x_{i} (and the sign of the initial velocity, as we explain later).

Importantly, the initial position x_{i} for the optimal trajectory (solution of Eq. (7.25)) in the weak-noise asymptotic regime differs from the 'physical' initial condition $x(0)$ considered in the path integral (7.6) and sampled with P_{st}. Indeed, the underlying Langevin dynamics is dissipative, so that the biased distribution $\Pi_\tau(x, \lambda)$ converges to a steady state at large finite time τ after a transient; then, the optimal trajectory that obeys the non-dissipative evolution (7.25) describes the most probable loci of $\Pi_\tau(x, \lambda)$. In other words, there is a transient regime for the 'physical' initial distribution $P_{\mathrm{st}}(x)$ to reach a distribution $\Pi_\tau(x, \lambda)$ that falls into a consistent weak-noise description. As a result, the initial distribution $P_{\mathrm{st}}(x)$ becomes irrelevant after this transient regime and can thus be forgotten in the weak-noise evaluation of the path-integral (7.6), since it does not fall in general in the weak-noise large-deviation regime.

On the other hand, Eq. (7.25) has an infinite number of solutions, only one of them being the actual optimal trajectory that minimises the action $S_\tau^\lambda[x(t)]$. To determine this optimal trajectory, one has to parameterise each solution of Eq. (7.25) by the initial position x_{i} and the energy $\mathcal{E}$, but again, x_{i} differs from the 'physical' initial condition $x(0)$.

In the following, we consider finite-size spatially periodic systems, for which $F(x + 1) = F(x)$, $h(x + 1) = h(x)$ and $g(x + 1) = g(x)$ (we took the spatial period as the unit length, without loss of generality). Such periodic systems have been studied in previous works, especially in the weak-noise asymptotics [85], but for a specific additive observable such as the entropy production [261–263] or the

current [85, 264, 265] and using a numerical approach based on a Fourier–Bloch decomposition [85, 262]. Our aim is to keep the form of the additive observable A_τ generic and the approach analytical for as long as possible in the study of the problem at hand, in order, in particular, to fully characterise dynamical phase transitions that are known to occur [85, 261, 262, 264] in this problem but that were not completely understood (the order of such transition for instance remained unclear).

For such spatially periodic systems, the optimal trajectory minimising the action $S_\tau^\lambda[x(t)]$ becomes independent of $x(0)$ for large enough time τ, so that the only relevant parameter to characterise the trajectories in this limit is their energy. To determine the sCGF $\mu(\lambda)$, one has to evaluate the action $S_\tau^\lambda[x(t)]$ for any of the optimal trajectories given by Eq. (7.25), and to find the optimal trajectory that minimises the action. In practice, this last step consists in minimising the action over the energy of the trajectories. Using Eqs. (7.9) and (7.26), the action $S_\tau^\lambda[x(t)]$ can be written as

$$S_\tau^\lambda[x(t)] = \int_0^\tau dt\, \mathcal{L}(\dot{x}(t), x(t)) \tag{7.28}$$

with a Lagrangian

$$\mathcal{L}(\dot{x}, x) = \frac{1}{2}\dot{x}^2 - \mathcal{V}(x) + \dot{x}\big(\lambda g(x) - F(x)\big). \tag{7.29}$$

Note that the last term, proportional to $\dot{x}$, in Eq. (7.29) plays no role in Eq. (7.25) since it is a total derivative, but it has to be included in the Lagrangian to correctly evaluate (and minimise) the action.

Assuming that the force field $F(x)$ and the function $h(x)$ are bounded, the potential $\mathcal{V}(x)$ is also bounded. We denote as $\mathcal{V}_{\mathrm{max}}$ the maximum value of the potential:

$$\mathcal{V}_{\mathrm{max}} = \max_x \mathcal{V}(x). \tag{7.30}$$

The value $\mathcal{V}_{\mathrm{max}}$ allows one to classify the optimal trajectories $x^\star(t)$ into periodic and propagative solutions, according to their energy $\mathcal{E}$ (for convenience, we include constant trajectories as a special case of the periodic ones). For $\mathcal{E} < \mathcal{V}_{\mathrm{max}}$, optimal trajectories are confined by the potential $\mathcal{V}(x)$, and are periodic in time. For $\mathcal{E} > \mathcal{V}_{\mathrm{max}}$, the potential no longer confines the optimal trajectories, which are then propagative, with a constant sign of the velocity $\dot{x}$. As a result, the sCGF $\mu(\lambda)$ is obtained by minimising the action over both sets of periodic and propagative optimal trajectories. One can thus write, taking into account the minus sign in Eq. (7.24),

$$\mu(\lambda) = \max\left\{\mu_{\mathrm{per}}(\lambda), \mu_{\mathrm{prop}}(\lambda)\right\} \tag{7.31}$$

where $\mu_{\text{per}}(\lambda)$, $\mu_{\text{prop}}(\lambda)$ are defined by minimising the action over the sets of periodic and propagative trajectories respectively:

$$\mu_{\text{per}}(\lambda) = -\lim_{\tau \to \infty} \left\{ \frac{1}{\tau} \inf_{\mathcal{E} < \mathcal{V}_{\text{max}}} S_\tau^\lambda[x^\star(t)] \right\}, \tag{7.32}$$

$$\mu_{\text{prop}}(\lambda) = -\lim_{\tau \to \infty} \left\{ \frac{1}{\tau} \inf_{\mathcal{E} > \mathcal{V}_{\text{max}}} S_\tau^\lambda[x^\star(t)] \right\}. \tag{7.33}$$

In the following, we successively evaluate $\mu_{\text{per}}(\lambda)$ and $\mu_{\text{prop}}(\lambda)$.

7.3.2 Time-periodic trajectories

We start by evaluating $\mu_{\text{per}}(\lambda)$. A particular type of periodic trajectories are the time-independent ones, for which $\dot{x}^\star = 0$ and $x^\star = x_0$, implying $\mathcal{V}'(x_0) = 0$ from Eq. (7.25). For such trajectories, one has $\mathcal{L}(\dot{x}^\star, x^\star) = -\mathcal{V}(x_0)$, so that minimising the action over time-independent trajectories selects points x_0 that are at the location(s) of the maximum of the potential $\mathcal{V}(x)$; hence:

$$\lim_{\tau \to \infty} \left\{ \frac{1}{\tau} \inf_{x(t) = x_0} S_\tau^\lambda[x^\star(t)] \right\} = -\mathcal{V}_{\text{max}}. \tag{7.34}$$

Considering now a generic time-periodic optimal trajectory, the action reads, with $x^\star \equiv x^\star(t)$

$$
\begin{aligned}
\frac{1}{\tau} S_\tau^\lambda[x^\star(t)] &= \underbrace{\frac{1}{2\tau} \int_0^\tau dt\, (\dot{x}^\star)^2}_{\geq 0} \underbrace{- \frac{1}{\tau} \int_0^\tau dt\, \mathcal{V}(x^\star)}_{\geq -\mathcal{V}_{\text{max}}} \\
&+ \underbrace{\frac{1}{\tau} \int_0^\tau dt\, \dot{x}^\star \left(\lambda g(x^\star) - F(x^\star) \right)}_{\to 0 \text{ when } \tau \to \infty}.
\end{aligned} \tag{7.35}
$$

The proof that the last integral in (7.35) goes to 0 when $\tau \to \infty$ comes from a change of variable from t to x:

$$\frac{1}{\tau} \int_0^\tau dt\, \dot{x}^\star \left(\lambda g(x^\star) - F(x^\star) \right) = \frac{1}{\tau} \int_{x^\star(0)}^{x^\star(\tau)} dx \left(\lambda g(x) - F(x) \right) \tag{7.36}$$

which goes to 0 when $\tau \to \infty$ because $[\lambda g(x) - F(x)]$ is bounded on the finite interval $[x^\star(0), x^\star(\tau)]$. It is tempting to take the $\tau \to \infty$ limit and to conclude from (7.32) that $\mu_{\text{per}}(\lambda) \leq \mathcal{V}_{\text{max}}$ but this would require to exchange the $\inf$ and the $\tau \to \infty$ limit in (7.32), which enters in conflict with our goal since we are

121

interested in how the small-noise and large-time limits commute. To avoid this exchange, one writes from (7.35) that for any time-periodic optimal trajectory,

$$\frac{1}{\tau} \inf_{\mathcal{E} < \mathcal{V}_{\max}} S_\tau^\lambda[x^\star(t)] \geq -\mathcal{V}_{\max} - \frac{1}{\tau} \inf_{\mathcal{E} < \mathcal{V}_{\max}} \int_{x^\star(0)}^{x^\star(\tau)} dx \left(\lambda g(x) - F(x) \right) \quad (7.37)$$

so that taking the $\tau \to \infty$ limit one finds

$$\lim_{\tau \to \infty} \left\{ \frac{1}{\tau} \inf_{\mathcal{E} < \mathcal{V}_{\max}} S_\tau^\lambda[x^\star(t)] \right\} \geq -\mathcal{V}_{\max} , \quad (7.38)$$

because the integrand on the r.h.s. of (7.37) is a bounded function on an interval of fixed finite length. From the definition (7.32), we obtain $\mu_{\mathrm{per}}(\lambda) \leq \mathcal{V}_{\max}$. Remarking now from (7.28-7.29) that this bound is realised for time-independent trajectories $x^\star = x_0$ we conclude that

$$\mu_{\mathrm{per}}(\lambda) = \mathcal{V}_{\max}(\lambda) \quad (7.39)$$

where the λ-dependence of $\mathcal{V}_{\max}$ has been made explicit. Therefore, for $\mathcal{E} < \mathcal{V}_{\max}$, the optimal trajectories sustaining a given fluctuations are time-independent of the form $x^\star = x_0$, where x_0 are the points maximising the potential $\mathcal{V}(x_0) = \mathcal{V}_{\max}$.

7.3.3 Propagative trajectories

To evaluate $\mu_{\mathrm{prop}}(\lambda)$, one now has to compute the minimum of the action over all propagative optimal trajectories, *i.e.*, trajectories for which $\mathcal{E} > \mathcal{V}_{\max}$. Then, from energy conservation, one has

$$\dot{x}^\star = \sigma \sqrt{2 \left(\mathcal{E} - \mathcal{V}(x^\star) \right)} \quad (7.40)$$

where $\sigma = \pm 1$ is the sign of $\dot{x}^\star$ (we recall that the sign of $\dot{x}^\star$ is constant all along propagative trajectories). Propagative trajectories are pseudo-periodic, in the sense that $x^\star(t + T) = x^\star(t) + \sigma$, which may be identified with $x^\star(t)$ due to the spatial periodicity of the system; $T = T(\mathcal{E})$ is the pseudo-period $T(\mathcal{E})$, determined as

$$T = \int_0^T dt = \int_0^1 \frac{dx}{\sqrt{2 \left(\mathcal{E} - \mathcal{V}(x) \right)}} , \quad (7.41)$$

where we have used Eq. (7.40) to change the integration variable from t to x. Using the relation

$$\mathcal{L}(\dot{x}^\star, x^\star) = \mathcal{E} - 2\mathcal{V}(x^\star) + \dot{x}^\star \left(\lambda g(x^\star) - F(x^\star) \right) , \quad (7.42)$$

the action of a propagative optimal trajectory on the time interval $[0, T(\mathcal{E})]$ is, expanding the Lagrangian (7.29),

$$S^\lambda_{T(\mathcal{E})}[x^\star(t)] = \sigma \int_0^1 \big(\lambda g(x) - F(x)\big) dx + T(\mathcal{E})\mathcal{E} - \int_0^1 \frac{2\mathcal{V}(x)}{\sqrt{2\big(\mathcal{E} - \mathcal{V}(x)\big)}}\, dx\,. \tag{7.43}$$

To lighten notations, we define

$$B = \int_0^1 \big(\lambda g(x) - F(x)\big) dx\,, \qquad R(\mathcal{E}) = \int_0^1 \frac{2\mathcal{V}(x)}{\sqrt{2\big(\mathcal{E} - \mathcal{V}(x)\big)}}\, dx\,. \tag{7.44}$$

Note that the term $F(x)$ in the integral defining B gives no contribution when the force $F(x)$ derives from a potential.

In the large-time limit, the value of the action over every interval $[nT(\mathcal{E}), (n+1)T(\mathcal{E})]$ is the same (by periodicity of the optimal trajectory). Furthermore, the optimal trajectory dependence on the initial value x_0 is now replaced by a pseudo-periodic boundary condition of the form $x(1) = x(0) + \sigma$. Hence the $\mu_{\text{prop}}(\lambda)$ defined in Eq. 7.33 is equal to:

$$\mu_{\text{prop}}(\lambda) = -\lim_{n\to\infty} \inf_{\mathcal{E}>\mathcal{V}_{\text{max}},\, \sigma=\pm 1} \left\{ \frac{1}{nT(\mathcal{E})} \int_0^{nT(\mathcal{E})} \mathcal{L}(\dot{x}^\star, x^\star)\, dt \right\} \tag{7.45}$$

$$= -\inf_{\mathcal{E}>\mathcal{V}_{\text{max}},\, \sigma=\pm 1} \left\{ \frac{1}{T(\mathcal{E})} \int_0^{T(\mathcal{E})} \mathcal{L}(\dot{x}^\star, x^\star)\, dt \right\} \tag{7.46}$$

$$= -\inf_{\mathcal{E}>\mathcal{V}_{\text{max}},\, \sigma=\pm 1} \left\{ \mathcal{E} + \frac{\sigma B - R(\mathcal{E})}{T(\mathcal{E})} \right\} \tag{7.47}$$

where in (7.45)-(7.46) the optimal trajectory $x^\star(t)$ is the propagative solution of the saddle-point equation, with an energy $\mathcal{E}$ and a pseudo-period $T(\mathcal{E})$ that depends on $\mathcal{E}$, as inferred from (7.41). Determining $\mu_{\text{prop}}(\lambda)$ thus amounts to finding, for both $\sigma = \pm 1$, the infimum of the function

$$\Psi_\sigma(\mathcal{E}) = \mathcal{E} + \frac{\sigma B - R(\mathcal{E})}{T(\mathcal{E})}\,. \tag{7.48}$$

The function $\Psi_\sigma(\mathcal{E})$ is defined over the interval $(\mathcal{V}_{\text{max}}, +\infty)$. When $\mathcal{E} \to \mathcal{V}_{\text{max}}$, both $R(\mathcal{E})$ and $T(\mathcal{E})$ diverge to infinity (assuming $\mathcal{V}(x)$ is regular close to $\mathcal{V}_{\text{max}}$), but their ratio $R(\mathcal{E})/T(\mathcal{E}) \to 2\mathcal{V}_{\text{max}}$, so that $\Psi_\sigma(\mathcal{E}) \to -\mathcal{V}_{\text{max}}$. In the opposite limit $\mathcal{E} \to \infty$, $T(\mathcal{E}) \sim R(\mathcal{E}) \sim 1/\sqrt{\mathcal{E}}$, yielding $\Psi_\sigma(\mathcal{E}) \to +\infty$. Consequently, if $\Psi_\sigma(\mathcal{E})$ has no minimum for $\mathcal{E} \in (\mathcal{V}_{\text{max}}, +\infty)$, one has:

$$\inf_{\mathcal{E}>\mathcal{V}_{\text{max}}} \Psi_\sigma(\mathcal{E}) = -\mathcal{V}_{\text{max}}\,. \tag{7.49}$$

We now proceed to determine if $\Psi_\sigma(\mathcal{E})$ has a minimum $\mathcal{E}_\sigma^*$, satisfying $\Psi_\sigma'(\mathcal{E}_\sigma^*) = 0$. The derivative $\Psi_\sigma'(\mathcal{E})$ reads

$$\Psi_\sigma'(\mathcal{E}) = \frac{1}{T(\mathcal{E})^2}\left[T(\mathcal{E})^2 - R'(\mathcal{E})T(\mathcal{E}) + R(\mathcal{E})T'(\mathcal{E}) - \sigma B T'(\mathcal{E})\right]. \quad (7.50)$$

From the definition (7.44) of $R(\mathcal{E})$, one finds that

$$R'(\mathcal{E}) = T(\mathcal{E}) + 2\mathcal{E}T'(\mathcal{E}) \quad (7.51)$$

so that $\Psi_\sigma'(\mathcal{E})$ can be rewritten as

$$\Psi_\sigma'(\mathcal{E}) = \frac{T'(\mathcal{E})}{T(\mathcal{E})^2}\left[R(\mathcal{E}) - 2\mathcal{E}T(\mathcal{E}) - \sigma B\right]. \quad (7.52)$$

Since $T'(\mathcal{E}) \neq 0$ for all $\mathcal{E}$, the condition $\Psi_\sigma'(\mathcal{E}_\sigma^*) = 0$ is equivalent to

$$R(\mathcal{E}_\sigma^*) - 2\mathcal{E}_\sigma^* T(\mathcal{E}_\sigma^*) - \sigma B = 0 \quad (7.53)$$

which determines $\mathcal{E}_\sigma^*$. If a solution $\mathcal{E}_\sigma^*$ exists, one has from Eqs. (7.48) and (7.53)

$$\Psi_\sigma(\mathcal{E}_\sigma^*) = \mathcal{E}_\sigma^* + \frac{\sigma B - R(\mathcal{E}_\sigma^*)}{T(\mathcal{E}_\sigma^*)} = -\mathcal{E}_\sigma^*. \quad (7.54)$$

Using Eqs. (7.51) and (7.53), one can show that the second derivative $\Psi_\sigma''(\mathcal{E}_\sigma^*)$ takes the simple form

$$\Psi_\sigma''(\mathcal{E}_\sigma^*) = -\frac{T'(\mathcal{E}_\sigma^*)}{T(\mathcal{E}_\sigma^*)} = \frac{\int_0^1 \left(\mathcal{E}_\sigma^* - \mathcal{V}(x)\right)^{-3/2} dx}{2\int_0^1 \left(\mathcal{E}_\sigma^* - \mathcal{V}(x)\right)^{-1/2} dx} > 0, \quad (7.55)$$

so that $\mathcal{E}_\sigma^*$ is a local minimum. The fact that it is a global minimum comes from a unicity argument, which goes as follows. Eq. (7.53) can be rewritten using Eqs. (7.41) and (7.44) as

$$\int_0^1 \sqrt{2\left(\mathcal{E}_\sigma^* - \mathcal{V}(x)\right)}\, dx = -\sigma B. \quad (7.56)$$

The integral on the l.h.s. of Eq. (7.56) spans the interval

$$(\int_0^1 \sqrt{2(\mathcal{V}_{\max} - \mathcal{V}(x))}\, dx, +\infty) \quad (7.57)$$

as a function of $\mathcal{E}_\sigma^*$. Hence a solution $\mathcal{E}_\sigma^*$ exists if

$$- \sigma B > \int_0^1 \sqrt{2\big(\mathcal{V}_{\max} - \mathcal{V}(x)\big)}\, dx \qquad (7.58)$$

where we recall that B is defined in Eq. (7.44). Since $\int_0^1 \sqrt{2(\mathcal{E} - \mathcal{V}(x))}\, dx$ is an increasing function of $\mathcal{E}$, the solution $\mathcal{E}_\sigma^*$ is unique if it exists. Hence the function $\Psi_\sigma(\mathcal{E})$ has at most one stationary point, so that its local minimum $\mathcal{E}_\sigma^*$ is, if it exists, a global minimum. In addition, if $\mathcal{E}_\sigma^*$ exists, then $\mathcal{E}_{-\sigma}^*$ does not exist, since Eq. (7.58) cannot be simultaneously satisfied for σ and $-\sigma$. This implies that $\mathcal{E}_\sigma^*$ can exist only for

$$\sigma = -\text{sign}(B)\,, \qquad (7.59)$$

and Eq. (7.58) can be rewritten as

$$|B| > \int_0^1 \sqrt{2\big(\mathcal{V}_{\max} - \mathcal{V}(x)\big)}\, dx\,. \qquad (7.60)$$

If Eq. (7.60) is satisfied, one has for $\sigma = -\text{sign}(B)$ that

$$\inf_{\mathcal{E}>\mathcal{V}_{\max}} \Psi_\sigma(\mathcal{E}) = -\mathcal{E}_\sigma^*, \quad \text{and} \quad \inf_{\mathcal{E}>\mathcal{V}_{\max}} \Psi_{-\sigma}(\mathcal{E}) = -\mathcal{V}_{\max}\,. \qquad (7.61)$$

As a result, Eq. (7.47) implies

$$\mu_{\text{prop}}(\lambda) = -\min\{-\mathcal{E}_\sigma^*, -\mathcal{V}_{\max}\} = \max\{\mathcal{E}_\sigma^*, \mathcal{V}_{\max}\} = \mathcal{E}_\sigma^* \qquad (7.62)$$

(with $\sigma = -\text{sign}(B)$) if Eq. (7.60) holds.

In the opposite case, if Eq. (7.60) is not satisfied,

$$\inf_{\mathcal{E}>\mathcal{V}_{\max}} \Psi_\sigma(\mathcal{E}) = \inf_{\mathcal{E}>\mathcal{V}_{\max}} \Psi_{-\sigma}(\mathcal{E}) = -\mathcal{V}_{\max}\,, \qquad (7.63)$$

so that

$$\mu_{\text{prop}}(\lambda) = \mathcal{V}_{\max}\,. \qquad (7.64)$$

Since from Eq. (7.39) $\mu_{\text{per}}(\lambda) = \mathcal{V}_{\max} \leq \mu_{\text{prop}}(\lambda)$, Eq. (7.31) implies that for all λ

$$\mu(\lambda) = \mu_{\text{prop}}(\lambda)\,. \qquad (7.65)$$

To summarise, we have shown that when a propagative optimal solution exists, it is unique and the value of the corresponding sCGF is given by the *energy* $\mathcal{E}_\sigma^*$ of such trajectory; otherwise, the value of the sCGF is given by the maximum

value $\mathcal{V}_{\max}$ of the potential $\mathcal{V}(x)$. This result is surprisingly simple in view of the complicated optimisation problem one is initially facing, and it is key to the explicit determination of the sCGF. We emphasise that although the search of optimal trajectories (coming as a standard consequence of the weak-noise approach) is formulated in the framework of Lagrangian mechanics, the result we have obtained goes one step beyond: in Lagrangian mechanics indeed the conserved energy $\mathcal{E}$ of trajectories is given and fixed, while in our problem of interest the energy itself has to be optimised. It is precisely the optimal energy $\mathcal{E}^*$ that benefits of the unexpected property that the action of its corresponding optimal trajectory becomes equal to $\mathcal{E}^*$ – a non-trivial fact, as we have shown. Such result could be of interest in different contexts where Lagrangian mechanics is used to solve optimisation problems. We note last that our result is not directly related to the optimisation principle put forward by Nemoto and Sasa in [264, 265] (since these are not based on a weak-noise framework).

In conclusion, the evaluation of $\mu(\lambda)$ generically goes as follows. Note as a starting point that the criterion given by Eq. (7.60) for the existence of an optimal propagative solution can be interpreted as a condition on λ; using explicit notations, one has that if the condition:

$$\left| \lambda \int_0^1 g(x)\, dx - \int_0^1 F(x)\, dx \right| > \int_0^1 \sqrt{2\mathcal{V}_{\max}(\lambda) + F(x)^2 + 2\lambda h(x)}\; dx \tag{7.66}$$

is satisfied, then the optimal trajectory is propagative. For each value of λ, one checks whether Eq. (7.66) is satisfied. If it holds, one determines $\mathcal{E}^*_\sigma$ by solving Eq. (7.53) with $\sigma = -\mathrm{sign}(B)$, i.e.,

$$R(\mathcal{E}^*_\sigma) - 2\mathcal{E}^*_\sigma T(\mathcal{E}^*_\sigma) + |B| = 0\,, \tag{7.67}$$

leading to $\mu(\lambda) = \mathcal{E}^*_\sigma(\lambda)$. If Eq. (7.66) is not satisfied, then $\mu(\lambda) = \mathcal{V}_{\max}(\lambda)$. This result allows one to determine the existence of possible dynamical phase transitions in the fluctuations of the additive observable A_τ. When varying λ, one can indeed jump from a situation where the optimal trajectory is time-independent (when Eq. (7.66) is not satisfied) to a situation where the optimal trajectory is time-dependent. Such a transition between two classes of optimal trajectories is illustrated in Fig. 7.1 and corresponds to a breaking of the 'additivity principle' [149]).

For an density-type observable A_τ ($g(x) = 0$) in the presence of a conservative force $F(x) = -U'(x)$, the l.h.s. of Eq. (7.66) is equal to 0, so that Eq. (7.66) is never satisfied. It follows that $\mu(\lambda) = \mathcal{V}_{\max}(\lambda)$ for all λ, meaning that the optimal trajectory is always time-independent in this case (in other words, there is
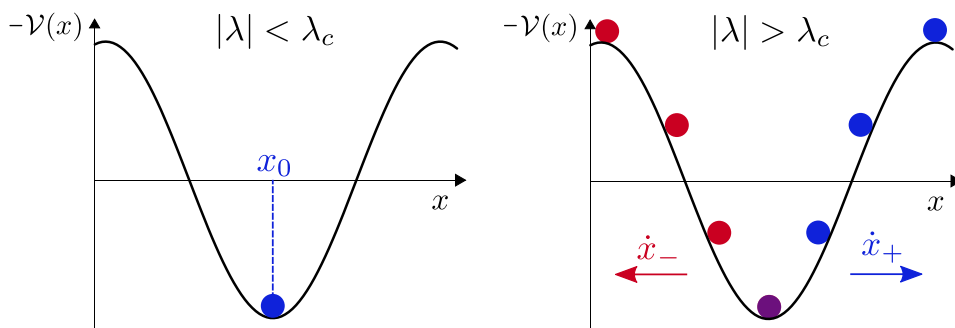
Figure 7.1: The different classes of optimal trajectories of interest: On the left, stationary ones, with x_0 the location of the maximum of $\mathcal{V}(x)$, defined in Eq. (7.26); On the right, propagative ones, either increasing or decreasing in time. Periodic trajectories which oscillate around x_0 without being propagative have a larger action than the stationary one in x_0, as shown in Subsection 7.3.2. The criterion for the existence of propagative trajectories is given by Eq. (7.66).

no breaking of the additivity principle). This however does not forbid dynamical phase transitions since, as seen from the expression (7.26) of $\mathcal{V}(x)$ the 'tilting' contribution $-\lambda h(x)$ can make the location of the maximum of $\mathcal{V}(x)$ switch from one position to another, if for instance $F(x)$ presents more than one equilibrium point. Such a situation occurs for instance in the large deviation of additive observables in driven diffusive systems [181].

We discuss below the determination of $\mu(\lambda)$ in the case of current-type additive observable, which generically leads to a phase transition between stationary and non-stationary trajectories – a common phenomenon in periodic systems in general [41, 85, 150, 272].

7.3.4 Determination of $\mu(\lambda)$ for current-type additive observable and conservative force $F(x)$

Considering a current-type additive observable (corresponding to $h(x) = 0$) as well as a conservative force $F(x) = -U'(x)$, Eq. (7.66) simplifies to

$$|\lambda| > \lambda_{\mathrm{c}} \equiv \frac{\int_0^1 |F(x)|\, dx}{\int_0^1 g(x)\, dx} \qquad (7.68)$$

where we have assumed that $\int_0^1 g(x)\, dx > 0$ (the case $\int_0^1 g(x)\, dx < 0$ is treated in the same way), and used the fact that $\mathcal{V}_{\max} = 0$ when $h(x) = 0$ (as inferred

from (7.26) and (7.30)). For $|\lambda| > \lambda_c$, $\mu(\lambda)$ is solution of the equation

$$\int_0^1 \sqrt{2\mu(\lambda) + F(x)^2} \, dx = |\lambda| \int_0^1 g(x) \, dx \qquad (7.69)$$

while for $|\lambda| < \lambda_c$, $\mu(\lambda) = \mathcal{V}_{\max} = 0$. Consequently, λ_c is the critical value at which the dynamical phase transition takes place. Note that $\mu(\lambda)$ is an even function of λ for current-type additive observable in a system with a conservative force, due to time-reversal invariance.

The singular behaviour of the sCGF close to the transition depends both on local and global properties of the force $F(x)$. If one naively expands for small $\mu(\lambda)$

$$\sqrt{F(x)^2 + 2\mu(\lambda)} = |F(x)| + \frac{\mu(\lambda)}{|F(x)|} + O\big(\mu(\lambda)^2\big) \qquad (7.70)$$

and integrates over $0 < x < 1$ in order to obtain an expansion of Eq. 7.69 for $\mu(\lambda)$, one finds a divergent integral $\int_0^1 dx/|F(x)|$ (if there is a fixed point $F(x_0) = 0$ with $F'(x_0) \neq 0$, which is the case in general). The expansion at small $\mu(\lambda)$ is thus ill-defined. The logarithmic divergence of $\int_0^1 dx/|F(x)|$ suggests a behaviour $\mu(\lambda) \sim (\lambda - \lambda_c)/|\log(\lambda - \lambda_c)|$ but the situation is better understood on a specific example first.

As an explicit example, we consider the case $F(x) = \sin(2\pi x)$, $h(x) = 0$ and $g(x) = 1$, where the force $F(x)$ is conservative, and the observable $A(t)$ is the integrated current (or the position at time t, counted with the number of turns). Such model and additive observable has been previously considered in Refs. [85, 262–264]. The sCGF $\mu(\lambda)$ was numerically evaluated in [264] at finite noise (the transition that appears in the weak-noise limit was not considered). In [262, 263] the weak-noise limit is considered and the singularity of the sCGF is described as a "kink", with no elucidation of its nature. In [85], numerical results in the weak but non-zero noise asymptotics are obtained, and described as suggesting a first-order transition with a cusp in the sCGF (compatible with the results of random-walk approximation of the problem), but the authors write that "the precise shape of the rate function around the cusp is yet to be determined analytically". Below, we elucidate the precise form of the dynamical phase transition that appears in the weak-noise asymptotics, showing that it is neither first nor second order, but continuous and intermediate between these two cases (it presents an essential singularity). For the location of the transition, Eq. (7.68) straightforwardly leads to

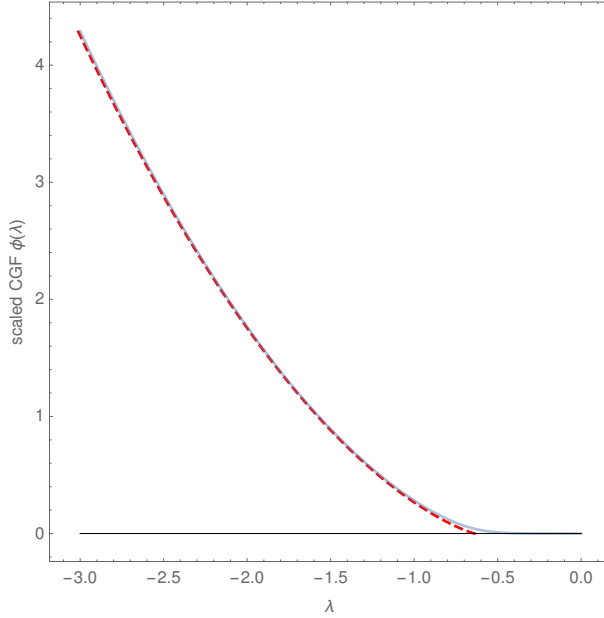$$\lambda_c = \frac{2}{\pi}. \qquad (7.71)$$

Figure 7.2: An example sCGF $\mu(\lambda)$, for $F(x) = \sin(2\pi x)$ and $h(x) = 0$ and $g(x) = 1$. Comparison of the evaluation of the sCGF $\mu(\lambda)$ between the weak-noise approach (deduced from (7.72)-(7.74), dashed red line) and the maximal eigenvalue of the deformed operator (7.10) of a lattice version of the dynamics (translucent blue line; 128 sites, $\varepsilon = 0.075$). In the negative regime of λ, the transition occurs at $\lambda = -\lambda_{\mathrm{c}} = -\frac{2}{\pi} \simeq -0.637$.

This result was already obtained in [85]. For $|\lambda| > \lambda_{\mathrm{c}}$, the sCGF $\mu(\lambda)$ is solution in $\mathcal{E}_\lambda$ of the equation

$$\lambda = \begin{cases} -\Lambda(\mathcal{E}_\lambda) & \text{for } \lambda < -\lambda_{\mathrm{c}} \\ \Lambda(\mathcal{E}_\lambda) & \text{for } \lambda > \lambda_{\mathrm{c}} \,, \end{cases} \tag{7.72}$$

with

$$\Lambda(\mathcal{E}) \equiv \frac{2}{\pi}\sqrt{2\mathcal{E}}\ \mathrm{E}\left(-\frac{1}{2\mathcal{E}}\right), \tag{7.73}$$

where $\mathrm{E}(\cdot)$ is the complete elliptic integral of the second kind (taking the definition used by Abramowitz & Stegun [273]). One thus obtains

$$\mu(\lambda) = \begin{cases} 0 & |\lambda| \le \lambda_{\mathrm{c}} \,, \\ \Lambda^{-1}(|\lambda|) & |\lambda| \ge \lambda_{\mathrm{c}} \,. \end{cases} \tag{7.74}$$

For $|\lambda| < \lambda_{\mathrm{c}}$, the sCGF $\mu(\lambda)$ and its associated optimal profiles are flat: one needs to consider large enough deviations of the current in order to actually observe a

travelling trajectory. In order to check the existence of the transition and the form of the sCGF, we evaluated $\mu(\lambda)$ from the maximal eigenvalue of the deformed operator (7.10) of a lattice version of the dynamics (at small temperature and for a large number of sites). Results are in good agreement with the present weak-noise approach (see Fig. 7.2).

For the expansion close to the transition points, one finds for $\lambda = \lambda_c + \delta\lambda$ with $\delta\lambda > 0$

$$\mu(\lambda_c + \delta\lambda) = \frac{\pi\,\delta\lambda}{|\ln\delta\lambda|} + o\left(\frac{\delta\lambda}{|\ln\delta\lambda|}\right). \tag{7.75}$$

This leads for the average velocity $\overline{v}$ of the particle (or, equivalently, the average current),

$$\overline{v}(\lambda_c + \delta\lambda) = -\mu'(\lambda_c + \delta\lambda) = -\frac{\pi}{|\ln\delta\lambda|} + o\left(\frac{1}{|\ln\delta\lambda|}\right). \tag{7.76}$$

As a result, the dynamical phase transition at λ_c is formally continuous since $\overline{v}(\lambda) \to 0$ when $\lambda \to \lambda_c$. However, for all practical purposes, the transition appears discontinuous as the convergence to zero is extremely slow. The higher-order derivatives $\mu^{(n)}(\lambda)$ diverge to $(-\infty)^n$ as $\lambda \to \lambda_c^+$ for $n \geq 2$, indicating an essential singularity of the sCGF in λ_c. This result, which is new to our knowledge and highly non-trivial, is to be contrasted with the standard depinning transition of a particle in a 'tilted' potential (*i.e.*, a particle subjected to a conservative force plus a uniform non-conservative driving force). For a regular potential, the depinning transition is continuous with a critical exponent $1/2$ [274]. The fact that the transition observed in the λ-biased dynamics is of a different nature shows that biasing the dynamics with λ does not only add a non-conservative uniform driving force to the original dynamics, but rather modifies the original dynamics in a more complex way. We describe in the next section how the λ-biased dynamics can be mapped onto a non-trivial effective driven process, which will allow us to better understand why the standard behaviour of the depinning transition of a particle in a potential is not recovered (see also [85] for a complementary approach).

7.4   Effective non-equilibrium dynamics of the conditioned equilibrium system

As we discussed in Section 7.2.3, the biased dynamics is governed by the deformed Fokker–Planck operator $\mathbb{W}_\lambda$ defined in (7.10), which does not preserve probability. This observation is at the basis of population dynamics algorithms [275–277] that allow one to study rare trajectories and to evaluate numerically the CGF by

representing the probability loss or gain through selection rules between copies of the system, in the spirit of Quantum Monte Carlo algorithms [278, 279] (see *e.g.* [280] for a review).

In fact, as shown recently in [72,73] and in [76] (inspired by [281,282]), there exists a change of basis, based on the explicit knowledge of the left eigenvector of $\mathbb{W}_\lambda$, that allows one to render the dynamics described by $\mathbb{W}_\lambda$ *probability-preserving*, up to a global normalisation. As studied in great depth in Refs. [77, 79, 259], this defines an 'auxiliary' or 'effective' dynamics $\mathbb{W}_\lambda^{\text{eff}}$ which is asymptotically equivalent to the biased dynamics described by $\mathbb{W}_\lambda$, if normalised appropriately (see Sec 7.4.4 for details). From a mathematical point of view, this construction is based on a generalised Doob's h-transform [79]. The interest of this effective dynamics is that it provides a physical (probability-preserving) dynamics whose typical trajectories are equivalent to the rare trajectories of the original dynamics (7.1). Such effective dynamics can be defined for Langevin processes or for jump processes. Explicit examples of such dynamics have been determined in exclusion processes [72, 73, 80, 81], in zero-range processes [82–84], in the current large deviation of Langevin dynamics [85] or in open quantum systems [86, 87]. They illustrate in general that the effective forces governing the dynamics described by $\mathbb{W}_\lambda^{\text{eff}}$ modify the original dynamics (7.1) on a global scale.

In this section, we recall how to identify the effective process as a Langevin dynamics with a force $F_\lambda^{\text{eff}}(x)$ that defines a λ-modified probability-preserving dynamics [79,259]. We then show that the determination of $F_\lambda^{\text{eff}}(x)$ can be done in a rather explicit way in the weak-noise limit, without having to determine explicitly the left eigenvector. We also explain how the determination of the effective process allows one to show that the small-noise and large-time limits can be exchanged in periodic systems for our LDF problem.

7.4.1 Derivation of the effective force

One defines $\langle L|$ as the left eigenvector[1] of $\mathbb{W}_\lambda$ associated to the maximal eigenvalue $\varphi_\varepsilon(\lambda)$. Following Refs. [72, 73, 76], one introduces a diagonal operator $\hat{L}$ whose elements are the components of $\langle L|$. Then, the definition $\langle L|\mathbb{W} = \varphi_\varepsilon(\lambda)\langle L|$ of the left eigenvector implies that

$$\langle -|\mathbb{W}_\lambda^{\text{eff}} = 0 \quad \text{with} \quad \mathbb{W}_\lambda^{\text{eff}} = \hat{L}\mathbb{W}_\lambda\hat{L}^{-1} - \varphi_\varepsilon(\lambda)\mathbf{1} \,. \tag{7.77}$$

---

[1]It is unique up to a multiplicative constant, since we have assumed that the conditions of validity of the Perron–Frobenius theorem are satisfied. Note also that this implies that all components of $\langle -|$ can be chosen to be strictly positive.

One reads from this relation that the operator $\mathbb{W}_\lambda^{\text{eff}}$ is probability-preserving and describes a *bona fide* dynamics (with positive transition rates). Since $\mathbb{W}_\lambda^{\text{eff}}$ is obtained from $\mathbb{W}_\lambda$ by a mere to a shift and a change of basis, it has to present the same physical content as $\mathbb{W}_\lambda$ – but in a sense that has to be specified. We refer to [76, 79, 259] for thorough studies of such a correspondence and to Section 7.4.4 for a self-contained presentation.

Let us now fix $\varepsilon > 0$ (not necessarily small) and send τ to infinity before taking the weak-noise limit. The Perron–Frobenius theorem ensures that the components of the eigenvectors associated to the large eigenvalue can be taken to be strictly positive, which allows one to introduce a function $\tilde{U}(x)$ such that the left eigenvector reads $L(x) = \exp\left[-\frac{1}{\varepsilon}\tilde{U}(x)\right]$. Note that this relation is simply a definition of $\tilde{U}(x)$, which may depend on ε at this stage. However, one expects[2] that in the weak-noise limit $\varepsilon \to 0$, $\tilde{U}(x)$ becomes independent of ε.

One finds by direct computation that

$$
\begin{aligned}
\mathbb{W}_\lambda^{\text{eff}}P(x) &= \frac{1}{2}\varepsilon P''(x) + \left[-F(x) + \lambda g(x) + \tilde{U}'(x)\right]P'(x) + \frac{1}{2\varepsilon}\Big[\lambda^2 g(x)^2 \\
&\quad - 2\lambda h(x) - 2\varepsilon\big(\varphi_\varepsilon(\lambda) + F'(x) - \lambda g'(x)\big) - 2F(x)\tilde{U}'(x) \\
&\quad + \tilde{U}'(x)^2 + 2\lambda g(x)(\tilde{U}'(x) - F(x)) + \varepsilon\tilde{U}''(x)\Big]P(x)\,. \qquad (7.78)
\end{aligned}
$$

Using the eigenvector equation for $L(x)$

$$
\begin{aligned}
\varphi_\varepsilon(\lambda)L(x) &= \frac{1}{2}\varepsilon L''(x) + \left[F(x) - \lambda g(x)\right]L'(x) \\
&\quad + \frac{\lambda}{\varepsilon}\left[\frac{1}{2}\lambda g(x)^2 - h(x) - F(x)g(x)\right]L(x) \qquad (7.79)
\end{aligned}
$$

which can be rewritten in terms of $\tilde{U}(x)$ as

$$
\begin{aligned}
\varphi_\varepsilon(\lambda) &= -\frac{1}{2}\tilde{U}''(x) \\
&\quad + \frac{1}{\varepsilon}\left[\frac{1}{2}\big(\lambda g(x) + \tilde{U}'(x)\big)\big(\lambda g(x) + \tilde{U}'(x) - 2F(x)\big) - \lambda h(x)\right] (7.80)
\end{aligned}
$$

one eliminates $\varphi_\varepsilon(\lambda)$ in (7.78) and one finds that $\mathbb{W}_\lambda^{\text{eff}}$ indeed takes the form of a probability-preserving Fokker–Planck evolution operator [79, 259]:

$$
\mathbb{W}_\lambda^{\text{eff}}\cdot = -\partial_x\left[\big(F(x) - \lambda g(x) - \tilde{U}'(x)\big)\cdot\right] + \frac{1}{2}\varepsilon\partial_x^2\cdot\,. \qquad (7.81)
$$

---

[2]This can be formally shown for instance by expanding $\tilde{U}(x)$ in a power series as $\tilde{U}(x) = \tilde{U}_0(x) + \varepsilon\tilde{U}_1(x) + \ldots$ following the standard WKB procedure [260].

It describes the evolution of a particle subjected to a force $F^{\text{eff}}(x) = F(x) - \lambda g(x) - \tilde{U}'(x)$. We note that the contribution $h(x)$ to the additive observable A defined in 7.2 does not appear explicitly in (7.81) but is still present implicitly through the potential $\tilde{U}(x)$ defined from the left eigenvector $L(x)$.

7.4.2 Effective dynamics in the weak-noise limit

Noting that $\varphi_\varepsilon(\lambda) \sim \frac{1}{\varepsilon}\mu(\lambda)$ in the weak-noise limit $\varepsilon \to 0$, and assuming that $\tilde{U}$ becomes independent of ε in this limit (as is usually the case in this WKB procedure [260]), the differential equation (7.80) for $\tilde{U}(x)$ becomes an ordinary, quadratic equation for $\tilde{U}'(x)$,

$$\frac{1}{2}\left(\lambda g(x) + \tilde{U}'(x)\right)\left(\lambda g(x) + \tilde{U}'(x) - 2F(x)\right) - \lambda h(x) = \mu(\lambda), \qquad (7.82)$$

whose solution reads

$$\tilde{U}'(x) = F(x) - \lambda g(x) - \sigma\sqrt{F(x)^2 + 2\lambda h(x) + 2\mu(\lambda)}, \qquad (7.83)$$

where $\sigma = \pm 1$ is an unknown sign that will be determined later on. Hence, the knowledge of $\mu(\lambda)$ allows for the determination of $\tilde{U}'(x)$, provided one is able to select the correct sign in Eq. (7.83). This can be done by evaluating the effective force $F^{\text{eff}}(x)$. Inserting Eq. (7.83) in the generic expression (7.81) of the effective Fokker–Planck operator, one finds

$$\mathbb{W}_\lambda^{\text{eff}}\cdot = -\partial_x\left[\sigma\sqrt{F(x)^2 + 2\lambda h(x) + 2\mu(\lambda)} \,\cdot\,\right] + \frac{1}{2}\varepsilon\partial_x^2 \cdot \ . \qquad (7.84)$$

It corresponds to the evolution of a particle subjected to an effective force

$$F^{\text{eff}}(x) = \sigma\sqrt{F(x)^2 + 2\lambda h(x) + 2\mu(\lambda)}. \qquad (7.85)$$

The two possible signs correspond to the two possible cases of Sections 7.3.3 and 7.3.4 when the optimal trajectory is either increasing or decreasing in time. We will see below that σ is given by $\sigma = -\text{sign}(B)$, consistently with the results of Section 7.3.3.

We have thus shown that in the weak-noise asymptotics, the explicit knowledge of the complete left eigenvector $\langle L|$ is not required in order to determine the effective force $F^{\text{eff}}(x)$: one only needs to know the sCGF $\mu(\lambda)$. Interestingly, for periodic systems, Eq. (7.83) also provides a way to determine $\mu(\lambda)$, without using the optimisation procedure described in Section 7.3. In a periodic system, $\tilde{U}(x)$ is

a periodic function of period 1, so that $\int_0^1 \tilde{U}'(x)\, dx = 0$. From Eq. (7.83), we thus have

$$\int_0^1 dx \left(F(x) - \lambda g(x) - \sigma \sqrt{F(x)^2 + 2\lambda h(x) + 2\mu(\lambda)} \right) = 0 \qquad (7.86)$$

and one recovers Eq. (7.53), given the definitions (7.44) and (7.26) of the parameter B, the function R and the potential $\mathcal{V}(x)$, as well as the identification of $\mu(\lambda)$ with $\mathcal{E}_\sigma^*$ when Eq. (7.53) has a solution — see Eqs. (7.62) and (7.65). Following the same reasoning as the one that leads to Eq. (7.59), we recover that $\sigma = -\text{sign}(B)$.

Note that recovering the same result as in Section 7.3 is non-trivial, because here we have made no optimisation of the action at finite time τ, but rather taken the infinite-time limit from the outset, by using first a spectral analysis (which yielded the eigenvector equation 7.79) and then a weak-noise expansion to go from (7.80) to (7.82). In other words, we have exchanged the order of the large-time and the weak-noise limit. It is interesting to see, as we previously mentioned, that both orders of limits yield the same result. Let us emphasise that this result strongly relies on the Perron–Frobenius theorem, which states that the eigenvector $\langle L|$ associated to the largest eigenvalue of $\mathbb{W}_\lambda$ only has strictly positive components (up to a sign convention) so that it can be written in an exponential form $L(x) = \exp\left[-\frac{1}{\varepsilon}\tilde{U}(x)\right]$ (with real $\tilde{U}(x)$), while other eigenvectors do not have all components of the same sign, and can thus not be written in such an exponential form. Looking for an eigenvector in an exponential form thus automatically selects the eigenvector associated to the largest eigenvalue thanks to the Perron–Frobenius theorem, without any explicit optimisation procedure.

For a conservative force $F(x)$ and current-type additive observables (*i.e.*, $h(x) = 0$), the condition $\sigma = -\text{sign}(B)$ boils down (if $g(x) > 0$) to $\sigma = -\text{sign}(\lambda)$, leading to an effective force

$$F^{\text{eff}}(x) = -\text{sign}(\lambda)\sqrt{F(x)^2 + 2\mu(\lambda)} \qquad (|\lambda| > \lambda_{\text{c}}), \qquad (7.87)$$

$$F^{\text{eff}}(x) = -\text{sign}(\lambda)\,|F(x)| \qquad (|\lambda| \le \lambda_{\text{c}}). \qquad (7.88)$$

Several comments are in order here. First, the effective force $F^{\text{eff}}(x)$ differs from the λ-dependent force appearing in the modified process defined by the Langevin equation (7.12). Second, $F^{\text{eff}}(x)$ can be decomposed into a uniform non-conservative part

$$f_{\text{eff}} = \int_0^1 F^{\text{eff}}(x)\, dx = \int_0^1 F(x)\, dx - \lambda \int_0^1 g(x)\, dx \qquad (7.89)$$

(where the last equality results from Eq. (7.86)) and a space-dependent conservative part

$$- U'_{\text{eff}} = F^{\text{eff}}(x) - f_{\text{eff}}. \qquad (7.90)$$

Note that the integrals in Eq. (7.89) should be understood as spatial averages (we recall that the length of the system is chosen as $L = 1$). In the specific case when the observable A is the current (*i.e.*, $g(x) = 1$ and $h(x) = 0$) and $F(x)$ is a conservative force, one recovers that $f_{\text{eff}} = -\lambda$. Yet, the conservative part $-U'_{\text{eff}}$ does not reduce to the original force $F(x)$. This can be seen explicitly by computing perturbatively the effective force $F^{\text{eff}}(x)$ in the large λ limit, yielding

$$F^{\text{eff}}(x) \underset{\lambda \to \infty}{=} -\lambda - \frac{1}{2\lambda} \left(F(x)^2 - \int_0^1 F(x')^2 \, dx' \right) + o\left(\frac{1}{\lambda} \right) \qquad (7.91)$$

From this last equation, the decomposition of the effective force $F^{\text{eff}}(x)$ into a uniform non-conservative force $f_{\text{eff}} = -\lambda$ and a conservative force becomes

$$- U'_{\text{eff}} = -\frac{1}{2\lambda} \left(F(x)^2 - \int_0^1 F(x')^2 \, dx' \right) + o\left(\frac{1}{\lambda} \right). \qquad (7.92)$$

The associated periodic potential U_{eff} reads

$$U_{\text{eff}}(x) = \frac{1}{2\lambda} \left(\int_0^x F(x')^2 \, dx' - x \int_0^1 F(x')^2 \, dx' \right) + o\left(\frac{1}{\lambda} \right). \qquad (7.93)$$

On the other side, it is instructive to determine how the effective force $F^{\text{eff}}(x)$ is modified as the dynamical transition is approached: we illustrate in Fig. 7.3 how a cusp singularity appears in $F^{\text{eff}}(x)$ as $\delta\lambda \to 0^+$ for $\lambda = \lambda_{\text{c}} + \delta\lambda$ in the example system studied at the end of Section 7.3.3. One sees from Eq. (7.87) that $F^{\text{eff}}(x)$ is a regular function of x as long as $\delta\lambda > 0$ but develops a cusp singularity at its stationary points as $\delta\lambda \to 0^+$, explaining why the transition is not of the same nature as that of the standard depinning transition [274] (see [85] for a numerical study of how singularities in the effective force $F^{\text{eff}}(x)$ are related to the dynamical phase transition, in the current large deviations of a particle a periodic sine potential).

To understand on a more general ground the relation between such depinning transition and the dynamical phase transition, we now consider the more generic case of an observable A with arbitrary g, $h \equiv 0$ and a force $F(x)$ presenting a stationary point x_0. We assume that F can be expanded around x_0 as $F(x) = (x-x_0)F_0 + o(x-x_0)$. In the effective dynamics, optimal trajectories are subjected
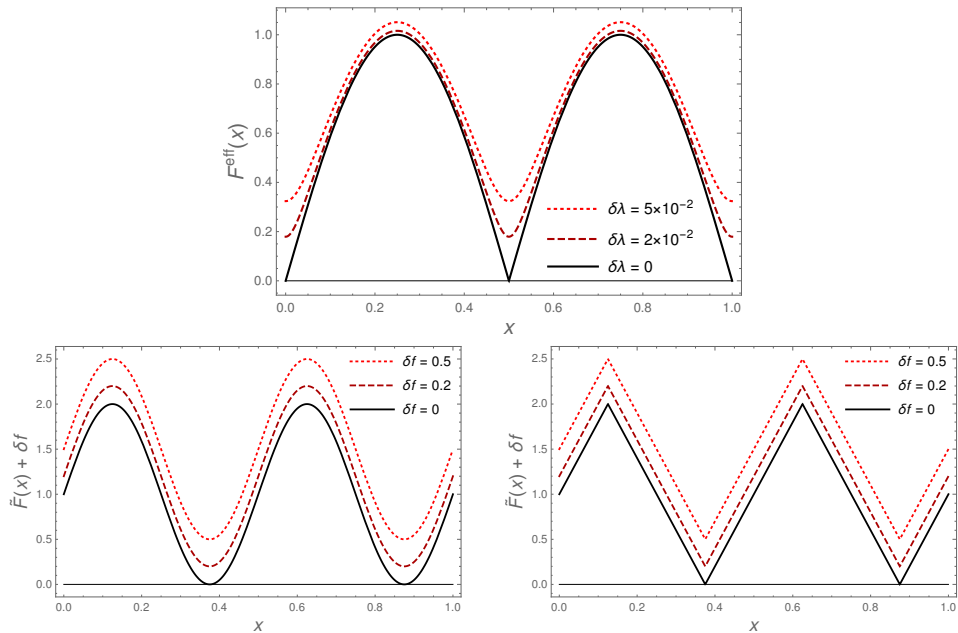
Figure 7.3: Comparison, on an example, of the criticality of the dynamical phase transition and of standard depinning transitions in 0d. (**Top**) The effective force $F^{\text{eff}}(x)$ at $\lambda = \lambda_c + \delta\lambda$ deforms and becomes a cuspy function of x close to the stationary points that develop as $\delta\lambda \to 0^+$, for the example model studied at the end of Section 7.3.3. (**Bottom left**) In the standard depinning transition in 0d, the depinning transition occurs when a regular force $\tilde{F}(x)$ possesses no stationary point any more when driven by a uniform force $\delta f > 0$. In this case, the force $\tilde{F}(x) + \delta f$ is a regular function of x and this implies that the transition is second-order [274], in contrast to our dynamical phase transition of interest. (**Bottom right**) If instead the force presents a cusp at all values of $\delta f \geq 0$ close to the $\delta f = 0$ stationary point, the transition becomes first-order [274], which is also different from our dynamical phase transition.

to the effective force defined in Eq. (7.85) which reads as follows close to the stationary point[3]:

$$F^{\text{eff}}(x) \simeq \sqrt{[(x - x_0)F_0]^2 + 2\mu(\lambda)}. \qquad (7.94)$$

As the dynamical phase transition is approached ($\mu(\lambda) \to 0$ as $\lambda \to \lambda_c^+$), this implies that the trajectories of the effective dynamics spend a longer and longer time close to x_0, meaning that the dynamics is mainly governed by the approximate form (7.94) of the effective force.

---

[3]We assume here that $\sigma = +1$ without loss of generality.

Effective trajectories are governed by the equation $\dot{x}(t) = F^{\text{eff}}(x(t))$, whose solution reads

$$x(t) = x_0 \pm \sqrt{2\mu(\lambda)} \, \frac{\sinh(F_0 t)}{F_0}, \tag{7.95}$$

(up to an arbitrary translation in time) in the regime where the approximation (7.94) holds. As usual for the depinning transition in 0d problems [274], the average velocity of the trajectory (counted positively) is $|\bar{v}| \sim L/T$, with L the spatial period (recall once again $L = 1$ in our settings) and T the period in time. Close to the transition, the time period T is for instance estimated from

$$x(T/2) - x(-T/2) = L = 1 \tag{7.96}$$

(since $x(0) = x_0$ with our choice of the origin of time, so that $x(t) - x_0$ is an odd function of time). In the large-time limit, one finds from (7.96) that at dominant order in $\mu(\lambda) \to 0$, one has $T \sim \frac{1}{F_0} |\ln \mu(\lambda)|$. Consequently, the average velocity of the trajectory behaves as:

$$|\bar{v}| \sim \frac{F_0}{|\ln \mu(\lambda)|}, \tag{7.97}$$

in good agreement with the result (7.76) for the example of the $\sin(2\pi x)$ force. In all, we have shown that the behaviour (7.94) of the effective force close to the stationary point of the effective depinning problem governs the logarithmic form of the velocity close to the transition for an arbitrary current-type additive observable A.

Furthermore, if the additive observable A is the velocity of the particle, the relation $v(\lambda) = -\mu'(\lambda)$ together with 7.97 leads to:

$$\mu'(\lambda) \sim \frac{1}{|\ln \mu(\lambda)|} \qquad \text{for } \lambda \to \lambda_c^+ . \tag{7.98}$$

Close to the transition point, writing $\lambda = \lambda_c + \delta\lambda$, one can integrate this equation and get:

$$\mu(\lambda) \ln \delta\lambda - \mu(\lambda) = -\delta\lambda. \tag{7.99}$$

so that at dominant order for $\delta\lambda \to 0^+$

$$\mu(\lambda) \sim \frac{\delta\lambda}{|\ln \delta\lambda|}. \tag{7.100}$$

which is compatible with the result (7.75) obtained for the example model $F(x) = \sin(2\pi x)$.

In conclusion, the effective depinning transition problem fully describes the unexpected $\delta\lambda/|\ln\delta\lambda|$ behaviour [see Eq. (7.75)] of the expansion of $\mu(\lambda)$ near the transition, that we computed exactly for the sine potential, but now for the generic case when the effective force takes the form (7.94) close to its stationary point.

7.4.3 Interpretation of the effective process in the path-integral formulation

It is now interesting to come back to the path integral formulation introduced in Section 7.2 to discuss the relationship between the effective non-equilibrium process and the original process biased by λ. To simplify the discussion, we specialise here to a conservative force $F(x) = -U'(x)$, so that we compare the effective non-equilibrium process with a λ-biased equilibrium process [4]. The aim of this subsection is to determine the possible relation between the action of the effective process and the biased action $S_\tau^\lambda[x(t)]$, in order to see how the trajectories corresponding to these actions compare, in the weak-noise limit where the results of Subsection 7.4.2 (that we will use) are valid.

A Langevin process with the effective non-equilibrium force $F^{\text{eff}}(x)$,

$$\dot{x}(t) = F^{\text{eff}}(x(t)) + \sqrt{\varepsilon}\,\zeta(t) \;, \tag{7.101}$$

leads to an Onsager–Machlup action which, in the small-noise limit, takes the form

$$S_\tau^{\text{eff}}[x(t)] = \int_0^\tau \frac{1}{2}\big(\dot{x} - F^{\text{eff}}(x)\big)^2 \, dt \;. \tag{7.102}$$

Expanding the square in the action and using the expression (7.85) of the effective force $F^{\text{eff}}(x)$, we end up with

$$S_\tau^{\text{eff}}[x(t)] = \int_0^\tau \left\{ \frac{1}{2}\dot{x}^2 + \frac{1}{2}F(x)^2 + \lambda h(x) + \mu(\lambda) - \dot{x}F^{\text{eff}}(x) \right\} dt \;. \tag{7.103}$$

Then, Eqs. (7.85) and (7.86) imply that

$$\int_0^\tau \dot{x}F^{\text{eff}}(x)\, dt = -\int_0^\tau \lambda\dot{x}g(x)\, dt \tag{7.104}$$

so that the action of the non-equilibrium process reads

$$S_\tau^{\text{eff}}[x(t)] = \int_0^\tau \left\{ \frac{1}{2}\dot{x}^2 + \frac{1}{2}F(x)^2 + \lambda\big(h(x) + \dot{x}g(x)\big) + \mu(\lambda) \right\} dt \;. \tag{7.105}$$

---

[4] The generalisation to a non-conservative force field $F(x)$ is straightforward and left to the reader.

Finally, from the expression (7.9) of the biased action $S_\tau^\lambda[x(t)]$, one obtains

$$S_\tau^\lambda[x(t)] = S_\tau^{\text{eff}}[x(t)] - \mu(\lambda)\tau \qquad (7.106)$$

This means that the action $S_\tau^\lambda[x(t)]$ of the biased process identifies, up to a constant, with the action $S_\tau^{\text{eff}}[x(t)]$ of the effective non-equilibrium process. The difference $-\mu(\lambda)\tau$ between these two actions has to be present since $S_\tau^\lambda[x(t)]$ describes a dynamics that does not preserve probability, while $S_\tau^{\text{eff}}[x(t)]$ describes a probability-preserving one. The remarkable feature of (7.106) is that this difference is independent of the trajectory, so that a simple normalisation $S_\tau^\lambda[x(t)] + \mu(\lambda)\tau$ of the biased action allows one to interpret it as the action of a probability-conserving process. This confirms that, in the weak-noise asymptotics we are working in, the effective non-equilibrium process defined by the force field $F^{\text{eff}}(x)$ describes the same statistics of trajectories as the original dynamics biased by λ (after an adequate normalisation). Let us emphasise that in Eq. (7.106), the actions $S_\tau^{\text{eff}}[x(t)]$ and $S_\tau^\lambda[x(t)]$ compare the non-equilibrium dynamics characterised by a force $F^{\text{eff}}(x) = -U'_{\text{eff}}(x) - \lambda$, with a λ-biased dynamics in the original conservative force field $F(x) = -U'(x)$.

7.4.4 Equivalence between the effective driven process and the λ-biased process

We have shown above, using the path-integral formalism in the specific case of a conservative force field $F(x)$, that the effective driven process described by $\mathbb{W}_\lambda^{\text{eff}}$ is equivalent to the original λ-biased process described by $\mathbb{W}_\lambda$. We provide here for completeness a more general and formal proof of this equivalence in an operatorial formalism, following Refs. [76, 276, 283]. The force field $F(x)$ is here no longer assumed to derive from a potential. We also refer the reader to Refs. [79, 259] for a more mathematical description.

We start by defining a 'λ-ensemble' as a normalised average $\langle \cdot \rangle_\lambda^{[0,\tau]}$ in the biased dynamics, namely

$$\langle \mathcal{O}[x(t)] \rangle_\lambda^{[0,\tau]} = \frac{\left\langle \mathcal{O}[x(t)]\, e^{-\frac{\lambda}{\varepsilon} A_\tau} \right\rangle}{\left\langle e^{-\frac{\lambda}{\varepsilon} A_\tau} \right\rangle}, \qquad (7.107)$$

where the observable $\mathcal{O}$ depends on the trajectory. We made explicit the time interval on the l.h.s. because the statistical properties of the λ-ensemble at times close to τ are different from those in the "bulk" of the time interval $[0, \tau]$. The numerator of (7.107) corresponds to the biased process described by the operator $\mathbb{W}_\lambda$ while the denominator represents the proper normalisation that ensures $\langle 1 \rangle_\lambda^{[0,\tau]} = 1$.

Let us now first focus on an observable $\mathcal{O}[x(t)] = \mathcal{O}_1(x(t_1))$ which depends only on the position of the particle at a time $t_1 \in [0, \tau]$. Denoting by $\hat{\mathcal{O}}_1$ the diagonal operator whose components are the values of $\mathcal{O}_1(x)$, one has by definition

$$\langle \mathcal{O}_1(x(t_1)) \rangle_\lambda^{[0,\tau]} = \frac{\langle -|e^{(\tau-t_1)\mathbb{W}_\lambda} \hat{\mathcal{O}}_1 \, e^{t_1 \mathbb{W}_\lambda}|P_{\mathrm{st}}\rangle}{\langle -|e^{\tau \mathbb{W}_\lambda}|P_{\mathrm{st}}\rangle} \,. \qquad (7.108)$$

Then, if both t_1 and $\tau - t_1$ are large compared to the inverse of the gap of $\mathbb{W}_\lambda$, that is to say, if t_1 is in the bulk of the time interval $[0, \tau]$, one can use the asymptotic behaviour (7.14) of $e^{t\mathbb{W}_\lambda}$, leading to

$$\langle \mathcal{O}_1(x(t_1)) \rangle_\lambda^{[0,\tau]} \xrightarrow[\tau \to \infty]{} \langle L|\hat{\mathcal{O}}_1|R\rangle = \int \mathcal{O}_1(x)L(x)R(x)\,dx \,. \qquad (7.109)$$

In other words, as well known [79, 276, 283], the intermediate-times λ-ensemble statistics is governed by the product of the left- and right-eigenvectors of $\mathbb{W}_\lambda$.

Consider now the effective dynamics described by the operator $\mathbb{W}_\lambda^{\mathrm{eff}}$. From its definition (7.77), one sees that the left- and right-eigenvectors associated to its largest eigenvalue 0 are respectively equal to $\langle -|$ and $|LR\rangle$. In analogy with (7.14), the large-time behaviour of the propagator $e^{\tau \mathbb{W}_\lambda^{\mathrm{eff}}}$ is thus given by

$$e^{\tau \mathbb{W}_\lambda^{\mathrm{eff}}} \underset{\tau \to \infty}{\sim} |LR\rangle\langle -| \,, \qquad (7.110)$$

where $|LR\rangle \equiv \hat{L}|R\rangle$. Hence, similarly to (7.109), one finds that the average $\langle \cdot \rangle_{\mathrm{eff}}^{[0,\tau]}$ of an observable for the effective dynamics is given in the steady state by

$$\langle \mathcal{O}_1(x(t_1)) \rangle_{\mathrm{eff}}^{[0,\tau]} \xrightarrow[\tau \to \infty]{} \langle -|\hat{\mathcal{O}}_1|LR\rangle = \int \mathcal{O}_1(x)L(x)R(x)\,dx \,, \qquad (7.111)$$

which is equal to the corresponding λ-ensemble average (7.109). The statistical properties of the biased dynamics, described by (7.107), are thus equal to those of the effective dynamics at any time t_1 in the bulk of $[0, \tau]$.

To go further and understand the equivalence at a trajectorial level, one has to consider more than one-time observables. Jack and Sollich [76] considered for instance a time-discrete settings and worked at the level of trajectory probabilities, showing that in the bulk of $[0, \tau]$ there is an equivalence between the trajectory probabilities of the effective process and of the (normalised) biased dynamics. Equivalently, one can formulate this equivalence using multi-time correlation functions of arbitrary observables (but now in continuous time) as follows. Using the identity $e^{t \mathbb{W}_\lambda^{\mathrm{eff}}} = e^{-t \varphi_\varepsilon(\lambda)} \, \hat{L} \, e^{t \mathbb{W}_\lambda} \hat{L}^{-1}$ inferred from the definition (7.77) of the

effective operator, the previous reasoning can be readily extended to observables of the form $\mathcal{O}[x(t)] = \mathcal{O}_1(x(t_1))\mathcal{O}_2(x(t_2))\ldots\mathcal{O}_n(x(t_n))$ depending on the position of the particle at different times $t_1, t_2, \ldots, t_n$ which are all in the bulk of the interval $[0, \tau]$ (but which can be arbitrarily close to each other). One finds:

$$\langle \mathcal{O}_1(x(t_1))\ldots\mathcal{O}_n(x(t_n))\rangle_{\text{eff}}^{[0,\tau]} \underset{t_1,\tau\to\infty}{\sim} \langle \mathcal{O}_1(x(t_1))\ldots\mathcal{O}_n(x(t_n))\rangle_{\lambda}^{[0,\tau]} \quad (7.112)$$

$$= \langle -|\mathcal{O}_n e^{(t_n-t_{n-1})\mathbb{W}_\lambda^{\text{eff}}}\ldots e^{(t_2-t_1)\mathbb{W}_\lambda^{\text{eff}}}\hat{\mathcal{O}}_1|LR\rangle \quad (7.113)$$

This corresponds to the notion of trajectorial asymptotic equivalence, developed by Chetrite and Touchette [79, 259], between the biased ensemble (7.107) and the effective dynamics.

7.5 Conclusions

In this work we have identified an effective probability-conserving dynamics turning the rare trajectories of a stochastic process into the typical histories of an explicit modified dynamics, in the case of a particle diffusing in a periodic one-dimensional generic force under a weak thermal noise. In this way, by using large-deviation techniques, we have determined the form of the force that a particle effectively withstands when conditioned to bear an atypical fluctuation for a long duration. Interestingly, the resulting effective non-equilibrium process does not only differ from the original λ-biased dynamics by the addition of a (λ-dependent) uniform driving force, but the conservative part of the force is also "renormalised" by the presence of λ, even in the simple case when the observable A_τ is the average current. Considering this result from a reversed perspective, we also learn that a particle in a potential driven by a uniform non-conservative force cannot be accurately represented by a λ-biased dynamics in the same potentials. This means that a tentative statistical approach that would try to evaluate (by analogy with equilibrium) mean values of physical observables by taking a flat average over configurations with the same current (as defined by the λ-biased dynamics) would be at best an approximation.

Along the way, we have analysed the fluctuations of time-integrated current-type observables in a periodic system. These display a rich phenomenology associated to the existence of dynamical phase transitions between a static fluctuating phase, characterised by a flat sCGF, and a phase with time-periodic travelling trajectories, associated to a sCGF being equal to the energy of a natural optimisation problem — which takes the form of a conservative Hamiltonian dynamics. Determining analytically how a finite noise rounds the observed transition (see for

instance Ref. [85]) is also an interesting open question. Furthermore, we have described an alternative way to compute the sCGF without using the variational techniques derived from the weak-noise analysis of the path-integral representation, that allowed us to show how the large-time and the weak-noise limits commute.

The obtained results also open a direction of research to characterise fluctuations in a given system by engineering a new system subjected to an additional external force. Such an approach has been used in recent studies on adaptive algorithms, based for instance on a feedback procedure to evaluate the effective force [283–286], improving the computational efficiency. The weak-noise regime has been seldom studied (it is in fact know to present specific difficulties [283]), and the results we present in this chapter could help to understand large-time fluctuations and their associated phenomenology both in experiments and simulations.

Chapter 8

Conclusions

Understanding the statistics of macroscopic fluctuations is a prominent challenge in modern theoretical physics. Their capital importance relies on the main role that fluctuations play out of equilibrium. Indeed, characterizing the probability distribution of observing a given (typical or rare) event lead to a description of the large deviation function, broadly considered a proper aspirant to act as marginal of thermodynamic potential in nonequilibrium situations. The knowledge of such a distribution and the associated LDF has been proved to be of special utility, providing very general results valid arbitrarily far from equilibrium . Furthermore, the figure of the most probable trajectory exhibited by the system to sustain a given fluctuation has been revealed as an essential element to describe many interesting phenomena such as symmetry-breakings or dynamic phase transitions at a fluctuating level. This situation has become even more relevant in last years, with (i) the development of new mechanisms to determine the effective drift which should apply to given system in such a way that the new effective dynamics reproduce as typical events the rare trajectories of the original one, and (ii) the rise of nanoelectronic technology where fluctuations considerably condition the behaviour of the system.

In this Thesis we have focused on the study of fluctuations of space- and time-integrated observables in different situations. In this way, under the framework of the Macroscopic Fluctuation Theory and Large Deviation Theory, we have characterized the properties of the probability distribution of fluctuations, their LDFs and associated optimal paths. As a fruit of this research, we have obtained interesting results which could help to clarify nonequilibrium behaviour, paving the way to further investigation. In the following we will detail the different conclusions we

can extract from this work.

Firstly, we have presented the main features of MFT and LDT, laying the foundations for the subsequent fluctuations studies. Starting from a mesoscopic description of the system at hand, we have provided the mathematical scheme that allows us to characterize the probability distribution of fluctuations. In particular, we have deduced that the problem of determining the LDF can be writen in terms of a spatio-temporal variational problem, whose solutions are the optimal trajectories leading to a fluctuation. Therefore, solving the Euler-Lagrange equations associated to such a problem is the main goal when studying the statistic of macroscopic fluctuations.

In the context of d-dimensional driven diffusive systems, we have adressed the problem of characterizing the structure of the most probable paths. Two main results can be derived from this study:

1. The optimal current fields satisfy a general fundamental requirement which strongly constraint their structure. In the particular, but frenquently observed, case of considering a system that exhibits a principal direction (e.g. a system subjected to a boundary gradient in one direction with periodic boundary conditions in all the orthogonal components) this relation implies a non-local behavior of the optimal current field and, consequently, on the current LDF, a typical feature of nonequilibrium situations.

2. Previous observations of structured current vector fields perfectly fit into this relation. Since this result does not rely on any boundary condition hypothesis, it therefore provides a fulcrum for new conjectures shedding light on the complex variational problem for the LDF in many general systems arbitrarily far from equilibrium.

The development of the previous relation has served as a starting point for our next study: the description of current fluctuations in a d-dimensional incompressible quiescent fluid subjected to a boundary temperature gradient in one direction. The main conclusions we have obtained from this research are the following:

3. We have computed the explicit expression for the most probable temperature fields, analyzing their properties for different values of the desired space- and time-integrated current, $\mathbf{q}$, and intensity of the temperature boundary gradient. In this way, we have realized that such optimal fields can be classified in families of universal profiles with the same mathematical structure, leading to a remarkable fact: systems subjected to different boundary gradients will exhibit the same optimal temperature curve if we look for an appropiated current $\mathbf{q}$ (different in each of these system).

4. Once the optimal temperature fields were determined, the corresponding LDF controlling the heat current probability distribution has been obtained. We have then observed that, while around the steady state deviations from gaussianity are small and such a distribution can be approximated by a deformed Gaussian, its long tails behaviour are far more complex enhancing the probability of observing rare events.

5. We have finally derived the analytic form of the spatio-temporal integrated n-points correlation functions, with $n \leq 3$, for the heat current field arbitrarily far from equilibrium, as well some interesting relations between low-order cumulants of the current distribution, which could be tested in further experimental investigations.

Thereupon, we have focused on one of the recently considered most interesting phenomena in nonequilibrium physics: the dynamic phase transitions. Indeed, we have analyzed the existence of DPTs in the current fluctuations for an anisotropic 2-dimensional driven diffusive system, arriving to the following results:

6. We have found a dynamic phase transition associated to the breaking of a spatiotemporal translation symmetry for large fluctuations of the current. This DPT separates an constant and structureless fluctuation phase with Gaussian current statistics and coherent jammed states in the form of one dimensional traveling waves with non-Gaussian distribution of currents, revealing the emergency of order for rare fluctuations with self-organized structures enhancing their probability of occur.

7. In the particular case of the weakly asymmetric exclusion process (WASEP), we have characterized such a DPT both from a mesoscopic level under the MFT framework and from a microscopic level by using extensive cloning Monte Carlo simulations, obtaining an outstanding agreement between both descriptions. Interestingly, the sCGF presents a non-analiticity in its second derivative at the transition, implying that the DPT is of 2nd-order. This outcome has been corroborated microscopically by defining a novel order parameter which vanishes for the structureless phase and increases upon crossing the transition point.

8. Lastly, fruit of the interplay between the external drift, anistropy and high-dimensionality ($d > 1$), a rich fluctuation phase diagram for the WASEP has been derived. Besides the previously mentioned 2nd-order dynamic phase transition, an interesting 1st-order DPT separating different traveling-wave

phases has been discovered, unveiling the existence of regions where such jammed states coexists.

In order to explore situations beyond the MFT, we have then studied the effects of fluctuations in dissipative systems with no conservation laws. In particular, we have extended the MFT techniques to characterize the distribution of fluctuations of the space- and time-integrated magnetization in the one-dimensional periodic stochastic Landau-Ginzburg model, with a dynamics given by the Hohenberg-Halperin model A. The following conclusions have been extracted from such analysis.

9. We have provided strong evidences of the existence of a dynamic phase transition for low values of the magnetization by studying the stability of uniform magnetization fields against spatio-temporal pertubations. This outcome holds deep implications in our understanding of nonequilibrium systems, constituting a new step forward on the discovery of DPTs in one-dimensional systems at a fluctuating level. Interestingly, the dynamic phase transition only takes place in situations in which the Landau-Ginzburg potential exhibits a double well structure.

10. We have found a new exotic dynamic phase that this model could exhibit beyond the transition. Indeed, to sustain rare fluctuations of the magnetization the system adopts a homogeneus structure which changes periodically with time. We have characterized such a solution, showing that the corresponding LDF is indeed lower than the one associated to uniform optimal fields.

Finaly, we have concentrated on the study of the effective probability-conserving dynamics under which rare events of the original dynamics become typical. The system at hand has been a single particle diffusing in a periodic one-dimensional generic force under the action of a weak thermal noise. We next detail the conclusions we have derived.

11. We have determined the effective dynamics turning rare trajectories into typical when studying fluctuations of general time-integrated additive observables, identifying the effective force under which the particle is conditioned to exhibit such an atypical events. This new dynamics has been proved to be not just a slightly modification of the original one by the application of a non-conservative constant drift, but it changes in a far more complex way.

12. For the case when the observable is of the time-integrated current-type, we have found that the system exhibits a dynamic phase transition between a

static fluctuation phase with a flat sCGF and time-periodic propagative trajectory presenting a more complex sCGF obtained as a solution of an optimisation problem. Interestingly, the form of the effective force near the transition reveals the highly non-trivial nature of the DPT, very different from standard depinning transitions.

13. As an interesting by-product, we have derived an alternative way to compute the sCGF for fluctuations of general time-integrated additive observables without the need to solve the complex variational problem derived from path integral formulation. This result unveils a relevant fact: in these situations, both weak noise and large time limits commute.

Optimal temperature field

In this Appendix we determine the analytical expression for the most probable temperature field. Moreover, we will exhaustively analyze its mathematical properties in order to better characterize the statistics of the heat current in our incompressible quiescent model fluid. For our particular model fluid, the optimal temperature field associated to a space\$time-averaged heat current fluctuation $\mathbf{q}$ is the solution of the following differential equation (see main text)

$$\frac{dT_{\mathbf{q}}}{dx} = 2s \left[q_x^2 + KT_{\mathbf{q}}^2 - \frac{T_{\mathbf{q}}^4}{A^2} \boldsymbol{J}_\perp^2 \right]^{1/2} , \tag{A.1}$$

with $s = \pm 1$ and where, for simplicity, we have fixed $L = 1$ without loss of generality. This expression can be rewritten in terms of the extrema $T_\pm$ of the optimal temperature field, i.e. the zeros of the quartic polynomial $q_x^2 + KT_{\mathbf{q}}^2 - \frac{T_{\mathbf{q}}^4}{A^2} \boldsymbol{J}_\perp^2$, resulting in

$$\frac{dT_{\mathbf{q}}}{dx} = 2s|q_x| \left[(1 - \eta_+ T_{\mathbf{q}}^2)(1 + \eta_- T_{\mathbf{q}}^2) \right]^{1/2} , \tag{A.2}$$

with the definition $\eta_\pm = \pm 1/T_\pm^2$, such that

$$(\eta_+ \eta_-)^{1/2} = \frac{|\boldsymbol{q}_\perp|}{A|q_x|} , \tag{A.3}$$

and we consider one of the η's constants fixed by boundary conditions. We can integrate Eq. (A.2) between two arbitrary spatial points (x_A, x_B) such that the

slope sign s is conserved in the interval

$$\int_{T_{\mathbf{q}}(x_A)}^{T_{\mathbf{q}}(x_B)} dT_{\mathbf{q}} \left[(1 - \eta_+ T_{\mathbf{q}}^2)(1 + \eta_- T_{\mathbf{q}}^2)\right]^{-1/2} = 2s|q_x|(x_B - x_A)\,. \quad (A.4)$$

It is now natural to transform eq. (A.4) into a Jacobi's integral of the first kind $F(\theta; k)$ [234, 235] by doing the change of variables $\cos\theta = \sqrt{\eta_+} T_{\mathbf{q}}$, leading to

$$\frac{2sQ_x T_1 \sqrt{\eta_+}}{\sqrt{1 - k^2}}(x_B - x_A) = F(\theta(x_A); k) - F(\theta(x_B); k)\,, \quad (A.5)$$

where

$$F(\theta; k) = \int_0^\theta d\bar{\theta} \frac{1}{(1 - k^2 \sin^2 \bar{\theta})^{1/2}}\,, \quad (A.6)$$

and where we have defined the modulas via $k^2 = (1 + \eta_+/\eta_-)^{-1}$, and $Q_x = |q_x|/T_1$. We can invert Eq. (A.5) by using the relation

$$\cos\theta = cn(F(\theta; k); k) \quad (A.7)$$

which defines the cosine-amplitude Jacobi function $cn(u; k)$ of modulus k [234, 235], resulting in

$$\tau(x_B) = \frac{1}{T_1\sqrt{\eta_+}} cn\left(-F(\theta(x_A); k) + \frac{2sQ_x T_1 \sqrt{\eta_+}}{\sqrt{1 - k^2}}(x_B - x_A); k\right)\,, \quad (A.8)$$

with $\tau_{\mathbf{q}}(x) = T_{\mathbf{q}}(x)/T_1$. Since the $cn(u; k)$ function appearing in Eq. (A.8) has a positive maximum and a negative minimum, and taking into account that $\tau_{\mathbf{q}}(x)$ is defined positive, the optimal temperature field presents at most two possible behaviors, namely: (i) a monotonous decreasing profile or (ii) a single-maximum profile. We analyze next each case separatedly.

A.1 Monotonous profile

In this case, assuming without loss of generality that $T_0 > T_1$, we have that $s = -1$ for all $x \in [0, 1]$. Therefore, considering Eq. (A.8) with $x_A = 0$ and $x_B = x$, the optimal temperature field takes the form

$$\tau_{\mathbf{q}}(x) = \frac{cn\left[F_0 + (F_1 - F_0)x; k\right]}{cn(F_1; k)}\,, \quad (A.9)$$

with $F_{0,1} \geq 0$ two constants. In order to completely compute the temperature field $T_{\mathbf{q}}(x)$ we need to fix the values of F_0, F_1 and k through boundary conditions and the clausure equation

$$A = \int_0^1 dx \, \sigma[T_{\mathbf{q}}(x)] \, . \tag{A.10}$$

Indeed, taking into account the boundary conditions, both Eq. (A.5) and the constraint $\tau(0) \equiv \tau_0 = T_0/T_1$ lead to

$$Q_x = \frac{\sqrt{1 - k^2}(F_1 - F_0)}{2 \, \mathrm{cn}(F_1; k)} \tag{A.11}$$

$$\tau_0 = \frac{\mathrm{cn}(F_0; k)}{\mathrm{cn}(F_1; k)}, \tag{A.12}$$

respectively, and from (A.10) we obtain

$$Q_\perp = \frac{E_1 - E_0 - (1 - k^2)(F_1 - F_0)}{2k \, \mathrm{cn}(F_1; k)} \, , \tag{A.13}$$

with $Q_\perp = |\boldsymbol{q}_\perp|/T_1$, and where

$$E_{0,1} = E(\mathrm{am}(F_{0,1}; k); k) \, , \tag{A.14}$$

being $\mathrm{am}(u; k)$ the amplitude Jacobi function and $E(\theta; k)$ the Jacobi integral of the second kind [234, 235]. Remarkably, as a consequence of assuming $\tau_0 \geq 1$, we find that $F_0 \in [0, \mathbf{K}(k)]$, $F_1 \in [\mathrm{cn}^{-1}(\tau_0^{-1}; k), \mathbf{K}(k)]$ with $F_1 \geq F_0$ and $\mathbf{K}$ the Jacobi complete elliptic integral of the first kind (using the notation used by Gradshteyn & Ryzhik [234]).

A.2 Single-maximum profile

In this case $s = +1$ for $x \in [0, x^*]$ while $s = -1$ for $x \in [x^*, 1]$, being x^* the maximum location where $d\tau_{\mathbf{q}}(x)/dx|_{x=x^*} = 0$. This maximum position can be obtained from Eq.(A.8) by taking $x_A = 0$, $x_B = x^*$ and forcing the argument of $\mathrm{cn}(u; k)$ to be equal to zero, arrivieng at

$$x^* = \frac{F_0 \sqrt{1 - k^2}}{2Q_x T_1 \sqrt{\eta_+}} \, . \tag{A.15}$$

In this way, the optimal temperature profile can be determined by considering Eq. (A.8) both for $x > x^*$ and $x < x^*$, resulting in

$$\tau_{\mathbf{q}}(x) = \frac{\mathrm{cn}\left[-F_0 + (F_1 + F_0)x; k\right]}{\mathrm{cn}(F_1; k)} \, , \tag{A.16}$$

where the values of $F_0, F_1 \geq 0$ and k are fixed again by the boundary conditions and the clausure equation (A.10), leading again to Eq. (A.12) and

$$Q_x = \frac{\sqrt{1-k^2}(F_1+F_0)}{2\,\mathrm{cn}(F_1;k)} \tag{A.17}$$

$$Q_\perp = \frac{E_1+E_0-(1-k^2)(F_1+F_0)}{2k\,\mathrm{cn}(F_1;k)}\,. \tag{A.18}$$

Interestingly, Eqs.(A.16), (A.17) and (A.18) corresponding to the single-maximum case map onto Eqs. (A.9), (A.11) and (A.13) corresponding to the monotonous behavior by changing $F_0 \to -F_0$; this allows us to write both solutions in an unified way. In particular, from now on, given Q_x, $Q_\perp$ and τ_0 fixed by boundary conditions and Eq. (A.10), the values of F_0, F_1 and k are determined from equations (A.12), (A.17) and (A.18) with $F_0 \in [-\mathbf{K}(k), \mathbf{K}(k)]$, $F_1 \in [\mathrm{cn}^{-1}(\tau_0^{-1};k), \mathbf{K}(k)]$ and $k \in [0,1]$ which includes both posibilities: $F_0 < 0$ for the monotonous case and $F_0 > 0$ for the single-maximum case.

A.3   Convexity behavior

Furthermore, once the solution (A.16) has been determined, we can now characterize the convexity behavior of the optimal termperature field as a function of the parameters $(\tau_0, Q_x, Q_\perp)$. Indeed, since the second derivative of $\mathrm{cn}(u;k)$ takes the form $d^2\mathrm{cn}(u;k)/du^2 = -\mathrm{cn}(u;k)(1-2k^2+2k^2\,\mathrm{cn}(u;k))$, there are no inflection points for $k^2 < 1/2$ and the profile is always concave in this regime. For $k^2 > 1/2$ we observe that, for a fixed value of τ_0, both $(Q_x, Q_\perp)$ are parametrized by (F_0, k), leading to the following regions with different number of inflection points. First, for $\tau_0 \leq \sqrt{2}$ we have

- If $F_0 > F_0^{(1)}(k)$ and $k^2 \geq 1/2$, with $F_0^{(1)}(k) = \mathrm{cn}^{-1}(B(k);k)$ and $B(k) = ((2k^2-1)/(2k^2))^{1/2}$, the optimal temperature profile presents two inflection points located at

$$x_{1,2} = (F_0 \pm F_0^{(1)}(k))/(F_0 + \mathrm{cn}^{-1}(1/\tau_0;k))\,. \tag{A.19}$$

- If $F_0^{(2)} \leq |F_0| \leq F_0^{(1)}$ and $k^2 \geq 1/2$, with $F_0^{(2)}(k) = \mathrm{cn}^{-1}(\tau_0 B(k);k)$, the optimal profile presents only one inflection point located at x_1.

On the other hand, for $\tau_0 \geq \sqrt{2}$

- If $F_0 > F_0^{(1)}(k)$ and $k^2 \geq 1/2$, we find that the profiles present two inflection points at x_1 and x_2.

- If $F_0^{(2)} \leq |F_0| \leq F_0^{(1)}$ and $1/2 \leq k^2 \leq \tau_0^2/(2(\tau_0^2 - 1))$, the optimal temperature profile has only one inflection point located at x_1.

- If $0 \leq |F_0| \leq F_0^{(1)}$ and $1 \geq k^2 \geq \tau_0^2/(2(\tau_0^2 - 1))$, the optimal profile presents again only one inflection point located at x_1.

Finally, outside these regions, no inflection points appear for any value of the parameters.

Resumen

1 Introducción

1.1 Antecedentes

Desentrañar los misterios de la Naturaleza ha sido siempre uno de los principales desafíos de la humanidad. A lo largo de los siglos, hemos intentado resolver preguntas como: *¿De qué están compuestas las diferentes sustancias?, ¿por qué llueve?, ¿por qué el sol sale y se pone todos los días?* La búsqueda de respuestas para esas cuestiones fundamentales abre la puerta a un nuevo dilema interesante: a la luz de esta nueva información, ¿es posible anticipar lo que va a ocurrir? En otras palabras, ¿somos capaces de detectar patrones generales a partir de estas respuestas y usarlas para predecir un comportamiento futuro? Estos elementos constituyen los pilares en los cuales se sustenta la física. En líneas generales, la física persigue entender los fenómenos naturales caracterizando sus causas y deduciendo principios básicos y teorías que permiten hacer predicciones cuantitativas sobre observaciones futuras[1]. En este sentido, la física ocupa un lugar especial entre los diferentes campos que componen las Ciencias Naturales. En palabras de Richard P. Feynman: "La física es la más fundamental e inclusiva de todas las ciencias [...]. Estudiantes de todos los campos se encuentran estudiando Física dado el papel fundamental que juega en todos los fenómenos" [1]. En efecto, la física, como ciencia que pretende obtener las leyes generales que gobiernan la Naturaleza, posee un amplio

---

[1]No pretendemos establecer en este texto una definición formal de lo que es la física, sino más bien señalar, desde el punto de vista del autor, algunos de los objetivos más importantes de esta ciencia.

grado de aplicabilidad en Química, Biología, Geología e incluso en las Ciencias Sociales.

El espectro de fenómenos descritos por la física abarca desde los sistemas más pequeños (por ejemplo, las partículas que constituyen la materia y la radiación) hasta los más grandes (galaxias, cúmulos de galaxias, supercúmulos...). Cuando lidiamos con la ambiciosa tarea de entender el universo, nos damos cuenta de que la naturaleza presenta una estructura jerárquica. La realidad se divide en diferentes *niveles de descripción*, cada uno de los cuales está definido por unas *escalas de longitud y tiempo* típicas. Por ejemplo, imaginemos un litro de agua dentro de un vaso Dewar. Las escalas de longitud y tiempo que podemos medir a simple vista en un laboratorio definen el *nivel macroscópico*. Sin embargo, es bien conocido que el litro de agua se compone por un número de moléculas H_2O del orden del número de Avogadro, N_A. Estas escalas de longitud y tiempo mucho más pequeñas definen un nuevo nivel de descripción llamado *nivel microscópico*[2]. Al estudiar las propiedades de cada nivel por separado, nos damos cuenta de que éstos poseen unos observables propios que los caracterizan, que a su vez satisfacen ciertas relaciones. Esas *leyes* gobiernan el comportamiento de cada estructura jerárquica. En el ejemplo del agua, el nivel macroscópico está completamente caracterizado por magnitudes tales como la temperatura, el volumen, la presión, etc. Asimismo, existe una teoría macroscópica que establece relaciones entre esos observables: la Termodinámica. Por otra parte, cuando pensamos en las moléculas que componen el agua, su comportamiento es descrito por su posición, velocidad, energía, etc., y las leyes que gobiernan su evolución están definidas por la Mecánica Clásica o Cuántica. Algunos ejemplos de esta división jerárquica se muestran en la Figura 1.

La clara separación entre diferentes escalas lleva a una cuestión fundamental: si todos los niveles de descripción forman parte de la misma realidad, ¿cuál es la conexión entre los niveles microscópico y macroscópico? El campo de estudio que intenta encontrar una solución a este dilema es la *Mecánica Estadística*, cuyo principal objetivo es describir las propiedades macroscópicas de un sistema a partir de las leyes que gobiernan el mundo microscópico. Pensemos de nuevo en el ejemplo del agua en el vaso Dewar. Por simplicidad, asumamos que las leyes que describen el comportamiento de las moléculas de agua vienen dadas por la Mecánica Clásica. De esta forma, las ecuaciones que definen la dinámica de cada partícula son deterministas, es decir, su evolución está completamente determinada una vez

---

[2]Esta división no es única y representa una versión simplificada de la realidad. Ciertamente, las moléculas de H_2O están compuestas por diferentes partículas subatómicas tales como electrones, quarks, etc., que poseen sus respectivas escalas. Es más, el litro de agua podría ser simplemente una pequeña fracción del Océano Atlántico, que a su vez presenta sus propias escalas de longitud y tiempo típicas.
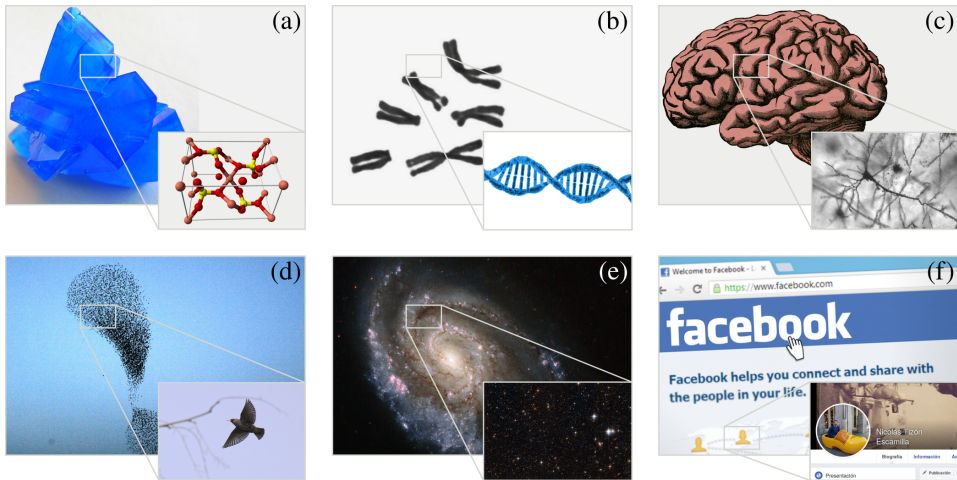
Figura 1: Ejemplos de distintos sistemas vistos a diferentes escalas. (a) El sulfato de cobre(II) es un cristal de estructura triclínica formada por átomos de Cu, S y O. (b) Cada célula humana contiene, dentro de su núcleo, 46 cromosomas de un tamaño del orden de $10^{-4} - 10^{-6}$ m. En los cromosomas, el ADN se encuentra en una estructura enrollada, sin embargo si se estirara fuera de la célula, el ADN formaría un hilo muy delgado de aproximadamente 3 metros de largo [2]. (c) El cerebro humano posee un volumen del orden de 10^3 m^3 y está compuesto de alrededor de 10^{10} neuronas, cuya longitud varía en el intervalo $10^{-6} - 10^{-4}$ m. [3]. (d) Una bandada de pájaros y un único estornino. (e) La galaxia espiral NGC 6984 es una de las 10^{11} galaxias en el universo observable, y cada una de esas galaxias se estima que contiene unas 10^{11} estrellas [4]. (f) El número de usuarios activos en la mayor red social es del orden de 10^{10}. Imágenes obtenidas de las siguientes fuentes: Wikimedia Commons, the free media repository (a, b, c), ESA/Hubble (e), Facebook (f), Graphodatsky et al., Molecular Cytogenetics 2011, 4-22 (b), Pixabay (b, d), COBBS (Universidad de la Sapienza, Roma) (d).

que se fijan las condiciones iniciales de cada molécula. Sin embargo, aunque este sistema es formalmente resoluble, encontrar una solución a N_A ecuaciones diferenciales acopladas es, en general, impracticable. Es más, resulta imposible fijar y determinar experimentalmente N_A condiciones iniciales. Como consecuencia, la existencia de tal cantidad de partículas nos conduce a un tratamiento estadístico del problema. La Mecánica Estadística trata con los numerosos grados de libertad microscópicos con el objetivo de obtener leyes estadísticas que nos permitan entender el complejo comportamiento macroscópico. Bajo este marco, podemos determinar la *media* o *valor promedio* de un observable macroscópico, que corresponde al valor típico que obtendremos al medir en el laboratorio[3]. Sin embargo,

---

[3]Este no será siempre el caso. Un sistema que satisface esta condición se llama *sistema ergódico*. Probar que un sistema es ergódico no es tarea fácil en absoluto, y solo se ha conseguido en unos pocos

podemos encontrar *desviaciones* respecto al valor medio de dicha magnitud como consecuencia de su naturaleza estadística. En este caso, se dice que el valor del observable *fluctúa* [7–9]. Por tanto, las fluctuaciones se entienden como reminiscencias microscópicas en el mundo macroscópico. El estudio de las fluctuaciones es un objeto fundamental en la física moderna, y constituye el tema central de esta Tesis.

En 1905, Albert Einstein introdujo un formalismo para describir el movimiento browniano, esto es, el movimiento aleatorio de una partícula suspendida en un fluido, basado en una descripción estadística del fenómeno [10–13]. Este trabajo es ampliamente considerado una de las primeras evidencias de la determinante influencia de las fluctuaciones. La aleatoriedad en el movimiento de la partícula emerge de sus colisiones con las moléculas que componen el fluido. De esta forma, Einstein fue capaz de determinar el número de Avogadro y, como consecuencia, el tamaño de las moléculas del fluido mediante el análisis de la estadística de las fluctuaciones del desplazamiento de la partícula. Podemos encontrar muchos otros ejemplos en los que destaca la importancia de las fluctuaciones, tales como los fenómenos críticos, hidrodinámica o incluso cosmología, donde el estudio de las fluctuaciones de la radiación de fondo de microondas ha proporcionado información crucial para entender el origen del universo.

1.2   ¿Por qué estudiar fluctuaciones macroscópicas?

La probabilidad de observar una fluctuación dada, normalmente, decae con el número de partículas del sistema. Como consecuencia de ello, medir una desviación del valor promedio de una magnitud macroscópica en un laboratorio es, en general, poco probable. La situación es incluso más dramática si estamos interesados en grandes desviaciones. Para ilustrar este hecho, imaginemos que nos encontramos aislados en una habitación y, en un momento dado, todo el aire del lugar se condensa en la esquina superior de la estancia. Este evento es un ejemplo paradigmático de lo que se entiende por una gran fluctuación. Aunque este evento raro no está prohibido por la física, la probabilidad de que tenga lugar es tan pequeña que en la práctica, por suerte, nunca ocurrirá. En la naturaleza, existen varios fenómenos conocidos por ser fruto de tal comportamiento, lo que generalmente tiene graves consecuencias (ver Figura 2). Por tanto, la cuestión que surge de manera natural es: ¿por qué nos interesamos en el estudio de fenómenos que rara vez suceden? O reformulando la pregunta, ¿por qué la caracterización de fluctuaciones arbitrariamente grandes tiene especial relevancia en física? En las siguientes líneas se van a

casos particulares (véase, por ejemplo, el sistema de billares de Sinai [5, 6]). En la mayoría de los casos, se asume que esta propiedad se satisface, suposición que se conoce como *Hipótesis Ergódica*.

Figura 2: Ola gigante en Avila Bay (California), un ejemplo paradigmático de grandes fluctuaciones presentes en la Naturaleza. Estas olas pueden alcanzar los 30 metros de altura. Su rareza e imprevisibilidad las convierte en un fenómeno extremadamente peligroso.

proporcionar tres argumentos de peso que sustentan la importancia de analizar la estadística de grandes desviaciones.

Dilema del no equilibrio. Describir el comportamiento macroscópico en términos de la dinámica microscópica es una ardua tarea, suponiendo aún un desafío en la mayoría de los casos. Imaginemos un sistema aislado que no presenta histéresis. Bajo estas condiciones, tras transcurrir un tiempo transitorio, el sistema se asentará en un estado en el que las variables macroscópicas no cambien con el tiempo, conocido como *estado de equilibrio termodinámico*. En lo que se refiere a sistemas en equilibrio, la Mecánica Estadística ha alcanzado un gran éxito, proporcionando una teoría general capaz de conectar ambos niveles de descripción (microscópico y macroscópico): la *teoría de colectividades*. En este marco teórico, se pueden construir y relacionar las diferentes magnitudes termodinámicas macroscópicas (entropía, energía libre, temperatura, presión, ...) desde el conocimiento de las leyes de la Mecánica Clásica (o Cuántica) que controlan la evolución de los componentes microscópicos. De esta manera, postulando que cada estado

microscópico que da lugar a un estado macroscópico de equilibrio dado tiene *a priori* la misma probabilidad de ocurrir (llamado *postulado de igual probabilidad a priori*), la Mecánica Estadística establece que la entropía (observable macroscópico) puede ser relacionada con el número de microestados $\Omega(U, \Delta U; V, N)$ compatibles con macroestados de energía $E \in [U, U + \Delta U]$ (con $\Delta U << U$), volumen V y número de partículas N, de la forma:

$$S(U, V, N) = k_\mathrm{B} \ln \Omega(U, \Delta U; V, N) \,, \tag{20}$$

donde k_B es la constante de Boltzmann. La relación entre estas dos magnitudes fue establecida por primera vez por Ludwig Boltzmann en 1875 [14], y más tarde formulada como (20) por Max Planck a principios de 1900 [8]. El número de microestados Ω es el principal elemento de la *colectividad microcanónica*, en la cual se describe un sistema caracterizado por $E \in [U, U + \Delta U]$, V y N. Sin embargo, es complicado fijar experimentalmente la energía del sistema. Por el contrario, usando un baño térmico, podemos controlar su temperatura, dejando fluctuar la energía. Por lo tanto, se puede definir la colectividad *canónica* describiendo un sistema caracterizado por T, V y N. La función de densidad de probabilidad de observar un estado microscópico α está ahora dada por la distribución de Gibbs:

$$\rho(\alpha) = \frac{1}{Z(T, V, N)} e^{-\beta E(\alpha)} \,, \tag{21}$$

donde $\beta = (k_\mathrm{B} T)^{-1}$, $E(\alpha)$ es la energía asociada al microestado α y $Z(T, V, N)$ es la *función de partición*, objeto central de la colectividad canónica. Esta colectividad proporciona una definición de la *energía libre*, también llamado *potencial de Helmhotz*, $F(T, V, N)$, en términos de la función de partición, a saber:

$$F(T, V, N) = -\beta^{-1} \ln Z(T, V, N) \,, \tag{22}$$

Además, se puede escribir Ω en términos de Z a través de una relación similar a una transformada de Laplace, mientras que la entropía y la energía libre pueden relacionarse, tal y como predice la Termodinámica, por la transformada de Legendre:

$$F = U - TS \,. \tag{23}$$

En el contexto de la Mecánica Estadística del equilibrio, las fluctuaciones juegan un papel destacado, ya que, caracterizando su estadística se pueden calcular los potenciales termodinámicos más relevantes. Una relación particularmente interesante está dada por la fórmula de Einstein [7, 8, 15] la cual permite escribir las

fluctuaciones de la energía E del sistema en términos de una magnitud macroscópica medible, la capacidad calorífica a volumen constante $C_V = \left(\frac{\partial U}{\partial T}\right)_{V,N}$:

$$\langle \Delta E \rangle \equiv \langle E^2 \rangle - \langle E \rangle^2 = k_{\mathrm{B}} T^2 C_V \,, \tag{24}$$

donde $U = \langle E \rangle$ y $\langle \cdot \rangle$ indica el valor medio de la magnitud correspondiente sobre la distribución canónica (Gibbs).

Considerar que un sistema real está en equilibrio termodinámico se ha convertido en una excelente aproximación en muchas situaciones, donde la Mecánica Estadística ha alcanzado predicciones sobresalientes. Sin embargo, en la naturaleza no existen sistemas reales en equilibrio (los cuales requerirían, por ejemplo, materiales aislantes perfectos). Es más, la mayoría de los fenómenos que encontramos en la naturaleza están *fuera del equilibrio*. Pensemos en nosotros mismos. Nuestro cerebro está compuesto por miles de millones de neuronas en continua actividad, enviando y recibiendo señales eléctricas, lo que conduce a una estructura altamente compleja que trabaja lejos del equilibrio. En nuestro corazón entra un flujo sanguíneo que luego es bombeado a todo el cuerpo a través de un proceso puramente fuera del equilibrio, en el que diferentes partes se contraen y se expanden de manera no trivial. Otros mecanismos como la respiración, la división celular o la replicación del ADN son algunos ejemplos más de procesos fuera del equilibrio que tienen lugar en nuestro cuerpo. Además de en los organismos vivos, en la naturaleza abundan sistemas que operan lejos del equilibrio en todas las escalas. Por ejemplo, cristales líquidos bajo la acción de campos eléctricos o magnéticos externos, los cuales se encuentran en membranas celulares o pantallas LCD; los mares y los océanos donde los flujos complejos y turbulentos son paradigmas de su comportamiento; o las estrellas, las cuales presentan altos gradientes de presión y temperatura, fenómenos de convección, etc. En general, se trata de sistemas abiertos o con histéresis, que a menudo se encuentran bajo la acción de fuerzas externas o fuentes de ruido, sujetos a flujos de masa o energía. Una situación interesante surge cuando el sistema evoluciona a un estado en el que sus variables macroscópicas permanecen constantes en el tiempo. Decimos entonces que el sistema se encuentra en un *estado estacionario* fuera del equilibrio. Dichos estados son los más similares a las situaciones de estados de equilibrio, siendo el principal objeto de estudio en la mayoría de los trabajos característicos de los fenómenos del no equilibrio.

A pesar de su ubicuidad, no existe una teoría general que sea capaz de predecir el comportamiento macroscópico a partir de las leyes microscópicas en sistemas lejos del equilibrio. El papel crucial desempeñado por la dinámica microscópica fuera del equilibrio dificulta el desarrollo de un esquema que conecte ambos niveles de

descripción. Como consecuencia de ello, las *trayectorias* o *historias* del sistema, es decir, las secuencias de estados seguidas por el sistema durante su evolución, emergen como elemento central para caracterizar las propiedades de no equilibrio. En general, tales trayectorias vienen descritas por ecuaciones fenomenológicas que se obtienen al usar aproximaciones *ad hoc* en cada situación particular, como por ejemplo las ecuaciones de Langevin, Fokker-Planck o Navier-Stokes. Además, de manera similar a lo que sucede en equilibrio, se pueden encontrar fenómenos relacionados con la ruptura de una simetría, auto-organización, coexistencia de fases, etc., lejos del equilibrio en el espacio de trayectorias. Las inestabilidades detrás de estos procesos se conocen como *transiciones de fase dinámicas* (DPTs, por sus siglas en inglés), las cuales separan regiones donde las historias que caracterizan la evolución del sistema presentan diferentes propiedades y estructuras.

Hoy en día, inspirados por la fórmula de Einstein y por la destacada relevancia de las fluctuaciones en el equilibrio, se espera que una comprensión más profunda de las fluctuaciones macroscópicas fuera del equilibrio pueda rellenar en parte la carencia de una teoría general que vincule ambos niveles de descripción [16–19]. Para respaldar esta idea, en las siguientes líneas describimos brevemente las principales características de la *Teoría de Grandes Desviaciones* (LDT, por sus siglas en inglés), el marco matemático que describe el comportamiento de grandes fluctuaciones [19–26] y su conexión con la Mecánica Estadística del equilibrio. La LDT se basa en un principio estadístico fundamental, piedra angular del estudio de los eventos raros. Sea A_n una variable aleatoria dependiente del parámetro n, y sea $p(A_n = a)$ la probabilidad de tener un valor dado $A_n = a$. Decimos que $p(A_n = a)$ satisface un *principio de grandes desviaciones* si el límite:

$$G(a) = \lim_{n \to \infty} \left\{ -\frac{1}{n} \ln p(A_n = a) \right\} \tag{25}$$

existe [19]. La función $G(a)$ es conocida como *Función de las Grandes Desviaciones* (LDF, por sus siglas en inglés), elemento central de la LDT que caracteriza la estadística de las fluctuaciones. A partir de la Ec. (25), se puede escribir:

$$p(A_n = a) \asymp e^{-nG(a)}, \tag{26}$$

donde "$\asymp$" representa "equivalencia logarítmica asintótica". La LDF es una función positiva $G(a) \geq 0 \; \forall a$. Suponiendo que $G(a)$ posee un único cero y un mínimo[4], puede demostrarse que éste se encuentra en $a^* = \lim_{n \to \infty} \langle A_n \rangle_{\mathrm{r}}$, denominado valor *típico* o *esperado*, donde $\langle \cdot \rangle_{\mathrm{r}}$ representa el promedio sobre ruido. Es

---

[4]Este será el caso general en esta Tesis.

importante remarcar que $p(A_n = a^*)$ no decae exponencialmente, y por tanto la LDF indica cómo la probabilidad $p(A_n = a)$ se estrecha alrededor de a^* cuando $n \to \infty$, la cual no es más que una expresión de la Ley de Grandes Números. Por último, dentro de este esquema es posible estudiar fluctuaciones alrededor del valor típico a^* expandiendo la LDF:

$$G(a) \approx \frac{1}{2}G''(a^*)(a - a^*)^2 + \mathcal{O}((a - a^*)^3) \,, \tag{27}$$

la cual en el primer orden distinto de cero lleva, como era de esperar, a fluctuaciones de tipo gaussiano:

$$p(A_n = a) \asymp e^{-n\frac{1}{2}G''(a^*)(a-a^*)^2} \,. \tag{28}$$

Por tanto, la Teoría de Grandes Desviaciones puede ser considerada como una generalización del Teorema Central del Límite (CLT, por sus siglas en inglés), ya que proporciona información acerca de lo que ocurre tanto cerca del valor esperado (donde la LDT y el CLT concuerdan), como para grandes desviaciones de a^*, donde la aproximación gaussiana ya no es válida. Recomendamos al lector consultar la publicación de Touchette [19], donde se estudian en profundidad las características de la Teoría de Grandes Desviaciones.

La teoría de colectividades, núcleo de la Mecánica Estadística del equilibrio, se puede entender en términos de la Teoría de Grandes Desviaciones [19, 24, 25, 27–36]. Vamos a mostrar de forma breve esta correspondencia. En efecto, si la variable aleatoria, cuyas fluctuaciones van a ser estudiadas, es la energía del sistema E_N, a partir de (25) se puede definir[5]:

$$G(e) = \lim_{N \to \infty} \left\{ -\frac{1}{N} \ln P(e_N \in [e, e + de]) \right\} \,, \tag{29}$$

donde N es, de nuevo, el número de partículas, $e_N = E_N/N$ es la energía por partícula (o energía molar) y $P(e_N \in [e, e + de])$ es la probabilidad de observar una energía $e_N \in [e, e + de]$. Como dicha probabilidad es proporcional al número de microestados $\Omega(e, de; v)$ compatible con $e_N \in [e, e + de]$ (siendo v=V/N), puede demostrarse que [19]:

$$G(e) = \lim_{N \to \infty} \left\{ -\frac{1}{N} \ln \Omega(e, de; v) \right\} \,. \tag{30}$$

---

[5]Esto puede demostrarse de forma trivial (ver [19]) usando $P(E_N \in [E, E+dE]) = p(E_N = E)dE$

Escribiendo $G(e) = -s(e)/k_B$ y de acuerdo con las propiedades de la LDF previamente mencionadas, nos damos cuenta de que ésta última expresión no es más que (20), siendo $s = S/N$ la *entropía por partícula*. Por tanto, la LDF para la energía se corresponde con la entropía en sistemas en equilibrio. Puede definirse la *Función Generadora de Cumulantes escalada* (sCGF, por sus siglas en inglés) de la distribución $P(e_N \in [e, e + de])$ como:

$$\mu(T) = \lim_{N \to \infty} \left\{ -\frac{1}{N} \ln Z_N(T) \right\} , \tag{31}$$

siendo T la temperatura y $Z_N(T) = \langle e^{-n\beta e_N} \rangle$ la función de partición (cabe destacar que, en este caso, $\langle \cdot \rangle$ representa el promedio sobre $P(e_N \in [e, e + de])$). Definiendo $\mu(T) = \beta f(T)$, de nuevo nos damos cuenta de que la ecuación previa equivale a (22) con $f = F/N$ la *energía libre por partícula*. Por tanto, en equilibrio, la sCGF se corresponde con la energía libre. Además, de acuerdo con el Teorema de Gärtner-Ellis [19, 24, 37], G y μ están relacionadas a través de la transformada de Legendre-Fenchel:

$$s(e) = \inf_{T} \left\{ \frac{e - f(T)}{T} \right\} , \tag{32}$$

en completa analogía con (23). Finalmente, nos centramos en las fluctuaciones alrededor del valor medio $u = \langle e_N \rangle$, que según (28), conducen a:

$$\langle e_N^2 \rangle - \langle e_N \rangle^2 = -k_B s''(u) . \tag{33}$$

Escribiend $C_V = -N \frac{1}{T^2} \left(\frac{\partial^2 s(u,v)}{\partial u^2} \right)_v$, nos damos cuenta que la expresión anterior no es más que la fórmula de Einstein (24).

La conexión entre la teoría de colectividades en equilibrio y la Teoría de Grandes Desviaciones abre nuevos caminos para profundizar en el estudio de situaciones fuera del equilibrio. La metodología de la LDT proporciona un esquema robusto del cual se podrían derivar predicciones generales lejos del equilibrio. En el núcleo de este marco teórico, las funciones de grandes desviaciones podrían ser consideradas, en una extensión natural, como análogos del no equilibrio de los potenciales termodinámicos, estableciendo un puente entre los niveles de descripción microscópico y macroscópico. Adicionalmente, se espera que la LDF muestre una estructura mucho más compleja fuera del equilibrio, conteniendo información clave sobre propiedades de no equilibrio[6]. Sin embargo, estas ideas no están exentas

---

[6]Por ejemplo, la LDF será en general no local, hecho que refleja la existencia de correlaciones de largo alcance características de situaciones lejos del equilibrio.

de problemas. Una de las principales dificultades es la identificación de observables macroscópicos relevantes. La ausencia de una teoría como la Termodinámica fuera del equilibrio conduce a una brecha en la definición correcta (si existe) de las magnitudes que caracterizan completamente el comportamiento de un sistema macroscópico (elemento esencial en el desarrollo de la teoría de colectividades en equilibrio). Para aquellos sistemas que pueden ser descritos a través de la evolución de algunas magnitudes conservadas (como la temperatura, la energía, la densidad de partículas, ...), es ampliamente aceptado que los observables esenciales de no equilibrio son las corrientes o flujos asociados que surgen en respuesta a las fuerzas o gradientes externos que hacen que el sistema se encuentre fuera del equilibrio. De hecho, hoy en día uno de los principales objetivos en la física de no equilibrio es caracterizar las fluctuaciones de las corrientes, convirtiéndose en una fuente de numerosos y muy generales resultados [16–18, 38–52]. En otras situaciones, podrían ser buenos candidatos determinados observables integrados en el espacio y en el tiempo, pero en general, estos dependen fuertemente de las características de cada sistema particular.

Aún lográndose identificar los observables relevantes que caracterizan el comportamiento de no equilibrio, la obtención de la función de grandes desviaciones es aún una tarea altamente compleja, ya que, en general no conocemos la estructura de la distribución de probabilidad de los estados (dinámicos) microscópicos, o incluso si tal distribución existe. El cálculo de la LDF a partir de la dinámica microscópica solo ha tenido éxito en unos pocos sistemas muy simplificados como son los gases reticulares estocásticos [16, 17]. Sin embargo, en las últimas décadas, Bertini, De Sole, Gabrielli, Jona-Lasinio y Landim han formulado una teoría para estudiar fluctuaciones dinámicas en sistemas difusivos lejos del equilibrio: la *Teoría de Fluctuaciones Macroscópicas* (MFT, por sus siglas en inglés) [16, 38, 53–55]. Partiendo de una descripción mesoscópica del sistema en términos de hidrodinámica fluctuante (completamente caracterizadas por tan solo unos pocos coeficientes de transporte, los cuales pueden ser fácilmente determinados a partir de experimentos o simulaciones), la MFT ofrece predicciones detalladas para las funciones de grandes desviaciones de interés en los límites de grandes tiempos y tamaños.[7]. Hay que tener en cuenta que el tiempo y el tamaño juegan el papel del parámetro n en la LDT. Como interesante subproducto, la MFT también determina la *trayectoria más probable* seguida por el sistema para mantener una fluctuación dada. Comprender las propiedades y la estructura espacio-temporal de estas trayectorias óptimas es de suma importancia, ya que contienen información sobre posibles

---

[7]En este tipo de situaciones, gran tamaño quiere decir grandes órdenes de magnitud de separación entre las escalas de los distintos niveles de descripción.

transiciones de fase dinámicas que aparecen en fluctuaciones [18, 41, 52, 56–63], mientras que sus propiedades de simetría conducen a nuevos teoremas de fluctuación [44, 46, 48–50, 64–71]. Se ha demostrado que la aplicación de dicho esquema proporciona resultados profundos y muy generales que nos ayudan a mejorar nuestra comprensión sobre el comportamiento de no equilibrio.

Dinámica efectiva. La segunda razón que justifica la importancia de estudiar eventos raros está relacionada con la determinación de lo que se denomina dinámica efectiva. Como se mencionó anteriormente, en general es casi imposible medir una fluctuación rara en un experimento. Sin embargo, avances recientes han demostrado que las fluctuaciones admiten una interpretación activa en términos de una teoría de control [72–77]. De esta forma, mediante el uso de una versión generalizada de la transformada h de Doob [78, 79], se puede construir una dinámica efectiva cuyas trayectorias típicas se correspondan con los eventos raros de la dinámica original. Además, este mecanismo proporciona la fuerza efectiva externa que debe aplicarse para hacer que dichos eventos raros se vuelvan típicos. En los últimos años se han realizado muchos avances, incluidos ejemplos explícitos, sobre la determinación de tales dinámicas efectivas [72, 73, 80–88]. A la luz de estos mecanismos, la determinación de la distribución de probabilidad de eventos raros, así como la caracterización de fenómenos interesantes tales como DPTs, rupturas de simetría, emergencia de estructuras ordenadas, etc., son, en la actualidad, más accesibles tanto en simulaciones como en experimentos. Ciertamente, esta metodología abre la puerta a un nuevo mundo de posibles aplicaciones de la gran cantidad de resultados y técnicas desarrolladas en estudios de grandes fluctuaciones.

Sistemas pequeños. Finalmente, el último argumento que respalda el interés en las grandes fluctuaciones se basa en el papel fundamental que éstas desempeñan cuando tratamos con sistemas pequeños. Hemos visto que la probabilidad de observar una desviación del valor promedio decae exponencialmente con el número de partículas del sistema, razón por la cual los eventos raros apenas tienen lugar en experimentos. Sin embargo, si el sistema es pequeño, la diferencia de escalas entre las descripciones microscópica y macroscópica se reduce notablemente, presentando además un número de partículas menor. En consecuencia, las grandes fluctuaciones se vuelven mucho más probables, convirtiéndose en elementos esenciales para entender el comportamiento del sistema. Este hecho tendrá una importancia crucial en, por ejemplo, dispositivos nanoelectrónicos, donde las fluctuaciones condicionan severamente sus propiedades y características y cuyos efectos deben tenerse en cuenta [89–92].

1.3 Estructura de la Tesis

A la luz de lo expuesto anteriormente, no cabe duda de que el estudio de las fluctuaciones es un objetivo esencial para la física moderna. El propósito de esta Tesis será indagar en el papel que juegan las fluctuaciones arbitrariamente fuera del equilibrio bajo los marcos de la Teoría de Fluctuaciones Macroscópicas y la Teoría de Grandes Desviaciones. En las siguientes páginas exploraremos los dos primeros argumentos expuestos anteriormente y sus profundas implicaciones, desarrollando diferentes herramientas, técnicas y resultados para un amplio espectro de situaciones que abarcan desde sistemas difusivos completamente generales hasta sistemas compuestos por una sola partícula bajo la acción de una fuerza externa, tanto fuera como en equilibrio. De esta forma, los capítulos 2, 3, 4, 5, 6 estarán dedicados al estudio y caracterización de la MFT y sus consecuencias, mostrando resultados generales en la estructura de las trayectorias que sostienen una determinada fluctuación, LDFs y transiciones de fase dinámicas. Por otro lado, el Capítulo 7 se centrará en la construcción de una dinámica efectiva asociada a fluctuaciones de observables completamente generals para una partícula en un anillo bajo la acción de un campo externo y una fuente de ruido térmico. A continuación detallamos, por tanto, la estructura de la presente Tesis.

En el **Capítulo 2** presentamos una introducción de la Teoría de Fluctuaciones Macroscópicas. Centrándonos en sistemas caracterizados por una ley de conservación, describiremos su evolución a nivel mesoscópico, que servirá como punto de partida para desarrollar los distintos aspectos que caracterizan la MFT. En particular, mostraremos cómo el estudio de la distribucion de probabilidad de las fluctuaciones de observables relevantes se torna en un problema variacional cuyas soluciones son las trayectorias óptimas que llevan a una fluctuación dada, lo que conduce a determinar la correspondiente LDF. Asimismo, presentaremos algunos resultados esenciales y generales sobre fluctuaciones y los traduciremo al lenguaje de grandes desviaciones y MFT. Finalmente, describiremos brevemente la evolución mesoscópica de otras clases de sistemas, tales como sistemas sin magnitudes conservadas, para los cuales podrán ser generalizadas algunas de las diferentes técnicas de la MFT.

Como hemos visto, las trayectorias más probables que conducen a una fluctuación dada codifican información clave sobre sus propiedades estadísticas. Esto hace que la comprensión de las características de tales historias sea una cuestión fundamental. En el **Capítulo 3** derivaremos una relación fundamental que condiciona fuertemente la arquitectura de estos caminos óptimos para sistemas difusivos d-dimensionales generales fuera del equilibrio, lo que implica una estructura no trivial para los campos vectoriales de corriente. Esta relación general pone de

manifiesto la no localidad espacio-temporal de la estadística de las corrientes y de las trayectorias óptimas asociadas. Además, mostraremos cómo esta relación engloba y explica muchos de los resultados obtenidos anteriormente en el campo de las grandes desviaciones.

El **Capítulo 4** está dedicado al estudio de las fluctuaciones de la corriente térmica en un modelo de fluido incompresible d-dimensional sacado fuera de equilibrio mediante un gradiente de temperatura. Macroscópicamente, este sistema obedece la ley de Fourier de la conducción térmica y su comportamiento se encuentra totalmente caracterizado por el campo de temperatura a lo largo del mismo. Encontraremos que los campos de temperatura más probables que sostienen valores atípicos de la corriente pueden clasificarse naturalmente en un conjunto infinito de curvas, lo que nos permite analizar exhaustivamente sus propiedades topológicas y definir perfiles universales sobre los que colapsan todos los campos óptimos. También calcularemos la distribución de probabilidad de la corriente térmica empírica, donde encontramos, entre otros resultados, un decaimiento logarítmico de las colas de dicha distributión para fluctuaciones grandes de la corriente en dirección ortogonal al gradiente térmico. Finalmente, determinaremos explícitamente los cumulantes de orden menor de la distribución de corrientes, estableciendo notables relaciones entre ellos.

En el **Capítulo 5** nos centramos en el estudio de las transiciones de fase dinámicas a nivel fluctuante en el espacio de las trayectorias, uno de los fenómenos más intrigantes de la física de no equilibrio. Aquí descubriremos una transición de fase dinámica estudiando la distribución del vector corriente en un sistema difusivo bidimensional ($2d$) bajo la acción de un campo externo, caracterizando además sus propiedades mediante la MFT. Como curiosidad, éste es el primer trabajo que analiza DPTs de un observable d'-dimensional en sistemas d'-dimensionales con $d' > 1$, una situación que hasta ahora había sido una incógnita. La compleja interacción entre el campo externo, la anisotropía del sistema y las corrientes vectoriales en $2d$ da lugar a un rico diagrama de fases dinámicas, con diferentes fases de fluctuación en las que se rompe la simetría espacio-temporal del sistema, sparadas por lineas de DPTs de primer y segundo orden. Notablemente, distintos tipos de soluciones unidimensionales en forma de ondas viajeras de densidad emergen para obstaculizar el transporte en el caso de fluctuaciones de baja corriente, revelando una conexión entre eventos raros y estructuras auto-organizadas que aumentan la probabilidad de que estos tengan lugar.

Originariamente, la MFT fue desarrollada para estudiar grandes fluctuaciones en sistemas difusivos. Sin embargo, estas técnicas podrían extenderse a otras situaciones caracterizadas por ecuaciones de evolución mesoscópicas. De esta for-

ma, en el **Capítulo 6**, caracterizaremos las fluctuaciones en el modelo de Landau-Ginzburg en equilibrio. Estos sistemas están descritos por un campo escalar que evoluciona siguiendo una dinámica no conservada localmente cuyas ecuaciones mesoscópicas vienen dadas por el modelo A de Hohenberg-Halpering [93]. Una de las principales propiedades de estos sistemas es que presentand dos regímenes de comportamiento diferentes caracterizados por la existencia de uno o dos estados de equilibrio. Nos centraremos en las fluctuaciones de la magnetización, es decir, del campo escalar integrado en el espacio y en el tiempo, revelando la existencia de una DPT al analizar la probabilidad de medir valores reducidos de dicho observable en el régimen de "pozo doble". Además, mostraremos una trayectoria exótica, homogénea pero periódica en el tiempo, que podría aparecer por debajo del punto de transición.

En el **Capítulo 7** determinamos explícitamente la dinámica efectiva (con probabilidad conservada) en el caso de fluctuaciones de observables generales integrados en el espacio y en el tiempo para una partícula que se difunde en un potencial periódico unidimensional en los límites de tiempos largos y ruido débil (que ahora desempeñará el papel del parámetro n en la LDT). Para observables aditivos de "tipo corriente", encontramos los criterios que marcan la emergencia de una trayectoria propagativa para desviaciones suficientemente grandes, revelando la existencia de una transición de fase dinámica a nivel fluctuante, cuyo comportamiento singular se encuentra entre primer y segundo orden. Asimismo, proporcionaremos un nuevo método para determinar la sCGF de observables generales sin tener que resolver el problema variacional derivado de la MFT. Esto nos permitirá demostrar que, en este caso, los límites de ruido débil y de tiempos grandes conmutan. Finalmente, mostraremos cómo la dinámica original puede ser mapeada en la práctica a una dinámica efectiva explícita, la cual toma la forma de una dinámica de Langevin con un potencial efectivo. La forma no trivial de este potencial efectivo es clave para entender el vínculo entre la transición de fase dinámica en las grandes desviaciones de corriente y la transición de fase estándar en un sistema formado por una partícula sometida a una fuerza conservativa más una fuerza de deriva uniforme no conservativa.

Por último, en el **Capítulo 8** resumiremos los diferentes resultados expuestos a lo largo de esta Tesis, señalando las principales implicaciones y novedades que tales aportaciones suponen para el campo de las fluctuaciones macroscópicas y, en general, para la Mecánica Estadística.

2 Conclusiones

Caracterizar la estadística de las fluctuaciones macroscópicas es uno de los grandes desafíos de la física teórica moderna. Su importancia radica en el rol fundamental que éstas representan en sistemas fuera del equilibrio. En efecto, la determinación de la distribución de probabilidad de observar un evento dado (típico o raro) conduce a una descripción de la función de grandes desviaciones, la cual se considera, en general, un buen aspirante para desempeñar el papel de un potencial termodinámico en situaciones de no equilibrio. El conocimiento de tal distribución y de la LDF asociada ha demostrado ser de gran utilidad, proporcionando resultados muy generales válidos arbitrariamente lejos del equilibrio. Además, la figura de la trayectoria más probable que el sistema exhibe para llevar a cabo una fluctuación dada ha resultado ser un elemento esencial en la descripción de muchos fenómenos de interés, como rupturas de simetría o transiciones de fase dinámicas a nivel fluctuante. Esta situación se ha vuelto aún más relevante en los últimos años, con (i) el desarrollo de nuevos mecanismos para determinar la fuerza externa efectiva que ha de aplicarse a un sistema dado para que la nueva dinámica efectiva reproduzcan, como evento típico, las trayectorias raras de la dinámica original, y (ii) el auge de tecnología nanoelectrónica donde las fluctuaciones condicionan considerablemente el comportamiento de los sistemas en cuestión.

En la presente Tesis, nos hemos centrado en el estudio de fluctuaciones de observables integrados en el espacio y en el tiempo en diferentes situaciones. De esta forma, en el marco de la Teoría de Fluctuaciones Macroscópicas y la Teoría de Grandes Desviaciones, hemos caracterizado las propiedades de la distribución de probabilidad de las fluctuaciones, así como sus LDFs y los caminos óptimos asociados. Como fruto de esta investigación, hemos obtenido interesantes resultados que podrían arrojar luz sobre el comportamiento de sistemas fuera del equilibrio , allanando el camino para nuevas investigaciones futuras. A continuación detallaremos las diferentes conclusiones que podemos extraer de este trabajo.

En primer lugar, se han presentado las principales características de la MFT y la LDT, sentando las bases para posteriores estudios de fluctuaciones. Partiendo de una descripción mesoscópica del sistema en cuestión, hemos desarrollado un formalismo matemático que nos permitirá caracterizar la distribución de probabilidad de las fluctuaciones. En concreto, hemos deducido que el problema de determinar la LDF se puede escribir en términos de un problema variacional espacio-temporal, cuyas soluciones son las trayectorias óptimas que conducen a una fluctuación. Por lo tanto, el objetivo principal al estudiar la estadística de las fluctuaciones macroscópicas será la resolución de las ecuaciones de Euler-Lagrange asociadas a este

problema.

En el contexto de sistemas difusivos d-dimensionales bajo la acción de un campo externo, nos hemos enfrentado al problema de caracterizar la estructura de los caminos más probables. De este estudio se infieren dos resultados principales:

1. Los campos de corriente óptimos satisfacen una relación fundamental completamente general que restringe fuertemente su estructura. En el caso particular, aunque frecuentemente observado, de considerar un sistema que muestra una dirección privilegiada (por ejemplo, un sistema sometido a un gradiente en una dirección con condiciones de contorno periódicas en todas las componentes ortogonales), dicha relación implica un comportamiento no local del campo de corriente óptimo y, por consiguiente, en la LDF de la corriente, reflejo de una de las principales características en situaciones fuera del equilibrio.

2. Las observaciones previas de campos vectoriales de la corriente con estructura encajan perfectamente en esta relación. Dado que este resultado no se basa en ninguna hipótesis sobre las condiciones de contorno, proporciona un importante sustento para nuevas conjeturas que arrojen luz sobre el complejo problema variacional para la LDF en muchos sistemas generales arbitrariamente alejados del equilibrio.

El desarrollo de la relación anterior ha servido como punto de partida para nuestro siguiente estudio: la descripción de las fluctuaciones de corriente en un fluido d-dimensional quiescente e incompresible sometido a un gradiente térmico en una dirección. A continuación se detallan las principales conclusiones que hemos obtenido de esta investigación:

3. Hemos calculado la expresión explícita de los campos de temperatura más probables, analizando sus propiedades para distintos valores de la corriente integrada en el tiempo y en el espacio, $\mathbf{q}$ y de la intensidad del gradiente térmico. De esta manera, hemos comprobado que estos campos óptimos se pueden clasificar en familias de perfiles universales con la misma estructura matemática, lo que conduce a un hecho relevante: los sistemas sometidos a diferentes gradientes térmicos exhibirán el mismo perfil de temperatura óptima para una corriente determinada $\mathbf{q}$ (que, obviamente, será distinta en cada uno de estos sistemas).

4. Una vez que determinados los campos de temperatura óptimos, se ha obtenido la LDF correspondiente que controla la distribución de probabilidad de la

corriente térmica. Con ello hemos observado que, mientras que las desviaciones de dicha distribución respecto de la gaussiana son pequeñas en torno al estado estacionario, por lo que ésta puede ser aproximada por una gaussiana deformada, su comportamiento para grandes desviaciones es mucho más complejo, lo que aumenta la probabilidad de observar eventos raros.

5. Finalmente, hemos derivado la forma analítica de las funciones de correlación a n puntos integradas en el espacio y en el tiempo, con $n \leq 3$, para el campo de corriente térmica arbitrariamente lejos del equilibrio, así como algunas relaciones interesantes entre los cumulantes de orden inferior de la distribución de corrientes, elementos que pueden ser testeados en futuras investigaciones experimentales.

Tras la obtención de estos resultados, nos hemos centrado en uno de los fenómenos recientemente considerados como más interesantes en el campo de la física de no equilibrio: las transiciones de fase dinámicas. De hecho, hemos analizado la existencia de las DPTs en las fluctuaciones de corrientes para un sistema difusivo anisotrópico bidimensional bajo la acción de un campo externo, lo cual ha conducido a los siguientes resultados:

6. Hemos encontrado una transición de fase dinámica asociada a la ruptura de una simetría de traslación espacio-temporal para grandes fluctuaciones de la corriente. Esta DPT separa una fase de fluctuación constante y sin estructura con una estadística de corrientes gaussiana asociada, de otra caracterizada por estrucutas coherentes que se mueven en forma de ondas viajera unidimensionales con distribución de corriente no gaussiana, revelando la aparición de orden para fluctuaciones raras con estructuras auto-organizadas, lo cual aumenta la probabilidad de que éstas ocurran.

7. En el caso particular del modelo conocido como proceso de exclusión simple débilmente asimétrico, o *weakly asymmetric simple exclussion process*, (WASEP, por sus siglas en inglés), hemos caracterizado tal DPT tanto desde un nivel mesoscópico bajo el marco MFT, como desde un nivel microscópico mediante el uso de simulaciones Monte Carlo extensivas con algoritmos de clonación, obteniendo un extraordinario acuerdo entre ambas descripciones. Curiosamente, la sCGF presenta una no analiticidad en su segunda derivada a lo largo de la línea de transición, lo que implica que la DPT es de segundo orden. Este resultado ha sido corroborado microscópicamente mediante la definición de un nuevo parámetro de orden que toma un valor igual a cero para la fase sin estructura y aumenta al cruzar el punto de transición.

8. Por último, fruto de la interacción entre el campo externo, la anistropía y la alta dimensionalidad considerada ($d > 1$), se ha obtenido un rico e interesante diagrama de fases dinámicas para el WASEP. Además de la ya mencionada transición de fase dinámica de segundo orden, se ha descubierto una interesante DPT de primer orden que separa diferentes fases de onda viajera, revelando la existencia de regiones en las que ambas coexisten.

Con el objetivo de explorar situaciones más allá de la MFT, hemos estudiado los efectos de las fluctuaciones en sistemas disipativos sin leyes de conservación. En particular, hemos ampliado las técnicas de la MFT para caracterizar la distribución de las fluctuaciones de la magnetización integrada en el espacio y en el tiempo en el modelo estocástico periódico unidimensional de Landau-Ginzburg, cuya dinámica viene dada por el modelo A de Hohenberg-Halperin. A partir de dicho análisis se han extraído las siguientes conclusiones.

9. Hemos proporcionado evidencias sólidas de la existencia de una transición de fase dinámica para valores bajos de la magnetización mediante el estudio de la estabilidad de los campos de magnetización uniformes frente a pertubaciones espacio-temporales. Este resultado posee profundas implicaciones en la comprensión de los sistemas fuera del equilibrio, lo que constituye un nuevo paso adelante en el descubrimiento de DPTs en sistemas unidimensionales a nivel fluctuante. Por otro lado, es interesante remarcar que la transición de fase dinámica solo tiene lugar en situaciones en las que el potencial de Landau-Ginzburg muestra una estructura de doble pozo.

10. Hemos encontrado que este modelo presenta una nueva fase dinámica exótica más allá de la transición. De esta forma, para realizar fluctuaciones raras de la magnetización, el sistema adopta una estructura homogénea que cambia periódicamente con el tiempo. Hemos caracterizado dicha solución, mostrando que la LDF correspondiente es, ciertamente, menor que la asociada a los campos óptimos uniformes.

Finalmente, nos hemos concentrado en el estudio de la dinámica efectiva con probabilidad conservada bajo la cual los eventos raros de la dinámica original se vuelven típicos. El sistema considerado ha sido una sola partícula que se difunde en una dimensión bajo la acción de una fuerza periódica completamente general y ruido aleatorio débil. A continuación detallamos las conclusiones que hemos obtenido.

11. Hemos determinado la dinámica efectiva relativa al estudio de las fluctuaciones de observables integrados en el tiempo y el espacio completamente

generales, identificando la fuerza efectiva bajo la cual se fuerza a la partícula a exhibir comportamientos atípicos. Esta nueva dinámica ha demostrado no ser exclusivamente una ligera modificación de la original bajo la aplicación de un campo constante no conservativo, sino que implica una transformación mucho más compleja.

12. Para el caso en que el observable es de "tipo corriente", hemos encontrado que el sistema exhibe una transición de fase dinámica entre una fase de fluctuación estática con una sCGF constante y una trayectoria propagativa periódica en el tiempo a la que se asocia una sCGF mucho más compleja cuyo valor puede obtenerse como la solución de un problema de optimización. Curiosamente, la forma de la fuerza efectiva cerca de la transición revela la naturaleza altamente no trivial de la DPT, muy diferente de aquellas que se observan para sistemas compuestos por una partícula bajo la acción de un campo conservativo más una fuerza constante no conservativa.

13. Como subproducto interesante, hemos deducido una forma alternativa de calcular la sCGF para las fluctuaciones de observables integrados en tiempo y espacio generales sin necesidad de resolver el complejo problema variacional derivado de la formulación en términos de integrales de camino. Este resultado revela un hecho de vital transcendencia: en estas situaciones, los límites de tiempos grandes y ruido débil conmutan.

References

[1] R.P. Feynman, R.B. Leighton, and M. Sands. *The Feynman Lectures on Physics, Vol. I: The New Millennium Edition: Mainly Mechanics, Radiation, and Heat*. The Feynman Lectures on Physics. Basic Books 2011.

[2] Neil A Campbell, Lawrence G Mitchell, Jane B Reece, and Jacqueline Bishop. *Biology: concepts & connections*. Number QH308. 2 C35 1996. Benjamin Cummings Menlo Park, Calif. 1997.

[3] Christopher S. Bartheld, Jami Bahney, and Suzana Herculano-Houzel. The search for true numbers of neurons and glial cells in the human brain: A review of 150 years of cell counting. *Journal of Comparative Neurology* **524**, 3865–3895 (2016).

[4] J. Richard Gott, III, Mario Jurić, David Schlegel, Fiona Hoyle, Michael Vogeley, Max Tegmark, Neta Bahcall, and Jon Brinkmann. A Map of the Universe. *The Astrophysical Journal* **624**, 463 (2005).

[5] Y.G. Sinai. On the foundations of the ergodic hypothesis for a dynamical system of statistical mechanics. *Dokl. Akad. Nauk SSSR* **153**, 1261–1264 (1963).

[6] Y.G. Sinai. Dynamical systems with elastic reflections. *Russian Mathematical Surveys* **25**, 137 (1970).

[7] L.D. Landau and E.M. Lifshitz. *Course of Theoretical Physics. Volume 5: Statistical Physics*. Elsevier Science 2013.

References

[8] R.K. Pathria and P.D. Beale. *Statistical Mechanics*. Academic Press. Butterworth-Heinemann 2011.

[9] Morikazu Toda, Ryogo Kubo, Nobuhiko Saitō, and Natsuki Hashitsume. *Statistical physics I: equilibrium statistical mechanics* volume 30. Springer Science & Business Media 1983.

[10] A. Einstein. Über die von der molekularkinetischen Theorie der Wärme geforderte Bewegung von in ruhenden Flüssigkeiten suspendierten Teilchen. *Annalen der Physik* **322**, 549–560 (1905).

[11] A. Einstein. Eine neue Bestimmung der Moleküldimensionen. *Annalen der Physik* **324**, 289–306 (1906).

[12] A. Einstein. Zur Theorie der Brownschen Bewegung [AdP 19, 371 (1906)]. *Annalen der Physik* **14**, 248–258 (1906).

[13] A. Einstein. *Investigations on the Theory of the Brownian Movement*. Dover Books on Physics Series. Dover Publications 1956.

[14] P. Perrot. *A to Z of Thermodynamics*. Supplementary Series; 27. Oxford University Press 1998.

[15] A. Einstein. Theorie der Opaleszenz von homogenen Flüssigkeiten und Flüssigkeitsgemischen in der Nähe des kritischen Zustandes. *Annalen der Physik* **33**, 1275 (1910).

[16] L. Bertini, A. De Sole, D. Gabrielli, G. Jona-Lasinio, and C. Landim. Macroscopic fluctuation theory. *Rev. Modern Phys.* **87**, 593–636 (2015).

[17] B. Derrida. Non-equilibrium steady states: fluctuations and large deviations of the density and of the current. *J. Stat. Mech.* page P07023 (2007).

[18] P. I. Hurtado, C. P. Espigares, J. J. del Pozo, and P. L. Garrido. Thermodynamics of Currents in Nonequilibrium Diffusive Systems: Theory and Simulation. *J. Stat. Phys.* **154**, 214–264 (2014).

[19] H. Touchette. The large deviation approach to statistical mechanics. *Phys. Rep.* **478**, 1–69 (2009).

[20] M. D. Donsker and S. R. S. Varadhan. Asymptotic evaluation of certain markov process expectations for large time, I. *Comm. Pure Appl. Math.* **28**, 1–47 (1975).

[21] MD Donsker and SRS Varadhan. Asymptotic evaluation of certain Markov process expectations for large time, II. *Communications on Pure and Applied Mathematics* **28**, 279–301 (1975).

[22] M. D. Donsker and S. R. S. Varadhan. Asymptotic evaluation of certain Markov process expectations for large time—III. *Comm. Pure Appl. Math.* **29**, 389–461 (1976).

[23] M. D. Donsker and S. R. S. Varadhan. Asymptotic evaluation of certain markov process expectations for large time. IV. *Comm. Pure Appl. Math.* **36**, 183–212 (1983).

[24] Richard S Ellis. Large deviations for a general class of random vectors. *The Annals of Probability* **12**, 1–12 (1984).

[25] Richard S Ellis. An overview of the theory of large deviations and applications to statistical mechanics. *Scandinavian Actuarial Journal* **1995**, 97–142 (1995).

[26] Mark I. Freidlin and Alexander D. Wentzell. *Random Perturbations of Dynamical Systems*. Grundlehren der mathematischen Wissenschaften. Springer-Verlag Berlin Heidelberg 3 edition 2012.

[27] David Ruelle. *Statistical mechanics: Rigorous results*. World Scientific 1999.

[28] Richard S Ellis. *Entropy, Large Deviations, and Statistical Mechanics*. Springer, New York 1985.

[29] Richard S Ellis. The theory of large deviations: from Boltzmann's 1877 calculation to equilibrium macrostates in 2D turbulence. *Physica D: Nonlinear Phenomena* **133**, 106–136 (1999).

[30] Oscar E. Lanford. *Entropy and equilibrium states in classical statistical mechanics* volume 20 of *A. Lenard (Ed.), Statistical Mechanics and Mathematical Problems, Lecture Notes in Physics*. Springer, Berlin 1973.

[31] J. T. Lewis. The large deviation principle in statistical mechanics: an expository account. In *Stochastic Mechanics and Stochastic Processes* page 141–155. Springer 1988.

References

[32] John T Lewis, C-E Pfister, and Wayne G Sullivan. Large deviations and the thermodynamic formalism: a new proof of the equivalence of ensembles. In *On three levels* page 183–192. Springer 1994.

[33] John T Lewis, Charles-Edouard Pfister, and Wayne G Sullivan. Entropy, concentration of probability and conditional limit theorems. *Markov Process. Relat. Fields* **1**, 319–386 (1995).

[34] John T Lewis and C-E Pfister. Thermodynamic probability theory: some aspects of large deviations. *Russian Mathematical Surveys* **50**, 279–317 (1995).

[35] Yoshitsugu Oono. Large deviation and statistical physics. *Progress of Theoretical Physics Supplement* **99**, 165–205 (1989).

[36] Anton Amann and Harald Atmanspacher. Introductory remarks on large deviation statistics. *Journal of Scientific Exploration* **13**, 639–664 (1999).

[37] Jürgen Gärtner. On large deviations from the invariant measure. *Theory of Probability & Its Applications* **22**, 24–39 (1977).

[38] L. Bertini, A. De Sole, D. Gabrielli, G. Jona-Lasinio, and C. Landim. Current fluctuations in stochastic lattice gases. *Phys. Rev. Lett.* **94**, 030601 (2005).

[39] B. Derrida, J. L. Lebowitz, and E. R. Speer. Exact large deviation functional of a stationary open driven diffusive system: The asymmetric exclusion process. *J. Stat. Phys.* **110**, 775–810 (2003).

[40] T. Bodineau and B. Derrida. Current fluctuations in nonequilibrium diffusive systems: An additivity principle. *Phys. Rev. Lett.* **92**, 180601 (2004).

[41] T. Bodineau and B. Derrida. Distribution of current in nonequilibrium diffusive systems and phase transitions. *Phys. Rev. E* **72**, 066110 (2005).

[42] T. Bodineau and M. Lagouge. Current Large Deviations in a Driven Dissipative Model. *J. Stat. Phys.* **139**, 201–218 (2010).

[43] U. Seifert. Stochastic thermodynamics, fluctuation theorems and molecular machines. *Reports On Progress In Phys.* **75**, 126001 (2012).

[44] G. Gallavotti and E. G. D. Cohen. Dynamical ensembles in nonequilibrium statistical-mechanics. *Phys. Rev. Lett.* **74**, 2694–2697 (1995).

[45] P. I. Hurtado and P. L. Garrido. Test of the Additivity Principle for Current Fluctuations in a Model of Heat Conduction. *Phys. Rev. Lett.* **102**, 250601 (2009).

[46] P. I. Hurtado, C. Pérez-Espigares, J. J. del Pozo, and P. L. Garrido. Symmetries in fluctuations far from equilibrium. *Proc. Natl. Acad. Sci. USA* **108**, 7704–7709 (2011).

[47] Yongjoo Baek, Yariv Kafri, and Vivien Lecomte. Dynamical Symmetry Breaking and Phase Transitions in Driven Diffusive Systems. *Phys. Rev. Lett.* **118**, 030604 (2017).

[48] J. Kurchan. Fluctuation theorem for stochastic dynamics. *J. Phys. A* **31**, 3719–3729 (1998).

[49] J. L. Lebowitz and H. Spohn. A Gallavotti-Cohen-type symmetry in the large deviation functional for stochastic dynamics. *J. Stat. Phys.* **95**, 333–365 (1999).

[50] D. J. Evans, E. G. D. Cohen, and G. P. Morriss. Probability of second law violations in shearing steady-states. *Phys. Rev. Lett.* **71**, 2401–2404 (1993).

[51] D. J. Evans and D. J. Searles. Equilibrium microstates which generate 2nd law violating steady-states. *Phys. Rev. E* **50**, 1645–1648 (1994).

[52] N. Tizón-Escamilla, C. Pérez-Espigares, P. L. Garrido, and P. I. Hurtado. Order and Symmetry Breaking in the Fluctuations of Driven Systems. *Phys. Rev. Lett.* **119**, 090602 (2017).

[53] L. Bertini, A. De Sole, D. Gabrielli, G. Jona-Lasinio, and C. Landim. Fluctuations in stationary nonequilibrium states of irreversible processes. *Phys. Rev. Lett.* **87**, 040601 (2001).

[54] L. Bertini, A. De Sole, D. Gabrielli, G. Jona-Lasinio, and C. Landim. Macroscopic fluctuation theory for stationary non-equilibrium states. *J. Stat. Phys.* **107**, 635–675 (2002).

[55] L. Bertini, A. De Sole, D. Gabrielli, G. Jona-Lasinio, and C. Landim. Non Equilibrium current fluctuations in stochastic lattice gases. *J. Stat. Phys.* **123**, 237–276 (2006).

[56] P. I. Hurtado and P. L. Garrido. Spontaneous Symmetry Breaking at the Fluctuating Level. *Phys. Rev. Lett.* **107**, 180601 (2011).

[57] C. Pérez-Espigares, P. L. Garrido, and P. I. Hurtado. Dynamical phase transition for current statistics in a simple driven diffusive system. *Phys. Rev. E* **87**, 032115 (2013).

[58] L. Zarfaty and B. Meerson. Statistics of large currents in the Kipnis–Marchioro–Presutti model in a ring geometry. *Journal of Statistical Mechanics: Theory and Experiment* **2016**, 033304 (2016).

[59] S. Vaikuntanathan, T. R. Gingrich, and P. L. Geissler. Dynamic phase transitions in simple driven kinetic networks. *Phys. Rev. E* **89**, 062108 (2014).

[60] K. D. N. T. Lam, J. Kurchan, and D. Levine. Order in Extremal Trajectories. *J. Stat. Phys.* **137**, 1079–1093 (2009).

[61] D. Chandler and J. P. Garrahan. Dynamics on the Way to Forming Glass: Bubbles in Space-Time. *Annual Review of Physical Chemistry* **61**, 191–217 (2010). PMID: 20055676.

[62] O. Shpielberg and E. Akkermans. Le Chatelier Principle for Out-of-Equilibrium and Boundary-Driven Systems: Application to Dynamical Phase Transitions. *Phys. Rev. Lett.* **116**, 240603 (2016).

[63] Y. Baek, Y. Kafri, and V. Lecomte. Dynamical Symmetry Breaking and Phase Transitions in Driven Diffusive Systems. *Phys. Rev. Lett.* **118**, 030604 (2017).

[64] G. Gallavotti and E. G. D. Cohen. Dynamical ensembles in stationary states. *J. Stat. Phys.* **80**, 931–970 (1995).

[65] D. Andrieux and P. Gaspard. A fluctuation theorem for currents and nonlinear response coefficients. *J. Stat. Mech.* page P02006 (2007).

[66] G. Gallavotti. *Nonequilibrium and Irreversibility*. Springer International Publishing 2014.

[67] R. Villavicencio-Sanchez, R. J. Harris, and H. Touchette. Fluctuation relations for anisotropic systems. *Europhys. Lett.* **105**, 30009 (2014).

[68] D. Lacoste and P. Gaspard. Isometric Fluctuation Relations for Equilibrium States with Broken Symmetry. *Phys. Rev. Lett.* **113**, 240602 (2014).

[69] P. Gaspard. Multivariate fluctuation relations for currents. *New J. Phys.* **15**, 115014 (2013).

[70] C. Pérez-Espigares, F. Redig, and C. Giardina. Spatial fluctuation theorem. *J. Phys. A* **48**, 35FT01 (2015).

[71] N. Kumar, H. Soni, S. Ramaswamy, and A. K. Sood. Anisotropic isometric fluctuation relations in experiment and theory on a self-propelled rod. *Phys. Rev. E* **91**, 030102 (2015).

[72] Damien Simon. Construction of a coordinate Bethe ansatz for the asymmetric simple exclusion process with open boundaries. *J. Stat. Mech.* **2009**, P07017 (2009).

[73] Vladislav Popkov, Gunter M. Schütz, and Damien Simon. ASEP on a ring conditioned on enhanced flux. *J. Stat. Mech.* **2010**, P10007 (2010).

[74] Raphaël Chetrite and Hugo Touchette. Nonequilibrium Markov Processes Conditioned on Large Deviations. *Annales Henri Poincaré* **16**, 2005–2057 (2015).

[75] Raphaël Chetrite and Hugo Touchette. Variational and optimal control representations of conditioned and driven processes. *Journal of Statistical Mechanics: Theory and Experiment* **2015**, P12001 (2015).

[76] Robert L. Jack and Peter Sollich. Large Deviations and Ensembles of Trajectories in Stochastic Models. *Prog Theor Phys* **184**, 304–317 (2010).

[77] R. L. Jack and P. Sollich. Effective interactions and large deviations in stochastic processes. *Eur. Phys. J. Spec. Top.* **224**, 2351–2367 (2015).

[78] J.L. Doob. *Classical Potential Theory and Its Probabilistic Counterpart: Advanced Problems*. Grundlehren der mathematischen Wissenschaften. Springer New York 1984.

[79] Raphaël Chetrite and Hugo Touchette. Nonequilibrium Markov Processes Conditioned on Large Deviations. *Ann. Henri Poincaré* **16**, 2005–2057 (2015).

[80] V. Popkov and G. M. Schütz. Transition Probabilities and Dynamic Structure Function in the ASEP Conditioned on Strong Flux. *J Stat Phys* **142**, 627–639 (2011).

[81] V. Belitsky and G. M. Schütz. Microscopic Structure of Shocks and Antishocks in the ASEP Conditioned on Low Current. *J Stat Phys* **152**, 93–111 (2013).

References

[82] Rosemary J. Harris, Vladislav Popkov, and Gunter M. Schütz. Dynamics of Instantaneous Condensation in the ZRP Conditioned on an Atypical Current. *Entropy* **15**, 5065–5083 (2013).

[83] Ori Hirschberg, David Mukamel, and Gunter M. Schütz. Density profiles, dynamics, and condensation in the ZRP conditioned on an atypical current. *J. Stat. Mech.* **2015**, P11023 (2015).

[84] Paul Chleboun, Stefan Grosskinsky, and Andrea Pizzoferrato. Lower Current Large Deviations for Zero-Range Processes on a Ring. *J Stat Phys* **167**, 64–89 (2017).

[85] Pelerine Tsobgni Nyawo and Hugo Touchette. Large deviations of the current for driven periodic diffusions. *Phys. Rev. E* **94**, 032101 (2016).

[86] Juan P. Garrahan and Igor Lesanovsky. Thermodynamics of Quantum Jump Trajectories. *Physical Review Letters* **104**, 160601 (2010).

[87] Federico Carollo, Juan P. Garrahan, Igor Lesanovsky, and Carlos Pérez-Espigares. Making rare events typical in Markovian open quantum systems. *Physical Review A* **98**, 010103 (2018).

[88] Nicolás Tizón-Escamilla, Vivien Lecomte, and Eric Bertin. Effective driven dynamics for one-dimensional conditioned Langevin processes in the weak-noise limit. *arXiv:1807.06438* (2018).

[89] Xu Du, Ivan Skachko, Anthony Barker, and Eva Y. Andrei. Approaching ballistic transport in suspended graphene. *Nature Nanotechnology* **3**, 491–495 (2008).

[90] Yu-Ming Lin, Joerg Appenzeller, Joachim Knoch, Zhihong Chen, and Phaedon Avouris. Low-Frequency Current Fluctuations in Individual Semiconducting Single-Wall Carbon Nanotubes. *Nano Letters* **6**, 930–936 (2006). PMID: 16683828.

[91] Asen Asenov. Random dopant induced threshold voltage lowering and fluctuations in sub 50 nm MOSFETs: a statistical 3D 'atomistic' simulation study. *Nanotechnology* **10**, 153 (1999).

[92] T.-H. Kim A.-P. Li C. Zeng, P.R.C. Kent and H.H. Weitering. Charge-order fluctuations in one-dimensional silicides. *Nature Materials* **7**, 539–542 (2008).

[93] P. C. Hohenberg and B. I. Halperin. Theory of dynamic critical phenomena. *Rev. Mod. Phys.* **49**, 435–479 (1977).

[94] J.W. Gibbs. *Elementary Principles in Statistical Mechanics: Developed with Especial Reference to the Rational Foundations of Thermodynamics.* Elementary Principles in Statistical Mechanics: Developed with Especial Reference to the Rational Foundation of Thermodynamics. C. Scribner's sons 1902.

[95] Jesús Biel Gayé. *Curso sobre el formalismo y los métodos de la termodinámica.* Reverté 1997.

[96] Herbert B Callen. Thermodynamics and an Introduction to Thermostatistics 1998.

[97] Melville S. Green. Markoff Random Processes and the Statistical Mechanics of Time-Dependent Phenomena. *The Journal of Chemical Physics* **20**, 1281–1295 (1952).

[98] Melville S. Green. Markoff Random Processes and the Statistical Mechanics of Time-Dependent Phenomena. II. Irreversible Processes in Fluids. *The Journal of Chemical Physics* **22**, 398–413 (1954).

[99] Ryogo Kubo. Statistical-Mechanical Theory of Irreversible Processes. I. General Theory and Simple Applications to Magnetic and Conduction Problems. *Journal of the Physical Society of Japan* **12**, 570–586 (1957).

[100] R. Kubo. Fluctuation-dissipation theorem. *Reports On Progress In Phys.* **29**, 255–& (1966).

[101] Ryogo Kubo, Morikazu Toda, and Natsuki Hashitsume. *Statistical physics II: nonequilibrium statistical mechanics* volume 31. Springer Science & Business Media 2012.

[102] Lars Onsager. Reciprocal relations in irreversible processes. I. *Physical review* **37**, 405 (1931).

[103] Lars Onsager. Reciprocal relations in irreversible processes. II. *Physical review* **38**, 2265 (1931).

[104] Lars Onsager and S Machlup. Fluctuations and irreversible processes. *Physical Review* **91**, 1505 (1953).

References

[105] Harald Cramér. Sur un nouveau théorème-limite de la théorie des probabilités. In Colloque consacré à la théorie des probabilités. **736**, 2–23 (1938).

[106] Monroe D Donsker and SR Srinivasa Varadhan. Asymptotic evaluation of certain Markov process expectations for large time, I. *Communications on Pure and Applied Mathematics* **28**, 1–47 (1975).

[107] MD Donsker and SRS Varadhan. Asymptotic evaluation of certain Markov process expectations for large time, III. *Communications on pure and applied Mathematics* **29**, 389–461 (1976).

[108] Monroe D Donsker and SR Srinivasa Varadhan. Asymptotic evaluation of certain Markov process expectations for large time, IV. *Communications on Pure and Applied Mathematics* **36**, 183–212 (1983).

[109] L.D. Landau and E.M. Lifshitz. *Fluid Mechanics*. Number v. 6. Elsevier Science 2013.

[110] Jose M Ortiz De Zarate and Jan V Sengers. *Hydrodynamic fluctuations in fluids and fluid mixtures*. Elsevier 2006.

[111] P Mazur. Mesoscopic nonequilibrium thermodynamics; irreversible processes and fluctuations. *Physica A: Statistical Mechanics and its Applications* **274**, 491–504 (1999).

[112] P.L. Garrido. Notes about the Macroscopic Fluctuation Theory. *In preparation*.

[113] H. Spohn. *Large Scale Dynamics of Interacting Particles*. Theoretical and Mathematical Physics. Springer Berlin Heidelberg 2012.

[114] Claude Kipnis and Claudio Landim. *Scaling limits of interacting particle systems* volume 320. Springer Science & Business Media 2013.

[115] Gregory Eyink, Joel L Lebowitz, and Herbert Spohn. Hydrodynamics of stationary non-equilibrium states for some stochastic lattice gas models. *Communications in mathematical physics* **132**, 253–283 (1990).

[116] Raúl Toral and Pere Colet. *Stochastic numerical methods: an introduction for students and scientists*. John Wiley & Sons 2014.

[117] J.P. Boon and S. Yip. *Molecular Hydrodynamics*. Dover books on physics. Dover Publications 1991.

[118] W. van Saarloos, D. Bedeaux, and P. Mazur. Non-linear hydrodynamic fluctuations around equilibrium. *Physica A: Statistical Mechanics and its Applications* **110**, 147–170 (1982).

[119] Shankar P. Das and Gene F. Mazenko. Fluctuating nonlinear hydrodynamics and the liquid-glass transition. *Phys. Rev. A* **34**, 2265–2282 (1986).

[120] Christian B. Mendl and Herbert Spohn. Dynamic Correlators of Fermi-Pasta-Ulam Chains and Nonlinear Fluctuating Hydrodynamics. *Phys. Rev. Lett.* **111**, 230601 (2013).

[121] Herbert Spohn. Nonlinear Fluctuating Hydrodynamics for Anharmonic Chains. *Journal of Statistical Physics* **154**, 1191–1227 (2014).

[122] Christian B Mendl and Herbert Spohn. Current fluctuations for anharmonic chains in thermal equilibrium. *Journal of Statistical Mechanics: Theory and Experiment* **2015**, P03007 (2015).

[123] D.N. Zubarev and V.G. Morozov. Statistical mechanics of nonlinear hydrodynamic fluctuations. *Physica A: Statistical Mechanics and its Applications* **120**, 411–467 (1983).

[124] Herbert Spohn. *Large scale dynamics of interacting particles*. Springer Science & Business Media 2012.

[125] Beate Schmittmann and Royce KP Zia. Statistical mechanics of driven diffusive systems. *Phase transitions and critical phenomena* **17**, 3–214 (1995).

[126] C. Kipnis, C. Marchioro, and E. Presutti. Heat-flow in an exactly solvable model. *J. Stat. Phys.* **27**, 65–74 (1982).

[127] N. Tizón-Escamilla, P. I. Hurtado, and P. L. Garrido. Structure of the optimal path to a fluctuation. *Physical Review E* **95**, 032119 (2017).

[128] Nicolaas Godfried Van Kampen. *Stochastic processes in physics and chemistry* volume 1. Elsevier 1992.

[129] K. Ito. *On Stochastic Differential Equations*. Memoirs of the American Mathematical Society. American Mathematical Society 1951.

[130] R.L. Stratonovich. *Topics in the Theory of Random Noise*. Number v. 1 in Mathematics and its applications. Gordon and Breach 1963.

References

[131] M.Á. Muñoz. *Ecuaciones de Fokker-Planck y Teoría de Campos Fuera del Equilibrio*. Tesis Doctoral. Universidad de Granada 1994.

[132] Norbert Wiener. Differential-Space. *Journal of Mathematics and Physics* **2**, 131–174 (1923).

[133] Norbert Wiener. The Average value of a Functional*. *Proceedings of the London Mathematical Society* **s2-22**, 454–467 (1924).

[134] R.P. Feynman and A.R. Hibbs. *Quantum mechanics and path integrals*. International series in pure and applied physics. McGraw-Hill 1965.

[135] Leticia F Cugliandolo and Vivien Lecomte. Rules of calculus in the path integral representation of white noise Langevin equations: the Onsager–Machlup approach. *Journal of Physics A: Mathematical and Theoretical* **50**, 345001 (2017).

[136] Leticia F Cugliandolo, Vivien Lecomte, and Frédéric Van Wijland. Building a path-integral calculus. *arXiv preprint arXiv:1806.09486* (2018).

[137] Jean Zinn-Justin. *Quantum field theory and critical phenomena*. Clarendon Press 1996.

[138] Julien Tailleur, Jorge Kurchan, and Vivien Lecomte. Mapping out-of-equilibrium into equilibrium in one-dimensional transport models. *Journal of Physics A: Mathematical and Theoretical* **41**, 505001 (2008).

[139] R. S. Ellis. *Entropy, Large Deviations, and Statistical Mechanics*. Grundlehren der mathematischen Wissenschaften. Springer-Verlag New York 1985.

[140] Richard S. Ellis. An overview of the theory of large deviations and applications to statistical mechanics. *Scandinavian Actuarial Journal* **1995**, 97–142 (1995).

[141] Richard S. Ellis. The theory of large deviations: from Boltzmann's 1877 calculation to equilibrium macrostates in 2D turbulence. *Physica D: Nonlinear Phenomena* **133**, 106–136 (1999).

[142] Hugo Touchette. The large deviation approach to statistical mechanics. *Physics Reports* **478**, 1–69 (2009).

[143] Lorenzo Bertini, Alberto De Sole, Davide Gabrielli, Giovanni Jona-Lasinio, and Claudio Landim. Macroscopic fluctuation theory. *Rev. Mod. Phys.* **87**, 593–636 (2015).

[144] Hugo Touchette. Introduction to dynamical large deviations of Markov processes. *arXiv:1705.06492 [cond-mat]* (2017). arXiv: 1705.06492.

[145] J. Gärtner. On Large Deviations from the Invariant Measure. *Theory Probab. Appl.* **22**, 24–39 (1977).

[146] Richard S. Ellis. Large Deviations for a General Class of Random Vectors. *Ann. Probab.* **12**, 1–12 (1984).

[147] Bernard Derrida and Joel L. Lebowitz. Exact Large Deviation Function in the Asymmetric Exclusion Process. *Phys. Rev. Lett.* **80**, 209–213 (1998).

[148] Jorge Kurchan. Fluctuation theorem for stochastic dynamics. *Journal of Physics A: Mathematical and General* **31**, 3719–3729 (1998).

[149] T. Bodineau and B. Derrida. Current Fluctuations in Nonequilibrium Diffusive Systems: An Additivity Principle. *Phys. Rev. Lett.* **92**, 180601 (2004).

[150] Lorenzo Bertini, Andrea De Sole, Davide Gabrielli, Giovanni Jona-Lasinio, and Claudio Landim. Current Fluctuations in Stochastic Lattice Gases. *Phys. Rev. Lett.* **94**, 030601 (2005).

[151] V. Lecomte, C. Appert-Rolland, and F. van Wijland. Chaotic Properties of Systems with Markov Dynamics. *Phys. Rev. Lett.* **95**, 010601 (2005).

[152] Vivien Lecomte, Cécile Appert-Rolland, and Frédéric Wijland. Thermodynamic Formalism for Systems with Markov Dynamics. *J. Stat. Phys.* **127**, 51–106 (2007).

[153] C. Giardina, J. Kurchan, and L. Peliti. Direct evaluation of large-deviation functions. *Phys. Rev. Lett.* **96**, 120603 (2006).

[154] C. Giardina, J. Kurchan, V. Lecomte, and J. Tailleur. Simulating Rare Events in Dynamical Processes. *J. Stat. Phys.* **145**, 787–811 (2011).

[155] V. Lecomte and J. Tailleur. A numerical approach to large deviations in continuous time. *J. Stat. Mech.* page P03004 (2007).

[156] Christoph Dellago, Peter G. Bolhuis, and Phillip L. Geissler. *Transition Path Sampling* chapter 1, page 1–78. Wiley-Blackwell 2003.

References

[157] C. Dellago, P.G. Bolhuis, and P.L. Geissler. *Transition Path Sampling Methods* page 349–391. Springer Berlin Heidelberg Berlin, Heidelberg 2006.

[158] Christoph Dellago and Peter G. Bolhuis. *Transition Path Sampling and Other Advanced Simulation Techniques for Rare Events* page 167–233. Springer Berlin Heidelberg Berlin, Heidelberg 2009.

[159] R. J. Harris and G. M. Schuetz. Fluctuation theorems for stochastic dynamics. *J. Stat. Mech.* page P07020 (2007).

[160] G.N. Bochkov and Yu.E. Kuzovlev. General theory of thermal fluctuations in nonlinear systems. *Sov. Phys. JETP* **45**, 125 (1977).

[161] G.N. Bochkov and Yu.E. Kuzovlev. Nonlinear fluctuation-dissipation relations and stochastic models in nonequilibrium thermodynamics: I. Generalized fluctuation-dissipation theorem. *Physica A: Statistical Mechanics and its Applications* **106**, 443–479 (1981).

[162] J Javier Brey, M J Ruiz-Montero, and Álvaro Domínguez. Work fluctuation theorems and free energy from kinetic theory. *Journal of Statistical Mechanics: Theory and Experiment* **2018**, 013207 (2018).

[163] C. Jarzynski. Equilibrium free-energy differences from nonequilibrium measurements: A master-equation approach. *Phys. Rev. E* **56**, 5018–5035 (1997).

[164] C. Jarzynski. Nonequilibrium equality for free energy differences. *Phys. Rev. Lett.* **78**, 2690–2693 (1997).

[165] Gavin E Crooks. Entropy production fluctuation theorem and the nonequilibrium work relation for free energy differences. *Physical Review E* **60**, 2721 (1999).

[166] T. Hatano and S. Sasa. Steady-state thermodynamics of Langevin systems. *Phys. Rev. Lett.* **86**, 3463–3466 (2001).

[167] Jorge Kurchan. A quantum fluctuation theorem. *arXiv preprint cond-mat/0007360* (2000).

[168] Massimiliano Esposito and Shaul Mukamel. Fluctuation theorems for quantum master equations. *Physical Review E* **73**, 046129 (2006).

[169] B. Derrida, B. Douçot, and P.-E. Roche. Current Fluctuations in the One-Dimensional Symmetric Exclusion Process with Open Boundaries. *Journal of Statistical Physics* **115**, 717–748 (2004).

[170] T. Bodineau and B. Derrida. Current large deviations for asymmetric exclusion processes with open boundaries. *J. Stat. Phys.* **123**, 277–300 (2006).

[171] S. Pilgram, A. N. Jordan, E. V. Sukhorukov, and M. Büttiker. Stochastic Path Integral Formulation of Full Counting Statistics. *Phys. Rev. Lett.* **90**, 206801 (2003).

[172] Andrew N. Jordan, Eugene V. Sukhorukov, and Sebastian Pilgram. Fluctuation statistics in networks: A stochastic path integral approach. *Journal of Mathematical Physics* **45**, 4386–4417 (2004).

[173] P. I. Hurtado and P. L. Garrido. Large fluctuations of the macroscopic current in diffusive systems: A numerical test of the additivity principle. *Phys. Rev. E* **81**, 041102 (2010).

[174] M. Gorissen and C. Vanderzande. Current fluctuations in the weakly asymmetric exclusion process with open boundaries. *Phys. Rev. E* **86**, 051114 (2012).

[175] Thierry Bodineau and Bernard Derrida. Cumulants and large deviations of the current through non-equilibrium steady states. *Comptes Rendus Physique* **8**, 540–555 (2007).

[176] C. Pérez-Espigares, P. L. Garrido, and P. I. Hurtado. Weak additivity principle for current statistics in d dimensions. *Phys. Rev. E* **93**, 040103 (2016).

[177] Vivien Lecomte, Uwe C Täuber, and Frédéric van Wijland. Current distribution in systems with anomalous diffusion: renormalization group approach. *Journal of Physics A: Mathematical and Theoretical* **40**, 1447 (2007).

[178] T. Bodineau, B. Derrida, and Joel L. Lebowitz. Vortices in the Two-Dimensional Simple Exclusion Process. *Journal of Statistical Physics* **131**, 821–841 (2008).

[179] R. L. Jack, I. an R. Thompson, and P. Sollich. Hyperuniformity and Phase Separation in Biased Ensembles of Trajectories for Diffusive Systems. *Phys. Rev. Lett.* **114**, 060601 (2015).

References

[180] R. Toral K. Proesmans and C. Van den Broek. Bose-Einstein phase transition in persistent and run-and-rumble walks. *arXiv:1808.09715* (2018).

[181] Yongjoo Baek, Yariv Kafri, and Vivien Lecomte. Dynamical Symmetry Breaking and Phase Transitions in Driven Diffusive Systems. *Phys. Rev. Lett.* **118**, 030604 (2017).

[182] D. Karevski and G. M. Schütz. Conformal Invariance in Driven Diffusive Systems at High Currents. *Phys. Rev. Lett.* **118**, 030601 (2017).

[183] J. P. Garrahan and I. Lesanovsky. Thermodynamics of Quantum Jump Trajectories. *Phys. Rev. Lett.* **104**, 160601 (2010).

[184] C. Ates, B. Olmos, J. P. Garrahan, and I. Lesanovsky. Dynamical phases and intermittency of the dissipative quantum Ising model. *Phys. Rev. A* **85**, 043620 (2012).

[185] I. Lesanovsky, M. van Horssen, M. Guta, and J. P. Garrahan. Characterization of Dynamical Phase Transitions in Quantum Jump Trajectories Beyond the Properties of the Stationary State. *Phys. Rev. Lett.* **110**, 150401 (2013).

[186] J. P. Garrahan, R. L. Jack, V. Lecomte, E. Pitard, K. van Duijvendijk, and F. van Wijland. Dynamical First-Order Phase Transition in Kinetically Constrained Models of Glasses. *Phys. Rev. Lett.* **98**, 195702 (2007).

[187] Juan P Garrahan, Robert L Jack, Vivien Lecomte, Estelle Pitard, Kristina van Duijvendijk, and Frédéric van Wijland. First-order dynamical phase transition in models of glasses: an approach based on ensembles of histories. *Journal of Physics A: Mathematical and Theoretical* **42**, 075007 (2009).

[188] Lester O. Hedges, Robert L. Jack, Juan P. Garrahan, and David Chandler. Dynamic Order-Disorder in Atomistic Models of Structural Glass Formers. *Science* **323**, 1309–1313 (2009).

[189] Pitard, E., Lecomte, V., and van Wijland, F. Dynamic transition in an atomic glass former: A molecular-dynamics evidence. *EPL* **96**, 56002 (2011).

[190] Thomas Speck, Alex Malins, and C. Patrick Royall. First-Order Phase Transition in a Model Glass Former: Coupling of Local Structure and Dynamics. *Phys. Rev. Lett.* **109**, 195703 (2012).

[191] Rattachai Pinchaipat, Matteo Campo, Francesco Turci, James E. Hallett, Thomas Speck, and C. Patrick Royall. Experimental Evidence for a Structural-Dynamical Transition in Trajectory Space. *Phys. Rev. Lett.* **119**, 028004 (2017).

[192] Juan P. Garrahan, Andrew D. Armour, and Igor Lesanovsky. Quantum trajectory phase transitions in the micromaser. *Phys. Rev. E* **84**, 021115 (2011).

[193] Sam Genway, Juan P. Garrahan, Igor Lesanovsky, and Andrew D. Armour. Phase transitions in trajectories of a superconducting single-electron transistor coupled to a resonator. *Phys. Rev. E* **85**, 051122 (2012).

[194] D. Manzano and P. I. Hurtado. Symmetry and the thermodynamics of currents in open quantum systems. *Phys. Rev. B* **90**, 125138 (2014).

[195] Daniel Manzano and Elica Kyoseva. An atomic symmetry-controlled thermal switch. *Scientific Reports* **6**, 31161 (2016).

[196] D. Manzano and P.I. Hurtado. Harnessing symmetry to control quantum transport. *Advances in Physics* **67**, 1–67 (2018).

[197] C. N. Yang and T. D. Lee. Statistical Theory of Equations of State and Phase Transitions. I. Theory of Condensation. *Phys. Rev.* **87**, 404–409 (1952).

[198] Peter F. Arndt. Yang-Lee Theory for a Nonequilibrium Phase Transition. *Phys. Rev. Lett.* **84**, 814–817 (2000).

[199] R. A. Blythe and M. R. Evans. Lee-Yang zeros and phase transitions in nonequilibrium steady states. *Phys. Rev. Lett.* **89**, 080601 (2002).

[200] S. M. Dammer, S. R. Dahmen, and H. Hinrichsen. Yang-Lee zeros for a nonequilibrium phase transition. *J. Phys. A* **35**, 4527–4539 (2002).

[201] R.A. Blythe and M.R. Evans. The Lee-Yang theory of equilibrium and nonequilibrium phase transitions. *Braz. J. Phys.* **3** (2003).

[202] Christian Flindt and Juan P. Garrahan. Trajectory Phase Transitions, Lee-Yang Zeros, and High-Order Cumulants in Full Counting Statistics. *Phys. Rev. Lett.* **110**, 050601 (2013).

[203] James M. Hickey, Christian Flindt, and Juan P. Garrahan. Intermittency and dynamical Lee-Yang zeros of open quantum systems. *Phys. Rev. E* **90**, 062128 (2014).

References

[204] Kay Brandner, Ville F. Maisi, Jukka P. Pekola, Juan P. Garrahan, and Christian Flindt. Experimental Determination of Dynamical Lee-Yang Zeros. *Phys. Rev. Lett.* **118**, 180601 (2017).

[205] M. Gorissen, A. Lazarescu, K. Mallick, and C. Vanderzande. Exact Current Statistics of the Asymmetric Simple Exclusion Process with Open Boundaries. *Phys. Rev. Lett.* **109**, 170601 (2012).

[206] A. Lazarescu. The physicist's companion to current fluctuations: one-dimensional bulk-driven lattice gases. *J. Phys. A* **48**, 503001 (2015).

[207] E. Akkermans, T. Bodineau, B. Derrida, and O. Shpielberg. Universal current fluctuations in the symmetric exclusion process and other diffusive systems. *Epl* **103**, 20001 (2013).

[208] T. Becker, K. Nelissen, and B. Cleuren. Current fluctuations in boundary driven diffusive systems in different dimensions: a numerical study. *New J. Phys.* **17**, 055023 (2015).

[209] R. Villavicencio-Sanchez and R. J. Harris. Local structure of current fluctuations in diffusive systems beyond one dimension. *Phys. Rev. E* **93**, 032134 (2016).

[210] P. C. Martin, E. D. Siggia, and H. A. Rose. Statistical Dynamics of Classical Systems. *Phys. Rev. A* **8**, 423–437 (1973).

[211] G.B. Arfken, H.J. Weber, and F.E. Harris. *Mathematical Methods for Physicists: A Comprehensive Guide*. Elsevier Science 2013.

[212] K. Saito and A. Dhar. Additivity Principle in High-Dimensional Deterministic Systems. *Phys. Rev. Lett.* **107**, 250601 (2011).

[213] P.L. Garrido, P.I. Hurtado, and N. Tizón-Escamilla. Infinite family of universal profiles for heat current statistics in Fourier's law. *arXiv:1810.10778* (2018).

[214] S.R. De Groot and P. Mazur. *Non-Equilibrium Thermodynamics*. Dover Books on Physics. Dover Publications 2013.

[215] F. BONETTO, J. L. LEBOWITZ, and L. REY-BELLET. *FOURIER'S LAW: A CHALLENGE TO THEORISTS* page 128–150.

[216] Pablo I Hurtado and Pedro L Garrido. A violation of universality in anomalous Fourier's law. *Scientific Reports* **6**, 38823 (2016).

[217] S.G. Tuttle, B.W. Webb, and M.Q. McQuay. Convective heat transfer from a partially premixed impinging flame jet. Part I: Time-averaged results. *International Journal of Heat and Mass Transfer* **48**, 1236–1251 (2005).

[218] S.G. Tuttle, B.W. Webb, and M.Q. McQuay. Convective heat transfer from a partially premixed impinging flame jet. Part II: Time-resolved results. *International Journal of Heat and Mass Transfer* **48**, 1252–1266 (2005).

[219] David D. Hall and Issam Mudawar. Critical heat flux (CHF) for water flow in tubes—II.: Subcooled CHF correlations. *International Journal of Heat and Mass Transfer* **43**, 2605–2640 (2000).

[220] Shu-yuan Zhao, Bo-ming Zhang, and Shan-yi Du. Probabilistic modeling of transient heat transfer and assessment of thermal reliability of fibrous insulation under aerodynamic heating conditions. *International Journal of Thermal Sciences* **48**, 1302–1310 (2009).

[221] Kristina B. Katsaros, W. Timothy Liu, Joost A. Businger, and James E. Tillman. Heat thermal structure in the interfacial boundary layer measured in an open tank of water in turbulent free convection. *Journal of Fluid Mechanics* **83**, 311–335 (1977).

[222] J. P. Gollub, J. Clarke, M. Gharib, B. Lane, and O. N. Mesquita. Fluctuations and transport in a stirred fluid with a mean gradient. *Phys. Rev. Lett.* **67**, 3507–3510 (1991).

[223] Masanori Hayashi, Shigeru Aso, and Anzhong Tan. Fluctuation of heat transfer in shock wave/turbulent boundary-layer interaction. *AIAA Journal* **27**, 399–404 (1989).

[224] P. A. Coppin, M. R. Raupach, and B. J. Legg. Experiments on scalar dispersion within a model plant canopy part II: An elevated plane source. *Boundary-Layer Meteorology* **35**, 167–191 (1986).

[225] Sudeesh Krishnamurthy, Subho Ghosh, Dipankar Chatterji, Rajesh Ganapathy, and A. K. Sood. A micrometre-sized heat engine operating between bacterial reservoirs. *Nature Physics* **12**, 1134 EP– (2016).

[226] C. Garnier, J. Currie, and T. Muneer. Integrated collector storage solar water heater: Temperature stratification. *Applied Energy* **86**, 1465–1469 (2009).

References

[227] Miles G. McPhee. Turbulent heat flux in the upper ocean under sea ice. *Journal of Geophysical Research: Oceans* **97**, 5365–5379 (1992).

[228] Dean Vickers and L. Mahrt. Quality Control and Flux Sampling Problems for Tower and Aircraft Data. *Journal of Atmospheric and Oceanic Technology* **14**, 512–526 (1997).

[229] F. H. Champagne, C. A. Friehe, J. C. LaRue, and J. C. Wynagaard. Flux Measurements, Flux Estimation Techniques, and Fine-Scale Turbulence Measurements in the Unstable Surface Layer Over Land. *Journal of the Atmospheric Sciences* **34**, 515–530 (1977).

[230] Jon E. Mound and Christopher J. Davies. Heat transfer in rapidly rotating convection with heterogeneous thermal boundary conditions. *Journal of Fluid Mechanics* **828**, 601–629 (2017).

[231] Lev Davidovich Landau and Evgenii Mikhailovich Lifshitz. *Statistical physics: course of theoretical physics* volume 5. Elsevier 2013.

[232] L. Bertini, A. De Sole, D. Gabrielli, G. Jona-Lasinio, and C. Landim. Stochastic interacting particle systems out of equilibrium. *J. Stat. Mech.* page P07014 (2007).

[233] L. Bertini, A. De Sole, D. Gabrielli, G. Jona-Lasinio, and C. Landim. Towards a Nonequilibrium Thermodynamics: A Self-Contained Macroscopic Description of Driven Diffusive Systems. *J. Stat. Phys.* **135**, 857–872 (2009).

[234] I. S. Gradshteyn and I. M. Ryzhik. *Table of integrals, series, and products*. Elsevier/Academic Press, Amsterdam seventh edition 2007.

[235] P.F. Byrd and M.D. Friedman. *Handbook of elliptic integrals for engineers and scientists*. Grundlehren der mathematischen Wissenschaften. Springer-Verlag 1971.

[236] J. J. Binney, N. J. Dowrick, A. J. Fisher, and M. Newman. *The Theory of Critical Phenomena: An Introduction to the Renormalization Group*. Oxford University Press, Inc. New York, NY, USA 1992.

[237] J. Zinn-Justin. *Quantum Field Theory and Critical Phenomena; 4th ed.* Internat. Ser. Mono. Phys. Clarendon Press Oxford 2002.

[238] R. Graham and T. Tél. Weak-noise limit of Fokker-Planck models and non-differentiable potentials for dissipative dynamical systems. *Phys. Rev. A* **31**, 1109–1122 (1985).

[239] H. R. Jauslin. Nondifferentiable potentials for nonequilibrium steady states. *Physica A: Statistical Mechanics and its Applications* **144**, 179–191 (1987).

[240] Mark I. Dykman, Mark M. Millonas, and Vadim N. Smelyanskiy. Observable and hidden singular features of large fluctuations in nonequilibrium systems. *Physics Letters A* **195**, 53–58 (1994).

[241] Pelerine Tsobgni Nyawo and Hugo Touchette. A minimal model of dynamical phase transition. *EPL* **116**, 50009 (2016).

[242] R. Colin B. Abou, and, V. Lecomte, E. Pitard, and F. van Wijland. Activity statistics in a colloidal glass former: experimental evidence for a dynamical transition. *arXiv:1705.00855* (2017).

[243] Raphaël Chetrite and Hugo Touchette. Variational and optimal control representations of conditioned and driven processes. *Journal of Statistical Mechanics: Theory and Experiment* **2015**, P12001 (2015).

[244] B. Derrida. An exactly soluble non-equilibrium system: The asymmetric simple exclusion process. *Phys. Rep.* **301**, 65–83 (1998).

[245] B. Derrida, J. L. Lebowitz, and E. R. Speer. Large deviation of the density profile in the steady state of the open symmetric simple exclusion process. *J. Stat. Phys.* **107**, 599–634 (2002).

[246] P. I. Hurtado and P. L. Garrido. Current fluctuations and statistics during a large deviation event in an exactly solvable transport model. *J. Stat. Mech.* page P02032 (2009).

[247] T. Nemoto, F. Bouchet, R. L. Jack, and V. Lecomte. Population dynamics method with a multi-canonical feedback control. *arXiv:1601.06648* (2016).

[248] B.U. Felderhof. Spin relaxation of the Ising chain. *Reports on Mathematical Physics* **1**, 215–234 (1971).

[249] F.C. Alcaraz, M. Droz, M. Henkel, and V. Rittenberg. Reaction-Diffusion Processes, Critical Dynamics, and Quantum Chains. *Annals of Physics* **230**, 250–302 (1994).

References

[250] R. B. Stinchcombe and G. M. Schütz. Application of Operator Algebras to Stochastic Dynamics and the Heisenberg Chain. *Phys. Rev. Lett.* **75**, 140–143 (1995).

[251] Robin Stinchcombe. Stochastic non-equilibrium systems. *Advances in Physics* **50**, 431–496 (2001).

[252] N. D. Mermin and H. Wagner. Absence of Ferromagnetism or Antiferromagnetism in One- or Two-Dimensional Isotropic Heisenberg Models. *Phys. Rev. Lett.* **17**, 1133–1136 (1966).

[253] L.D. Landau and E.M. Lifshitz. *Statistical Physics*. Number v. 5. Elsevier Science 2013.

[254] S. Machlup and L. Onsager. Fluctuations and Irreversible Process. II. Systems with Kinetic Energy. *Phys. Rev.* **91**, 1512–1515 (1953).

[255] Joel L. Lebowitz and Herbert Spohn. A Gallavotti–Cohen-Type Symmetry in the Large Deviation Functional for Stochastic Dynamics. *Journal of Statistical Physics* **95**, 333–365 (1999).

[256] B. Derrida and C. Appert. Universal Large-Deviation Function of the Kardar–Parisi–Zhang Equation in One Dimension. *Journal of Statistical Physics* **94**, 1–30 (1999).

[257] Rosemary J. Harris and Hugo Touchette. Phase transitions in large deviations of reset processes. *Journal of Physics A: Mathematical and Theoretical* **50**, 10LT01 (2017).

[258] H. D. Miller. A Convexity Property in the Theory of Random Variables Defined on a Finite Markov Chain. *The Annals of Mathematical Statistics* **32**, 1260–1270 (1961).

[259] Raphaël Chetrite and Hugo Touchette. Nonequilibrium Microcanonical and Canonical Ensembles and Their Equivalence. *Phys. Rev. Lett.* **111**, 120601 (2013).

[260] Frank William John Olver. *Asymptotics and Special Functions*. Academic Press 1974.

[261] T. Speck, V. Blickle, C. Bechinger, and U. Seifert. Distribution of entropy production for a colloidal particle in a nonequilibrium steady state. *EPL (Europhysics Letters)* **79**, 30002 (2007).

[262] Jakob Mehl, Thomas Speck, and Udo Seifert. Large deviation function for entropy production in driven one-dimensional systems. *Physical Review E* **78**, 011123 (2008).

[263] Thomas Speck, Andreas Engel, and Udo Seifert. The large deviation function for entropy production: the optimal trajectory and the role of fluctuations. *Journal of Statistical Mechanics: Theory and Experiment* **2012**, P12001 (2012).

[264] Takahiro Nemoto and Shin-ichi Sasa. Variational formula for experimental determination of high-order correlations of current fluctuations in driven systems. *Physical Review E* **83**, 030105 (2011).

[265] Takahiro Nemoto and Shin-ichi Sasa. Thermodynamic formula for the cumulant generating function of time-averaged current. *Physical Review E* **84**, 061113 (2011).

[266] Bernard Derrida and Tridib Sadhu. Large deviations conditioned on large deviations I: Markov chain and Langevin equation. *arXiv:1807.06543 [cond-mat, physics:math-ph, physics:physics]* (2018). arXiv: 1807.06543.

[267] Bernard Derrida and Karol Proesmans. Large deviation theory of a Brownian particle on a ring: a WKB approach. (2018). Preprint.

[268] Bernt Øksendal. *Stochastic differential equations: an introduction with applications*. Universitext. Springer Berlin 6. ed., 6. corrected printing edition 2013. OCLC: 935584333.

[269] S. R. S. Varadhan. Asymptotic probabilities and differential equations. *Comm. Pure Appl. Math.* **19**, 261–286 (1966).

[270] Juan P Garrahan, Robert L Jack, Vivien Lecomte, Estelle Pitard, Kristina van Duijvendijk, and Frédéric van Wijland. First-order dynamical phase transition in models of glasses: an approach based on ensembles of histories. *Journal of Physics A: Mathematical and Theoretical* **42**, 075007 (2009).

[271] T. Bodineau and C. Toninelli. Activity Phase Transition for Constrained Dynamics. *Communications in Mathematical Physics* **311**, 357–396 (2012).

References

[272] Lorenzo Bertini, Alberto De Sole, Davide Gabrielli, Giovanni Jona-Lasinio, and Claudio Landim. Lagrangian phase transitions in nonequilibrium thermodynamic systems. *Journal of Statistical Mechanics: Theory and Experiment* **2010**, L11001 (2010).

[273] M. Abramowitz and I.A. Stegun. *Handbook of Mathematical Functions: With Formulas, Graphs, and Mathematical Tables*. Applied mathematics series. Dover Publications 1965.

[274] Serguei Brazovskii and Thomas Nattermann. Pinning and sliding of driven elastic systems: from domain walls to charge density waves. *Advances in Physics* **53**, 177–252 (2004).

[275] Peter Grassberger. Go with the winners: a general Monte Carlo strategy. *Computer Physics Communications* **147**, 64–70 (2002).

[276] Cristian Giardinà, Jorge Kurchan, and Luca Peliti. Direct Evaluation of Large-Deviation Functions. *Phys. Rev. Lett.* **96**, 120603 (2006).

[277] Julien Tailleur and Jorge Kurchan. Probing rare physical trajectories with Lyapunov weighted dynamics. *Nat Phys* **3**, 203–207 (2007).

[278] James B. Anderson. A random-walk simulation of the Schrödinger equation: H_3^+. *The Journal of Chemical Physics* **63**, 1499–1503 (1975).

[279] Mohamed El Makrini, Benjamin Jourdain, and Tony Lelièvre. Diffusion Monte Carlo method: Numerical Analysis in a Simple Case. *ESAIM: Mathematical Modelling and Numerical Analysis* **41**, 189–213 (2007).

[280] Cristian Giardinà, Jorge Kurchan, Vivien Lecomte, and Julien Tailleur. Simulating Rare Events in Dynamical Processes. *J. Stat. Phys.* **145**, 787–811 (2011).

[281] R. M. L. Evans. Rules for Transition Rates in Nonequilibrium Steady States. *Phys. Rev. Lett.* **92**, 150601 (2004).

[282] A. Baule and R. M. L. Evans. Invariant Quantities in Shear Flow. *Phys. Rev. Lett.* **101**, 240601 (2008).

[283] Takahiro Nemoto, Freddy Bouchet, Robert L. Jack, and Vivien Lecomte. Population-dynamics method with a multicanonical feedback control. *Phys. Rev. E* **93**, 062123 (2016).

[284] Takahiro Nemoto, Robert L. Jack, and Vivien Lecomte. Finite-Size Scaling of a First-Order Dynamical Phase Transition: Adaptive Population Dynamics and an Effective Model. *Phys. Rev. Lett.* **118**, 115702 (2017).

[285] Ushnish Ray, Garnet Kin-Lic Chan, and David T. Limmer. Exact Fluctuations of Nonequilibrium Steady States from Approximate Auxiliary Dynamics. *Physical Review Letters* **120**, 210602 (2018).

[286] Grégoire Ferré and Hugo Touchette. Adaptive Sampling of Large Deviations. *Journal of Statistical Physics* (2018).